THESIS

UNCERTAINTY IN MEASURING SEEPAGE FROM EARTHEN IRRIGATION CANALS USING THE INFLOW-OUTFLOW METHOD AND IN EVALUATING THE EFFECTIVENESS OF POLYACRYLAMIDE APPLICATIONS FOR SEEPAGE REDUCTION

Submitted by

Chad Allen Martin

Department of Civil and Environmental Engineering

In partial fulfillment of the requirements

For the Degree of Master of Science

Colorado State University

Fort Collins, Colorado

Spring 2015

Master's Committee:

Advisor: Timothy K. Gates

Daniel S. Cooley
Ryan T. Bailey

ABSTRACT

UNCERTAINTY IN MEASURING SEEPAGE FROM EARTHEN IRRIGATION CANALS USING THE INFLOW-OUTFLOW METHOD AND IN EVALUATING THE EFFECTIVENESS OF POLYACRYLAMIDE APPLICATIONS FOR SEEPAGE REDUCTION

Seepage losses from unlined irrigation canals account for a large fraction of the total volume of water diverted for agricultural use, and reduction of these losses can provide significant water quantity and water quality benefits. Quantifying seepage losses in canals and identifying areas where seepage is most prominent are crucial for determining the potential benefits of using seepage reduction technologies and materials. In recent years, polymers have been studied for their potential to reduce canal seepage, and the use of linear-anionic polyacrylamide (PAM) was studied as part of this analysis. To quantify seepage reduction, seepage rates must be estimated before and after application of linear-anionic polyacrylamide (LA-PAM). In this study, seepage rates from four earthen irrigation canals in the Lower Arkansas River Valley (LARV) of southeastern Colorado were estimated with repeated measurements using the inflow-outflow volume balance procedure. It is acknowledged that a significant degree of measurement error and variability is associated with using the inflow-outflow method; however, as is often the case, it was selected so that canal operations were not impacted and so that seepage studies could be conducted under normal flow conditions. To account for uncertainty related to using the inflow-outflow procedure, detailed uncertainty analysis was conducted by assigning estimated probability distribution functions to volume balance components then performing Monte Carlo simulation to calculate possible seepage

values with associated probabilities. Based upon previous studies, it was assumed that flow rates could be measured with +/- 5% accuracy, evaporation at +/- 20% accuracy, and water stage within 0.04 to 0.06 feet (all over the 90% interpercentile range). Spatial and temporal variability in canal hydraulic geometry was assessed using field survey data and was incorporated into the uncertainty model, as were temporal variability in flow measurements. Monte Carlo simulation provided a range of seepage rates that could be expected for each inflow-outflow test based upon the pre-defined probable error ranges and probability distribution functions.

Using the inflow-outflow method and field measurements directly for assessing variables, deterministic seepage rates were estimated for 77 seepage tests on four canals in the LARV. Canal flow rates varied between 25.8 and 374.2 ft^3/s and averaged 127.9 ft^3/s, while deterministic estimates of seepage varied between -0.72 and 1.53 (ft^3/s) per acre of wetted perimeter with an average of 0.36 (ft^3/s)/acre for all 77 tests. Deterministic seepage results from LA-PAM application studies on the earthen Lamar, Catlin, and Rocky Ford Highline canals in southeastern Colorado indicated that seepage could be reduced by 34-35%, 84-100%, and 66-74% for each canal, respectively.

Uncertainty analysis was completed for 60 seepage tests on the Catlin and Rocky Ford Highline canals. To describe hydraulic geometry within the seepage test reaches of these canals, canal cross-sections were surveyed at 25 and 16 locations, respectively. Probability distribution functions were assigned to parameters used to estimate wetted perimeter and top width for each cross-section to account for measurement error and spatial uncertainty in hydraulic geometry. Probability distributions of errors in measuring canal flow rates and stage, and in calculating water surface evaporation also were accounted for. From stochastic analysis of these 60 seepage tests, mean values of estimated seepage were between -0.73 (ft^3/s)/acre (gain) and 1.53

(ft^3/s)/acre, averaging 0.32 (ft^3/s)/acre. The average of the coefficient of variation values computed for each of the tests was 240% and the average 90^{th} interpercentile range was 2.04 (ft^3/s)/acre. For the Rocky Ford Highline Canal reaches untreated with LA-PAM sealant, mean values of canal seepage rates ranged from -0.26 to 1.09 (ft^3/s)/acre, respectively, and averaged 0.44 (ft^3/s)/acre. For reaches on the Catlin Canal untreated with LA-PAM, mean values of seepage ranged from 0.02 to 1.53 (ft^3/s)/acre, respectively, and averaged 0.63 (ft^3/s)/acre. For reaches on the Rocky Ford Highline Canal and Catlin Canal treated with LA-PAM, mean canal seepage rates values ranged from 0.25 to 0.57 (ft^3/s)/acre, averaging 0.33 (ft^3/s)/acre, and from -0.73 to 0.55 (ft^3/s)/acre, averaging -0.01 (ft^3/s)/acre, respectively. Comparisons of probability distributions for several pre- and post-PAM inflow-outflow tests suggest likely success in achieving seepage reduction with LA-PAM.

Sensitivity analysis indicates that while the major effect on seepage uncertainty is error in measured flow rate at the upstream and downstream ends of the canal test reach, but that the magnitude and uncertainty of storage change due to unsteady flow also is a significant influence. Based upon the findings, recommendations for future seepage studies were provided, which have the ability to account for and reduce uncertainty of inflow-outflow measurements.

ACKNOWLEDGMENTS

Thank you to the United States Bureau of Reclamation (USBR), Desert Research Institute, Colorado Agricultural Experiment Station, Southeastern Colorado Water Conservancy District, and the Lower Arkansas Valley Water Conservancy District for providing direct funding my Master's research. Thank you Del Smith of USBR for your guidance and support. Special thanks to the Desert Research Institute, particularly Rick Susfalk, Margaret Shanafield, Brian Fitzgerald, Brian Epstein, and others who partnered in this research with countless hours of data collection and testing. Thank you to fellow graduate and undergraduate students who helped collect data, perform applications, and provide support including Alex Herting, Nik Hallberg, Eric Morway, Chad Hall, Matt Bostrom, and Kyle Davis. Thank you to graduate committee members Dr. Dan Cooley and Dr. Ryan Bailey for your time and invaluable input. Thanks to the good people from the Lower Arkansas River Valley, including Mike Bartolo, for your kindness and hospitality.

I would especially like to thank canal company boards and superintendants in the Lower Arkansas River Valley who allowed for this research to be conducted including Dan Henrichs (Rocky Ford Highline Canal), Greg Williams (Catlin Canal), John Carver (Lamar Canal), and Manny Torrez (Fort Lyon Canal). Without your participation this research would not have been possible.

Most of all, I would like to thank my advisor Dr. Tim Gates. I appreciate all your patience during the long process of completing my degree and for keeping faith that I would get it completed. I am one of countless students who have benefitted from your teachings, example, enthusiasm, and encouragement. Thank you so much.

TABLE OF CONTENTS

LIST OF TABLES

LIST OF FIGURES

LIST OF SYMBOLS AND ABBREVIATIONS

Symbols

a	albedo (decimal)
A_P	area of wetted perimeter (acre)
A_{WS}	area of water surface (acre)
c_a	heat capacity of air (MJ/kg/K)
C_i	hydraulic geometry coefficient for variable i determined from at-a-cross-section regression
$\hat{C}_i$	component of hydraulic geometry coefficient for variable i predicted by the "along-the-canal" deterministic trend equation for that location
C_i'	random "along-the-canal" component associated with predicting hydraulic geometry coefficient for variable i
C_{P1}, C_{P2}, C_{P3}	fitted "at-a-cross-section" regression coefficients for P using survey data
C_{T1}, C_{T2}, C_{T3}	fitted "at-a-cross-section" regression coefficients for T_w using survey data
d	water depth (ft)
D_{TH}	thalweg depth (ft)
E	free-water evaporation rate or depth (mm/day, ft)
EL_{PT}	relative elevation of a pressure transducer
e_a	vapor pressure (kPa)
e_a^*	saturated vapor pressure (kPa)
h	canal flow stage (ft)
H	canal stage (ft)

H_{DS}	canal stage measured at the downstream boundary of the canal test reach (ft)
H_{US}	canal stage measured at the upstream boundary of the canal test reach (ft)
K	net solar shortwave radiation [MJ / (m^2/day)]
K_E	coefficient of vertical transport of water (kPa^{-1})
K_{in}	shortwave radiation entering earth's atmosphere [MJ / (m^2/day)]
K_{sat}	saturated hydraulic conductivity (cm/s)
L	longwave radiation [MJ / (m^2/day)]
L_j	length of subreach j along the canal test reach
O_i	measured data point
P	wetted perimeter or precipitation depth (ft)
P_{abs}	absolute pressure (lbs/in^2)
P_{baro}	atmospheric pressure (lbs/in^2)
P_{gage}	gage pressure (lbs/in^2)
Q	discharge (ft^3/s)
Q_D	diversion rate (ft^3/s)
Q_{DS}	canal outflow rate through the downstream cross section (ft^3/s)
$Q'_{DS,1}$	flow rate at the downstream boundary of the canal test reach at time t_1 estimated using Q vs. H relationship during "unmeasured" time period Δt_B (ft^3/s)
$Q'_{DS,2}$	flow rate at the downstream boundary of the canal test reach at time t_2 estimated using Q vs. H relationship during "unmeasured" time period Δt_B (ft^3/s)
$Q_{DS,3-4}$	measured flow rate at the downstream boundary of the canal test reach during unmeasured time period Δt_B (ft^3/s)
Q_E	evaporation rate (ft^3/s)

Q_I	inflow discharge (ft^3/s)
Q_P	volumetric precipitation rate (ft^3/s)
Q_s	seepage rate (ft^3/s)
Q_{US}	canal inflow rate through the upstream cross section (ft^3/s)
$Q_{US,1-2}$	measured flow rate at the upstream boundary of the canal test reach between t_1 and t_2 during unmeasured time period Δt_A (ft^3/s)
$Q'_{US,3}$	flow rate at the upstream boundary of the canal test reach at time t_3 estimated using Q vs. H relationship during "unmeasured" time period Δt_A (ft^3/s)
$Q'_{US,4}$	flow rate at the upstream boundary of the canal test reach at time t_4 estimated using Q vs. H relationship during "unmeasured" time period Δt_A (ft^3/s)
r	correlation factor for Q_{US} and Q_{DS} flow measurements (decimal)
St	measurement cross-section station (mi)
t	time (sec)
t_1	time at the start of the Q_{US} measurement
t_2	time at the end of the Q_{US} measurement
t_3	time at the start of the Q_{DS} measurement
t_4	time at the end of the Q_{DS} measurement
Δt	flowing water-balance test duration
Δt_A	"unmeasured" time period for Q_{US}, between t_2 and t_4
Δt_B	"unmeasured" time period for Q_{DS}, between t_1 and t_3
T_a	air temperature (°C)
T_w	canal top width at the water surface (ft)
$\overline{T}_{w\,j}$	average canal top width over subreach j along the canal test reach (ft)

$UO_i(l)$	lower uncertainty boundary
$UO_i(u)$	upper uncertainty boundary
$\bar{v}$	average cross-section flow velocity (ft/sec)
v_a	wind speed (m/s)
W	average water surface top width (ft)
W_a	relative humidity (decimal)
x	position along the thalweg axis of the canal test reach (mi)
z_o	roughness of water surface (m)
z_d	zero-place displacement (m)
z_m	height at which wild and air vapor are measured (m)
$\frac{\Delta S}{\Delta t}$	rate of change of stored water volume (ft^3/s)
Δ	slope of relation between saturation vapor pressure and temperature (kPa/K)
γ	psychometric constant (kPa/K)
γ_w	density of water (lbs/ft^3)
ε_{qt}	atmospheric emissivity (decimal)
ε_w	emissivity of water (decimal)
$\varepsilon_{H_{abs}}$	random error associated with measuring p_{abs} for use in estimating H(ft)
$\varepsilon_{H_{baro}}$	random error associated with measuring p_{baro} for use in estimating H (ft)
$\varepsilon_{H_{SG}}$	random error in manual staff gage readings (ft)
ε_P	random error associated with measuring P "at-a-station" (ft)
$\varepsilon_{P_{trend}}$	random error in estimating P by projecting a linear trend line (ft)
$\varepsilon_{Q_{DS},1}$	random error in estimating $Q'_{DS,1}$ (ft)

$\varepsilon_{Q_{DS},2}$ random error in estimating $Q'_{DS,2}$ (ft^3/s)

$\varepsilon_{Q_{DS},3-4}$ random error in estimating $Q_{DS,3-4}$ (ft^3/s)

$\varepsilon_{Q_{US},1-2}$ random error in estimating $Q_{US,1-2}$ (ft^3/s)

$\varepsilon_{Q_{US},3}$ randomly generated flow rate error for estimation of $Q'_{US,3}$ (ft^3/s)

$\varepsilon_{Q_{US},4}$ randomly generated flow rate error for estimation of $Q'_{US,4}$ (ft^3/s)

ε_{TH} random error associated with estimating TH_{el} (ft)

ε_{Tw} random error in measuring T_w "at-a-station" (ft)

λ_v latent heat of vapor (MJ/kg)

ρ_w mass density of water (kg/m^3)

σ Stephen-Boltzmann constant [$4.90(10)^{-9}$ $MJ/(m^2day^1K^4)$]

Abbreviations

ADCP acoustic Doppler current profiler

ADV acoustic Doppler velocimeter

AMD unpolymerized acrylamide

ANCID Australian National Committee for Irrigation and Drainage

BOD biological oxygen demand

ft^3/s cubic feet per second

CR county road

CV coefficient of variance

DOC dissolved organic carbon

DST daylight savings time

EC	eddy covariance or electric conductivity
EPA	United States Environmental Protection Agency
FDA	Food and Drug Administration
ft	foot or feet
g	gram
GPS	global positioning system
GUM	ISO's "Guide to Expression of Uncertainty in Measurement"
ha	hectare
IR	interpercentile range
ISO	International Standardization Organization
L	liter
LA-PAM	linear anionic polyacrylamide
LARV	Lower Arkansas River Valley
mg	milligram
mi	mile
mol	mole
NRCS	Natural Resources Conservation Service
PAM	polyacrylamide
PC	personal computer
PER	probable error range
PDF	probability distribution function
PT	pressure transducer
R	gas constant

RFH	Rocky Ford Highline
s	second
sec	second
Sta	channel station
Stdev	standard deviation
UN-FAO	United Nations Food and Agriculture Organization
USGS	United States Geological Survey
UTM	Universal Transverse Mercator
WHO	World Health Organization
WSE	water surface elevation
XPAM	cross-linked polyacrylamide

1 INTRODUCTION AND LITERATURE REVIEW

1.1 PURPOSE

This thesis has two purposes: (1) evaluate and attempt to quantify the effectiveness of granular, LA-PAM application for reducing water seepage from earthen irrigation canals and (2) quantify error and uncertainty related to using the inflow-outflow method for estimating seepage rates from earthen canals and recommend ways in which to reduce measurement uncertainty.

The objective of field data collection was to measure seepage rates using the inflow-outflow method. These measurements were conducted before and after LA-PAM applications (if an application was conducted). Field data collection included measurement of in-stream flow rates, water levels, and atmospheric data. Data was processed and implemented in the inflow-outflow seepage measurement equations to obtain a seepage rate for a given measurement. Pre- and post-application seepage rates were then compared to estimate a reduction in seepage.

It is recognized that measurement error can have a significant impact on the accuracy of seepage measurement, so as part of the study, uncertainty analysis and Monte Carlo simulation was conducted on the volumetric water balance approach for the purpose of considering the accuracy at which seepage can be measured and practices that can be followed to minimize error. Probability distributions were assigned to measured and calculated values within the volumetric water balance equation for the purpose of simulating a probable expected range of seepage rates for a given measurement. Sensitivity analysis was conducted for various parameters related to inflow-outflow seepage measurements to study which sources of error and variability led to the highest degree of uncertainty.

1.2 PROBLEM DEFINITION

1.2.1 Canal Seepage Loss

Seepage from irrigation canals can have the following impacts on water quality and water quantity: (1) reduced water volumes and flow rates delivered to agricultural fields, (2) higher canal diversion rates from rivers leading to less in-stream river flows, (3) increased water table elevations that can lead to salinity problems and reduce crop yield, (4) and reduction in water quality as groundwater from canal seepage picks up and transports salts, selenium, uranium, nutrients, and other compounds from aquifers to the rivers and streams (Burkhalter and Gates 2005; Burt et al. 2010; USGS 1990).

Seepage from unlined canals can account for a large percentage of the total water volume diverted for irrigation use. A wide variety of seepage percentage have been estimated by several sources, some unique to a particular region. Seepage losses in semi-arid regions can account for 20-30% of the total flow volume in unlined, earthen canals, according to (Tanji and Kielen 2002). USGS (1990) suggests that 17% of water conveyed for irrigation in 1985 in the United States was lost to evaporation or seepage to groundwater; Kinzli et al. (2010) found that earthen canals in the Middle Rio Grande Valley of New Mexico can lose more than 40% of the diverted water volume to seepage; Yussuff et al. (1994) suggests that unlined canals around the world can loses 25% to 50% of the total diverted flow to seepage; Fipps (2005) estimated that conveyance efficiency from the point of diversion to the field in canals in the Lower Rio Grande Valley in Texas was 69.7%; and Sharma (1975) estimated that irrigation canals and laterals in New Delhi lose 45% of the total diverted flow rate before water reaches agricultural fields. Despite the variety of estimates, it is clear that significant volumes of water diverted for irrigation purposes never reach agricultural fields due to seepage.

Seepage rates in unlined canals are mainly affected by (1) the hydraulic conductivity of soils composing the wetted perimeter of the channel and of subsoils; (2) suspended sediment concentrations; (3) hydraulic characteristics of the canal water including stage, flow velocity, and shear stress on the wetted perimeter; (4) hydraulic gradient between the canal water surface and the underlying groundwater surface of an unconfined aquifer; (5) channel geometry; and (6) vegetation located along the channel banks (Johnson and Heil 1996; Swamee et al. 2000; Yussuff et al. 1994). Each of these factors changes temporally and spatially along a canal reach.

1.2.2 Uncertainty Related to Estimating Canal Seepage Loss

Quantifying seepage rates can be difficult due to uncertainty related to field measurements and modeling. The validity of hydrologic model parameters often goes unconsidered or uninvestigated (Haan 1989). R.W. Herschy (2002) states that "the result of a measurement is only an estimate of the true value of the measurement and is therefore only complete when accompanied by a statement of its uncertainty." One of the purposes of this thesis is to investigate the impacts that parametric uncertainty has on seepage calculations when using the inflow-outflow seepage method. Parametric uncertainty is derived from:

- measurement error
- spatial variability
- temporal variability
- limited sampling

1.2.3 Expensive Canal Lining Methods

Conventional canal lining materials include concrete, rubber, geomembranes, fluid-applied membranes, and compacted clay. Advantages of these types of linings include large seepage reductions and durability of the materials after construction. Swihart and Haynes (2002)

estimated through controlled studies that conventional canal lining can reduce the effective seepage rate of a water delivery canal by 70% to 95% while maintaining effectiveness for a duration of 10 to 60 years. The disadvantage of these materials is the large costs related to materials, construction, and maintenance (ANCID 2004). Typically, these materials are only used when the value of increased crop yield and salvaged water exceeds these high costs. As such, cheaper canal lining techniques and materials are of great interest to canal companies. The effectiveness of applying PAM, which is significantly cheaper than conventional lining materials, to canals for seepage reduction was studied and results are provided in this report.

1.3 CANAL SEEPAGE

1.3.1 Factors Affecting Seepage

1.3.1.1 Soil Properties

According to Darcy's Law, the discharge rate through a porous media is directly related to the permeability of the porous media (Darcy 1856). As such, the permeability of soils or canal lining materials affects the canal's seepage rate. The permeability of soils increases as void space increases. Therefore, the type of soil that composes an earthen irrigation canal and the compaction of those soils affect the seepage rate. The following soils are listed in order of increasing permeability: clays, silts, sands, then gravels (Milligan 1976). For rocks, permeability increases as the level of fracturing increases (Milligan 1976).

Compacting the soil that comprises the channel perimeter can have a significant impact on reducing seepage as the soil permeability is decreased (Burt et al. 2010). Kahlown and Kemper (2004) conducted ponding tests in channels to study the effects that channel bank condition and composition have on seepage losses and concluded that loss rates are impacted by soil texture but are even more impacted by the presence of holes and leaks cause by organic

material, sod, and burrows from animals, worms, and insects. In their study, channels were reconstructed and seepage was reduced to 5-16% of the previous loss rate by compacting new soil with foot pressure on the channel perimeter that was low in organic matter.

1.3.1.2 Shape of Channel

The shape of a channel cross-section can have an impact on loss rates from both lined and unlined canals (Swamee 1995; Swamee et al. 2000) as the hydraulic radius (the ratio between flow area and wetted perimeter) plays an important role in flow efficiency. For a given area, less wetted perimeter results in increased flow efficiency and less area through which canal water can infiltrate from the channel. Additional wetted perimeter increases the area through which water can seep, while additional top width increases the area from which water can evaporate. Swamee (1995) used explicit equations to estimate seepage losses in rectangular, triangular, and trapezoidal channels and concluded that trapezoidal channels have the least seepage loss. The study did not take into account influencing factors other than shape, such as perimeter materials, adjacent groundwater levels, boundary conditions, vegetation, etc.

1.3.1.3 Aquifer Table Elevation

Darcy's Law indicates that flow through a porous media (i.e. soils composing a canal perimeter) has a direct relationship to the hydraulic gradient (Darcy 1856). The hydraulic gradient is the change in hydraulic head over a given distance and in a given direction. For canals, flow through the soil of the channel perimeter is related to the groundwater gradient between the canal interface and underlying aquifer, and the gradient is variable around the channel perimeter. Upadhyaya and Chauhan (2001) and Yussuff et al. (1994) both analytically studied the relationships between canal seepage and adjacent aquifer elevations, indicating that

groundwater elevation increases with canal seepage and canal seepage decreases as groundwater elevation increases.

Islam (1999) attributed intra-seasonal variations in seepage rates from lined and unlined canal sections to variations in groundwater table elevations in West Bengal, India. Higher groundwater tables in wet seasons caused seepage rates to be less than during dry seasons when the groundwater table was lower and the groundwater gradient was steeper. Similarly, Sheng et al. (2003) performed ponding seepage tests during and after the irrigation season on a canal in Texas and found that seepage rates were 50% higher after the irrigation season than during the irrigation season due to lower groundwater tables.

1.3.1.4 Season and Vegetation

Vegetation along canal banks varies seasonally and can have an impact on seepage rates by direct consumption of water by root extraction, as well as by increasing hydraulic conductivity due to root systems which can create preferential flow pathways. Vegetation in canals also creates an increase in flow resistance which increases flow depths (Chow 1959), and thereby increases the wetted perimeter through which seepage can occur. Decreasing channel roughness by removing vegetation lowers flow depth and consequently reduces water loss rates (Akram et al. 1981). Organic matter and sod in the soil composing the channel banks also influences seepage rates from earthen canals (Kahlown and Kemper 2004). This is related to the decomposition of organic material which results in potential flow pathways and is related to the food source that vegetation provides to worms, ants, beetles and other insects which form burrow holes through the soils of the channel perimeter.

1.3.1.5 Sedimentation and Erosion

Sediment layers formed by a sediment deposition event in a canal are often characterized with large sediment particles on the bottom and smaller particles on the top, and the gradation of the sediment layer has been found to reduce infiltration through the layer, thereby reducing channel seepage (Bouwer et al. 2001). Channel infiltration rates are typically less when inflow water contains sediment, likely due to clogging of soil pores (Sirjacobs et al. 2000).

Rodrick D. Lentz and Freeborn (2007) discuss three ways that sediment can reduce infiltration in ponded and flowing water. The three sediment sealing mechanisms are referred to as thick-layer deposits, thin-layer seals, and wash-in seals. Thick-layer sediment deposits are created by the settling of bedload and suspended sediments in water, which form horizontal layers that reduce permeability. Thin-layer seals are thinner than thick-layer deposits and are formed from suspended sediment that deposits in flowing water. The thin layer is held in place and compacted by negative subsurface pressures, which forms a seal. Wash-in seals form when suspended sediments flow into soil pores and are deposited within the upper layers of the soil. Sediment thereby plugs the soil voids and forms a seal.

1.3.1.6 Flow Velocity

Stone et al. (2008) conducted laboratory experiments on the impacts that shear stress has on soil treated with PAM and discovered that shear stress can cause the PAM layer to scour and result in an increase in seepage through the treated soil column, especially if imperfections in the PAM layer were present and the beginning of the experiment.

1.3.2 Technologies to Reduce Canal Seepage Losses

1.3.2.1 Concrete Lining

Concrete lining is perhaps the most effective option to reduce seepage in water conveyance channels due to low permeability, durability, longevity, and hydraulic efficiency (ANCID 2004).

Concrete liners can be applied with a variety of combinations in technique and technologies including: conventional concreting, applying shotcrete (pneumatically applied concrete or mortar), roller compacting concrete, applying concrete with or without reinforcement, applying concrete over a geomembrane or impermeable fabric, etc. (ANCID 2004; Swihart and Haynes 2002). It is a more expensive option for canal lining, but Swihart and Haynes (2002) and ANCID (2004) indicate a 70% to 90% long-term reduction in seepage with a life span of 40 to 60 years. The cost of the liner is dependent upon many factors including concrete thickness, concrete strength, reinforcement (if any), constructability, etc.. Many canals are not lined with concrete because high capital cost of construction is large or outweighs the monetary benefit of the potential water savings. In addition, concrete liners can be susceptible to damage from expansive soils, groundwater pressure, buoyancy of the liner if the groundwater table elevation exceeds the water level in the canal, and undermining (ANCID 2004).

1.3.2.2 Flexible Membrane Lining

A variety of flexible membrane liners are used for the purpose of seepage reduction in earthen canals. Such materials include rubber, plastic, high density polyethylene, geosynthetic clay, polypropylene, geomembrane, fluid applied geomembrane, and thin layered asphalt (ANCID 2004; Swihart and Haynes 2002). Flexible liners are generally a cheaper option than concrete liners, however, the disadvantages include lower durability, susceptibility to damage

(ultraviolet damage, animal traffic, plant growth, etc.), higher maintenance cost, and less of a reduction in seepage. Swihart and Haynes (2002) found that exposed geomembranes and fluid applied geomembranes have a durability of 10 to 25 years and 10 to 15 years, respectively, with an average long term seepage reduction of around 90%. ANCID (2004) states that covered flexible membrane liners generally have a life span 40 years with an earth cover and reduce seepage by at least 95%. It also states that uncovered flexible membranes reduce seepage by at least 85% with a life span between 20 and 40 years.

1.3.2.3 Soil Compaction

Compaction of existing and imported soils that compose the bottom and side slopes of an earthen canal can be an effective means for reducing seepage loss, as the hydraulic conductivity of compacted soil is reduced (ANCID 2004; Burt et al. 2010). Seepage can be reduced by 70% to 90% when in-situ or imported soil is compacted on the perimeter of earthen canals (ANCID 2004). Soil is typically compacted mechanically using vibratory plates, rollers (e.g. sheepsfoot rollers, smooth drum rollers, or rubber tired rollers - some of which may also be vibratory), or impact compactors (e.g. rammers, tampers, or jumping jacks). In-situ soil compaction one of the least expensive options for reducing seepage in unlined canals and the estimated effective life is up to 30 years (ANCID 2004).

Burt et al. (2010) describes a study in which in-situ canal soils were compacted in an effort to reduce seepage in earthen canals in California. Seepage tests were conducted before and after compacting the soil of the canal bottom and/or banks using the ponding method. The study results indicated that short-term seepage rates were reduced by approximately 90% when the canal bottom and sides were compacted and by 16-31% when only the sides were compacted. Longevity of the canal soil compaction efforts for seepage reductions were not studied.

1.3.2.4 Polyacrylamide (PAM)

Polyacrylamide (PAM) is a synthetic polymer composed of thousands of acrylamide monomers (-CH2CHCONH2-), as shown in Figure 1-1, linked together. (Budd 1996; Seybold 1994; Sojka et al. 2007). Polymers are long chains of molecules connected by strong covalent bonds (Seybold 1994). The length, charge density, and molecular weight of the PAM polymer can be altered chemically (Green and Stott 2001; Seybold 1994), and PAM is often altered to obtain an ionic charge (cationic or anionic) that is more beneficial for flocculation, depending upon the purpose of its use (Budd 1996). PAM with linear linked molecules is water soluble, while PAM with cross linked molecules is water absorbent but not water soluble (Sojka et al. 2007).

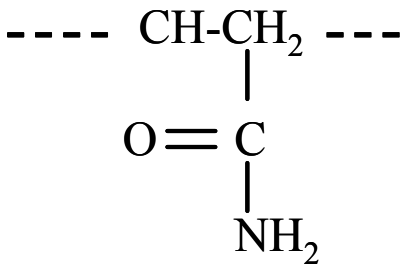

Figure 1-1 Molecular structure of the acrylamide monomer

Polyacrylamide can be manufactured to have one of three electrical states: (1) near non-ionic (no appreciable net charge, although it is slightly anionic), (2) anionic (a negatively charged ion), and (3) cationic (a positively charged ion) (Seybold 1994; Sojka et al. 2007; R. Susfalk et al. 2008). If ionic strength of the PAM is increased, repulsive forces are overcome more easily, allowing for particles to come into closer contact thereby increasing their overall attracting forces (Gregory 1996). Molecular weight varies between less than 1 Mg mol-1 and 20 MG mol-1, depending upon the type of PAM (Barvenik 1994). As the molecular weight

increases, the length of the polymer and the viscosity of the solution increases (Green and Stott 2001). As such, PAM with high molecular weight tends to be more effective for seepage reduction than PAM with lower molecular weight (Green and Stott 2001).

Global production of water soluble acrylamide polymer was a multi-billion dollar industry as of 1996 with a projected annual world-wide sales growth rate of 5-8% for water and wastewater treatment (Hunkeler and Hernandez-Barajas 1996). Sojka et al. (2007) reports that the wholesale cost of PAM has risen significantly in the past few years as the cost of natural gas, used for PAM synthesis, has increased. The report states that PAM prices increased 30% between 2000 and 2006. Nonetheless, PAM remains a very cost effective option for various applications that require particulate flocculation or water absorption.

1.3.2.4.1 Forms of Polyacrylamide

Cationic PAM

Cationic PAM has a low molecular weight (M. Young et al. 2007a), electrostatically bonds to negatively charged soil particles (Seybold 1994), and has been shown to have adverse ecological impacts. Beim and Beim (1994) found that cationic PAM is toxic to fish, invertebrates, and algae, and Muir et al. (1997) found that cationic polymers have negative impacts on trout as they tend to bond to their negatively charged gills. Since it is possible that a portion of PAM applied to water-delivery canals can return to rivers, streams, and other bodies of water, cationic PAM is not considered a safe option for environmental applications. Also, canals develop their own ecological habitats over time, supporting the growth and inhabitance of numerous aquatic animals such as fish, frogs, snakes, turtles, and crawfish, as observed in the canals of the LARV.

Non-ionic PAM

Nonionic PAM has a much lower reactivity and less ability to flocculate with suspended sediment particles in water (Mason et al. 2005). It will bond to clay particles as the molecules are attracted with weak van der Waals forces (Gregory 1996; Theng 1982). Nonionic PAM would be much less effective than charged PAMs in reducing seepage from earthen canals since flocculate formations are unlikely and since reactivity to charged soil particles is low.

Anionic PAM

Anionic PAM, with molecular structure shown in Figure 1-2, as typically used for agricultural applications has a molecular weight between 10 and 20 Mg mol^{-1} (Green and Stott 2001; Lu et al. 2002; Sojka et al. 2007; M. Young et al. 2007a). The anionic polymer uses cation-bridging to bond to negatively charged soil particles that are principally found in natural environments (Seybold 1994; Sojka et al. 2007; Theng 1982). Cations form the bridge between the negatively charged polymer and negatively charged particulate surfaces that would otherwise repel one another. It has been found that divalent cations commonly found in surface water, such as Mg^{2+} and Ca^{2+}, are very effective in forming the cation-bridges required to form the bonds, more so than monovalent cations, such as Na^{+} and K^{+} (Gregory 1996; Lu et al. 2002; R. Susfalk et al. 2008). The divalent ion Ca^{2+} also has been found to be more effective in the flocculation process than the monovalent ion Na^{+} because it has a smaller hydrated radius that enables closer proximity of molecules and promotes floc formation (Sojka et al. 2007).

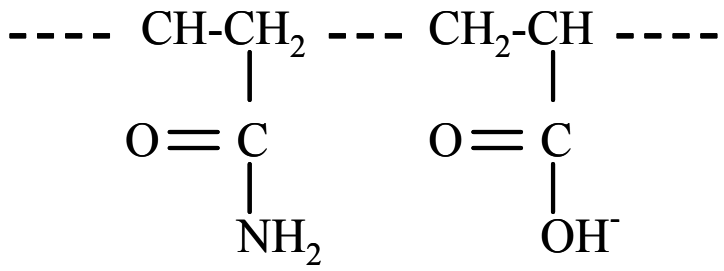

Figure 1-2 Molecular structure of anionic PAM

Based upon research findings and recommended PAM application guidelines created by multiple organizations, anionic PAM appears to be the safest form for reducing seepage in earthen canal systems (Sojka et al. 2007; M. Young et al. 2007a). However, environmental and human health risks are still present when applying anionic PAM, due to the presence of unpolymerized acrylamide (AMD). Anionic PAM used for most applications contains less than 0.05% AMD by weight of the total mixture (Sojka et al. 2007). AMD is a neurotoxin and is suspected to be a human carcinogen (Seybold 1994; WHO 1985; M. Young et al. 2007a), although it is used for numerous municipal purposes such as food processing, food packaging, and water treatment. The United States Environmental Protection Agency (EPA) and the Food and Drug Administration (FDA) limit AMD concentrations depending upon the type of use of PAM (M. Young et al. 2007a).

There are different forms of anionic PAM including linear-anionic PAM (LA-PAM) and cross-linked PAM (XPAM) (Sojka et al. 2007). XPAM is not recommended for use in canal systems due to increased ecological and environmental impacts caused by the greater presence of AMD.

LA-PAM is the most commonly used type of PAM for environmental applications including: reducing seepage in canals, ponds, and landfill; minimizing erosion of irrigation

furrows, construction sites, and ditches; and enhancing infiltration in irrigation furrows (Sojka et al. 2007). Anionic PAM has minimal impacts on the environment when the acrylamide content within the PAM mixture is minimized and when applied at reasonable and advised rates (Seybold 1994; M. Young et al. 2007a). R. B. Susfalk et al. (2007) discusses application procedures of anionic PAM to canal waters that are expected to result in effective seepage reduction while minimizing environmental and human health risks. Similar guidelines for PAM applications were developed by the USDA Natural Resources Conservation Service (NRCS 2005). The NRCS guidelines recommend that only non-cross-linked LA-PAM be used in canal treatments (NRCS 2005).

1.3.2.4.2 Flocculation of Adsorbed Polymers

Flocculation of polymers and particles typically occur from either the process of polymer bridging or the process of charge neutralization, or both processes working simultaneously (Gregory 1996; Theng 1982). Natural waters predominately contain negatively charged particles in suspension (Gregory 1996). Thus, anionic polymers alone are resistant to these negatively charged suspended particles and require cationic-bridging to flocculate, while cationic polymers require charge neutralization to adsorb to negatively charged suspended particles (Gregory 1996; Theng 1982).

Polymers mainly interact with clay particles in soils (Seybold 1994). The interaction is dependent upon the ionic surface charge, molecular size and weight, and configuration of the polymers; and the pH level, ionic strength, type of ions, and amount of clay particles of the soil in solution (Seybold 1994).

1.3.2.4.3 Bridging of Polymers

Sections of a polymer can adsorb to multiple particles, bridging the particles and polymers together forming flocs (Gregory 1996). The bonding of the particles and polymers through polymer bridging provides stronger attachment forces than those of van der Waals forces; consequently, the large number of links that characterize flocs are less likely to break from shear stresses caused by agitation of the solution (Gregory 1996; Ray and Hogg 1987). Extreme shear stresses on bridged flocs can cause breakage that is irreversible (Gregory 1996; Ray and Hogg 1987). Since most natural waters contain negatively charged suspended particles, the bridging process typically is associated with the use of anionic polymers that use positively charged particles to form the bridge to other anionic polymers, referred to as "cationic-bridging" (Gregory 1996; R. Susfalk et al. 2008; Theng 1982).

Polymer bridging allows for a rearrangement of flocculating particles, resulting in stronger and more dense flocs (Gregory 1996).

1.3.2.4.4 Charge Neutralization of Polymers

Charge neutralization most often is associated with cationic polymers (Gregory 1996). The cationic polymers can form flocs by adsorbing directly to negatively charged suspended particles (coagulation), although particle bridging can play a role depending upon the molecular weight of the cationic polymer (Gregory 1996).

1.3.2.4.5 Mixing

Gregory (1996) suggests that mixing of polymers with solution should be conducted immediately upon application to obtain the greatest flocculation effectiveness. If adequate mixing does not take place, an uneven distribution of polymers can form, causing restabilization of the adsorbed polymer molecules which, as previously stated, leads to the separation of flocs.

Flocculation occurs after a certain period of time has passed after PAM application due to factors including water chemistry, flow velocity, suspended sediment concentration and size (R. Susfalk et al. 2008), as supported and explained by Gregory (1996). In the presence of fluid motion, such as that of flowing canal water, Gregory (1996) states that polymer adsorption is slow relative to the rate of particle collisions required for the flocculation of polymers and suspended particles.

1.3.2.4.6 Hydration Process

The hydration process of PAM begins upon addition to water. Hydrogen bonding and dipole interactions between the polymer and water molecules begins the process of PAM uncoiling (Seybold 1994; R. Susfalk et al. 2008). Anionic polymers are more reactive on their outer surface area and less reactive in the inner layers of the coil (Lu et al. 2002; Theng 1982), so anionic PAM becomes more reactive to positively-charged soil particles as the hydration process progresses. The polymer can potentially bond with larger suspended soil particles as the polymer becomes more hydrated and the coils extend further from the core (Seybold 1994). Agitation of the water creates particle collisions, advancing the bonding process (Gregory 1996). However, extreme agitation can cause the bonds to break and the agglomerates to fall apart if hydrodynamic forces exceed the strength of the flocculate bonds (Ray and Hogg 1987). As the flocculation process between the polymer and soil continues, soil continues to bond to the polymer and small flocs join together becoming larger flocs as they are attracted through electrostatic forces (R. Susfalk et al. 2008). The flocs continue to join and increase in size until the hydrodynamic forces required to keep them suspended in the water are exceeded by the weight of the flocs. Once the weight of the flocs exceeds the required hydrodynamic forces for suspension in flowing water, the flocs settle to the channel perimeter (R. Susfalk et al. 2008).

1.4 USES OF WATER-SOLUBLE PAM

PAM typically is used for industrial, municipal, and agricultural applications involving flocculation of suspended particles in aqueous solutions (Budd 1996). It is one the most commonly used polymeric flocculants in industrial applications (Gregory 1996). Water-soluble PAM was introduced first in 1954 after a process for polymerizing acrylamide (Minsk et al. 1949) was patented (Sojka et al. 2007). Since this time, water-soluble PAM has been used most commonly for paper manufacturing, drinking water and wastewater treatment, food packaging, thickening and dewatering, mineral processing, oil recovery, soil stabilization, and soil conditioning (Gregory 1996; Hunkeler and Hamielec 1991; Sojka et al. 2007).

1.4.1 Studies of PAM Effectiveness

1.4.1.1 Agricultural Applications

Studies involving synthetic polymers for agricultural applications first began in the 1950's when PAM was being used as a soil conditioner to alter soil properties in crop fields (Green and Stott 2001; Seybold 1994; Sojka et al. 2007). The majority of agricultural-related research since this time has revolved around the use of polymers as soil conditioners that flocculate suspended particles and stabilize soil aggregates in furrows to reduce erosion and sediment runoff, improve plant growth, increase water infiltration, and improve water quality (De Boodt 1975; Green and Stott 2001; Seybold 1994; Sojka et al. 2007). However, high costs of soil-conditioning polymers limited demand and field application until the 1980's and 1990's when chemistry advances lead to improved production and when studies targeting optimum application rates made polymeric treatment significantly more affordable and more effective (R. D. Lentz and Sojka 2000; Sojka et al. 2007; Wallace and Wallace 1990). As a result, the number of studies of water soluble polymers, specifically PAM, for agricultural application has greatly

increased over the last few decades. Recent research, although limited, has focused on using PAM and other synthetic polymers as seepage-inhibiting sealants for unlined canals. It has been confirmed through research studies that small application rates of PAM can increase infiltration while larger applications rates combined with other factors can decrease infiltration (Ajwa and Trout 2006; Green and Stott 2001; Gregory 1996; R. D. Lentz 2003; Rodrick D. Lentz 2007; Seybold 1994).

1.4.1.1.1 Soil Conditioners

(Sojka et al. 2007) stated that beginning in the 1950's soil conditioners were applied directly to surface and subsurface soils. This process was labor intense and required significant polymer amounts which resulted in expensive applications and consequently limited demand and research studies (Sojka et al. 2007). It was later discovered that water-soluble polymers could be added as dry granulars or as a stock solution to irrigation water prior to entering furrows for soil conditioning, rather than directly to the soil. This technique treated only the upper few millimeters of soil and was found to be a more cost-effective and less labor intensive mechanism for conditioning crop fields (Sojka et al. 2007). The primary benefits of soil conditioning are related to increased infiltration rates and decreased erosion of furrow soils (Bjorneberg et al. 2000; R. D. Lentz and Sojka 2000). Once application to irrigation water, the polymers will bond to suspended solids and settle to the soil surface after flocculation. Upon settlement, the conditioning flocs stabilize the existing soil surface structure and provide additional resistance to the shear stresses caused by flowing water (Seybold 1994). The stabilized soil structure reduces erosion and allows for fluids to pass through the surface pores. As a result of fluid passages, crop production is increased, especially for fields with drainage problem or limited irrigation schedules, as water and nutrients can easily be delivered to plant roots. Drainage and aeration

also minimizes bacteria and fungus growth that can be harmful for crops (Sojka et al. 2007). By preventing erosion, sediment and other solids are kept on the agricultural fields instead of being transported downstream. This prevents potential problems with sediment deposition of streams, ponds, wetlands, and other bodies of water. Biological oxygen demand (BOD) and dissolved organic carbon (DOC) levels are reduced by preventing sediment runoff (R D Lentz et al. 1998), which can transport pesticides, nutrients, and organic materials. This potentially increases dissolved oxygen levels, inhibits excessive algae growth, and improves aquatic habitat in downstream water bodies.

R. D. Lentz and Sojka (2000) tested several application techniques and rates. The studies found that a large PAM doses (>7 kg ha^{-1}) reduced sediment loss by 93% while increasing infiltration rates 20% compared to a control, and that smaller PAM doses (<7 kg ha^{-1}) reduced soils losses by an average of 70% compared to a control, although results were variable. The studies also found that erosion rates were much lower when using a PAM solution as opposed to granular PAM. Mitchell (1986) suggests that even larger PAM doses (32.2 kg ha^{-1}) improve soil stability and increased infiltration rates by 30-57% during the first four hours after application to silty clay loam furrows. Studies completed by R. D. Lentz et al. (1992) found that PAM concentrations of 10 g m^{-3} reduced the sediment loads in treated furrows by 97% compared to untreated furrows during a treatment. The percentage reduction was discovered to decrease to 50% during an untreated irrigation event following the PAM application. Yu et al. (2003) found that soil conditioning with a mixture of anionic PAM and gypsum was most effective as infiltration rates were increased by 400% and erosion rates were reduced by 30% when compared to a control.

1.4.1.1.2 Canal and Ditch Sealants

Higher PAM concentrations have been found to decrease infiltration rates in irrigation furrows, ditches, and canals. As discussed later in this section, a balance between suspended sediment concentration and PAM concentration must be achieved to adequately inhibit infiltration and seepage. R. Susfalk et al. (2008) and Sojka et al. (2007) propose three principal physical mechanisms that result in seepage reduction upon settlement of PAM-sediment flocs: (1) settled flocs fill soil pores around the channel perimeter; (2) a thin layer of low hydraulic conductivity is formed on the channel perimeter by the flocs; and (3) viscosity is increased by the presence of PAM which inhibits the flow, and therefore infiltration, of water between soil void spaces around the channel perimeter.

Laboratory studies by M. H. Young et al. (2007b) and Moran (2007) found that linear anionic PAM can have a significant impact of the hydraulic conductivity of soil. Three soils were tested, two types of sand and a loam soil, in soil column experiments. Results suggested that the hydraulic conductivity (K_{sat}) of the two sands decreased by 80% and 81%, and K_{sat} of the loam soil was reduced by 52%. Through conceptual model studies, Zhu and Young (2009) concluded that PAM treatments are more effective at reducing seepage rates if the soil underlying the canal is coarse-textured. Constant head soil column studies by M. H. Young et al. (2009) indicated that PAM treatments to sand reduced hydraulic conductivity by 40 to 98% and that PAM treatments to loamy sand reduced hydraulic conductivity by 0 to 56%. The study also concluded that combining suspended sediment and PAM during a soil treatment reduced hydraulic conductivity of the sand by 8 to 11 times more than PAM without suspended sediment. Seepage reduction was attributed to increased viscosity from dissolved PAM and plugging of larger soil pores near the surface of the soil.

Laboratory studies also have shown that anionic PAM can significantly reduce infiltration in irrigation furrows or storage ponds when applied to dry soils prior to filling with water. Lentz (2003) conducted soil column and miniflume experiments using cross-linked PAM on clay loam and silt loam soils. Seepage rates were determined for ponded and flow scenarios. PAM concentrations applied to the dry soil ranged between 125 and 1000 mg/L and were found to reduce infiltration by up to 90%, with reduction rates greater for the higher concentrations. Relative to controls, PAM concentrations of 125 mg/L and 1000 mg/L were found to reduce K_{sat} by 25% and 60-90%, respectively. Rodrick D. Lentz (2007) performed soil column and miniflume studies on silt loam, loam, loamy sand, and clay loam soils with cross-linked anionic PAM. The soils and PAM were mixed prior to water saturation at treatment levels of 2.5-10 g/kg. It was determined that seepage rates decreased with increasing treatment levels. Seepage was reduced by up to 87% for 5g/kg treatments and 94% for 10 g/kg treatments. Ajwa and Trout (2006) used soil column experiments with sandy loam soils to investigate the effects of anionic PAM applications on infiltration rates. Granular PAM and emulsified PAM continuously were applied during the experiments at concentrations of 5-20 mg/L. Relative to controls, granular and emulsified PAM at concentrations of 5 mg/L were found to reduce seepage by 64% and 35% and at concentrations of 20 mg/L reduced seepage by 77% and 58%, respectively.

Field studies regarding the effectiveness of PAM in seepage reduction are limited in number but results have proved similar to laboratory studies. A canal seepage reduction demonstration was completed in the Arkansas River Valley of eastern Colorado by Valliant (2000) who tested two types of anionic PAM, a cross-linked PAM solution called HYDROGEL and LA-PAM, in unlined lateral canals. Flume and flow meter (Marsh-McBirney) measurements were conducted in a control reach and in a study reach of the lateral canal to estimate seepage

losses. Results using the cross-linked PAM were highly variable and showed no significant evidence of seepage reduction after application. The LA-PAM was found to reduce seepage rates by 41-73%, relative to the seepage rates in the control section prior to application. A variety of application rates and methods were tested on the same reach over a 3-year period. A total of 9 treatments were conducted between 1998 and 2000. The seepage rate in the treated canal reach was found to decrease after each application and the treatments appeared to remain effective to some extent, although variable, between irrigation years. Another field study investigated the effect of PAM on seepage reduction in earthen reservoirs. R. D. Lentz and Kincaid (2008) applied LA-PAM and cross-linked PAM to sections of a dry soil-lined irrigation reservoir prior to its being filled. The LA-PAM was applied at a concentration of 1000 mg/L and the cross-linked PAM was combined with three different salt (NaCl) concentrations that were expected to enhance the solution's performance. Each of the four treatments showed significant seepage reduction once the reservoir was filled with water. The average seepage rate of all treatments was 50% less than that of an untreated control. The study also confirmed that the presence of NaCl in cross-linked PAM treatments reduces amounts of XPAM required for an application while retaining treatment effectiveness.

1.4.1.2 Ineffectiveness of PAM

If an excess amount of PAM is adsorbed, particles can restabilize causing the bridging of polymers to become less effective and flocs to break apart (Gregory 1996). This occurs when particles become so saturated with polymers that they no longer are attracted to, or link to, other particles (Gregory 1996). Segments of the polymers adsorbed to particles will extended out from the particle into the aqueous solution, increasing the distance between particles and making the attractive forces too weak to hold flocs together (Gregory 1996; McLaughlin and Bartholomew

2007). The floc sizes consequently will decrease and can potentially become too small to effectively fill the spaces between soil particles along channel perimeters. The soil is given more strength and structure along the channel perimeter, without clogging soil pores, which is a possible explanation for increases in seepage in furrows and canals when the ratio between PAM application rate and suspended sediment concentration is high. For these reasons, it is important to find an optimum polymer concentration so that restabilization does not occur and so that enough polymers are present in the water to enable bridging (Gregory 1996).

1.5 SEEPAGE CALCULATION METHODS

The common methods for direct measurement of seepage in earthen channels are (1) the inflow-outflow method, (2) the ponding method, and (3) point measurements (ANCID 2003). Seepage detection also can be conducted using infrared remote sensing (Engelbert et al. 1997), but this method will not be discussed herein since it is used for detection purposes only, as opposed to direct measurement of seepage rates. Each seepage measurement method has advantages and disadvantages related to cost, constructability, accuracy, hydraulics, and canal operation that must be considered when choosing a method that is most feasible for a particular canal study reach. Each technique for quantifying seepage losses is discussed in this section, and a comparison among the methods is provided.

1.5.1 Ponding Method

The ponding method uses a volume balance approach for calculating seepage rates in an isolated reach of channel. Temporary impervious dams must be constructed within the channel to form upstream and downstream boundaries, between which water is ponded. With the impervious dams in place, inflow and outflow into the control volume from the upstream and downstream boundaries are eliminated and the section is filled with water to a typical operating

level (ANCID 2003). After accounting for evaporation, precipitation, diversions, and inflow sources, the seepage rate can be calculated by measuring the change in water level over a given period of time with staff gages, water level recorders, or other equipment. Assuming that there are no active diversions and that evaporation, precipitation, and seepage are the only inflows and outflows, seepage rates for the ponding test are calculated using the following equation (Alam and Bhutta 2004; ANCID 2003):

$$Q_s = \frac{\overline{T}_W L[(d_1 - d_2) - E + P]}{(t_2 - t_1)} \quad (1.1)$$

Where: Q_s = seepage rate (ft^3/s)

$\overline{T}_W$ = average water surface top width between times t_1 and t_2 (ft)

L = length of channel between dams (ft)

d_1 = water level at time t_1 (ft)

d_2 = water level at time t_2 (ft)

E = evaporation depth between times t_1 and t_2 (ft)

P = precipitation depth between times t_1 and t_2 (ft)

t_1 = time at first measurement of water level (sec)

t_2 = time at subsequent measurement of water level (sec)

A depiction of the ponding method is provided in Figure 1-3.

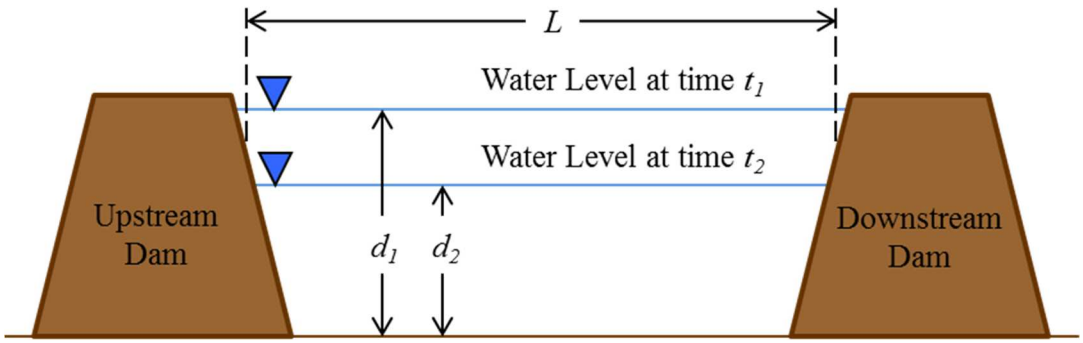

Figure 1-3 Depiction of the Ponding Method

The ponding method poses advantages and disadvantages relative to other seepage measurement techniques. Advantages include measurement accuracy and relatively low operational costs, and disadvantages include dam construction costs, taking a channel out of use, and altering channel hydraulics such that the channel is not under normal operating conditions (ANCID 2003). These advantages and disadvantages are discussed below.

1.5.1.1 Advantages of the Ponding Method

The ponding method often is regarded as the most accurate way of measuring seepage (Alam and Bhutta 2004; ANCID 2003). What makes the ponding method more accurate than the inflow-outflow method is that in-stream flow rate measurements, which typically provide the largest degree of measurement uncertainty in the inflow-outflow method, are not required at the upstream and downstream boundaries with the ponding method. In addition, unsteady flow conditions are non-existent as in-stream inflows are eliminated.

Channel diversions and inflows typically can be eliminated during ponding tests, such that the only measurement requirements are water level, channel length and width, and evaporation depth. The ponding method also can be used for measuring relatively low seepage rates, whereas the inflow-outflow method cannot be implemented with confidence without

seepage rates that significantly exceed the levels of uncertainty in measurement of inflow and outflow rates for the channel reach and changes in storage associated with water level fluctuations (Skogerboe et al. 1999).

Measurement costs associated with the ponding method are relatively low. Water level measurement devices are the only measurement equipment required. Staff gages and water level loggers are relatively inexpensive, and labor costs are relatively low because stage readings only need to be recorded twice at a minimum.

1.5.1.2 Disadvantages of the Ponding Method

A major disadvantage of the ponding method is the need for temporary shut-down of the canal for dam construction, seepage measurement, and dam removal. If it is not possible to take a canal out of commission due to irrigation demands or other water supply needs, then the ponding method is not an option for seepage measurement.

Another disadvantage is that channels are not operating under normal conditions during ponding tests. Flow velocities and shear along with associated sediment erosion and deposition are eliminated because water is ponded (ANCID 2003). In addition, suspended sediment that is present in the water upon filling the study reach can settle to the channel perimeter as hydrodynamic forces are eliminated, causing a potential reduction in seepage rates (Alam and Bhutta 2004; Skogerboe et al. 1999). Stone et al. (2008) found that shear stress from flow velocity can cause scouring of PAM layers and can result in an increased seepage flux. If a ponding test was conducted to observe seepage reduction due to a PAM application, shear stress on the channel perimeter would be eliminated as there would be no flow velocity; hence, seepage would not be measured under the typical hydraulic conditions that impact PAM's effectiveness. In addition, ponding water results in a horizontal water surface, as opposed to a sloping water

surface, which alters the hydrostatic loads placed on the channel perimeter (Skogerboe et al. 1999).

Dam construction poses disadvantages related to seepage around/under the dams and construction and removal costs (ANCID 2003). If a tight seal is not adequately formed between the dam and the channel perimeter, then water can leak around the dam. This leakage rate could be difficult or impossible to measure and should not be accounted for as seepage from the study reach. The upstream and downstream dams must be constructed using impervious materials such as plastic, clay, or concrete. Construction costs include materials, labor, equipment rental, and fuel during both dam installation and removal. Other labor and equipment costs are related to channel surveying, such that channel length and top width can be determined.

1.5.2 Point Measurements

A point test refers to a seepage measurement which tracks the movement of water through the channel bottom or banks at a single location (ANCID 2003; Bakry and Awad 1997). Point measurements can be conducted using tracers, seepage meters, or infiltrometers (ANCID 2003; Shepard et al. 1993). These technologies will not be discussed in detail in this thesis.

1.5.2.1 Advantages of point test

The main advantage of point tests is that a spatial distribution of seepage rates along a reach or cross-section can be obtained (ANCID 2003). Channel sections features that can contribute to higher seepage rates potentially can be identified using point tests. In addition, certain types of point measurements (e.g. infiltrometers) can be conducted whether the channel is operating or not, so that water delivery is not interrupted (ANCID 2003).

1.5.2.2 Disadvantages of point test

Point tests typically are not representative of seepage over large channel reaches due to spatial variations in channel materials, hydraulic conditions, groundwater gradients, and other factors, and are best used to estimate distribution of seepage as opposed to cumulative seepage losses over a given reach (ANCID 2003). A higher density set of point measurements decreases the level of uncertainty for seepage measurements, which in turn raises labor and equipment costs.

Point tests require skilled technicians and the least practical level of disturbance of bed material to provide reliable results (ANCID 2003). Without skilled technicians who are familiar with point measurement equipment and methods, the accuracy of seepage tests can be suspect. Skilled labor often increases measurement cost as well.

1.5.3 Inflow-Outflow Method

The inflow-outflow method uses a volume balance procedure to calculate seepage rates with inflows, outflows, and storage changes directly measured (Alam and Bhutta 2004). In-stream inflow and outflow at the upstream and downstream boundaries of the control volumes, respectively, must be measured accurately. These flow rates are measured typically with current meters (i.e. propeller meters, ADVs, or ADCPs) or with inline structures (i.e. flumes or weirs) with flow depth measurement gages (ANCID 2003; Sheng et al. 2003). The following mass balance equation typically is used to calculate seepage rates with the inflow-outflow method (ANCID 2003).

$$Q_s = Q_{US} - Q_{DS} + Q_I + Q_P - Q_D - Q_E - \frac{\Delta S}{\Delta t} \tag{1.2}$$

Where: Q_{US} = canal inflow rate through the upstream cross section (ft^3/s)

Q_{DS} = canal outflow rate through the downstream cross section (ft^3/s)

Q_I = total rate of inflows along the canal reach (ft^3/s)

Q_P = total rate of precipitation along the canal reach (ft^3/s)

Q_D = total rate of outflow diverted along the reach (ft^3/s)

Q_E = total rate of evaporation from the water surface along the reach (ft^3/s)

$\frac{\Delta S}{\Delta t}$ = rate of change of stored water volume within the canal reach (ft^3/s)

Inflow-outflow measurements are most appropriate when the channel flow rates can be measured with relative accuracy and when the seepage rates are relatively large (Skogerboe et al. 1999; Trout and Mackey 1988). Trout and Mackey (1988) concluded through analytical investigation that the most important factor for improving inflow-outflow seepage measurements is to measure a seepage that is as large as possible so that the measured seepage exceeds the flow measurement uncertainty. They also concluded that systematic flow measurement error is reduced if the same device is used at the upstream and downstream locations.

1.5.3.1 Advantages of the Inflow-Outflow Method

Canals and channels can remain in full operation during seepage tests using the inflow-outflow method. Measurement under normal operating conditions provides two main advantages: (1) hydraulic conditions and sediment loads which are unaltered during testing and (2) water continuing to flow downstream such that irrigation and water supply demands can be met during testing (ANCID 2003; Skogerboe et al. 1999). When canal operation cannot be interrupted or halted, then the inflow-outflow method is regarded as the best option for measuring seepage over large channel reaches.

Usually, no construction costs are required to implement the inflow-outflow method for seepage measurement. Installation of flumes and weirs can be conducted, which would create construction/installation costs. However, existing flumes and weirs typically are used to avoid

such costs, if these structures are to be used at all. In most cases, channel flow rates are estimated using area-velocity measurements from current meters such as propeller meters, electromagnetic meters, ADVs, and ADCPs.

1.5.3.2 Disadvantages of the Inflow-Outflow Method

The main disadvantage of the inflow-outflow method is the challenge of achieving highly accurate results. In-stream inflow and outflow measured at the upstream and downstream boundaries, respectively, often have a significant degree of measurement error. A discussion of flow measurement error is presented in Section 1.6.1.1. This can have a significant impact on the uncertainty of a seepage measurement, particularly for sections of channel that are short, have low flow rates, and/or have low seepage rates (Alam and Bhutta 2004; ANCID 2003). Under steady flow conditions, if the in-stream flow measurement error exceeds the calculated seepage rates, then seepage measurement has a large degree of uncertainty (Alam and Bhutta 2004).

Unsteady flow conditions also can lead to seepage measurement errors. Variations in diversion rates from rivers, opening and closing of canal diversion gates, and raising and lowering of inline canal structures (i.e. sluice gates and overshot gates) impact flowrate and water level stability. These changes impact inflow and outflow measurement as well as storage change measurements in the channel control volume during a seepage test.

Labor costs for equipment operation are associated with inflow-outflow method. These costs are relatively minor compared to construction costs, but they can become expensive as the number of seepage tests that are conducted increases. Labor also includes channel surveying and equipment setup. Equipment cost can be a large percentage of total seepage measurement costs.

Equipment required may include current meters, staff gages, tapes, pulleys, water level recorders, pressure transducers, weather station equipment, and survey equipment.

1.5.4 Comparison of Seepage Measurement Methods

Alam and Bhutta (2004) performed a comparative evaluation of the inflow-outflow and ponding seepage measurement techniques. The evaluation included a literature review along with results and statistical analysis for seepage tests conducted on five different canals using both ponding tests and inflow-outflow tests. The literature review concluded that opinions vary among investigators on which method is better. The main argument for ponding tests is that they are more accurate, whereas the main argument for inflow-outflow test is that the channels are under normal operating conditions during the measurement period. The seepage test results from Alam and Bhutta (2004) showed that the mean measured seepage rate, coefficient of variation, standard deviation and mean standard error for seepage conducting inflow-outflow tests was higher than when conducting ponding tests. In conclusion, the evaluation recommended using the ponding method and stated that the majority of arguments against the ponding tests are insignificant or somewhat avoidable.

Although seepage measurement may not be statistically as accurate for the inflow-outflow method as the ponding method, the inflow-outflow method often is the preferred measurement technique because tests must be conducted under normal operating conditions (Skogerboe et al. 1999).

Sheng et al. (2003) conducted ponding and inflow-outflow tests on a canal in Texas and compared the results. Ponding tests were conducted in January and November, and inflow-outflow tests were conducted between August and October. The average seepage rates measured with ponding tests were 20% to 50% of those measured with inflow-outflow tests. The author

was not able to develop a solid conclusion regarding the difference in seepage rates, other than unsteady flow conditions and potential measurement error; however, temporal variations in seepage also may have had an impact.

1.6 MEASUREMENT ERROR AND UNCERTAINTY

Measurement error and measurement uncertainty are two distinct things. Error is the difference between a measured value and the true value (Bell 1999; Reginald W. Herschy 2009), and uncertainty is the qualification of unknowingness of a measured value (Bell 1999).

Any water resources problem contains two fundamental types of informational uncertainties: (1) parameter uncertainty and (2) model uncertainty (Vicens et al. 1975). Parameter uncertainty is derived, in part, from measurement error or the difference between true and measured values (R.W. Herschy 2002). It is also derived from spatial and temporal variability. Even if a parameter value could be measured perfectly at a given point in space and time only a very limited number of points can be measured. Hence, the true space-time distribution of parameter values cannot be known with certainty. Due to this error and variability and the inability to know what the "true" values are, parameters estimates strictly should be treated as random variables (Haan 1989) and parameters that are functions of random variables should be treated themselves as random variables (Haan 1977).

Model uncertainty stems from the fact that hydrologic processes cannot be represented or approximated in a conceptual physical or mathematical form with total accuracy and completeness (Haan 1989) due to the complexities of natural systems. In relation to the mass balance equation used to estimate canal seepage loss, modeling free-water evaporation rates from the water surface of the canal is performed using an equation that does not completely account for all factors that affect evaporation rates. Evaporation is a complex process in that it is

dependent upon numerous atmospheric conditions, so equations are simplified because of lack of availability of data or the inability to measure all components that affect evaporation rates. Free-water evaporation equations implement atmospheric components such as relative humidity, wind speed, solar radiation, etc. but the equations themselves provide merely an estimate of evaporation (even if every variable within the equation could be measured with complete accuracy) due to the lack of completeness of the equation. The same is true for groundwater inflows into a canal, because they cannot be measured directly or completely along the entire study reach of the canal. As such, the model has to make certain assumptions about groundwater inflows which lead to incompleteness of the model.

1.6.1 Seepage Measurement Error and Uncertainty

The inflow-outflow seepage measurement procedure was adopted for the analysis presented in this thesis. As such, literature review of the parameters associated with this method will be discussed herein, including the uncertainty of estimating parameters values. Major components of uncertainty in seepage measurement using the inflow-outflow procedure include discharge measurements, free-water evaporation estimates, water stage measurements, and measurements of canal hydraulic geometry.

All physical measurements have a degree of uncertainty due to either random scatter errors (a.k.a. "standard errors") or systematic errors (Harmel and Smith 2007; ISO 1973). Errors related to computational procedures and measurement techniques can be classified as random scatter errors if they create scatter around the true mean, but if they cause a uni-directional bias in estimates then they are classified as systematic errors.

Standard errors cannot be easily assessed (Harmel and Smith 2007) but often are related to equipment's ability to make a measurement with accuracy or with random operation errors.

Measurement repetition reduces standard errors as the mean of the repeated measurements becomes closer to the true value (Bell 1999; ISO 1973), as long as the measurement error is scattered around the true mean.

Systematic errors typically are either positive or negative throughout a measurement set, and likely are caused by equipment bias or user bias (Bell 1999; Harmel and Smith 2007). As opposed to standard errors, repeated measurements will not reduce the uncertainty of systematic errors since the errors are biased in a given direction (ISO 1973). As such, the only ways to reduce systematic errors are through equipment calibration and proper equipment operation.

In addition to direct measurement error, uncertainties also stem from the procedures used to perform a measurement or used to calculate a value from measurements (Harmel and Smith 2007). Model uncertainty is related to the inability to adequately represent natural systems due to their complexity, dynamic nature, and the modeler's lack of understanding of the modeled system. It is also related to the methods, equations, and procedures used to calculate given parameters. Even if random scatter errors and systematic errors did not exist (i.e. sub-parameters could be measured with 100% accuracy) there is still uncertainty related to the equations and procedures used to attempt to quantify a given parameter. For example, when estimating free-water evaporation, if temperature, relative humidity, wind speed, solar radiation, and all other required components for a given equation were all measured with 100% accuracy, the estimation of free-water evaporation still would not be equivalent to the true value due to imperfections in the equation being used.

Spatiotemporal uncertainty is the result of systems that vary over time and space. Data can be collected at given point in space, but that data may not be representative of the physical area that it is assumed to represent due to variability in physical conditions. Similarly, data can

be collected at a given point in time, but changes in the system over time causes the measured parameter value to change (T. K. Gates and Al-Zahrani 1996b). For example, when using the velocity-area method to measure river discharge, water velocity is not measured at every location within a cross section so average velocity cannot truly be known but only estimated, which leads to spatial variability. Water velocity at a given location also changes temporally during a measurement leading to temporal variability.

1.6.1.1 Discharge Measurement Error and Uncertainty

The most common method for estimating stream flows is the velocity-area method (R. Herschy 1993). This method typically is conducted by summing the products of measured velocity and the corresponding flow area for a series of measurements within a channel cross-section (ISO 1979). Inflow-outflow seepage measurements can be conducted using Acoustic Doppler flow meters and other technologies that utilize the velocity-area method to measure upstream and downstream flow rates relatively quickly Kinzli et al. (2010). Additional descriptions of the velocity-area method for flow measurement with ADVs and ADCPs are provides in Section 3.1.1. Adoption of error ranges and probability distributions related to flow rate measurement with ADVs and ADCPs are discussed in Section 5.2. The sub-sections that immediately follow present a literature review of studies related to the measurement error and uncertainty of these flow measurement technologies.

1.6.1.1.1 Acoustic Doppler Velocimeters Error and Uncertainty

Rehmel (2007) compared flow rate measurements conducted using ADVs, Price AA propeller meters, and Price pygmy propeller meters. Based upon 55 measurements, the study concluded that ADV measurements are not statistically different than measurements taken by Price AA or Price pygmy meters and that ADV measurements were typically within 5% of Price

AA and Price Pygmy meters on average. Of the 55 measurement comparisons in Rehmel (2007), 76% of the ADV measurements were within 5%, and 89% were within 8%.

1.6.1.1.2 Acoustic Doppler Current Profilers Error and Uncertainty

Oberg and Mueller (2007) used large towing basins in a laboratory to estimate the accuracy of ADCP bottom-tracking and water-tracking velocities. They conclude that mean differences for bottom tracking velocity (pertains to area calculation) and water-tracking velocity (pertains to flow velocity) are -0.51% and -1.10%, respectively. The differences ranged between -2.33 to 0.99% and between -2.10 to 0.70%, respectively. Oberg and Mueller (2007) also attempted a field validation. Field measurements were taken at 22 sites in the US, Canada, Sweden, and the Nederlands, totaling 1,032 transects over 100 discharge measurements. ADCP measurements were compared to either Price AA-metered or rating curve discharges. The rating curves are stage-discharge relationships that were reportedly developed during stable flow conditions. The study verifies that uncertainty decreases as the number of transects taken increases. The range of uncertainty at 2 standard deviations for 4, 6, and 8 transects per measurement was ±5.4%, ±4.4%, and ±4.2%, respectively. The study also considered temporal impacts on the ADCP measurements, and concludes that a minimum of 2 transects of 720 second durations (minimum) should be taken.

1.6.1.2 Stage Error and Uncertainty

Stage (water level) readings are necessary for all seepage measurements. For ponding tests, they are important for measuring the change in water level over a given period of time. For inflow-outflow tests, they are important for observing the stability of a canal flow and for calculating varying storage changes along the canal reach. Upon surveying channel cross-sections, relationships between stage and canal wetted perimeter and between stage and canal top

width can be developed. As such, stage measurements during seepage tests can be used to estimate time-varying top width (used for evaporation calculations) and wetted perimeter (used to quantify seepage per wetted area). The accuracy of stage measurement using pressure transducers is discussed below.

Technical specifications for HOBO™ pressure transducers state that the maximum stage measurement error is ±0.03 ft and the average error is ±0.015 ft (ONSET 2008). They also state that barometric pressure may be assumed constant across a region (within 10 miles), with the exception of a fast moving storm. This is important when using atmospheric pressure to calculate gage pressure from absolute pressure measurements.

The technical specifications for the In-Situ Level Troll 300™ pressure transducer state that the accuracy for a Level Troll 300™ is ±0.035 feet (In-Situ 2009).

1.6.1.3 Free-Water Evaporation Error and Uncertainty

In measuring seepage from animal waste lagoons, Ham (2002) found that evaporation was the most significant source of uncertainty in the volume balance using the ponding method. He concluded that evaporation could be measured within ±10-20% of the true value when implementing a form of the Penman equation, and that wind was the largest factor affecting the level of uncertainty. Uncertainty was represented as the square root of the sum of the squared errors, using the products of uncertainty terms and partial derivatives for sensitivity coefficients.

Rosenberry et al. (2007) compared 15 methods for estimating free-water evaporation. The purpose was to check 14 methods against the Bowen-ratio energy budget (BREB) method, which is stated to be the standard method for estimating evaporation. The study concludes that the Priestley–Taylor, deBruin–Keijman, and Penman methods compare best with the BREB. Uncertainty analysis was not conducted as part of the study.

Tanny et al. (2008) compared evaporation estimates from field measurements using an eddy covariance (EC) system with equations typically used to calculate evaporation. The study concluded that the Penman–Monteith–Unsworth and Penman–Brutsaert methods result in daily evaporation rates closest to those measured by the EC system.

A derivation and comparison of three simplified Penman equations was completed by Valiantzas (2006). Commonly-measured weather data used in these equations include solar radiation, air temperature, relative humidity, and wind velocity. The study then compared each of the three simplified equations to the original Penman (1948) equation using data from 535 sites in the United Nations Food and Agriculture Organization's (UN-FAO) CLIMWAT (Smith, 1993) database. The database includes long-term monthly climatic data over thirteen countries that provide a range of values. The comparison of versions of the Penman equation revealed that the least-simplified version corresponds most closely with Penman (1948). Valiantzas (2006) also revealed that neglecting wind velocity data adds variability to the results, and compares least-closely to Penman (1948).

1.6.1.4 Channel Geometry Error and Uncertainty

Measurement error and spatial variability of channel geometry can create significant uncertainty in open-channel hydraulic analysis (Buhman et al. 2002). Using survey data from 1600 cross-sections in the Mississippi and Red Rivers, Buhman et al. (2002) observed significant spatial variability in hydraulic geometry parameters and concluded that hydraulic-geometry patterns are not completely random but rather oscillate and display large-scale and medium-scale spatial trends. They modeled the residuals around fitted trend equations as random variables with estimated probability distributions and spatial correlation.

Spatiotemporal variability creates uncertainty in predicting flow behavior including flow depth (T. K. Gates and Al-Zahrani 1996a), which affects the hydraulic geometry of a channel. Through stochastic analysis, T. Gates et al. (1992) concluded that hydraulic geometry in irrigation delivery systems varies spatiotemporally due to irrigation demands and patterns.

Measurement error related to channel geometry exists on two scales. The first is "at-a-station" errors related to uncertainty of parameter estimation using cross-sectional surveys, and the second are "longitudinal" errors related to uncertainty of hydraulic geometry in channel reaches between surveyed cross-sections where no survey data were collected.

1.6.2 Modeling Measurement Error and Uncertainty

Estimates of seepage can be made with either a deterministic approach (Kinzli et al. 2010) or probabilistic approach that accounts for parameter uncertainty (Oblinger et al. 2010; Shaw and Prepas 1990). Uncertainty analysis implementing Monte Carlo simulation is more commonly being used to develop ranges of expected seepage rates from water bodies (Keery et al. 2007; Oblinger et al. 2010; Shaw and Prepas 1990). In each of these studies, probability distribution functions were assigned to sets of parameters used to calculate seepage rates from water bodies, and distributions of expected seepage rates were developed via Monte Carlo simulation.

An extensive literature review was conducted, and it was found that the water balance uncertainty analysis conducted by Ham (2002) most closely reflects the method used in this thesis. Ham (2002) studied seepage rates from animal waste lagoons using the ponding method and assigned probable error ranges to measured data to consider the accuracy of the seepage measurements. Probable error ranges were assigned to atmospheric measurements (air temperature and relative humidity) used to calculate evaporation and to water depth measurements. Changes in flow depth were measured with float-based recorders and

atmospheric parameters, including humidity, air temperature, and wind speed, were measured on site with weather station equipment. Ham (2002) adopted "typical" and "best" probable error ranges based upon previous studies and manufacturer specifications for these variables and calculated ranges of seepage rates accordingly. The study concluded that evaporation uncertainty had the largest impact on accuracy of the seepage results, and that seepage studies should be conducted when evaporation rates are minimal to reduce error in seepage measurement.

Shaw and Prepas (1990) studied the accuracy of estimating seepage rates from lakes using seepage meters. The analysis used Monte Carlo simulation for 32 combinations of flow patterns, spatial variability of seepage flux, and placement and number of seepage meters within a transect. A total of 500 Monte Carlo simulations were performed for each combination to generate coefficients used to calculate seepage velocity. The stochastic analysis concluded that seepage meters have the ability to accurately quantify the average nearshore seepage flux and that the most important factor affecting the seepage flux measurement was spatial variability.

The widely-accepted standard for quantifying measurement uncertainty is the ISO's Guide to Expression of Uncertainty in Measurement (GUM) (ISO 1995). GUM classifies uncertainty evaluations as either being "Type A" or "Type B" and does not differentiate errors as being random or systematic (Cox et al. 2003; Reginald W. Herschy 2009). Type A evaluations are used to estimate a value using a probability distribution that was developed from repeated measurements, and Type B evaluations use standard deviations and assumed probability distributions obtained from scientific judgment, available information, and possible variability of a measurement (Cox et al. 2003; R. W. Herschy 2004). For example, the uncertainty evaluation used for a single river discharge measurement would be Type B if the error range and probability distribution of the measurement equipment and procedure is assumed from previous studies and

scientific judgment, and because a single measurement is taken at a given point in time such that a probability distribution of measurement could not be developed (i.e. due to temporal variations in flow rate).

The root mean square method is widely accepted for estimating the uncertainty related to measurement of water quantity and water quality (Harmel and Smith 2007; ISO 1995; Sauer et al. 1992), as presented in ISO (1995). Harmel and Smith (2007) describe this measurement uncertainty as the "probably error range", and quantify upper and lower uncertainty boundaries for measured data points as the following when attempting to specify an expected range of expected values:

$$UO_{i_u} = O_i + \frac{PER_i \times O_i}{100} \tag{1.3}$$

and

$$UO_{i_l} = O_i - \frac{PER_i \times O_i}{100} \tag{1.4}$$

Where: UO_{i_u} = upper uncertainty boundary

UO_{i_l} = lower uncertainty boundary

O_i = measured data point

PER_i = probable error range for measured data point O_i, (+/- %)

This approach for describing the probable error range (Harmel and Smith 2007) is applicable for PER_i that is known or assumed because no data is available to develop a probability distribution (i.e. Type B uncertainty evaluations).

2 CANAL STUDY REACH DESCRIPTIONS

All canal reaches that were selected for this study are located in earthen irrigation canals that offtake from the Arkansas River in the Lower Arkansas River Valley (LARV) in southeastern Colorado: on the Rocky Ford Highline Canal (RFH Canal), Catlin Canal, Fort Lyon Canal, and Lamar Canal. A general location map is presented as Figure 2-1. Descriptions of the canal study reaches and vicinity maps for each study reach are presented in Section 2.3 through Section 2.4.

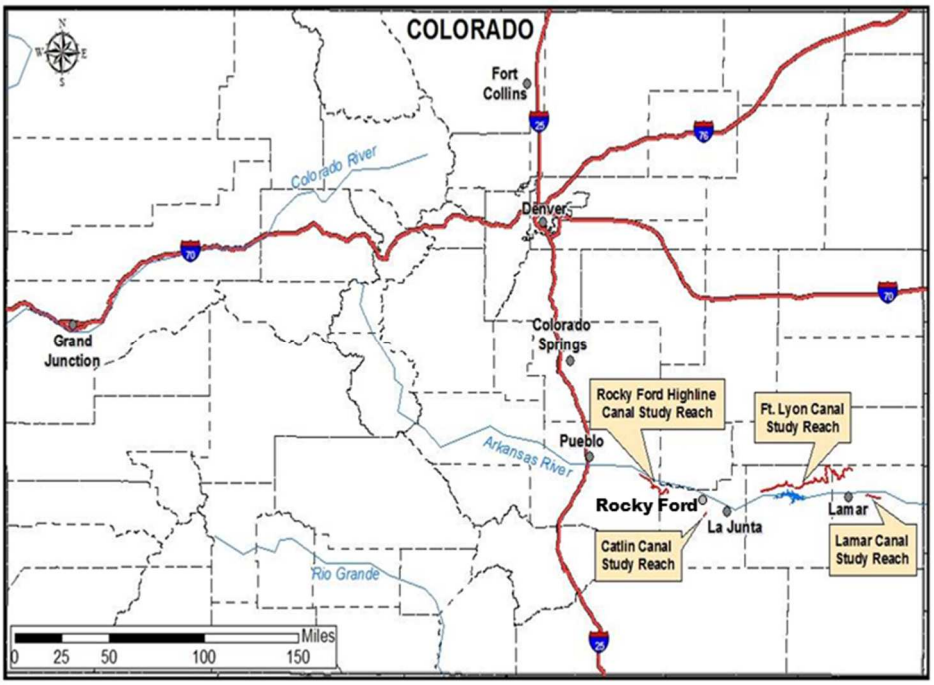

Figure 2-1 General map of the canal study reaches in the LARV

In the LARV, there are approximately 270,000 acres of irrigated land on around 14,000 fields (T. K. Gates et al. 2012), and the canal system includes over 1,000 miles of channels (T. K. Gates et al. 2006). The most common method of irrigation in the LARV is surface (furrow) irrigation, with a small percentage of fields irrigated with center-pivot sprinklers or drip lines.

Commonly-irrigated crops within the LARV include alfalfa, corn, wheat, sorghum, grass hay, onions, cantaloupe, and watermelon. Water for irrigation is diverted each year between March 15 to November 15. Irrigation-related problems in the LARV include "shallow groundwater tables (waterlogging), excessive salt buildup, and high selenium (Se) concentrations, both on the land and in the larger river ecosystem" (T. K. Gates et al. 2006).

2.1 SELECTION PROCESS OF CANAL STUDY REACHES AND FLOW MEASUREMENT LOCATIONS

Locating areas where seepage already was evident or likely to occur was a priority in selecting study reaches within LARV canals. Results from seepage measurements conducted by CSU prior to 2006, consultation with canal superintendents, and observing evidence of seepage (i.e. standing water adjacent to canal banks or wetland vegetation) were used to target canal reaches with relatively large seepage rates. Sites also were selected where channel conditions were conducive to accurate measurements using ADCP and ADV equipment. Such conditions include water with relatively low turbulence and eddies, no major obstructions to flow, no debris or rip-rap creating a highly irregular channel perimeter, minimal moving bed sediment, relatively straight reaches where the majority of flow is parallel to the banks, and locations that are easily and safely accessible. Once these study reaches were identified, cross sections on the upstream and downstream ends of the reaches were defined approximately perpendicular to the principal flow direction. They were marked by placing flags or T-posts in the canal banks and collecting GPS coordinates so that measurements could be taken consistently at the same locations. The total length of canal between the cross sections was designated as the study reach wherein seepage and the other water balance components were analyzed. The study reaches were chosen with the intent that the predicted seepage losses likely would exceed the measurement errors associated with the volume balance procedure, specifically in flow rate measurements. This

intent was not satisfied for all seepage measurements, however, due to temporal changes in seepage, hydraulic changes in the canal, variation in data collection methodology, etc. If possible, a control reach was designated upstream of the study reach so that seasonal seepage patterns could be observed uninfluenced by a PAM application. However, due to the limitations of long study reaches (i.e. increased number of diversions and greater potential for storage changes), a control reach was not practical on some canals or did not provide large enough seepage rates. Larger study reaches typically result in a larger cumulative seepage rate over the reach; however, they are characterized by more diversions, offtakes, and spatial changes in canal geometry and are more susceptible to significant storage changes which impact the total seepage measurement error. Overall, preliminary seepage data, visual evidence of seepage, and input from canal managers were all taken into account during the study reach selection process in an effort to identify and select reaches where seepage rates exceeded measurement errors. UTM coordinates for all flow measurement cross section locations are presented in Table 2-1.

Table 2-1 UTM coordinates and canal stations for flow measurement cross sections

Canal	Site Number	Canal Station (mi)	X Coordinate	Y Coordinate
RFH	200	21.9	569531	4228695
	201	19.9	572050	4226655
	202	17.4	575000	4224960
	203	16.1	576575	4224398
	204	13.4	577975	4221068
	205	11.1	579211	4220847
	206	0	587643	4215987
Catlin	201	2.4	612160	4201350
	202	0	614579	4203621
Fort Lyon	1 (CR 7)	42.2	650095	4218575
	2 (CR 12)	34.8	657978	4220391
	3 (CR 17)	27.4	665863	4223314
	4 (CR 24)	17.1	678920	4223828
	5	13.2	682511	4225259
	6	10.9	685528	4225677
	7 (CR 30)	6.5	688139	4227129
	8 (CR 34)	0.0	694583	4225408
Lamar	400	7.4	720965	4217881
	401	5.8	723307	4217619
	402	3.6	726109	4217081
	403	3.5	726169	4217018
	404	2.6	727299	4216573
	405	0	730650	4216195

2.2 ROCKY FORD HIGHLINE CANAL

A segment of the RFH Canal was included for seepage studies in 2006 and 2007 and for two PAM applications in 2006. The studied segment of canal was located east of Fowler, Colorado approximately 2.5 miles downstream of the headgate on the Arkansas River (Figure 2-2). Canal manager observations, visual evidence, and background seepage data suggested that this section of the canal had relatively high seepage rates. Inset into Figure 2-2 is a picture of standing water adjacent to the canal bank, a suspected result of seepage, taken from the canal bank near site 201. All studies on the RFH Canal included a control reach that extended 2.1 miles from site 200 to site 201. Two seepage studies and PAM applications were completed

during the 2006 water year. The first study included the entire 19.9-mile reach of canal located between sites 201 and 206. After a fairly unsuccessful first PAM application in 2006, the study reach was shortened to a 2.5-mile upstream section, located between sites 201 and 202, where the majority of the seepage was thought to occur. This second study reach received a PAM application later in the 2006 water year, as described in Section 4.2.

In 2007, the study reach again was modified by moving the Q_{DS} measurement sites further downstream. The re-modified study reach included either a 3.7-mile canal section between sites 201 and 203 or a 6.4-mile canal section between sites 201 and 204, depending upon the irrigation schedule. Multiple diversions that could not be accurately measured, and were equivalent to a large percentage of Q_{US}, were located between sites 203 and 204. When the diversions were active, the study reach extended from site 201 to site 203 to avoid potentially large errors in estimating Q_D. If the diversions were inactive, due to irrigation schedules or requests to the canal managers, the study reach extended from site 201 to site 204. The re-modification of the study reach was completed to improve conditions with seepage rates that were greater than potential measurement errors and because sites 203 and 204 were determined to be more conducive to ADCP measurements than site 202 due to the channel geometry and flow turbulence. A photograph of the RFH Canal, taken between sites 201 and 202 in 2006, is presented as Figure 2-3.

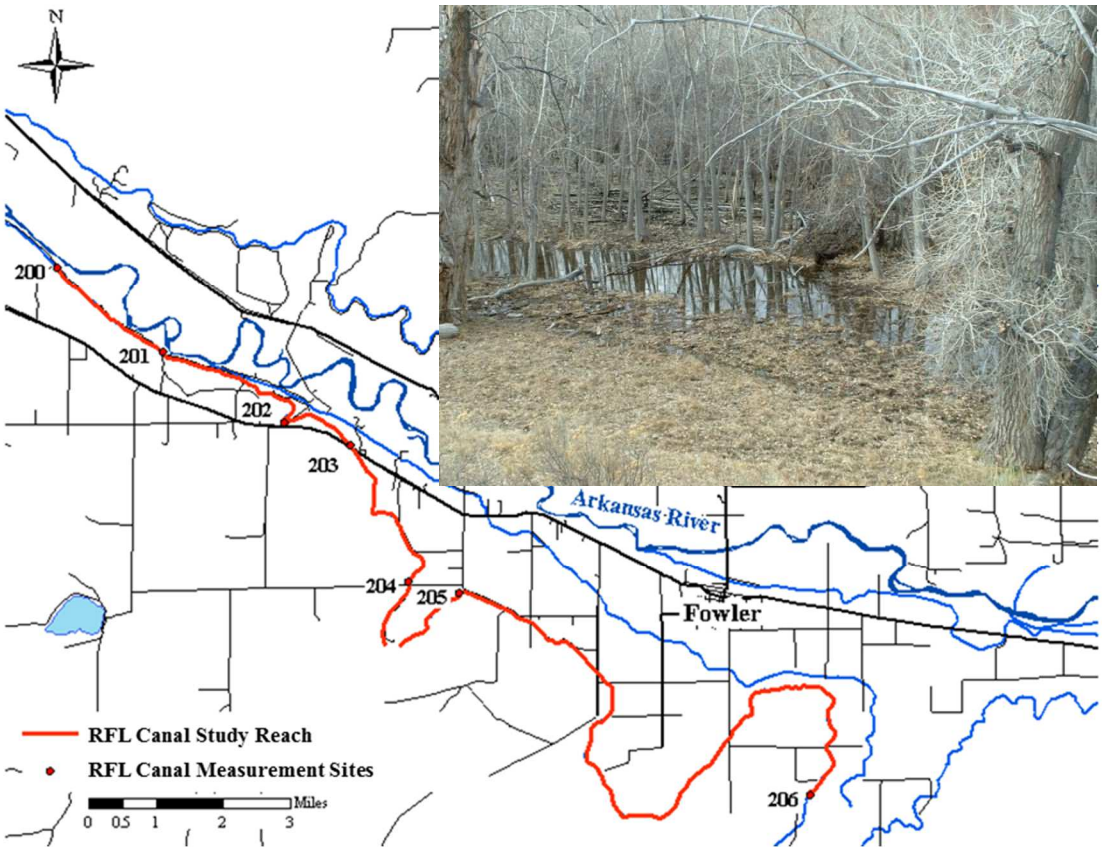

Figure 2-2 Map of the RFH Canal study reach and control reach with inset photograph showing evidence of seepage adjacent to the canal bank near site 201

Figure 2-3 Photograph the RFH Canal between stations 201 and 202 (2006)

2.3 CATLIN CANAL

A 2.4-mile stretch of the Catlin Canal located south of Rocky Ford, Colorado (Figure 2-4) was chosen as a study reach because of the relatively large seepage rates that had been known to characterize the area. Visual evidence of seepage (inserted in Figure 2-4), background seepage data, and communication with canal managers assisted in the decision to select this reach for seepage studies. Two flow measurement sites, designated as 201 and 202, were selected and determined to be suitable for measurements of Q_{US} and Q_{DS}, respectively, using ADVs and ADCPs. Due to the large number of diversions in the canal upstream and downstream of the study reach, no control reach was designated. Three small diversions were present between sites 201 and 202, although only one typically was active during seepage measurements at a given time. The positive qualities of the selected study reach included: fairly uniform hydraulic geometry; few active diversions, accounting for a small percentage of Q_{US} (typically less than 1%); relatively non-turbulent flows; easily accessible measurement sites; suspended sediment concentrations typically adequate for PAM applications; and large expected seepage rates over a relatively short length of canal. The principal negative quality of the study reach was its being located approximately 26 miles downstream of the canal headgate and about seven miles upstream of the end of the canal, making it susceptible to unsteady flow rates and storage changes caused by numerous diversions outside of the study reach. However, actions were taken to avoid unsteady flow rates and storage changes, as described later in Section 3.1.5. All studies on the Catlin Canal in 2006 and 2007 were completed on the reach highlighted red between sites 201 and 202, as presented in Figure 2-4. A photograph of a typical section on the Catlin Canal study reach, taken in 2008, is presented as Figure 2-5.

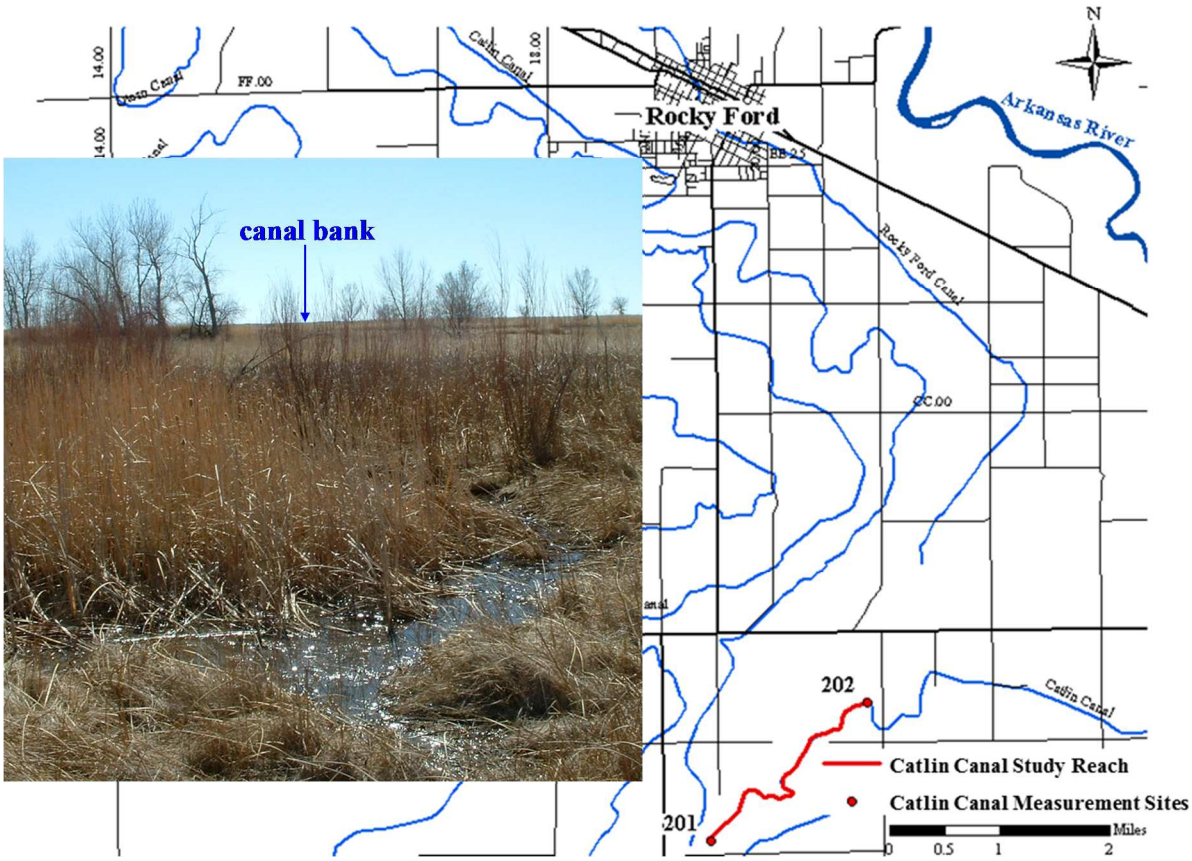

Figure 2-4 Map of the Catlin Canal study reach with inset photograph illustrating evidence of seepage adjacent to the canal bank

Figure 2-5 Photograph of a typical section of the Catlin Canal study reach (2006)

2.4 FORT LYON CANAL

Seepage studies were performed on two segments of the Fort Lyon (FL) Canal in 2007, although neither study reach was treated with PAM. The FL Canal is divided into four major divisions that operate on rotational irrigation schedules. Typically, only one division at a time contains active diversions. Once the diversion period ended in one division, the offtakes in that division were deactivated and the offtakes in another division were activated. This process was completed in a rotation, but could be altered based upon water availability, the growing season, and demand. The two middle divisions in the canal, the Las Animas Division and the Limestone Division, were designated as the two seepage study reaches (Figure 2-6). This study reach selection was made so that unsteady flow and major storage changes could be avoided to the greatest extent possible. Adjustable overshot weirs were located throughout each division. The weir crests were raised or lowered depending upon diversion demands, irrigation schedules, canal flow rates, and target diversion flow rates. Accordingly, stage measurements had to be conducted throughout seepage measurements to identify and estimate storage changes. This mainly was completed by placing temporary pressure transducers in the canal at measurement cross-sections and by installing long-term pressure transducers incrementally throughout a study reach (only performed on the Limestone Division since it was the reach primarily studied). Prior to seepage measurements, the canal manager was contacted regarding the diversion schedules. Based upon the canal manager's advice about when flow rates and water levels were expected to be relatively steady, the time periods for seepage measurements were chosen. Measurements only were conducted when each division was inactive in the diversion rotation; when Q_{US} was allowed enough time to stabilize from the upstream diversions becoming active or inactive; and when enough time was given for canal storage to stabilize from unsteady flow rates, adjustment of in-channel overshot weirs, and diversion activity.

The Las Animas division begins directly north of Las Animas, Colorado and is approximately 25 canal miles in length. The study reach on the Fort Lyon Canal's Las Animas Division spanned between sites 1 and 4, as presented in Figure 2-6. It is the second division downstream of the canal headgate by approximately 22 miles. Thus, diversion schedules had to be monitored carefully to avoid significantly unsteady flow rates caused by changes in diversion rates in the upstream La Junta Division and in the Las Animas division itself. Evidence of seepage was located on the downgradient side of the canal at a few locations along the reach in the form of standing water and wetland vegetation. Flow rate measurements for Q_{US} and Q_{DS} were conducted at four cross-sections within the division, as seen in Figure 2-6.

The upstream boundary of the Limestone Division study reach was located directly north of Hasty, Colorado. The study reach on the Fort Lyon Canal's Limestone Division spanned approximately 17.1 miles between sites 4 and 8, as shown in Figure 2-6. This division is the third division downstream of the canal headgate. Two divisions (the La Junta Division and the Las Animas Division) are located upstream of the Limestone Division. For this reason, knowing the diversion schedules of these three divisions was important in attempting to avoid major storage changes and unsteady flow rates. The division contained numerous offtake gates that were routinely checked during seepage measurements to ensure that they were inactive. The Limestone Division is appropriately named as the geology underlying the canal perimeter is mainly composed of limestone rock. Canal seepage was evident as standing water could be seen on the downgradient side of the canal throughout most of this division. The apparently high seepage rates are thought to be a result of the limestone rock that typically contains large fractures. Q_{US} and Q_{DS} were measured at up to five locations within the division, as shown in Figure 2-6.

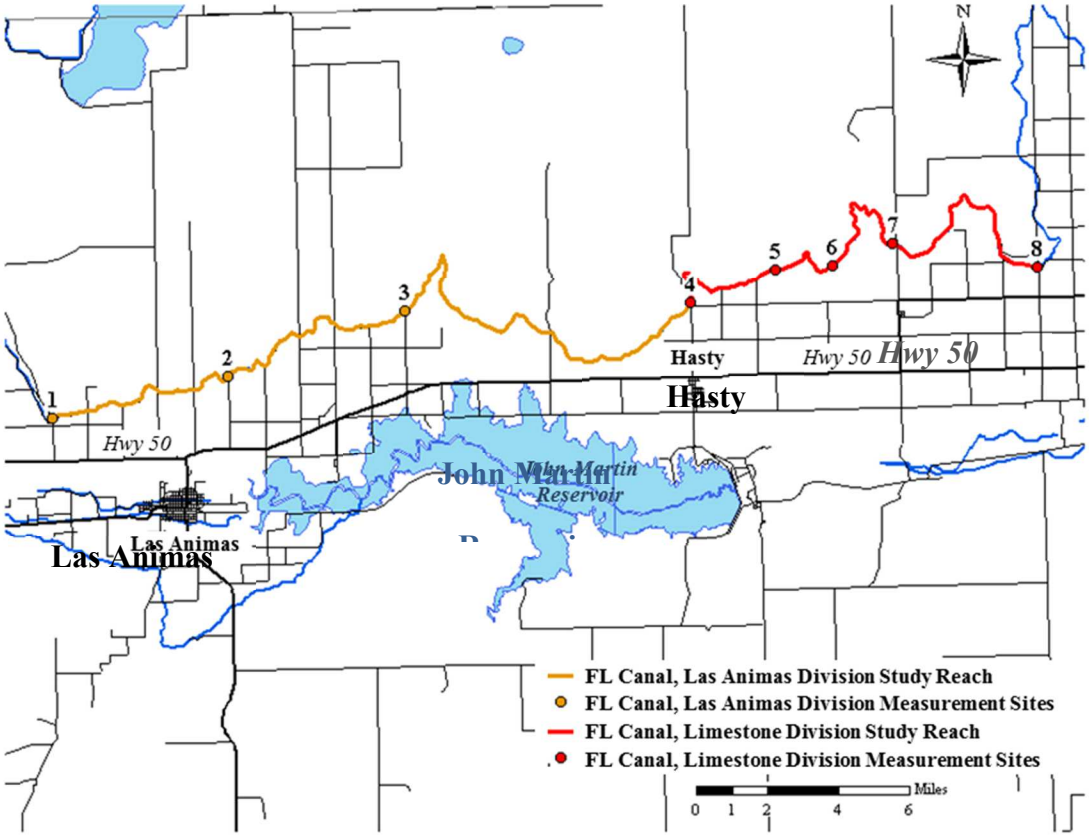

Figure 2-6 Map of the Fort Lyon Canal study reaches

2.5 LAMAR CANAL

Seepage studies on the Lamar Canal were completed over a 7.4-mile stretch of canal located east of Lamar, Colorado (Figure 2-7). A photograph of a typical section on the Lamar Canal study reach, taken in 2006, is presented as Figure 2-8. The upstream 1.6 miles, between sites 400 and 401, were designated as a control reach that would not receive a PAM application, and the remaining 5.8 miles of downstream canal, between sites 401 and 405, were designated as the study reach to which PAM would be applied. The control reach and the study reach were fairly uniform in geometry and typically were characterized by relatively shallow flows that rarely exceeded a two feet in depth. The study reach contained multiple diversions that were occasionally activate during seepage measurements, depending upon irrigation schedules. Some

of the diversions accounted for a significant percentage of Q_{US} (typically around 10% but as large as 26% of Q_{US}), so Q_D needed to be accurately measured in an effort to reduce errors in estimation of seepage rates. Positive features of the Lamar Canal included: the ability to have a control reach, relatively non-turbulent flows, spatial uniformity of the channel hydraulic geometry, and easily accessible measurement sites. Negative features of the selected canal reach included: multiple diversions that were potentially equivalent to a large percentage of Q_{US}; typically low suspended sediment concentrations that resulted from the Lamar Canal headgate being located downstream of John Martin Reservoir; being located approximately 10.5 miles downstream of the Lamar Canal headgate, increasing the likelihood of unsteady flow rates and storage changes; and shallow flows that resulted in a relatively large percentage of unmeasured flow area when using ADCPs to measure Q_{US} and Q_{DS}. In order to minimize potential measurement errors resulting from unsteady flows and large diversion rates along the canal, six flow measurement sites were installed along the Lamar Canal study reach. Some were installed to bracket the large diversions and to act as an additional measurement of Q_D (i.e. sites 402 and 403 bracketed a large offtake capable of diverting up to 6 ft^3/s). Others were installed along the canal for comparative purposes and to check that the flow rate was decreasing in the downstream direction as a result of all canal outflows, including Q_S and Q_D. All seepage studies were completed between sites 400 and 405 in the 2006 water year. The Lamar Canal was not studied in 2007 due to conditions that were observed to be unsuitable for PAM applications (i.e. typically low suspended sediment concentrations) and conditions that increased measurement uncertainty (i.e. substantially unsteady flow rates).

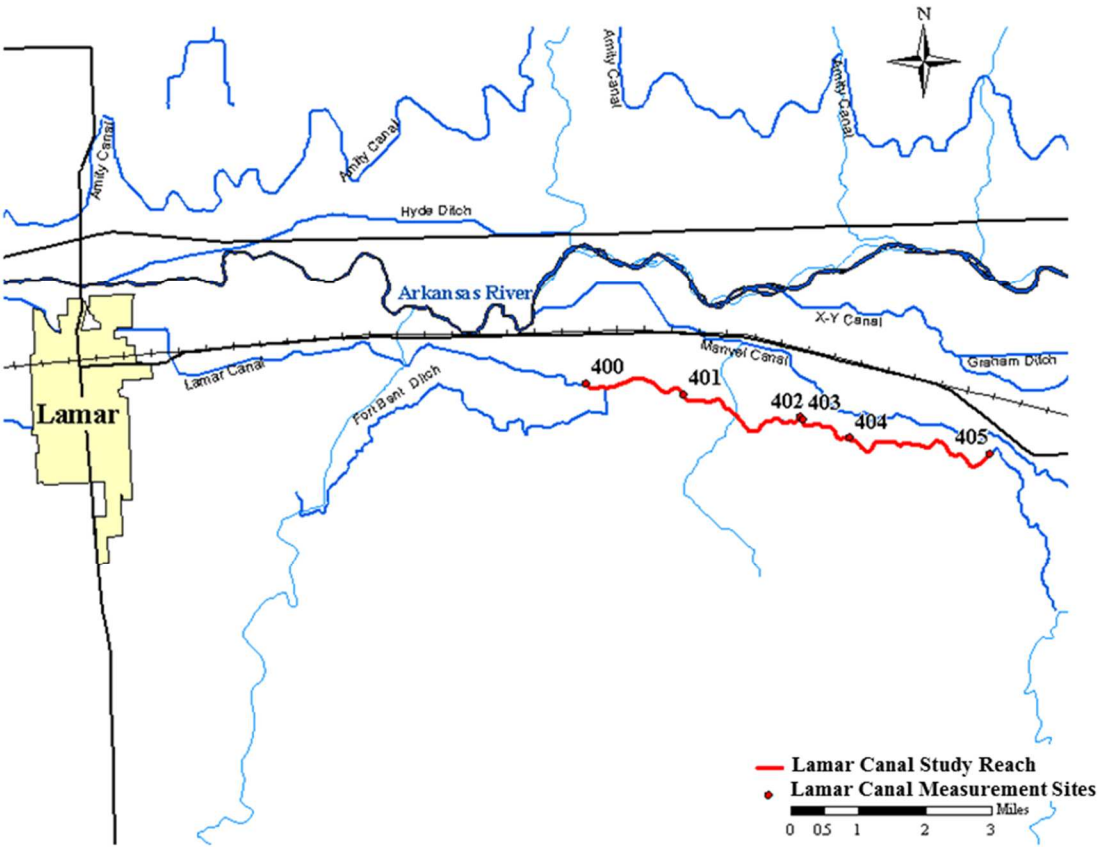

Figure 2-7 Map of the Lamar Canal study reach and control reach

Figure 2-8 Photograph of a typical section of the Lamar Canal study reach (2006)

3 CANAL SEEPAGE DATA COLLECTION METHODOLOGY

This chapter describes the canal seepage data collection methodology only. Data processing and uncertainty analysis of estimated canal seepage are presented in Section 5.

Canal seepage was calculated using a mass balance procedure, assuming that the density of water was constant over the study reach. It was quantified in terms of seepage rate (volume per unit time) per unit wetted perimeter area of the canal study reach to account for changes in canal stage and hydraulic geometry and therefore wetted perimeter area through which water can infiltrate from the channel. Seepage losses from a channel are likely to be higher when the canal stage is higher due to an increase in wetted perimeter area. Describing seepage rates in terms of discharge per unit of wetted perimeter area facilitates comparison to seepage rates in the same canal under different conditions or to seepage rates in other canals.

For cases when PAM was applied to a canal study reach, pre-application seepage rates and post-application seepage rates were compared to determine the effectiveness of an application. The effectiveness was quantified in terms of percent seepage reduction.

3.1 INFLOW-OUTFLOW VOLUME BALANCE PROCEDURE FOR ESTIMATING SEEPAGE

In applying the inflow-outflow volume balance procedure, a control volume was defined along the canal reach with boundaries at the upstream cross-section, the downstream cross-section, the wetted channel perimeter, and the free-water surface of the canal. A depiction of a canal study reach control volume is shown as Figure 3-1, where the dashed lines represent the boundaries.

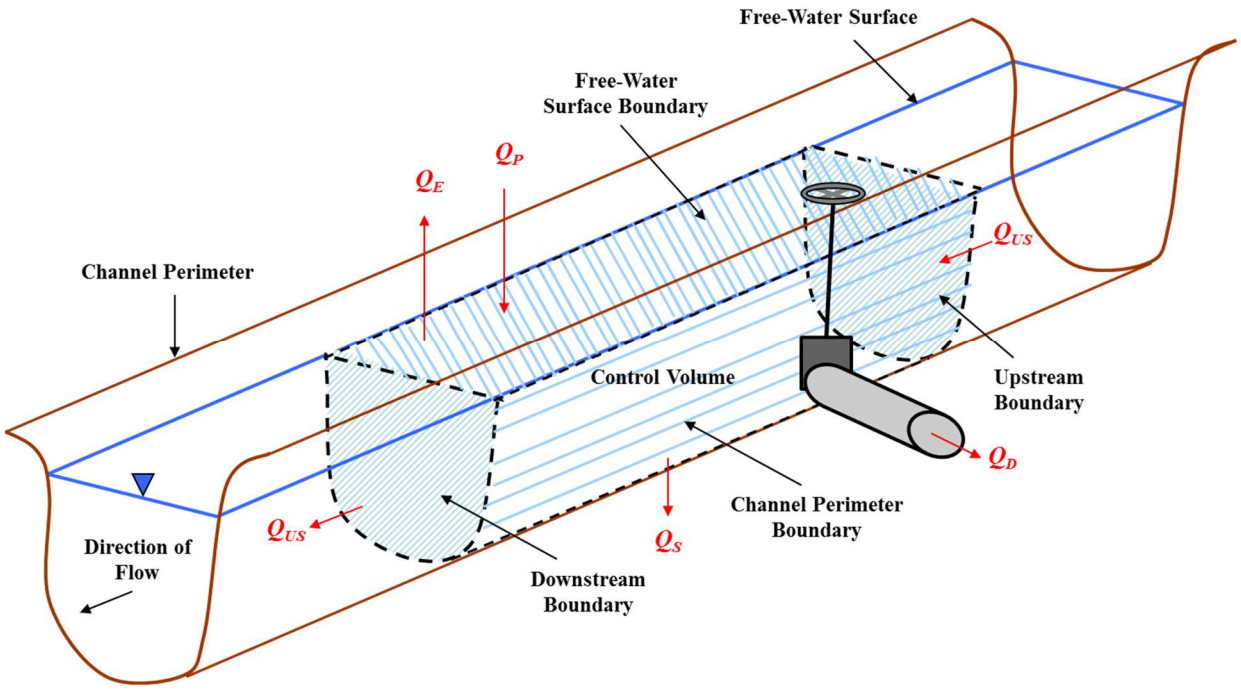

Figure 3-1 Depiction of a control volume for a canal seepage inflow-outflow test

Inflow, outflow, and storage change rates associated with this canal control volume were measured or calculated and used to estimate the unknown total seepage rate, Q_s (ft^3/s), through the wetted perimeter of the canal reach over the measurement time period Δt as:

$$Q_s = Q_{US} - Q_{DS} + Q_I - Q_D - Q_E + Q_P - \frac{\Delta S}{\Delta t} \tag{3.1}$$

Where:

Q_{US} = canal inflow rate through the upstream cross section (ft^3/s)

Q_{DS} = canal outflow rate through the downstream cross section (ft^3/s)

Q_I = total rate of inflows along the canal reach (ft^3/s)

Q_D = total rate of outflow diverted along the reach (ft^3/s)

Q_E = total rate of evaporation from the water surface along the reach (ft^3/s)

Q_P = total rate of precipitation from the water surface along the reach (ft^3/s)

$\frac{\Delta S}{\Delta t}$ = rate of change of stored water volume within the canal reach (ft^3/s)

Seepage estimations were calculated using Equation 3.1 for each inflow-outflow test conducted in this study. Descriptions of how each variable in Equation 3.1 was measured or calculated are provided in the following sections of this chapter. By calculating and comparing the seepage rates before and after a PAM application, the effectiveness of that application was evaluated.

Seepage was calculated using a deterministic approach for all seepage tests on all studied canals in 2006 and 2007, and a probability distribution of the expected seepage rate was calculated using a stochastic approach for all seepage tests on the Catlin and RFH canals in 2006 and 2007.

For deterministic estimates of seepage, Equation 3.1 was implemented using direct field measurements of Q_{US}, Q_{DS}, Q_I, Q_D, and Q_P; estimates of Q_E using the Penman Combination Method along with measured atmospheric data; and estimates of $\frac{\Delta S}{\Delta t}$ using stage data and hydraulic geometry survey data, as discussed in detail in the following sections of this chapter. For example of how to calculate Q_S using Equation 3.1 with a deterministic approach, the estimated values of $Q_{US,}$ $Q_{DS,}$ $Q_{I,}$ $Q_{D,}$ $Q_{E,}$ $Q_{P,}$ and $\frac{\Delta S}{\Delta t}$ were approximately 50.0 ft^3/s, 35.8 ft^3/s, 0 ft^3/s, 3.6 ft^3/s, 0.5 ft^3/s, 0 ft^3/s, and 0 ft^3/s, respectively, on the Lamar Canal on June 6, 2006. Upon applying these volumetric rates to Equation 3.1, the deterministic estimate of seepage was 10.1 ft^3/s. The total wetted perimeter area of the study reach was estimated to be 13.9 acres, making the estimated seepage rate per wetted perimeter area ($\hat{Q}_s$) approximately 0.73 ft^3/s per acre.

For stochastic calculations of Q_S, probability distributions were assigned directly to the variables within Equation 3.1 or to components used to calculate the variables in Equation 3.1.

Specifically, normal probability distribution functions (PDF) were assigned directly to Q_{US}, Q_{DS}, Q_I, and Q_D where the mean of the PDF was set to equal the volumetric rate that was measured in the field and the standard deviation of the PDF was based upon the expected error range in measuring or estimating those variables. A PDF was not assigned directly to $\frac{\Delta S}{\Delta t}$ but instead to stage measurements and hydraulic geometry parameters that were used to calculate the change in storage over the test duration. For Q_E, evaporation was calculated in units of depth per unit time using the Penman Combination Equation and a PDF was assigned to that evaporation rate to account for uncertainty in the estimate, based upon literature review of accuracy of calculating free-water evaporation. The calculated value had to be multiplied by the water surface area (A_{WS}) within the canal study reach to obtain the volumetric evaporation rate, and A_{WS} was calculated using stage readings with PDFs assigned to them as well as hydraulic geometry functions with components that were estimated using PDFs to account for spatial variability. Wetted perimeter area (A_P) was calculated in a similar manner and was used to quantify seepage rates in units of discharge per wetted area of canal ($\hat{Q}_s$). The procedures used for stochastic analysis are discussed in greater detail in Chapter 5.

3.1.1 Canal Flow Rate Measurements

Q_{US} and Q_{DS} were measured with a three-dimensional FlowTracker ADV manufactured by SonTek (similar to the one shown in Figure 3-2), or with a StreamPro ADCP manufactured by RDI Teledyne (similar to the one shown in Figure 3-3). Note that Figure 3-2 shows a two-dimensional two-pronged FlowTracker sensor, but a three-dimensional three-pronged FlowTracker was used for this study.

Figure 3-2 Manufacturer photo of the SonTek FlowTracker ADV (wading rod not shown)

Figure 3-3 Manufacturer photo of the RDI Teledyne StreamPro ADCP

An area-velocity method is used by both the ADV and ADCP equipment for calculating volumetric flow rates, in which incremental areas along a channel cross-section are measured and multiplied by measured point velocities that are approximately perpendicular to the cross-section within those areas. The resulting incremental discharges for each flow area are then summed to obtain a total flow rate for the cross-section.

The technologies of the ADCP and ADV are similar in that they both use acoustics to track the movement of suspended particles within the canal water to calculate flow velocity. Sound waves are emitted from the acoustic transmitters and reflect off of, or scatter, back from

collision with the suspended particles to acoustic sensors. Upon applying the Doppler theory, the frequency shift of the sound waves can be used to determine velocity. An adequate amount of suspended sediment must be present in the water for proper reflection of sound. Canal water, especially in the LARV, contains enough suspended sediment for acoustic Doppler measurement equipment to work sufficiently. The ADCP in mounted on a floatation device that can be traversed easily across a channel while remaining in the principal direction of flow. An acoustic signal, separate from that used to track sediment for water velocity calculations, is used to track the channel bed to measure flow depth and distance traveled across the channel (discussed in Section 3.1.1.2). The ADV must be placed on a wading rod within the channel to take point measurements of velocity at stations incrementally spread-out within a cross-section and at specific flow depths within each station.

Both types of equipment have advantages and disadvantages. The advantages of an ADV are it can be used for shallow channels, can measure flow velocity relatively close to channel banks without signal interference, and requires relatively little data processing. The disadvantages of the ADV are time consuming measurements which limit the amount of velocity data that can be collected over a given time period, making the measurements prone to error associated with temporal changes in the flow rate and water level, data storage capacity required for an individual measurement when using a function that automatically calculates discharge, and limitations in maximum flow depth that can be measured since the technician operating the ADV typically must be present in the canal. The ADV could be lowered from a bridge or other structure, but stabilization of the ADV and wading rod can be difficult due to hydrodynamic forces. Advantages of the ADCP include time-efficient measurements that allow large quantities of data that can be collected over a relatively short period of time, floatation of the device and

wireless operation of the equipment which prevent mandatory entrance a technician into the canal, and relatively easy data processing. Disadvantages of the ADCP include errors associated with a moving channel bed; limitations in how near the equipment can be set to channel banks, which creates unmeasured areas of flow; a decrease in signal strength caused by high suspended sediment loads or a soft (sandy or loosely-compacted) channel perimeter; and unmeasured flow area along the water surface due to minimum required transducer submergence and signal instability (discussed in Section 3.1.1.2).

One ADCP and multiple ADVs were available in 2006, so both types of flow measurement equipment were used for Q_{US} and Q_{DS} measurements during this irrigation season. This allowed for a comparison of measurements between the two technologies and increased the quantity of data collected. After the 2006 water year, it was deemed more advantageous to use ADCPs for a few reasons. Mainly, the time efficient measurements of ADCPs resulted in a reduction in labor costs and in a reduction of potential errors related to volume balance calculations associated with temporal changes in flow rates and in stored volume. In 2007, two additional ADCPs were available for use, so all measurements of Q_{US} and Q_{DS} in 2007 were conducted with ADCPs.

Canal flow rates varied throughout the 2006 and 2007 seasons, depending upon irrigation demands and the available flow rate and water level in the Arkansas River. Flow rates less than 20 ft^3/s and in excess of 500 ft^3/s were measured in the LARV canals using ADV and ADCP technology. A typical range of Q_{US} and Q_{DS} measured within the Catlin Canal study reach was from 90 to 160 ft^3/s, was 90 to 300 ft^3/s within the RFH study reaches, was 20 to 60 ft^3/s in the Lamar Canal study reach, and was 230 to 370 ft^3/s in the Fort Lyon Canal study reaches.

3.1.1.1 ADV Discharge Measurement Technique

The FlowTracker uses an area-velocity method to calculate flow rate, in which the channel cross-section is divided into n stations, St_i (i=1, n). The ADV operator began the measurement at one bank and proceeded across the channel from station to station, recording the total station flow depth (with a wading rod to which the ADV is mounted), recording the station distance from the reference position on one of the canal banks, and collecting a minimum of one velocity reading within each station. Refer to Figure 3-4 for a depiction of an ADV flow rate measurement, where d is the total flow depth at St_i, and W_i is the horizontal channel width between adjacent station midpoints. The equation used to calculate discharge via an ADV measurement (Q_{ADV}) is:

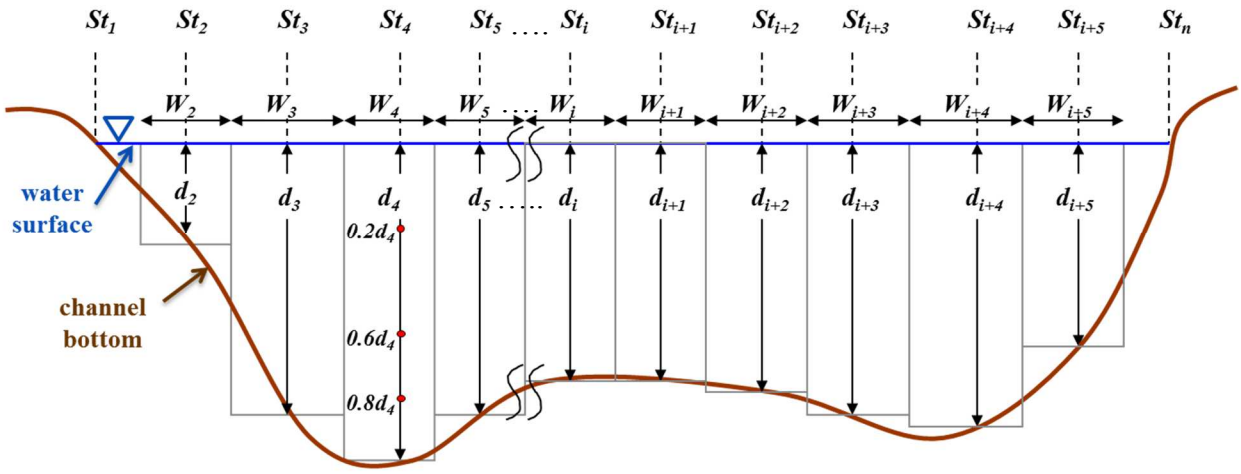

Figure 3-4 Depiction of an ADV flow rate measurement at a canal cross-section

$$Q_{ADV} = \sum_{n}^{i=1} (W_i d_i) \overline{V_i} \tag{3.2}$$

The area represented by each station St_i is the product of d_i and W_i. Velocity measurements within a station were collected using either a single-point method or three-point method. In the single-point method, velocity was measured at one point located 0.6 times the total station flow depth below the water surface, as illustrated in Figure 3-4. Under flow

conditions that are not highly turbulent, the average flow velocity, $\overline{V_i}$, in a column of water typically is located near this depth. The three-point method uses velocity measurements at 0.2, 0.6, and 0.8 times the total depth below the water surface, as illustrated in Figure 3-4. It then calculates $\overline{V_i}$ using a weighted average equation in which the 0.6 velocity measurement is given twice the weight as the 0.2 and 0.8 measurements. The three-point method is more accurate in estimating the average flow velocity in a water column that has a velocity profile affected by substantial turbulence. The three-point method was used for flow depths greater than 1 foot for all ADV measurements for seepage estimation. All point velocity measurements were averaged over a period of 30 seconds to reduce errors associated with turbulent flows and pulsating velocity. Thus, for a three-point velocity measurement, the total velocity measurement duration was 90 seconds per cross-section station. The wading rod, with mounted sensors, was held steady, pointing in the upstream direction, while 30 seconds of velocity data were collected. The depth-averaged velocity measurements, using either the single-point or three-point method, were multiplied by their respective station areas and summed over all of the stations to estimate the total discharge within a channel cross-section.

A diagnostic check of the FlowTrackers was completed at the beginning of the 2006 water year and periodically was conducted throughout the season, in accordance with SonTek operation specifications, to ensure that they were operating properly. This was completed by holding the sensors steady in a bucket of standing water, large enough that the walls of the bucket did not interfere with the sensor readings. The ADVs were connected to a computer containing SonTek software that tested the transmitters and sensors for signal strength, noise, and damage. Another diagnostic test of the recorder status, temperature data, battery power, raw

data measurements, and the system clock was completed prior to each FlowTracker use in the field. This was completed by following the manufacturer's protocol (SonTek, 2002).

Prior to an ADV measurement, rigid pins, such as rebar or T-posts, were placed firmly into the channel banks so that a tape measure, strung tautly across the channel and attached to the pins, was approximately perpendicular to the principal direction of flow. The tape measure was installed so the distance from the reference position on the canal bank could be entered into the FlowTracker. The FlowTracker can store a maximum of 100 velocity measurements per cross-section using the function that automatically calculates the total discharge. To collect as much data as possible in a cross-section using the three-point measurement method, the top width of the channel was measured then divided by 33 to obtain the spacing distances between stations. The ADV requires a measure of total dissolved solids concentration to adjust for signal travel velocity variations that are affected by the presence of dissolved salt ions in the water. A specific conductance probe was used to measure electric conductivity (EC) standardized to 25°C, which is proportional to total dissolved solids. Flow rate measurements with the ADVs generally were conducted simultaneously at the upstream and downstream cross-sections of a study reach in 2006 since multiple FlowTrackers were available. This process allowed for Q_{US} and Q_{DS} to be estimated over approximately the same time period, Δt. Lagged ADV measurements were conducted when available personnel was limited.

ADV measurements were conducted under near steady-state conditions in an effort to minimize errors associated with storage change calculations and with temporal flow rate variability. Near real time flow rate data at canal head gates were monitored on the Colorado Division of Water Resources website (http://www.dwr.state.co.us) to observe any changes in diversion rates from the river. Communication with canal managers and ditch riders also

assisted in determining the stability of flow in study reaches related to the head gate diversion and offtakes from the canal. Canal storage changes were monitored also by viewing stage data collected by pressure transducers and/or staff gages located at various sites within a study reach. Storage change calculations and monitoring methods are discussed in more detail in a following section.

3.1.1.2 ADCP Discharge Measurement Technique

The StreamPro is a broadband ADCP that measures three-dimensional flow velocity and tracks the channel bed using a transducer consisting of a thermistor and four transducer beams. Only three beams are required for three-dimensional velocity measurements, so the fourth beam is used to compute error velocity ["the difference between a velocity measured by one set of three beams versus a velocity measured by the other set of three beams during the same time frame" as defined by Simpson (2001)] or as a back-up if one of the other beams is obstructed (Simpson, 2001). The transducers beams, each angled at 20-30 degrees from the vertical, measure the speed of the suspended sediment particles traveling in the water, track their direction of travel, locate the depth of the channel bed, and measure the distance traveled along the cross-section (Simpson, 2001). The thermistor collects water temperature data, since the speed of sound used by the acoustic equipment is affected by temperature. The transducer is mounted to a device and points downward into the water. The device was designed so that it could be traversed across a water surface while remaining closely aligned with the principal direction of flow. However, improper operation, water surface waves, and highly turbulent flow can cause the device to "fishtail" (i.e. the downstream end of the device moves back and forth). Using Bluetooth technology, data are transmitted wirelessly from the StreamPro flotation unit to a portable iPAQ pocket PC, operated by a measurement technician on the channel bank, and

containing Teledyne WinRiver software that stores and processes the data. The StreamPro makes point velocity measurements at various depths below the water surface at a given station as it travels between banks. The depths at which velocity is measured depend upon the thalweg depth and the maximum number of depths at which flow velocity is to be measured (which determines the vertical spacing of each measurement), as specified by the StreamPro operator.

For an illustration of how the StreamPro collects data, refer to Figure 3-5 which displays a processed WinRiver data file. Water velocities, represented by the colored boxes (cells), at various flow depths are plotted versus the distance from the right bank for a StreamPro measurement taken on the Catlin Canal. Velocity is represented as an average over each cell and a station is defined as a vertical column of cells (ensemble). Increasing flow velocity is indicated as the color spectrum goes from blue to red. The representative flow area within each cell depends upon the total flow depth, the maximum flow depth entered into the iPAQ unit, and the StreamPro travel speed from bank to bank. Station velocity readings are taken every second, so the cells are narrower for a slower traveling StreamPro. The discharge for each cell equals the measured velocity within that cell times the cell's flow area. As seen in Figure 3-5, the StreamPro is not able to collect velocity data near the channel banks, within approximately 4 inches above the channel bed, and within approximately 6 inches below the water surface due to signal interference and instability. In order to calculate the flow velocities within these areas, the ADCP extrapolates measured velocity data to the channel banks, water surface, and channel bed, respectively. To obtain the maximum measured flow area, the StreamPro was placed as close to the channel banks as the signal would allow under manufacturer recommendations. Placing the ADCP transducer too close to the channel bank causes signal interference and thereby the

inability to measure flow velocity at that location. The total discharge of a cross-section equals the sum of the measured cell discharges plus the estimated discharge in the unmeasured areas.

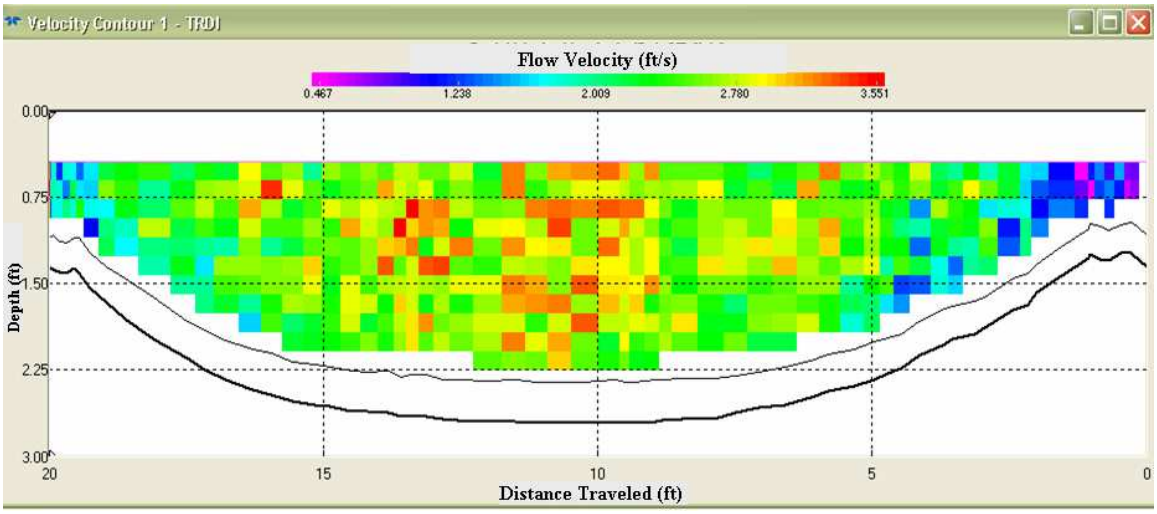

Figure 3-5 Processed ADCP StreamPro WinRiver II velocity data at a cross section on the Catlin Canal for a flow rate of 87.0 ft3/s on April 28, 2007

Prior to beginning a measurement, a rope was strung across the channel perpendicular to the channel banks. For the majority of measurements, the rope was attached to pulleys mounted to metal rods placed firmly in the banks (Figure 3-6 and Figure 3-7), allowing the StreamPro to be tethered to the rope and traversed manually from one channel bank to the other. In the summer of 2007, a mechanical device called a Cable Chimp was implemented, although rarely. The device was attached to a single rope strung across the channel and traveled at speeds controlled by a technician operating a wireless remote control. It was determined that the pulley system was more effective due to problems regarding the power and reliability of the Cable Chimp.

The ADCP was placed as close to each bank as possible until signal interference caused by the channel banks resulted in a minimum of at least two depths at which velocity could be

measured, as recommended by the manufacturer (Teledyne RDI, 2009). These locations were marked on the rope with tape, representing the starting and ending points of each transect. The distances from the starting and ending locations to their respective channel banks were measured and entered into the ADCP software on the iPAQ. The geometries of each bank were individually assigned a "bank coefficient" that is used to estimate the unmeasured flow area along the banks. The bank coefficients ranged between 0.35 and 0.91, depending upon the steepness and roughness of each bank (0.91 for steep banks and 0.35 for flatter banks), and were recorded in the data processing software. The bank coefficients were used to estimate the unmeasured flow area near each bank.

Figure 3-6 ADCP StreamPro measurement on the Lamar Canal (2006) looking toward the right bank

Figure 3-7 ADCP StreamPro measurement on the Lamar Canal (2006) looking upstream

With the initial setup complete, the discharge measurement proceeded. As directed by the data collection software, the StreamPro was held at rest at the starting locating for ten seconds while average flow velocities within the ensemble were collected. After ten seconds, the StreamPro was then moved by a technician operating the ropes in the direction of the opposite bank at a near-steady rate. Once the ending location at the opposite bank was reached, the StreamPro was held at rest to collect average flow velocity data within the final ensemble over ten seconds. Once this process was completed, the measurement procedure was started again and the StreamPro was traversed in the opposite direction as it collected another discharge measurement. Each pass across the water surface of the cross-section with the ADCP is referred to as a transect. Multiple transects were taken for each measurement, and the final discharge was calculated as the average of the transect discharges. USGS (2002) recommends that a minimum of four 3-minute transects be conducted at each cross-section. If the percent difference of any of the four transects exceeded 5% of the average discharge (of all the transects), four more transects were conducted before ending the measurement. However, experience from this study proved that to reduce suspected error, transects at some cross-sections needed to be conducted in less than three minutes. For narrow cross-sections (typical of the studied LARV canals), the StreamPro had to travel at very slow speeds for a minimum of 3-minute transects to be obtained. When the ADCP traveled across a cross-section at too low of a speed, it had a tendency to fishtail which tended to create more variability in the measurements as distance traveled across the cross-section altered from positive to negative with the transducer moving back and forth due to fishtailing. To minimize these errors, the StreamPro was traversed between banks at speeds that reduced fishtailing, often resulting in transect durations less than three minutes. Therefore, the targeted technique was to conduct more than four transects for each measurement so that at

least a total of 12 minutes of data (sum of the transect times) were still collected. This method was found to reduce variability in measurements and resulted in a final discharge calculated as an average over a greater sample set of transects. In some cases, where discharge measurements of all transects had a percent difference of less than 5% of the average discharge (of all transects), the number of collected transects was limited to four.

The ADCP tracks the canal bed using a sound wave with a frequency different than that used to track scatter (in measuring flow velocity). Bed tracking is completed using the Doppler theory under the assumption that the channel bed is motionless. Accordingly, moving bedload associated with sediment transport can potentially affect the measurement accuracy. To identify errors associated with a violation of the motionless bed assumption, a moving bed test was completed prior to or after a discharge measurement. A moving bed test consists of holding the ADCP stationary near the center of the channel for a time period between five to ten minutes. Since the ADCP is held stationary, any measured movement of the channel bed indicates a moving bed condition. This test was completed at all measurement cross-sections in the LARV under a variety of flow rates. If bedload did not appear to have an impact on the accuracy of ADCP measurements, the moving bed test was not completed in the future at that cross-section for similar flow rates.

When an adequate number of ADCPs and operators were available, Q_{US} and Q_{DS} measurements were conducted simultaneously at cross-section locations within a study reach. If simultaneous measurements were not possible, successive (time-lagged) measurements were conducted, generally moving downstream in a canal study reach. Over short reaches, successive measurements could result in measuring approximately the same bulk parcel of water at an upstream and downstream cross-section. The time duration required for the bulk flow at an

upstream cross-section to reach a downstream cross-section was estimated as the distance between the locations divided by the average flow velocity at the upstream cross-section.

3.1.2 Measurement of Diverted Outflows

Diversion structures, primarily vertical sluice gates, and pumps were located within of the LARV canal study reaches. The diversion gates and pumps on each structure could be operated by canal managers to approximate a desired diversion rate for agricultural use. The locations of diversion structures were identified by driving along the canal bank roads and through the assistance of canal managers. The size and number of diversions were taken into account in the selection process of study reaches so that: (1) the selected measurement cross-sections bracketed a minimal number of diversions, (2) any open or leaking diversions within a study reach could be measured as accurately and easily as possible, and (3) the total estimated Q_D (obtained through communication with canal managers) where less than the expected range of error associated with the measurement of Q_s. In some cases, active diversions could be shut off to minimize potential measurement errors upon request to canal managers. However, diversions sometimes were active during seepage measurements, depending upon irrigation schedules and demand.

A variety of techniques were used to measure Q_D, depending on the nature of the offtake structure, type of conveyance (open channel or pipe), available measurement equipment, and expected accuracy of the measurement. Q_D was measured using: (1) flumes located within the diversion channels immediately downstream of the canal offtake, (2) ADV FlowTracker measurements within the open channel served by the offtake, (3) pump rating curves developed for pumped diversions, (4) bracketing a diversion with flow rate measurements in the parent canal (measuring the flow rate immediately upstream and immediately downstream of a diversion structure), and/or (5) measuring the time required to fill a container of known volume

with flow from an offtake. Whenever possible, multiple measurement techniques were employed for a comparison of results. Flume readings were conducted by measuring the total flow depths at critical locations, typically from mounted staff gages, unique to each flume. A calibrated discharge rating curve for the type and size of flume then was used to calculate the flow rate. FlowTracker measurements were completed within the receiving channel at a location immediately downstream of the offtake that permitted the use of an ADV without compromising measurement accuracy. This type of FlowTracker measurement always was made for diversions except in cases where the flow depth in the receiving channel was too shallow, the flow was highly turbulent, or the channel was highly irregular. Pump rating curves were available from canal managers and used to calculate pumped diverted flow rates upon known operating power of the pumps. For large offtakes that diverted a significant percentage of the total upstream flow rate in the canal study reach, the diversion structure was bracketed with flow rate measurements in the study canal. The diversion discharge was calculated as the difference between the upstream and downstream flow rates. The diversion rate had to be significantly greater than the cumulative errors of the bracketing measurements for this technique to be justified. The bucket technique was used if offtake channels that did not contain a flume and did not permit the use of an ADV and if the cumulative measurement error associated with bracketing the offtake structure in the study canal was greater than the diversion discharge. Using the bucket technique, an open container of known volume was placed under a free-flowing feature (typically the end of a pipe or near the bottom of a steep drop in the channel) and the time required to fill the container was recorded. The volume of the container divided by the time required to fill the container was taken as the diversion discharge. This process was completed several times, and the final Q_D was estimated as an average.

Diversion schedules were obtained from canal managers to assist in the decision process for the timing of seepage measurements. The diverted flow not only affect the accuracy of the volume balance procedure regarding the measurement of Q_D, but also affect the accuracy of measuring $\frac{\Delta S}{\Delta t}$ since storage changes are affected by upstream and downstream offtake gates being open and closed.

The Lamar Canal study reach contained the most active diversions that could not be shut off upon request. Large diversions were bracketed in the study canal by flow measurement cross-sections in an attempt to accurately determine diversion discharges. Measured values of Q_D ranged from 3.6 to 12 ft^3/s on the Lamar Canal, or approximately 7% to 26% of the discharge at the upstream study boundary. These values were much greater than those typically observed on the other canals that were studied. Fortunately, on the RFH Canal, no major diversions were active within the canal study reach when seepage measurements were taking place. In 2007, a downstream reach of the canal contained multiple active diversions during certain water demand periods. When these diversions were active, the seepage study reach of the canal was reduced by approximately 2.7 miles so that none of these diversions lied within the seepage study reach. The maximum Q_D ever active on the RFH Canal during seepage measurements was 0.6 ft^3/s, less than one percent of Q_{US}. On the Catlin Canal, one pumped diversion was active typically and on two occasions a second diversion was active in 2006 and 2007. The total diversion rates on the Catlin Canal study reach ranged between 0 and 1.5 ft^3/s, never exceeding 1.1 percent of Q_{US}.

3.1.3 Accounting for Inflows

Inflows, particularly drainage from irrigated lands under an adjacent upper-contour of a canal, are not uncommon in the LARV. Drainage from irrigated lands commonly discharges into canals from ditches and culverts or by overland flow. Prior to the selection of canal study

reaches, potential Q_I sources were located with the assistance of canal managers. These sources were checked regularly during seepage measurement to account for any Q_I into the canal; however, no Q_I was observed during inflow-outflow measurements in 2006 or in 2007. No seepage measurements were conducted when precipitation events were occurring, so this source of inflow also was non-existent.

3.1.4 Free-Water Evaporation

The depth rate of free water evaporation, E (m day^{-1}), from the canal water surface over the inflow-outflow study reach was estimated using the Penman combination equation:

$$E = \frac{\Delta(K+L) + \gamma K_E \rho_w \lambda_v v_a e_a^* (1 - W_a)}{\varphi_w \lambda_v (\Delta + \gamma)} \tag{3.3}$$

Where: Δ = slope of relation between saturation vapor pressure and temperature (kPa°K^{-1})

K = Net solar shortwave radiation [MJ (m^2 day^{-1}) $^{-1}$]

L = Longwave radiation [MJ (m^2 day^{-1}) $^{-1}$]

γ = psychometric constant (kPa°K^{-1})

K_E = Coefficient of vertical transport of water (kPa^{-1})

ρ_w = Mass density of water (kg m^{-3})

λ_v = Latent heat of vapor (MJ kg^{-1})

v_a = Wind speed (m day^{-1})

e_a^* = Saturated vapor pressure (kPa), and

W_a = Relative humidity.

Dingman (2002) presents equations and detailed definitions for the variables within Equation 3.3; however, brief discussions of the variables and their methods of estimation are

included in this section. The majority of atmospheric data used to estimate the parameters of Equation 3.3 were obtained from local weather stations associated with Colorado State University's CoAgMet program (CoAgMet 2006 and 2007). Hourly atmospheric data is posted and can be accessed online for each of the CoAgMet weather stations (http://climate.colostate.edu/~coagmet/). Data from the station nearest to each canal study reach, typically within a few miles, were used in calculating the average E over inflow-outflow measurement time periods (refer to Table 3-1 for a list of CoAgMet weather stations used and distances from the study reach midpoints). These data include air temperature, relative humidity, vapor pressure, solar radiation, and average wind velocity. Water temperature data were obtained from the ADV and ADCP flow rate measurements in 2006 (the ADCP and ADV record the temperature at the thermistor for every stored velocity measurement) and from pressure transducers submerged within the canal water in 2007. Q_E was calculated as the product of E (depth per unit time) and the total estimated study reach water surface area, A_{WS}, which is described later in the chapter.

Table 3-1 CoAgMet weather stations used to calculate free water evaporation

Canal Study Reach	**CoAgMet Weather Station**	**Distance from Weather Station to Canal Study Reach Midpoint**
Catlin	rfd01	~5.3 miles
Lamar	lam01	~10.3 miles
Rocky Ford Highline	avn01	~13.7 miles
Fort Lyon	lam02	~15.5 miles

Δ is a function of the air temperature, T_a (°K):

$$\Delta = \left[\frac{2508.3}{(T_a + 237.3)^2} \right] \exp\left(\frac{17.3(T_a)}{T_a + 237.3} \right) \tag{3.4}$$

Air temperature data were obtained from the hourly atmospheric data posted by CoAgMet (CoAgMet 2006 and 2007).

Shortwave radiation entering the earth's atmosphere, K_{in}, was obtained from CoAgMet data. Only a portion of K_{in} that enters the atmosphere reaches the earth surface. Thus, K is used for estimating free-water evaporation and is calculated using an albedo term, a, that accounts for the dissipation of K_{in}:

$$K = K_{in}(1 - a) \tag{3.5}$$

$$a = (0.127)\exp(-0.0258K_{in}) \tag{3.6}$$

Albedo typically ranges between 0.05 to 0.10, resulting in the K equally approximately 90 to 95 percent of K_{in} (Dingman 2002).

The psychometric constant, γ, can be estimated from by the heat capacity of air, c_a, (assumed to equal 10^{-3} MJ/kg/°K) atmospheric pressure, P_{atm}, and λ_v:

$$\gamma = \frac{c_a P_{atm}}{0.622\lambda_v} \tag{3.7}$$

$$\lambda_v = 2.50 - 2.36(10)^{-3} T_a \tag{3.8}$$

Atmospheric pressure data were obtained from the National Oceanic and Atmospheric Administration's (NOAA) National Climatic Data Center website (NOAA 2006) for the 2006 seepage studies and from atmospheric pressure transducers located along the canal study reaches for 2007 seepage studies. All T_a data were acquired from CoAgMet weather stations.

A portion of the longwave solar radiation that reaches the canal water surface is reflected back into the atmosphere and does not contribute to the energy used for evaporation. Thus, the net longwave radiation, L, was estimated as:

$$L = \varepsilon_w \varepsilon_{at} \sigma (T_a + 273.15)^4 - \varepsilon_w \sigma (T_s + 273.15)^4 \quad (3.9)$$

The emissivity of water, ε_w, was assumed equal to 0.95 (typical for liquid water) and atmospheric emissivity, ε_{at}, was calculated from an equation developed for clear sky exposure (no forest canopy):

$$\varepsilon_{at} = 1.72 \left(\frac{e_a}{T_a + 273.2} \right)^{1/7} \quad (3.10)$$

The Stephen-Boltzmann constant, σ, equals $4.90(10)^{-9}$ $MJm^{-2}day^{-1}°K^{-4}$, and water surface temperature, T_s (°K), was assumed to equal the water temperatures measured by the ADVs and ADCPs during discharge measurements.

The value of K_E is dependent upon P and air density, ρ_a:

$$K_E = \left[\frac{0.622 \rho_a}{P \rho_a} \right] \frac{1}{6.25 \left[\ln \left(\frac{z_m - z_d}{z_o} \right) \right]^2} \quad (3.11)$$

with: $$\rho_a = \frac{P}{T_a R} \quad (3.12)$$

K_E is also a function of the zero-plane displacement, z_d, which is equal to zero since no vegetation is present (used for evapotranspiration calculations), the height at which the wind and air vapor pressure are calculated (2 meters), z_m, and the roughness of the water surface, z_o (estimated to be approximately 0.23 millimeters). The gas constant, R, found in Equation 3.12 equals 0.288 K^{-1} m^{-1}.

The latent heat of vaporization, λ_v, was estimated as a function of T_a measured in degrees Celsius:

$$\lambda_v = 2.50 - 2.36(10)^{-3} T_a \tag{3.13}$$

Vapor pressure, e_a, and relative humidity, W_a, data were obtained through CoAgMet. The value of e_a^*, was calculated as:

$$e_a^* = \frac{e_a}{W_a} \tag{3.14}$$

Values of Q_E along the LARV canal study reaches during measurement periods commonly ranged between 0.05 and 0.15 ft^3/s per mile. Values typically were less than 1% of Q_{US} and never exceeded 2% of Q_{US}. Greater values of Q_E were observed on longer canal reaches that had larger values of total A_{WS}. The ratio Q_E/Q_{US} (in percent) on the Catlin and RFH canal reaches was never greater than 1% and typically was less than 0.5%.

3.1.5 Storage Changes

Temporal variability in canal water levels are associated with changes in the volume of water stored within a canal control volume. Main sources of such variability include changes in the settings of regulating structures (i.e. overshot weirs), changes in diversion rates from the system, changing water levels and flow rates at the canal system's source (river), changes in hydraulic geometry, changes in hydraulic resistance, and atmospheric variability. Changes in stored volume were estimated by monitoring the water levels at all Q_{US} and Q_{DS} measurement cross-sections and, in some cases, at intermediate cross-sections over the time period of measurement, Δt. Staff gages were mounted at all Q_{US} and Q_{DS} measurement cross-sections so that stage readings could be collected during flow rate measurements. Pressure transducers also were used to monitor water levels, although they were not installed at all Q_{US} and Q_{DS}

measurement cross-sections and only were used in 2007. They were installed at upstream or downstream cross-section boundaries of the study reaches and/or at intermediate locations in between Q_{US} and Q_{DS} measurement cross-sections. Pressure transducers are beneficial in estimating storage changes in that they can be set to automatically record stage data without requiring a technician to be present during those readings. This allows for intermediate stage readings to be collected which greatly assist in identifying storage changes, in quantify storage change volumes, and in estimating the duration of time over which the storage changes occurred. Stage readings using staff gages typically were recorded every 5 to 15 minutes during inflow-outflow tests, and readings with pressure transducers were recorded every 15 minutes.

To minimize potential errors associated with the calculation of changing storage volumes, an effort was made to avoid major storage changes during seepage measurements by communicating with canal managers about diversion schedules, by monitoring flow rates at canal headgates as posted near real-time on the internet by the Colorado Division of Water Resources (CDWR 2006 and 2007), and by monitoring stage data from staff gages and pressure transducers.

The total volume of storage gained or lost in the control volume during a seepage measurement was calculated upon analyzing stage data throughout the study reaches. Rising or falling water levels were tracked and the total volume of water associated with the changes was calculated using the average bulk velocity of the changing wave. Once ΔS was calculated it was divided by the total duration of the seepage measurement, Δt, to obtain the storage change $\frac{\Delta S}{\Delta t}$, as described in Section 5.5.

Storage changes on the RFH Canal were minimal since the study reach was located immediately downstream of the canal headgate which regulates fairly steady flow rates entering

the canal from the Arkansas River. The Catlin Canal and Lamar Canal study reaches were located downstream of numerous irrigation diversions; thus, the water level in the canals had to be monitored carefully to identify and quantify storage changes.

3.1.6 Potential Sources of Error and Uncertainty in the Volume Balance Procedure

This section discusses potential sources of error and uncertainty in the inflow-outflow volume balance methodology for estimating canal seepage. Calculations and analysis related to quantifying levels of error and uncertainty associated with the volume balance procedure are discussed and presented in Section 5. The rationale and methodology that were adopted to model uncertainty for this study also are presented in Section 5.

There are a number of sources of uncertainty in estimating canal seepage losses using a volume balance procedure. Several major sources are briefly discussed in the following sections.

3.1.6.1 Potential Sources of Uncertainty in Flow Rate Measurements

Errors associated with the accuracy of ADCP and ADV measurements potentially have the greatest impact on field studies incorporating the volume balance procedure to estimate canal seepage since these technologies are used to estimate Q_{US}, Q_{DS}, and Q_D, all major components of the volume balance. The accuracy of ADCP and ADV measurements not only is affected by the errors associated with the technology itself but also by spatial and temporal variability within the canal system and by operational errors. Little research has been completed or published on the accuracy of FlowTracker and StreamPro equipment under a variety of different field conditions. However, some types of uncertainty associated with each technology can be identified and estimated.

3.1.6.1.1 Potential Sources of Uncertainty in ADCP Measurements

The benefit of ADCP technology is the large quantity of data that can be collected in a relatively short period of time. The amount of data collected in a channel transect is determined by the speed of traverse of the device, the number of velocity measurement cells in a water column, and the flow depth. By traversing the ADCP at a slower rate, the measurement time duration is extended, thereby increasing the amount of data collected. However, if Δt is too long it may encompass temporal variation in the flow rate. Gonzalez-Castro and Muste (2007) described uncertainty analysis for ADCP measurements, highlighting uncertainty associated with velocity ambiguity, side-lobe interference, Doppler noise, spatial resolution, instrument rotation, edge estimation, measuring environment, sampling duration, bottom tracking, and instrument operation. These specific sources of uncertainty will not be discussed further in this report. Rather, uncertainty as a whole related to ADCP measurements will be considered.

The flow area along the channel bed and banks is not measured by the StreamPro ADCP due to signal interference (side-lobe interference) (Simpson 2002). The proximity of an ADCP to a channel bank before side-lobe interference occurs depends upon the slope and geometry of the channel bank. Based upon experience from this study, the ADCP typically can travel to within 1 to 2.5 feet of the bank before signal interference becomes a problem on most canals. The ADCP usually was able to get closer to steeper channel banks than to flat channel banks. The estimated discharge calculated for the unmeasured channel bank areas is sensitive to the edge coefficients assigned to each bank. Depending upon the flow velocities of the closest measured station in the transect, discharge estimation along the banks can be sensitive to the chosen edge coefficient. For example, if high velocities are present within the unmeasured area near the canal bank, from which extrapolation takes place, the estimated discharge (calculated using an area-velocity formula) can vary substantially as the edge coefficient changes, since it

determines the unmeasured flow area along the bank. If flow velocities are relatively low near the measured flow adjacent to the banks, estimated flow rate is not as greatly affected by the selected edge coefficients. Selection of edge coefficients poses subjective errors by the equipment operator. This potential source of error was managed by remaining consistent in the assignment of edge coefficients for a range of water depths at a given cross-section. For example, if a discharge measurement was conducted on three different days at the same cross-section and the stage on all three days was approximately the same, the same edge coefficient was assigned for all three measurements. This approach assumes that cross-section geometry does not change temporally. Only major changes in geometry that could be easily identified would affect the selection of an edge coefficient, so the assumption always seemed adequate. In addition, the selection of an edge coefficient typically was decided upon by multiple equipment operators in an effort to eliminate subjective errors by a single operator.

The upper 0.46 feet (approximately 6 inches) of a water column cannot be sampled for flow velocity due to signal instability and transducer submergence (Simpson 2002). Regression equations, as selected in the WinRiver data processing software, are fit to the measured velocity data and extrapolated to this and other unmeasured regions of the flow area for velocity estimation. The extrapolation method creates uncertainty in ADCP measurement due to errors in the fitted equations. To minimize this uncertainty, the raw velocity data were analyzed upon processing each discharge data file so that appropriate regression equations could be assigned. If it was unclear which type of regression equation fitted the data best, the resulting discharge values using all regression equations were compared to see how Q_s varied among the methods. As long as the type of regression equation was consistently used for all discharge measurements

at every measurement location within a study reach, Q_s never seemed to change significantly among the methods, although Q_{US} and Q_{DS} changed.

3.1.6.1.2 Potential Sources of Uncertainty in ADV Measurements

ADV measurements are subject to uncertainty related to equipment accuracy, operation and setup errors, and subjective decisions and applications by the operating technician. They are also limited in the amount of data they collect when the operational mode that automatically calculates discharge is selected. A mode can be used that does not automatically calculate discharge so that more data could be collected, but doing so would have extended the length of the measurement greatly and would have made the seepage measurement more prone to temporal errors of storage changes and unsteady flow, both of which likely would have created higher levels of uncertainty than would quicker ADV measurements.

Causes of error related to the equipment's measurement accuracy (excluding operational errors) include, but may not be limited to: turbulent flows, signal interference caused by channel boundaries and debris, velocity spikes, low suspended sediment concentrations (scatter) in the water, low signal-to-noise ratios (weak signal reflected back to the sensors), and inaccurate estimations of electrical conductivity. Average velocity measurements within a water column are calculated from a weighted average equation using a maximum of three velocity measurements, but when this method is used for turbulent flows that have an inverted or highly irregular velocity profile, significant errors potentially can occur. Much of the potential uncertainty related to the equipment technology can be minimized through proper operation by the technician. Rehmel (2007) found that the ADV FlowTracker will produce, on average, flow rate measurements that are within 5% of traditional mechanical current meters, such as the Price pygmy and Price AA propeller meters when used in accordance with USGS measurement

protocols. SonTek, the manufacturer of the FlowTracker, suggests that individual ADV velocity readings are accurate to within 1% of the true velocity (SonTek/YSI 2003).

Operation and setup uncertainty arises mainly from inadequate calibration of the ADV prior to measurement, setting up and conducting measurements in a skewed cross-section that is not perpendicular to the canal alignment (results in an extended cross-section), sinking of the wading rod into the channel bed, and not holding the wading rod vertically during flow depth and velocity measurements, collecting average point velocities over too short of a time period so that turbulence and velocity spikes affected the average, sagging of the measuring tape strung across the cross-sections, measuring and recording flow depths and channel distances incorrectly, and choosing improper measurement sites that created conditions that exceeded the limitations of the equipment. If the setup and location of a measurement was inadequate, even perfect operation of the equipment would result in error and uncertainty. For example, if the equipment was not calibrated properly or the cross-section was skewed or setup in locations of high turbulence, the measurements likely will have a substantial degree of error even if the equipment is operating properly. The amount of error associated with incorrect operation and setup is very difficult to quantify and is dependent in part upon the hydraulic conditions of the flow, but it can be certain that the error is significant. For this reason, special attention was given to the operation and setup of ADV measurements during the studies in 2006 and 2007 in the LARV. In addition, ADV operators were given training regarding proper operation prior to conducting discharge measurements in 2006.

Subjective uncertainty can impact ADV measurement since operating technicians are required to conduct and record numerous distance and depth measurements. At every station in a cross-section where average velocity is measured, the total flow depth must be entered into the

ADV. Acoustic sensors must then be raised or lowered to depths of 0.2, 0.6, and 0.8 of the total flow depth for velocity measurements. The placement of the sensors is based upon a system of markings on the wading rod, which can be subjective to interpret for each individual technician. A difference in placement of the sensors results in velocity measurements not at the specified locations required to calculate an average. It is also somewhat subjective to determine if the wading rod is being held completely vertically or not, since no levels are mounted on wading rods. This can affect the accuracy of a measurement as discussed in the previous paragraph. Another error that can take place is measuring the distance from a station to the starting canal bank using the tape measure stretched across the channel.

3.1.6.2 Potential Sources of Uncertainty in Diverted Flow Rate Estimation

Diversion rates from the canals were estimated using ADVs, pump rating curves, or measurement flumes. Turbulent flows in the diversion channels potentially affected the accuracy of ADV measurements, as previously discussed. Uncertainty in estimating pumped flow rates using rating curves can be substantial, especially as pumps age and wear down. Fortunately, for this study, only one active pumped diversion was present (located within the Catlin Canal study reach). Estimations of the pumping rate were provided by the canal manager. On multiple occasions, these estimations were checked by placing a bucket of known volume under the pump discharge pipe and timing how long it took to fill the bucket. The discharge numbers provided by the canal manager and the measured flow rate using the buckets were closely comparable. The estimated diversion rate from the pump on the Catlin Canal never exceeded 1.5 ft^3/s or 1% of Q_{US}; thus, errors were expected to minimally affect the seepage calculations. Flume measurements also were uncertain for a variety of reasons. Flumes are required to be installed level in the channel for accurate measurements. As such, lateral and vertical settling cause flow

measurement errors (Abt et al. 1995). Submergence of flumes, especially Parshall flumes which are common in the LARV, creates measurement error since flumes are most accurate under free-flow conditions. To gain assurance of the accuracy of diversion rates, ADV and flume measurements were taken simultaneously and their results were compared. In all cases, the results were very similar.

3.1.6.3 Potential Sources of Uncertainty in Storage Change Estimation

Uncertainty of storage changes come from a variety of sources including errors in stage readings, in canal hydraulic geometry surveys, and from temporal and spatial variability in canal stage and hydraulic geometry.

Uncertainty in stage readings is unique to the type of equipment used. Manual staff gage readings can be affected by the observer's subjective interpretation of the water level, misreading of the staff gage, wave action, and high flow velocity causing a non-linear water surface across the staff plate. The staff gages used in this study could be read to 0.01 foot increments, so any subjective errors should be fairly minimal. Wave action was mainly an issue only when high winds were active in the study reach; however, seepage measurements typically were not conducted when wind velocity was large due to the negative effects it has on ADCP measurements. Measurement sites were chosen in locations of low turbulence which did not result is excessive wave action, and the staff gages were placed along the channel banks where flow velocities were relatively small so they could easily be read. Pressure transducers have an error associated with measurement accuracy and spatial variability. Onset, the manufacturer of the Hobo pressure transducers that were used for stage measurements, suggests that water levels can accurately be measured typically with 0.5 centimeters with a maximum error of 1 centimeter (Onset, 2008). However, if the equipment is not cared for properly the error can increase. The

conversion from absolute pressure (recorded by the pressure transducer) to gage pressure (used to calculate water depth) is subject to spatial variability since the atmospheric pressure transducers were placed near the center of study reaches, which was up to a few miles away from any pressure transducer in the canal water. Atmospheric conditions are typically very similar at locations spread by less than a few miles unless a storm is present, so spatial variability of atmospheric pressure likely was minimal under normal weather conditions.

Uncertainty is also associated with the spatial variability in hydraulic geometry characteristics of each channel that were determined by cross-sectional surveys, incrementally spaced along a canal study reach. Closely-spaced surveys improve accuracy of channel geometry calculations and thereby storage change estimates. If the surveyed cross-sections were not representative of the channel reaches they were designated to represent, related uncertainty can be significant since ΔV is directly dependent upon channel geometry.

Locating exactly where storage changes occurred in a control volume, the duration of the change, and the volume of the change can be difficult to quantify in a reach that is unsteady and has fluctuating water levels. Some locations in a canal reach may have rising water levels (i.e. from a weir being raised or from changing Q_{US}) while other locations having falling water levels (i.e. from downstream diversions becoming active or from changing Q_{US}). This makes the changes difficult to track since a change in storage is highly variable and no obvious pattern can be observed. The changes at locations where stage is measured are easy to identify in the data, but outside locations to which the change extended and the timing of those changes can be extremely difficult in areas where no stage data were collected. For this reason, attempts always were made to conduct seepage measurements when canal flow rates were expected to be relatively steady and diversion schedules were not expected to affect the study reaches. This was

completed through communication with canal managers, by monitoring flow rates diverted from the river at the canal headgates, by timing the measurements appropriately, and by conducting synoptic measurements if thought necessary. In some cases, storage changes could not easily be avoided or occurred unexpectedly and the associated uncertainty was significant, as indicated in the uncertainty analysis of Section 5.

3.1.6.4 Potential Sources of Uncertainty in Evaporation Rate Estimation

Free-water evaporation rate calculations are subject to temporal and spatial variability. The Penman-Combination equation was used to quantify free-water evaporation rates from the canal water surface based upon hourly atmospheric data collected at local weather stations. This equation has uncertainty related to its use and the accuracy of the weather data employed. Atmospheric data collection technologies at weather stations have associated measurement errors. Uncertainty due to temporal variability arises from hourly data that may not be a true representation of the time periods in which seepage measurements were conducted (seepage measurements did not begin and end on the hour, which is when atmospheric pressure data were measured), so averages of the atmospheric data were used to help reduce errors. The weather stations in the LARV typically were located within a few miles of canal study reaches, which poses spatial variability uncertainties. The weather conditions at weather stations likely varied from the true weather conditions along the canals during measurements; however, the difference is thought to be minimal under normal weather conditions. Free-water evaporation rates are often difficult to accurately estimate, but fortunately their estimates were a small percentage of the total outflows from studied canal reaches as calculated. Q_E estimates rarely exceeded 1% of Q_{US} in any of the study reaches.

3.2 DETERMINING HYDRAULIC GEOMETRY AND PROPERTIES

Components of the volume balance equation require hydraulic geometry data (i.e. channel top width and wetted perimeter area), and seepage estimates are expressed in terms of flow rate per unit of wetted perimeter area. Thus, the hydraulic geometry of a canal study reach plays an important role in the data analysis for seepage measurements. This data comes from a combination of stage data and survey data. The stage data can be used with survey data to determine where the water surface was located throughout a study reach of a canal during seepage measurements.

3.2.1 Cross-Sectional and Longitudinal Surveys

Cross-sectional surveys can be obtained at flow measurement locations from ADV and ADCP data. Both technologies collected cross-sectional data in order to calculate discharge using the area-velocity method. This data assisted in cross-sectional geometry calculations, however, the data it provided was limited to the sites at which flow rates were measured. The distances between sites were typically on the order of miles, so it was determined that denser cross-sections needed to be surveyed within the study reaches for more accurate hydraulic geometry calculations, due to spatial variability. Surveying was completed on the Catlin Canal and the RFH Canal. Surveying was not completed on the Lamar and Fort Lyons canals due to limitations of time and due to the lack of measured stage data. Without adequate stage data, water surfaces could not be interpolated, so surveying on these canals was determined to be less useful. Figure 3-8 and Figure 3-9 display locations surveyed on the Catlin and RFH canals, respectively.

A total of 16 cross-sections were surveyed over the 2.35-mile study reach of the Catlin Canal, and a total of 50 cross-sections were surveyed over the 8.49-mile study reach of the RFH Canal.

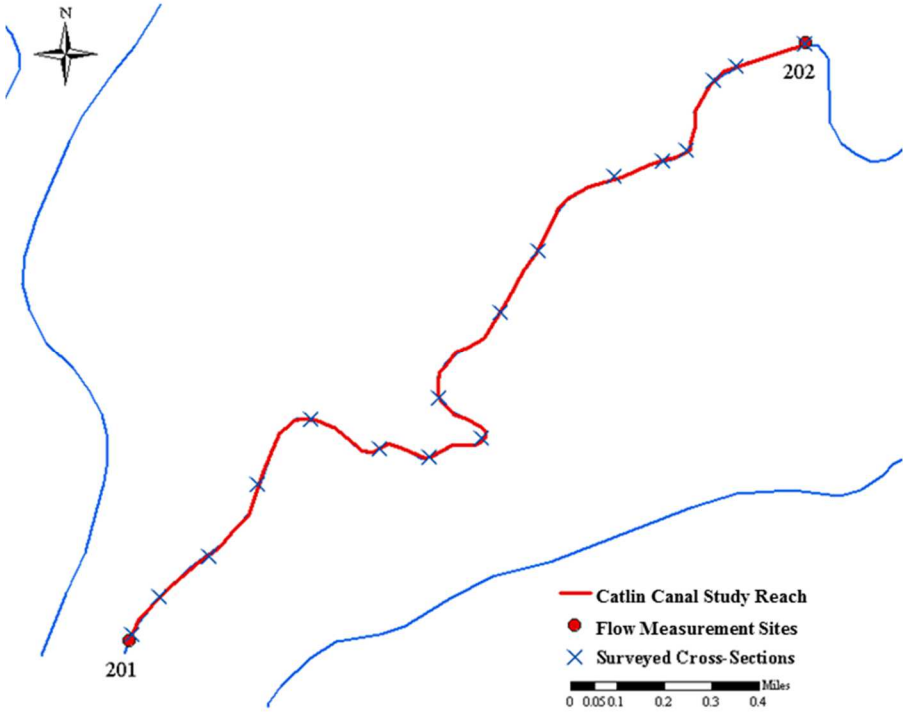

Figure 3-8 Map of surveyed cross-sections on the Catlin Canal

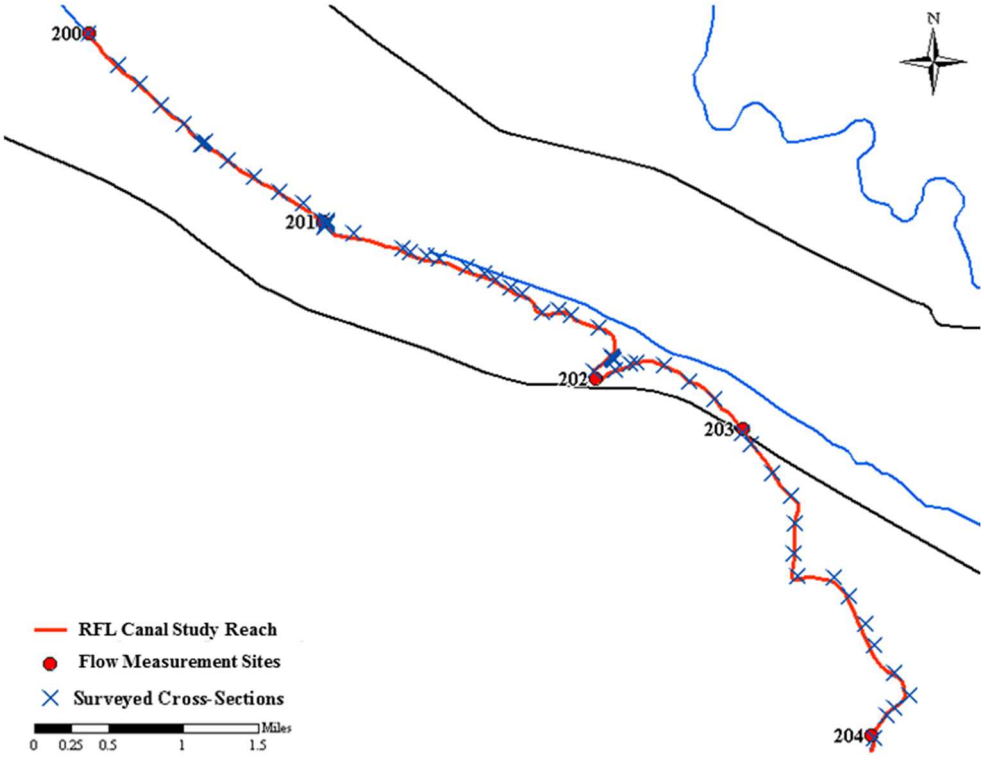

Figure 3-9 Map of surveyed cross-sections on the RFH Canal

Cross-sections were surveyed at least every 0.2 miles within canal study reaches using either a total station or a surveying level (Figure 3-10). Based upon observations of spatial variability of canal geometry, such as channel width and typical flow depth, this spacing of cross-sectional surveys was deemed adequate. In locations where the canal clearly was not uniform, denser surveys were conducted to limit errors associated with spatial variability. For example, some portions of the RFH Canal varied significantly in width over relatively short distance, so cross-sections were surveyed at least every 0.1 miles in these regions.

Figure 3-10 Cross-sectional survey on the Catlin Canal using a surveying level

A rigid pin was placed firmly into the canal bank at each surveyed location. A cross sectional survey would begin at this pin and proceed to the opposite bank. The survey was conducted so that the entire canal cross section was captured and the starting and ending locations were well above the maximum flow depth that was observed during seepage measurements. All major breaks in slope were captured within a cross-sectional survey to ensure that the geometry was properly captured. If a staff gage or pressure transducer was present within a cross-section being surveyed, a survey point was captured at that location so that the water surface elevation could be determined at that cross-section during times of seepage measurements. The data from each survey were processed, and the relative elevations and distances between survey points were calculated. Figure 3-11 depicts an example a surveyed cross-section on the RFH Canal.

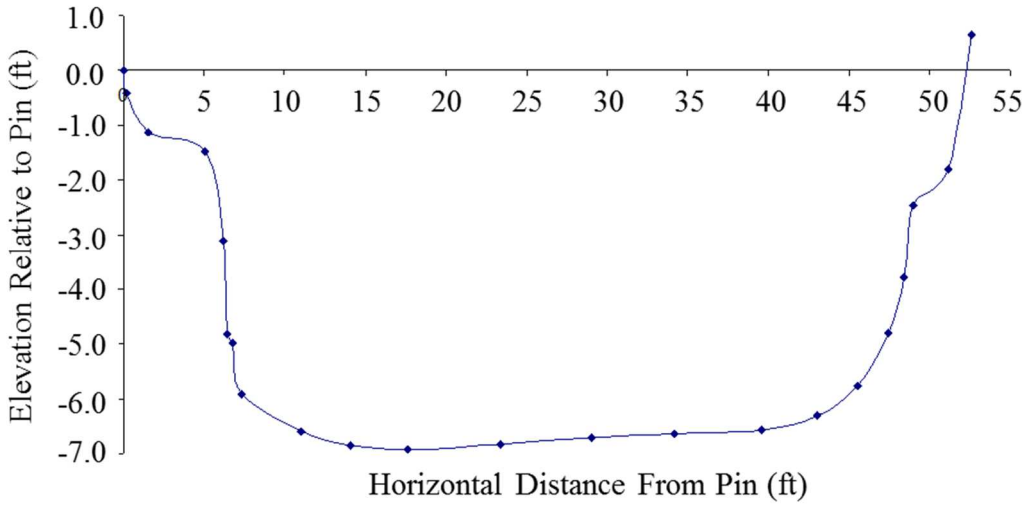

Figure 3-11 Processed total station cross-sectional survey on the RFH Canal near site 201

A longitudinal survey was conducted on each canal using a total station after all cross-sections were surveyed. This was done by capturing survey points at all cross-sections pins within the study reach. Upon calculating a relative elevation of each pin, the remaining surveyed points within a cross-section could be assigned a relative elevation. The purpose of this process was to link the elevations of each cross-section together so that their relative elevation could be calculated and a water surface could be interpolated from cross-sections where stage was measured to cross-sections that did not have stage data. A processed longitudinal survey of the Catlin Canal showing elevations of the tops of each pin and cross-section thalweg elevation is shown in Figure 3-12.

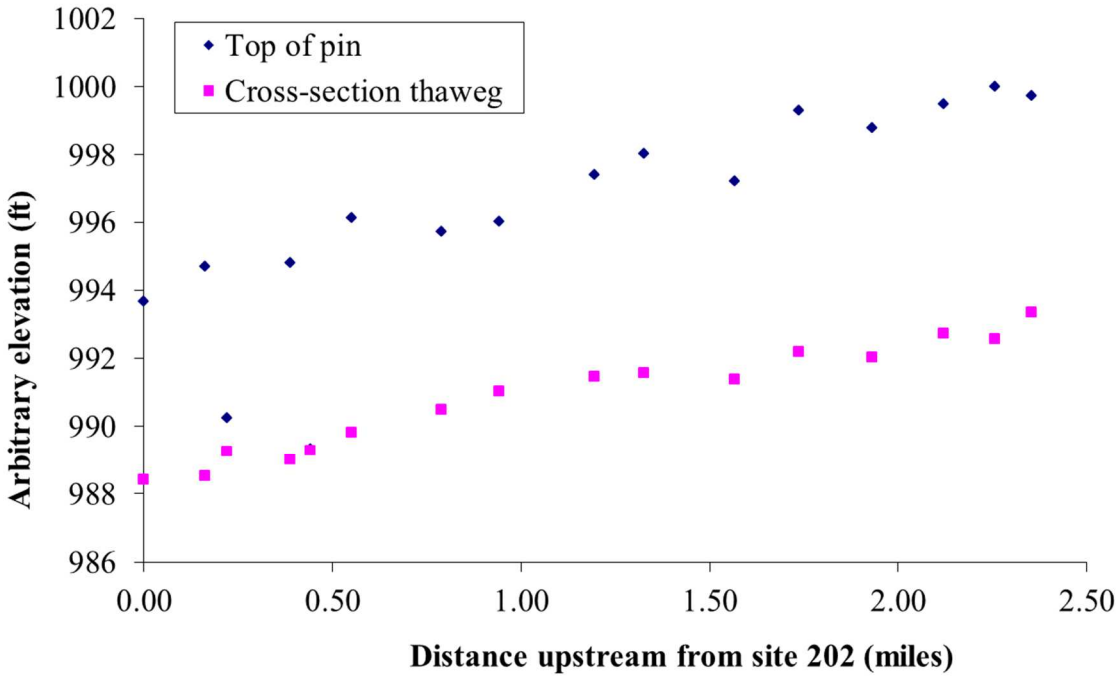

Figure 3-12 Longitudinal survey of the Catlin Canal showing pin and thalweg elevations

3.2.2 Stage Data

Stage data were collected through a variety of methods that were dependent upon the data collection location. Flow depths were recorded at the Q_{US} and Q_{DS} flow measurement locations using staff gages, ADV data, ADCP data, and/or pressure transducers. Pressure transducers were installed in the Catlin and RFH canals in 2007, which enabled data to be collected at locations in between measurement sites so that hydraulic properties could more accurately be calculated. Figure 3-13 shows a mounted staff gage and the location of a submerged pressure transducer at Site 202 of the Catlin Canal. Figures 3.11, 3.12, and 3.13 show the locations where stage data were collected and the source of the data on the RFH Canal, the Catlin Canal, and the Lamar Canal, respectively.

Figure 3-13 Picture of a staff gage and location of a submerged pressure transducer at Site 202 on the Catlin Canal

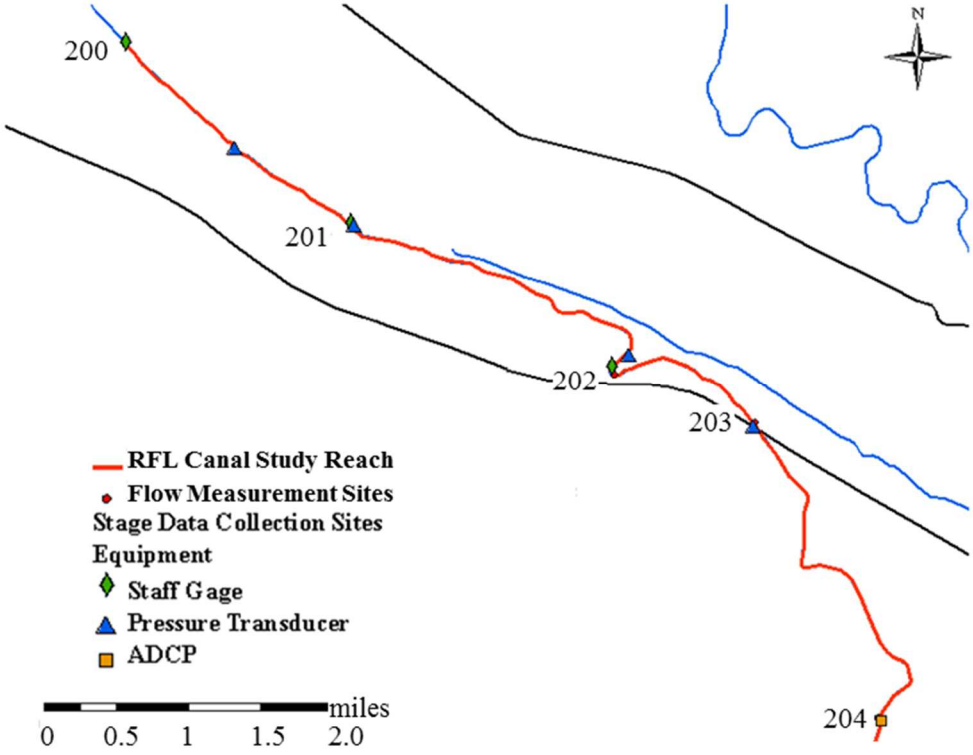

Figure 3-14 Map of the pressure transducers and staff gages on the RFH Canal

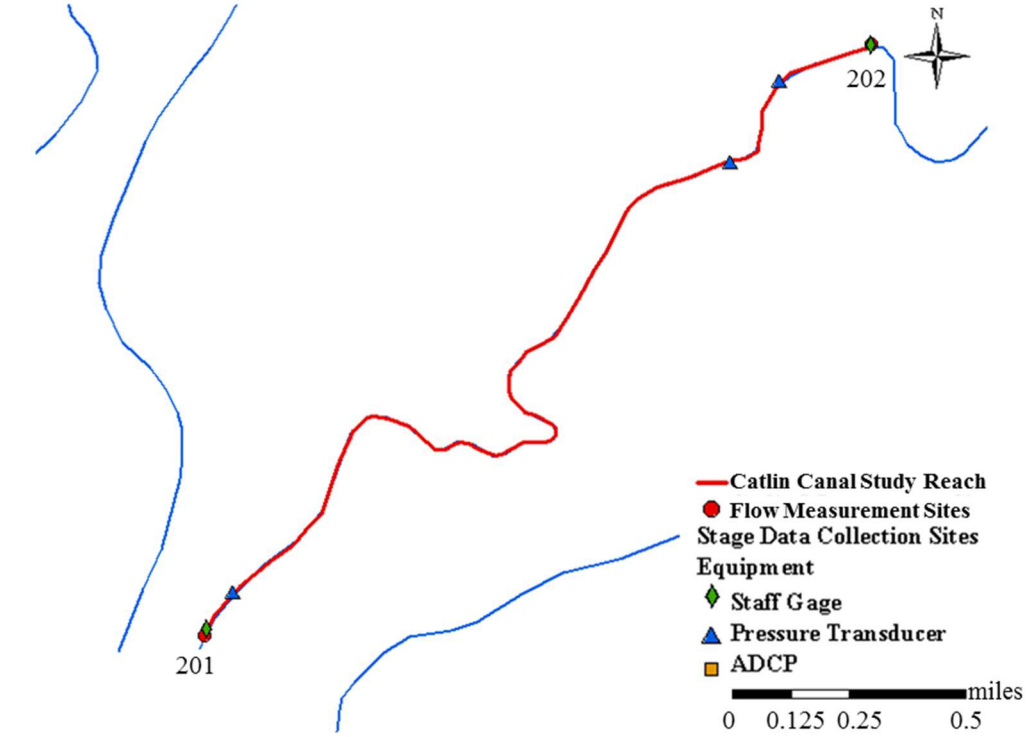

Figure 3-15 Map of the pressure transducers and staff gages on the Catlin Canal

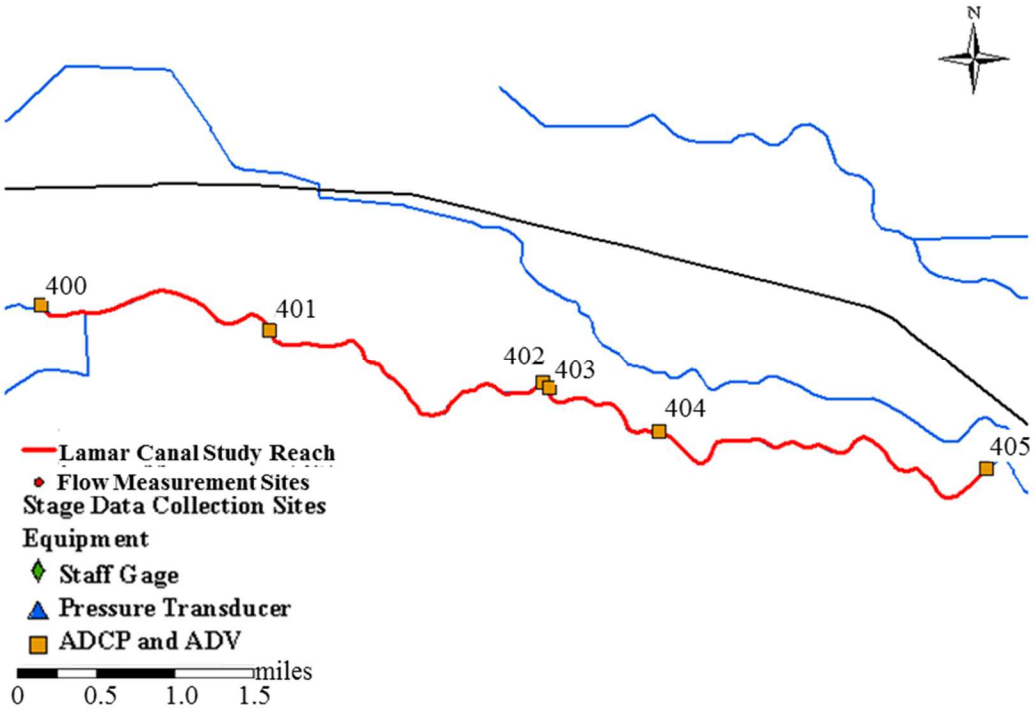

Figure 3-16 Map of the stage measurement locations on the Lamar Canal

3.2.2.1 Staff Gage Measurements

Staff gage plates were mounted to rigid t-posts at Q_{US} and Q_{DS} flow measurement sites, as indicated in Figure 3-14 through Figure 3-16. Each staff gage contained markings spaced every hundredth of a foot so that the flow depth could be read fairly accurately. They were placed near the canal banks where the flow velocity was relatively small so they could be easily read to minimize errors related to the interpretation of where the flow depth was located on the plate. During discharge measurements, stage was recorded by a measurement technician every 5 to 15 minutes, or more frequently if stage was rapidly changing. They remained installed through the end of the 2007 water year, allowing for comparisons of flow depth and allowing the 2006 depth measurements to be related to the cross-sectional surveys that were completed in 2007. They were observed to remain firmly in place during both water years as their elevations and locations appeared (visually) to remain unchanged.

3.2.2.2 Flow Depth Measurements with ADV and ADCP Equipment

The flow depth was measured manually and recorded at every velocity measurement station during ADV operation. The ADCP tracked the channel bed as it is traversed from one canal bank to the other during discharge measurements. From the data, the thalweg depth could be identified and tied to cross-sectional survey data under the assumption that significant temporal changes of the thalweg elevation did not occur. If a staff gage was present at the flow measurement site, the ADV or ADCP data were not used for the stage measurements for a variety of reasons. Principally, the staff gages remained at one location that was surveyed and did not depend upon the assumption that the thalweg elevation did not vary significantly over time, which likely was violated to some degree due to sediment deposition, bed erosion, and changing bedload that occurs under various flow velocities. Also, the wading rods used for

ADV measurement had markings spaced every 0.1 feet, as opposed to every 0.01 feet on the staff gages. In some cases, no staff gages or pressure transducers were present at measurement locations during flow rate measurements, so the ADV and ADCP were the only sources of stage data.

3.2.2.3 Pressure Transducer Measurements

After the studies in 2006, it was determined that stage measurements at locations between measurement sites would be more beneficial for accurately calculating hydraulic properties and identifying storage changes. Thus, in 2007, pressure transducers (Onset HOBOs and In-Situ LevelTROLL 300s) were installed within the Catlin, RFH, and Fort Lyon Canal study reaches and were used to automatically measure absolute pressure (converted into water depth) over short time increments (no longer than 15 minutes). The transducers were firmly mounted to rigid t-posts placed in the vicinity of a canal bank at locations intermediate to the Q_{US} and Q_{DS} flow measurement sites. The t-posts were pounded deep enough into the ground that they remained stable against the drag forces of flowing water and captured debris. Data from the pressure transducers were downloaded approximately once monthly to ensure they were operating properly and to prevent the loss of significant amounts of data if a problem did occur. All pressure transducers were calibrated prior to launching by placing them in a bucket of water and comparing the readings to manual water depth measurements. This process was completed using different depths of water, similar to those expected in the canals, to ensure that the pressure transducers were reading accurately. They were setup to measure absolute pressure, so in order to calculate gage pressure that was converted into water depth, at least one atmospheric pressure transducer, an In-Situ BaroTROLL, was installed near the middle of each canal study reach.

3.2.3 Water Surface Interpolation

A process for interpolating the location of the water surface was completed to estimate the stage at each surveyed cross-section where stage was not measured, based upon the longitudinal profile and collected stage data. Water surface slope between known stage elevations was calculated and a linear interpolation to intermediate cross-sections was conducted. This was completed using the following relationship:

$$WSE_2 = WSE_1 - L_{1-2}\left(\frac{WSE_1 - WSE_3}{L_{1-2} + L_{2-3}}\right) \tag{3.15}$$

As depicted in Figure 3-17, L is the canal length between cross-sections and WSE_i is the water surface elevation at cross-section i (measured at cross-sections 1 and 3 and interpolated to cross-section 2). The water surface slopes used for the interpolation process were the slopes between bounding cross-sections of known water surface elevations, not the average water surface slope over the entire reach.

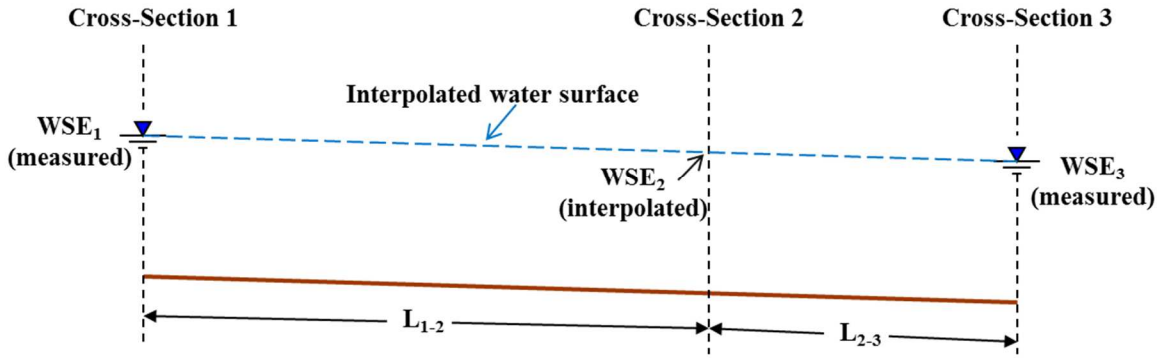

Figure 3-17 Depiction of a water surface interpolation

3.2.4 Calculation of A_{WS} and A_P

Canal free water surface area was used to calculate free-water evaporation and wetted perimeter area was used to quantify seepage rates in terms of flow rate per unit wetted area of channel. This method of reporting seepage was adopted to account for variations related to

different flow rates, stages, and wetted perimeter geometries among different seepage measurements.

Prior to calculating A_{WS} and A_P, T_w and P had to first be calculated at each surveyed cross-section based upon the stage data and water surface interpolation results. T_w and P were calculated for every 0.01 foot of flow depth above the thalweg for all surveyed cross-sections. Since survey points were not collected at every 0.01-ft increment above the thalweg, an interpolation had to be conducted in order to calculate T_w and P. For an example of how this interpolation was completed, refer to Figure 3-18, which depicts an example surveyed cross-section. The location where the water surface would intersect each channel bank had to be interpolated for each 0.01-ft flow depth increment. This process was completed using the following equations, where x_L represents the water surface intersection with the left bank, x_R represents the water surface intersection with the right bank, and D_{TH} represents the incremental flow depth above the thalweg:

$$x_L = x_0 + \left(D_{TH} - y_0\right)\left(\frac{x_i - x_0}{y_i - y_0}\right) \tag{3.16}$$

$$x_R = x_n + \left(D_{TH} - y_n\right)\left(\frac{x_f - x_n}{y_f - y_n}\right) \tag{3.17}$$

Where:

x_i = x-coordinate of survey point immediately to the right of the water surface on the left canal bank.

y_i = y-coordinate of survey point immediately to the right of the water surface on the left canal bank.

x_o = x-coordinate of survey point immediately to the left of the water surface on the left canal bank.

y_o = y-coordinate of survey point immediately to the left of the water surface on the left canal bank.

x_f = x-coordinate of survey point immediately to the right of the water surface on the right canal bank.

y_f = y-coordinate of survey point immediately to the right of the water surface on the right canal bank.

x_n = x-coordinate of survey point immediately to the left of the water surface on the right canal bank.

y_n = y-coordinate of survey point immediately to the left of the water surface on the right canal bank.

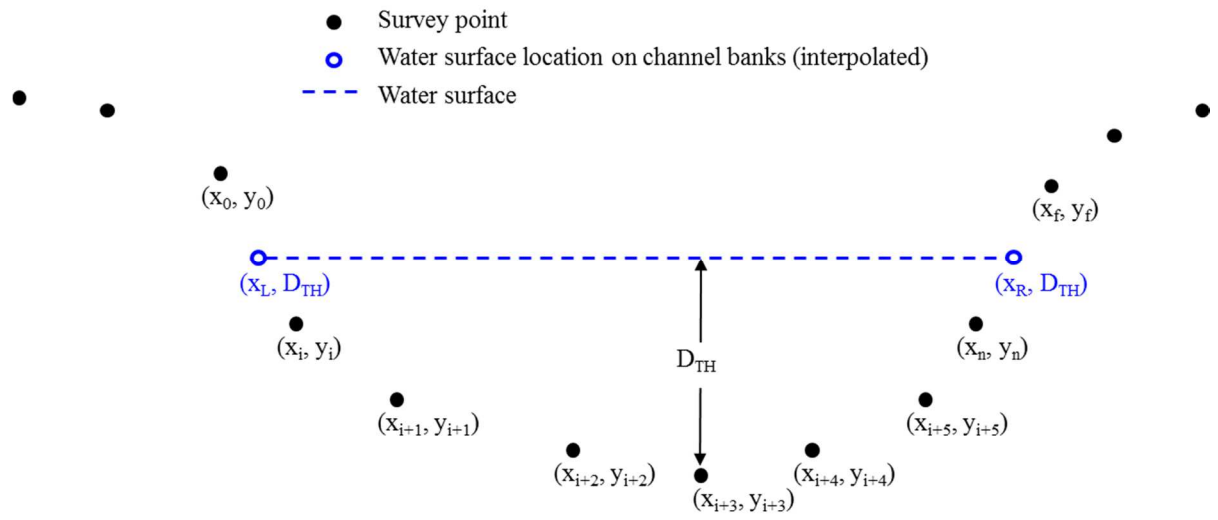

Figure 3-18 Depiction of an example cross-section to illustration the interpolation of T_w and P

The values of T_w and P for each incremental thalweg depth were calculated using the following equations:

$$T_w = |x_R - x_L| \tag{3.18}$$

$$P = \sqrt{(x_i - x_L)^2 + (D_{TH} - y_i)^2} + \sqrt{(x_R - x_n)^2 + (D_{TH} - y_n)^2} + \sum_{i+1}^{n} \sqrt{(x_{i+1} - x_i)^2 + (y_{i+1} - y_i)^2}$$

(3.19)

T_w was calculated simply as the straight line distance between the banks for each water depth, and P was calculated using the Pythagorean Theorem between survey points within a cross-section up to the specific flow depth.

With the water surface interpolated longitudinally over the length of the study reach, the flow depth at each cross section was calculated as the water surface elevation minus the thalweg elevation. The flow depth was then used to calculate T_w and P, as discussed in Section 5.1.2.

A weighted average technique was used to calculate both the average A_{WS} and average A_P over the time period in which seepage measurements were conducted, using the top width and wetted perimeter at each surveyed cross-section, respectively. A cross-section was assumed to represent the canal prism extending between that cross-section to the midpoint of the adjacent cross-sections. For an example of how this calculation was performed, please refer to the depiction of a canal study reach in Figure 3-19, where L_i and P_i represent channel length between cross-sections i and $i+1$ and wetted perimeter at cross-section i, respectively.

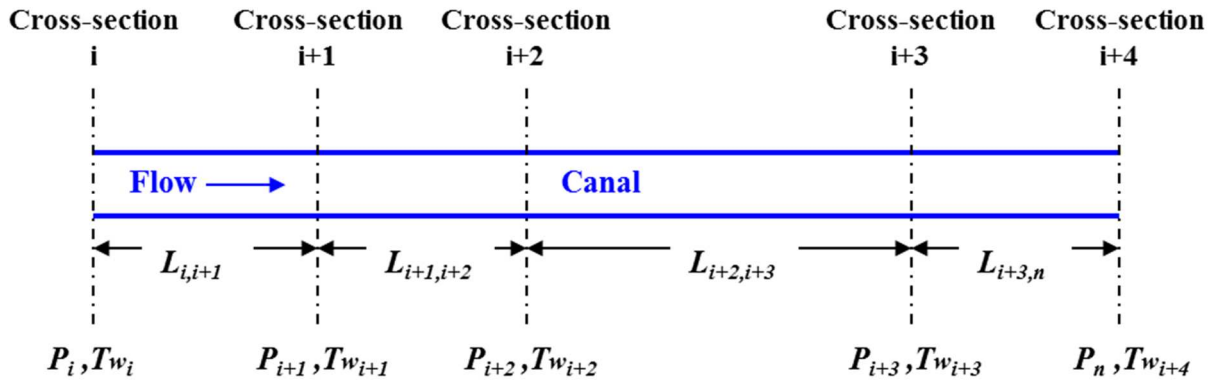

Figure 3-19 Depiction of a canal study reach

After calculating the wetted perimeter at each cross-section and the channel length between cross-sections, a total wetted perimeter area of the study reach, A_P, was computed as:

$$A_P = P_i\left(\frac{L_i}{2}\right) + P_{i+1}\left(\frac{L_i + L_{i+1}}{2}\right) + P_{i+2}\left(\frac{L_{i+1} + L_{i+2}}{2}\right) + P_{i+3}\left(\frac{L_{i+2} + L_{i+3}}{2}\right) + \ldots + P_n\left(\frac{L_{n-1}}{2}\right) \quad (3.20)$$

The total water surface area, A_{WS}, in a study reach was computed similarly:

$$A_{WS} = T_{w_i}\left(\frac{L_i}{2}\right) + T_{w_{i+1}}\left(\frac{L_i + L_{i+1}}{2}\right) + T_{w_{i+2}}\left(\frac{L_{i+1} + L_{i+2}}{2}\right) + T_{w_{i+3}}\left(\frac{L_{i+2} + L_{i+3}}{2}\right) + T_{w_n}\left(\frac{L_{n-1}}{2}\right) \quad (3.21)$$

Since water levels vary temporally during seepage measurements, even if only by a small amount, the top width and wetted perimeter of each cross-section changes. To account for this variation, average values of top width and wetted perimeter over the period of seepage measurement were used to calculate A_{WS} and A_P, respectively.

3.2.5 Potential Sources of Uncertainty in Calculating Hydraulic Geometry

If a cross-section is not adequately representative of its associated canal reach, errors will result related to spatial variability. In order to reduce this error, spacing between cross-sections where hydraulic geometry characteristics were measured was decreased based upon visual observations. The geometry of the studied canals seemed fairly uniform over short reaches, so it was assumed that cross-sectional surveys at intervals no greater than 0.2 of a mile were adequate.

Potential sources of measurement error related to the surveying process included: (1) not holding the surveying rod (when using the level) or prism pole (when using the total station) vertically, which would result in vertical distance measurements not truly representative of the surveyed points; (2) inadequate leveling of the survey instrument that is required to obtain accurate elevation differences among survey points; (3) temporal changes in the thalweg elevations caused by moving bedload; (4) sinking of the survey rod into the loose channel bed during cross-sectional surveying; (5) movement or settling of the pins placed into the ground at

each cross-section for the longitudinal survey as potentially caused by impact from vehicles, impact from people, settling, or movement from other sources; and (6) conducting a skewed cross-sectional survey that was not perpendicular to the channel banks and resulted in a inaccurately extended channel width. Proper surveying protocol and techniques were used to ensure than any potential errors were minimized or eliminated. A careful attempt was made to eliminate each of the listed sources of errors during cross-sectional surveying and longitudinal surveying; however, some degree of error likely occurred.

Potential errors in stage readings directly result in errors related to calculating the top width and wetted perimeter, both of which are important components to seepage characteristics. There errors could have come from a variety of sources since water levels were measured using multiple techniques. The major sources of uncertainty related to staff gage readings include: (1) subjective errors caused by technicians reading staff gages under their own individual interpretation; (2) reading the staff gages incorrectly; (3) movement of the staff gages over time due to impact from floating debris, hydrodynamic forces, or settling of the t-posts into the channel (causing them to no longer be vertical or to be surveyed at a location different than the locations when previous measurements were conducted). The major sources of uncertainty for pressure transducer readings include: (1) equipment problems leading to inaccurate pressure readings; (2) atmospheric pressure variations along a study reach, since typically only one atmospheric pressure transducer was deployed and was located near the center of the study reach; (3) movement of the t-post to which the pressure transducers were mounted as caused by floating debris, hydrodynamic forces, and settling of the channel bed; (4) movement of the pressure transducers on the t-post caused by the same sources as (3), which creates error related to the location at which they were surveyed; and (5) not re-attaching the pressure transducer to the t-

post at the exact same location each time after downloading data (which required temporary removal of the pressure transducer from the canal).

Temporal changes in cross-sectional geometry also could have affected the accuracy of results. Surveying was completed throughout 2007; however, canal geometry likely was different during the 2006 studies and was changing over the course of 2007. Possible sources of error related to these temporal canal changes include: (1) erosion caused by hydrodynamic forces; (2) erosion caused by people, livestock, or vehicles entering and exiting the canal; (3) sediment deposition; (4) bed erosion or changes in bedload; (5) removal or decay of vegetation from channel banks that could lead to erosion or an immediate channel changes; (6) placement of rip-rap or other erosion preventive materials along channel banks; and (7) construction or removal of in-channel structures and flow regulatory devices including weirs, gates, bridges, and flumes. However, no major changes to the canal were visually observed in either water year or between water years.

4 PAM APPLICATIONS

4.1 PAM APPLICATION METHODS

Applications of PAM were completed on canal study reaches by starting at the downstream boundary and traveling in the upstream direction, continuously dispersing granular PAM onto the canal water surface by either walking the canal or travelling in a small motorized boat. Traveling in the upstream direction prevented repeated application of PAM to the same parcel of water. PAM was dispensed with either an automated, battery-powered spreader mounted to a boat or with handheld spreaders. During the application process, protective gear including eye goggles, dust masks, and gloves were worn to prevent exposure of PAM to the body. During boat applications the travel velocity was great enough to cause PAM to fly back into the boat, so full-body coveralls were worn for protection.

Susfalk et al. (2008) concluded that turbidity levels of canal water should ideally exceed a minimum level of approximately 80 to 100 Ntu for the targeted application rates of 10 to 15 pounds of PAM per wetted canal acre for effective channel perimeter sealing. As such, PAM applications were completed during conditions when the measured turbidity levels met these standards.

The total amount of PAM to be applied during an application was calculated as the product of the target application rate (weight per unit area of wetted canal) and the estimated wetted perimeter area of the canal study reach. Since the type of PAM used was assumed to contain a 92% active ingredient and have a 4% moisture content, the weight of effective PAM was used for all measurements rather than the total weight of the Stokopam® granular product. For example, 10 pounds of Stokopam contains approximately 8.9 pounds of effective PAM

ingredient. The weight to be applied per 0.1 miles of canal was then measured and placed into small, sealing plastic bags. During an application, a truck was driven along the canal road to act as a pace-setter, to carry the PAM not yet dispersed, and to re-supply the applicators with PAM. The truck would drive ahead of the application technicians and stop at approximate 0.1 mile increments along the canal. The small bags of PAM were dispersed to the canal water at an even rate until the idle truck was reached. At this point, the spreader(s) were refilled with another bag of PAM and the truck would again drive ahead and stop at the next 0.1-mile increment. This process was completed throughout the length of the study reach in an attempt to apply PAM at a consistent rate.

A "clear zone" in canal water develops downstream of a PAM application point when flocculates of suspended sediment settle to the channel bottom resulting in less turbid water (Susfalk et al., 2008). Susfalk et al. (2008) suggested that PAM must be allowed a certain distance to travel downstream, which is dependent upon canal velocity, in order for flocculation and sediment deposition to be complete. Thus, PAM was applied an appropriate distance upstream of the upstream study reach boundary when LARV canal conditions and features allowed for such a procedure. This process ensured that PAM was allowed enough time for flocculation and that the entire study reach was fully treated.

Additional details regarding the evaluation of PAM applications can be found in Susfalk et al. (2008).

4.1.1 PAM Applications via Motorized Boat

The first method of application, which was predominantly used for the field experiments, included the use of a small boat equipped with an outboard motor powerful enough to travel upstream against the water current. The benefits of using a boat for PAM application include

time efficiency, increased hydration of PAM due to better mixing with canal water caused by the turbulence created by the boat motor, along with consequent well-balanced dispersion throughout the application area. PAM was dispersed onto the water surface using an automatic spreader (Herd, Logansport, IN), as shown in Figure 4-1, or with two hand-operated spreaders, as shown in Figure 4-2. PAM was discharged from the automated spreader over a window of approximately 180 degrees in front of the boat, allowing the full canal width to be covered. This process required one application technician and a boat driver. The power of the automated spreader was controlled by adjusting a lever mounted to the base of the spreader. The power controlled the rate of dispersion and controlled the distance that PAM could be ejected from the spreader. The power was adjusted so that PAM could be dispersed at a constant rate over the 0.1-mile increments and to eject PAM over the entire canal width while preventing it from reaching the canal banks. If numerous features were located in the canal, such as low-lying bridges and fences, that obstructed free passage of the elevated automated spreader, handheld spreaders were used to disperse PAM. In such cases, two application technicians within the boat were required (in addition to the boat driver) on each side of the boat facing each canal bank so that PAM could be spread evenly across the entire free water surface.

The automated spreader was more time-efficient, having the ability to disperse PAM more quickly than two technicians operating hand-powered spreaders. Time efficiency minimized application costs as labor was reduced. Operation of an automated spreader required one less technician than operation of hand-powered spreaders, which also reduced labor cost. Estimates from cost analysis show that labor costs using an automatic spreader are less than a third of the cost per mile of application than those using manual spreaders (discussed in Section 4.3). The main disadvantage of the automated spreader was less control over the landing area of

the ejected PAM. The increased boat speed and higher release height from the boat resulted in a larger quantity of PAM that flew back into the boat, never reaching the water surface. However, the amount of PAM that ended up in the boat was a very small percentage of the total application amount.

Figure 4-1 PAM application with a boat on the RFH Canal using an automatic spreader

Figure 4-2 PAM application with a boat on the Lamar Canal using handheld spreaders

4.1.2 PAM Applications via Walking the Canal

In cases when the use of a boat was not feasible, the boat was unavailable, or the boat was not operating, two application technicians walked within the canal traveling in the upstream direction and dispersed PAM onto the water surface using handheld spreaders (Figure 4-3). This application technique was more time consuming and did not mix the PAM with the canal water as effectively as did application from a boat. It resulted in much higher labor costs and potentially less seepage reduction. However, applying PAM by walking the canal was an acceptable option, especially when the canal was too shallow to use a boat, when the boat was not operational, or when too many obstacles (bridges, flumes, fences, and siphons) were present for efficient transport. Walking the canal during applications resulted in an even and continuous application over the canal reach and allowed for better control over the landing area of the dispersed PAM.

Figure 4-3 PAM application on the RFH Canal by walking the canal with handheld spreaders

4.2 FIELD PAM APPLICATION DESCRIPTIONS

Granular linear anionic PAM was used for all field applications to LARV canals in 2006 and 2007. PAM applications and seepage reduction studies were conducted on the Lamar, RFH, and Catlin canals, as described in the following sections. A summary of PAM applications in the LARV is presented in Table 4-1. Canal distances between measurement sites were presented in Table 2-1. Additional details of the field PAM applications can be found in R. Susfalk et al. (2008).

Linear anionic PAM was obtained from JT Water Management, LLC of Parker, Colorado. This particular type of PAM, called Stokopam®, had a minimum molecular weight of 12 million grams per mole, an anionic charge density of 30% ± 5%, and an assumed 92% active ingredient with a moisture content of 4%.

Table 4-1 Summary of PAM applications in the LARV

Canal	Application Date(s)	Reach Studied for Seepage Reduction	Reach Length (mi)	PAM Application Rate		Total Weight of Applied PAM (lbs)
				lbs/ac	lbs/mi	
Lamar	June 7, 2006	Site 401 to Site 405	7.4	11.2	27.2	201
RFH	June 29-30, 2006	Site 201 to Site 206	19.9	11.9	45.3	901
RFH	July 20, 2006	Site 201 to Site 202	3.8	12.7	64.4	245
Catlin	June 3, 2006	Site 201 to Site 202	3.0	16.3	49.0	147
Catlin	August 7, 2007	Site 201 to Site 203	2.4	10.8	42.1	101

4.2.1 PAM Application to Lamar Canal 2006

PAM was first applied to the Lamar Canal on May 18, 2006. However, canal flow rates were relatively low, suspended sediment concentrations were low, and seepage rates prior to PAM application were estimated to not exceed measurement errors; hence, the test was deemed inadequate. Additional details are presented in Susfalk et al. (2008).

As a result, a second PAM application was conducted on the Lamar Canal on June 7, 2006 when conditions were considered to be more suitable. The application began at Site 205 and granular PAM was dispersed with two hand spreaders traveling 7.4 miles in the upstream direction to Site 200. The average application rate was about 27.2 lbs/mi or 11.2 lbs/wetted acre.

4.2.2 First PAM Application to RFH Canal 2006

The first PAM application on the RFH canal in 2006 was conducted on a 19.9-mile reach between sites 201 and 205. The application spanned two days from June 29 to June 30. A total of 901 effective lbs (1012 total lbs) of PAM were applied at a rate of about 45.3 lbs/mi or 11.9 lbs/wetted acre. The granular PAM was applied from a motorized boat traveling in the upstream direction with PAM being dispersed from an automatic spreader.

4.2.3 Second PAM Application to RFH Canal 2006

The second PAM application on the RFH Canal in 2006 was conducted on July 20 when the observed turbidity levels in the canal water (270 Ntu) were much higher than normal due to a recent thunderstorm event that washed sediment into the Arkansas River upstream of the RFH Canal headgate. PAM was applied over a much shorter reach than was the first application. This segment of canal contained the majority of the seepage that was measured along the reach of the first application. The second application was conducted using a motorized boat that dispersed granular PAM with an automatic spreader starting at Site 202 and traveling 3.8 miles in the

upstream direction. A total of 245 effective lbs (275 total lbs) of PAM were applied to the canal's water surface for an application rate of about 64.4 lbs/mi or 12.7 lbs/wetted acre.

4.2.4 PAM Application to Catlin Canal 2006

PAM was applied to the Catlin Canal on June 3, 2006 using a motorized boat with two hand spreaders. The flow diversions within the application reach were shut down at the time of PAM application. A total of 147 effective lbs (165 total pounds) of granular PAM were applied over a 3 mile reach that extend 0.3 miles upstream and 0.3 miles downstream of sites 201 and 202, respectively, thereby encompassing the seepage reduction study reach between sites 201 and 202. The application rate was approximately 49.0 lbs/mi or 9.00 lbs/wetted acre.

4.2.5 PAM Application to Catlin Canal 2007

PAM again was applied to the Catlin Canal on August 7, 2007. The application technique again implemented a motorized boat driven in the upstream direction with two hand-operated spreaders used to disperse the PAM onto the canal's water surface. A total of 101 effective lbs (114 total pounds) of Stockopam were applied over a 3 mile reach of canal, for an application rate of about 33.8 lbs/mi or 10.8 lbs/wetted acre. Seepage rates were measured before and after application on August 7, as described in Section 6.

4.3 COST ANALYSIS OF POLYACRYLAMIDE APPLICATIONS

The cost of applying PAM to earthen irrigation canals includes the PAM, labor, equipment, and vehicle operation. Based upon the studies in the LARV, the unit price of granular PAM with a minimum of 90% active ingredient averaged about $4.00 per pound (Swihart 2007). Note that this cost analysis originally was provided for (Susfalk et al. 2008), but the results herein are updated to represent 2014 US dollars.

Labor costs for PAM applications depend upon the number of workers and their hourly wages. It also is dependant on the technique (using an automatic spreader requires one less technician) and speed of application (labor costs decrease as application speed increases). Based on research experience in the Arkansas River Valley over the past two years, it generally takes up to four technicians to complete the application process. Typically, one or two people spread the PAM over the canal water from inside a boat, one person drives the boat, and another person drives a truck alongside the canal road to carry the PAM and to refill the boat with PAM when necessary. If all four workers make between $15.00 and $20.00 per hour, the total cost of labor averages about $70.00 per hour. Using handheld spreaders, two workers are required to apply the PAM and the speed of application averages approximately one canal mile per hour. Using an automatic spreader, only one person is required to apply the PAM and the speed would average around three canal miles per hour. The actual speed of application is dependant upon the number of obstacles in the canal, experience of the technicians, dependability of equipment, and boat motor size. These variables can vary the speed of application greatly. In a canal with many low-lying bridges, fences, and other obstacles, more time should be expected for completion of the application process. The cost analysis presented herein is based upon average application time requirements from the 2006 and 2007 field studies in the LARV. In these studies, time of application varied from about 0.22 hours per mile to 1.22 hours per mile and averaged about 0.75 hours per mile over five applications. The cost of application planning, equipment cleaning and maintenance, and mobilization were included in the labor cost calculations. It was assumed that two people can complete the tasks of planning and cleaning per application over a time period of five hours. In order to convert the associated labor costs, the assumption was made that an average application would cover about 10 miles.

Equipment necessary for PAM application in canals includes a small boat, a low horsepower boat motor, protective gear, and hand-powered seed spreaders or an automatic spreader to discharge the PAM. It was assumed that a new boat and motor (5 to 10 horsepower) should be attainable for a total purchase price of $3,000. It also was assumed that handheld seed spreaders can be purchased new for about $10 apiece, totaling $20 for two technicians applying PAM. A new automatic spreader can be purchased for about $400. An automatic spreader must be mounted on the front of the boat which will likely require some custom fabrication with associated labor and supplies. It was assumed that all costs associated with the fabrication process would total about $300.

Protective gear should be used by everyone inside the boat while the PAM application is taking place. It was assumed that eye-protection and disposable respiratory masks cost $10 per person per application. Body protective suits such as Tyvek coveralls ($55.00 for a case of 25) should be worn to minimize skin contact and to prevent ruining clothing.

A truck, or other type of vehicle, is necessary to carry bags of PAM (each typically weighing 50-55 pounds) and to act as a pace setter. Due to stop-and-go driving and frequent idling of the vehicle, a fuel efficiency of about 10 miles per gallon (or less) can be expected from the vehicle. Clearly, this will vary depending on the type of vehicle and the idle time. Based upon the 2006 and 2007 studies, boat gas mileage was approximately 2 miles per gallon for a 10-horsepower boat motor. However, gas mileage may vary drastically from one motor to the next. For this analysis, the unit cost of gasoline was assumed to equal $3.25 per gallon.

The total cost of a PAM application varies with canal width and application technique. Estimated application costs on the Catlin, Lamar, and RFH canals are provided in Table 4-2. The average wetted perimeter for each canal varies, affecting the total application cost. In Table

4-2, it was assumed that labor wages total $70 per hour, PAM costs $4.00 per pound, gasoline prices total $1.95 per canal mile, and PAM application rates are either 10 or 15 pounds per wetted acre. Fuel economy related to boat speeds that vary by application technique was not accounted for in this analysis. A cost of vehicle operation was added to the table based upon a typical rental or compensation rate of $0.50 per mile.

Table 4-2 PAM application cost comparison for the Catlin, Lamar, and Rocky Ford Highline canals

Variable	Catlin Canal	Lamar Canal	RFH Canal
Avg. Canal Wetted Perimeter (ft)	25	20	35
Unit Area (wetted acres/mile)	3.03	2.42	4.24
PAM ($/mile)			
10 lbs/wetted acre	$121.21	$96.97	$169.70
15 lbs/wetted acre	$181.82	$145.45	$254.55
Labor ($/mile)			
Auto Spreader	$48.51	$48.51	$48.51
Manual Spreader	$84.77	$84.77	$84.77
Vehicle Use ($/mile)	$0.50	$0.50	$0.50
Gasoline ($/mile)			
Truck	$0.35	$0.35	$0.35
Boat	$1.75	$1.75	$1.75
Total Cost ($/mile)			
Minimum	$172.32	$148.08	$220.81
Maximum	$269.19	$232.82	$341.91
Average	$220.75	$190.45	$281.36

4.4 COST COMPARISON WITH CONVENTIONAL CANAL LININGS

Conventional canal lining materials include concrete, fluid-applied membrane, and geomembrane. These materials have a much greater cost per area for construction and maintenance than PAM applications; however, PAM must be applied at least once per year while the alternative materials will last between 10 and 60 years.

Table 4-3 presents a comparison among PAM application and conventional canal linings. All lining data, except those for PAM, were published originally by Swihart and Haynes (2002). Costs were adjusted to 2014 US dollars using the inflation rates (USDL 2014). The 10-year projected costs were calculated using a 3-percent annual inflation rate.

The total annual cost over 10 years for PAM applications is represented as a range in Table 4-3. The low end of the range represents one annual application at 10 lbs/acre and the upper end represents one application at a rate of 15 lbs/acre. This total cost includes granular polyacrylamide, labor, gasoline, application equipment (boat and spreaders), vehicle expenses, and protective gear. The equipment prices include the cost of a new boat and spreader that are assumed to function properly for 10 years at a work rate of 250 canal wetted acres per year.

PAM can be less effective than conventional lining materials in reducing seepage from earthen irrigation canals based upon Swihart and Haynes (2002) and the canal seepage data collected during the field studies of 2006 and 2007; however, the cost of application is significantly lower. For one PAM application per year to the same canal reach over 10 years, the greatest cost is $855 per acre, as shown in Table 4-3. This cost is approximately 0.5%, 0.7%, 1.2%, and 0.6% of the total average annual cost of fluid-applied membrane, concrete, exposed geomembrane, and geomembrane with a concrete cover canal linings, respectively.

Table 4-3 Cost comparison (2014 USD) between PAM applications and conventional canal lining materials

Lining Material	Construction Cost ($/acre)	Maintenance Cost ($/acre-year)	Durability (yr)	Effective Seepage Reduction	Total Average Cost over 10 years ($/acre)*
Fluid-applied membrane	$80,500 - $249,000	$575	10 - 15 yrs	90%	$171,500
Concrete	$110,400 - $134,000	$290	40 - 60 yrs	70%	$125,600
Exposed Geomembrane	$45,000 - $88,000	$575	10 - 25 yrs	90%	$73,200
Geomembrane with Concrete Cover	$140,000 - $146,000	$290	40 - 60 yrs	95%	$146,000
	Application Cost ($/acre/application)	**Re-Application Rate (App/year)**	**Durability (yr)**	**Effective Seepage Reduction**	**Total Average Cost over 10 years ($/acre)****
Polyacrylamide	$45 - $82	1 - 2 times	< 1 year	30% - 90%	$626 - $855

* Based upon 3% annual inflation rate for maintenance

** Based upon 1 application per year

5 UNCERTAINTY ANALYSIS OF CANAL SEEPAGE

Monte Carlo simulation was used to analyze the uncertainty in estimating canal seepage using measurements made with the inflow-outflow method. Monte Carlo simulation was conducted using Palisade's @RISK software (version 6.0), which is an add-on program for Microsoft Excel™. Uncertainty in the component variables of the inflow-outflow volume balance Equation 3.1 was addressed by modeling the components as random variables with associated probability distribution functions (PDF). Each variable in Equation 3.1 was a function of one or more variables or parameters that were directly measured during inflow-outflow tests using various instruments and methods as described in Chapter 4.

Each directly-measured variable was assumed subject to measurement error such that:

measured value = true value $\pm$ measurement error

Thus, the possible true value of each directly-measured variable was calculated as:

true value = measured value $\pm$ measurement error

An appropriate PDF was adopted for each directly-measured random variable where the mean value was assumed to be the measured value and Monte Carlo simulation was used to generate possible values of measurement error as prescribed percentages of the measured value distributed in probability according to the adopted PDF. Although the type of PDF varied among the different variables, the true value was assumed to have a mean value equal to the value measured in the field. It is acknowledged that the measured value is not the true value due to measurement error, but by assigning an appropriate PDF to each variable, a range of possible values with associated probabilities of occurrence was captured using Monte Carlo simulation.

An approach similar to that described in Harmel and Smith (2007) was used for the analysis, which constitutes analysis of a form of Type B uncertainty as described in Section 1.6.2. For example, if it is expected that a variable, like canal flow rate, can be measured within +/- 5% of the true value with 90% confidence, then the non-exceedance values associated with the probable error range (PER_i) for measuring flow rate were assumed to be equal to 95% and 105% of the measured value, respectively, when applying a normal distribution. Herein, the range of values between the 5th and 95th percentiles of a PDF will be referred to as the 90% interpercentile range (IR).

Uncertainty in some of the component variables in Equation 3.1, namely those dependent on canal stage and hydraulic geometry along the inflow-outflow test reach, is derived not only from measurement error but also from spatial and temporal variability, as described in Sections 3.1.6.3. Canal stage and hydraulic geometry could be measured at only a limited number of times and at only a limited number of locations along the channel reach of the inflow-outflow test. The statistical properties across measurements associated with canal stage and hydraulic geometry at different spatial and temporal locations, as well as the statistical properties associated with measurement error at each space-time location, were used to describe the PDFs associated with canal stage and hydraulic geometry parameters.

Table 5-1 provides a brief summary of probability distributions that were assigned to variables to account for uncertainty derived from measurement error and from spatial and temporal variability, as described in the following sections.

Table 5-1 Summary of probability distribution functions for Monte Carlo simulation

Measurement Type	Variables	Assumed Distribution Type	Error Range/ Confidence Interval*
Discharge Measurements	Q_{US}	normal	+/- 5% @ 90% IR
	Q_{DS}	normal	+/- 5% @ 90% IR
	Q_D	normal	+/- 5% @ 90% IR
	Q_I	normal	+/- 5% @ 90% IR
Predicting Q_{US} and Q_{DS} for unsteady-lagged tests	$\varepsilon_{Q_{US},1-2}$ and $\varepsilon_{Q_{DS},3-4}$	normal	+/- 5% @ 90% IR
	$\varepsilon_{Q'_{US},3}$ and $\varepsilon_{Q'_{US},4}$	normal	+/- 15% @ 90% IR
	$\varepsilon_{Q'_{DS},1}$ and $\varepsilon_{Q'_{DS},2}$	normal	+/- 15% @ 90% IR
Free-water Evaporation	Q_E	normal	+/- 20% @ 90% IR
Canal Stage			
Staff Gage	h	normal	+/- 0.04 feet @ 90% IR
Absolute Pressure	p_{abs}	normal	+/- 0.04 feet @ 90% IR
Atmospheric Pressure	p_{atm}	normal	+/- 0.04 feet @ 90% IR
Hydraulic Geometry *At-a-Station Cross-Section Geometry*	ε_P and ε_{T_w}	logistic	unique to each cross-section
Along-the-Canal Trendline Coefficients	C_{P1}', C_{P2}', C_{P3}'	logistic	unique to each coefficient
	C_{T1}', C_{T2}', C_{T3}'	logistic	unique to each coefficient
Thalweg Elevation	ε_{TH}	normal	unique to each canal reach

*Error ranges were varied in sensitivity analysis of Section 6.4.2.

5.1 HYDRAULIC GEOMETRY UNCERTAINTY ANALYSIS

Uncertainty in describing hydraulic geometry is due to (a) temporal variability, (b) spatial variability, and (c) measurement error. Hydraulic properties used in the inflow-outflow

procedure are functions of T_w and P. From T_w and P, the following parameters and variables in the inflow-outflow equation are calculated:

- A_P
    - Estimated as a function of P (Equation 3.20)
    - Used to normalize values of Q_S in relation to the surface area of the canal perimeter through which seepage occurred ($\hat{Q}_S$)
- A_{WS}
    - Function of T_w (Equation 3.21)
    - Used to calculate Q_E in terms of a the area through which evaporation occurs
- $\frac{\Delta S}{\Delta t}$
    - Function of T_w (refer to Section 5.5)
    - Used to estimate ΔS within the canal reach over the course of the inflow-outflow test

5.1.1 Temporal Variability in Canal Hydraulic Geometry

The perimeter shape of earthen canals changes over time due in part to sedimentation and erosion processes. Sediment in the water diverted from the river is transported into the canal. Sediment transported from tributary streams and overland runoff into the river during and immediately following a storm event usually results in above-average sediment entry into canals. As an example of sedimentation in the LARV, sandy soils were observed on the canal bed in the upstream portions of the RFH canal which were thought to be transported from the sandy bed of the Arkansas River and deposited at the upstream end of the canal due to deceleration of the flow.

Sandy beds were not observed in the lower reaches of the canal, indicating that only finer sediment particles were retained in suspension as the water moved further downstream. Erosion of sediments from the canal perimeter also can occur as a result of multiple factors including animal and human traffic, hydrodynamic forces from flowing water in zones of acceleration, decaying bank vegetation, scour caused by obstructions, etc. In the LARV, erosion caused by animal traffic (i.e. cattle crossings) and flowing water (i.e. bank undercutting) was not uncommon.

The RFH and Catlin canals were surveyed in both 2007 and 2008. Each cross section location was surveyed once, so temporal changes in hydraulic geometry could not be evaluated for the majority of cross-section unless they coincided with locations where ADV or ADCP data had been gathered. Temporal changes due to sediment deposition and erosion over the 2006 and 2007 irrigation seasons were thought to be minimal based upon visual observations. Therefore, temporal variability in hydraulic geometry was not accounted for directly in the uncertainty analysis. Instead, uncertainty associated with variability in hydraulic geometry observed and described along a canal and within a given cross section (at-a-station) was assumed to encompass uncertainty due to short-term temporal changes as well as spatial variability.

To illustrate temporal changes, or the lack thereof, in the RFH and Catlin canals, cross-section data gathered at different times of the year and/or in different irrigation seasons were compared. Examples are presented as Figure 5-1 through Figure 5-5. These data were obtained from cross-section surveys conducted using a total station, a level, ADV measurements, and ADCP measurements, as indicated on the figures. Total station and level survey data were collected in 2007 and 2008, the ADV data were collected in 2006, and the ADCP data were

collected in 2006 and 2007. Differences in the data may be attributed partially to measurement error and not completely to actual changes in canal geometry over the course of time.

In most cases, channel cross sections do not appear to have changed substantially over time, as seen in Figure 5-1 to Figure 5-5. Cross sections from ADV measurements conducted in 2006 match very well with total station and level survey data collected in 2007 and early 2008. The studies spanned only two irrigation seasons, which may not have been a long enough period of time to observe significant temporal changes in hydraulic geometry under the given flow conditions, at least at the locations were flow rate measurements were conducted.

Inflow-outflow tests were conducted over a short time frame (generally one to four hours). Sedimentation and erosion of canals, which can cause temporal variation, may be considered negligible over the short course of a test period, particularly when the canal is operating under normal conditions. As such, it was assumed that temporal variability of hydraulic geometry was negligible during the inflow-outflow measurements.

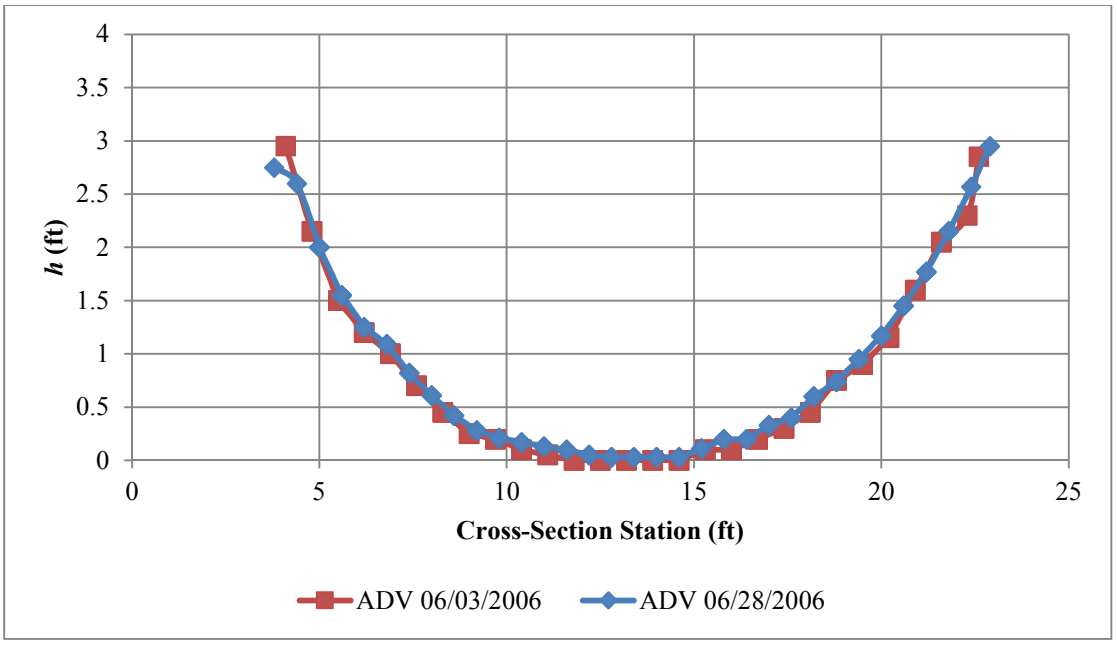

Figure 5-1 Comparison of cross-section geometry surveyed at Catlin Canal Site 201 at the beginning and end of a 25-day interval in 2006

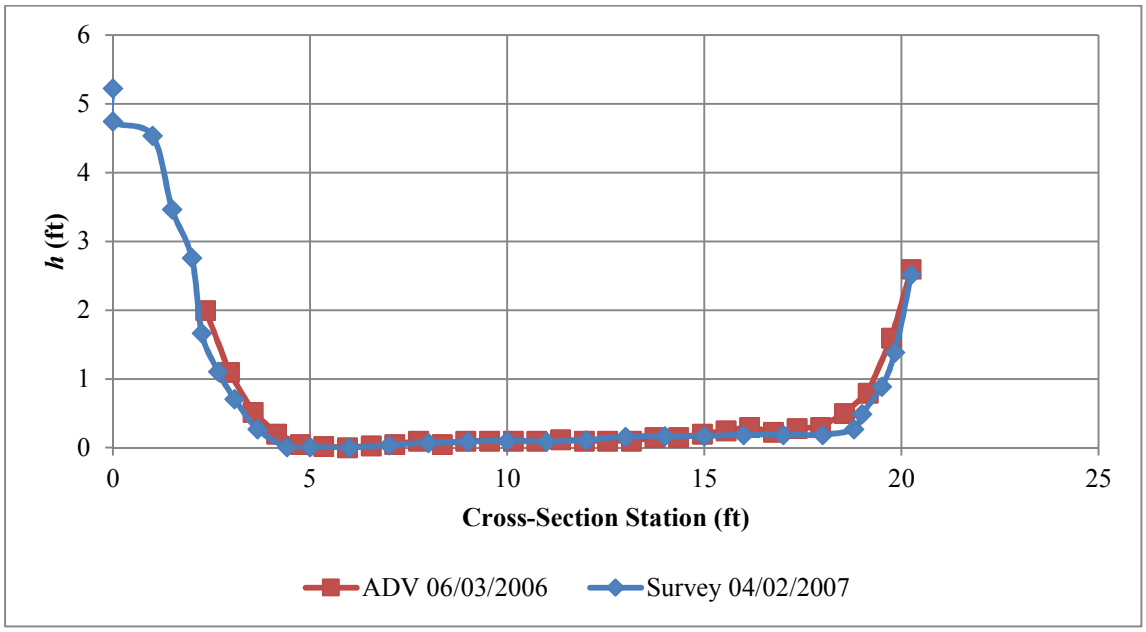

Figure 5-2 Comparison of cross-section geometry surveyed at Catlin Canal Site 202 in June 2006 and in April 2007

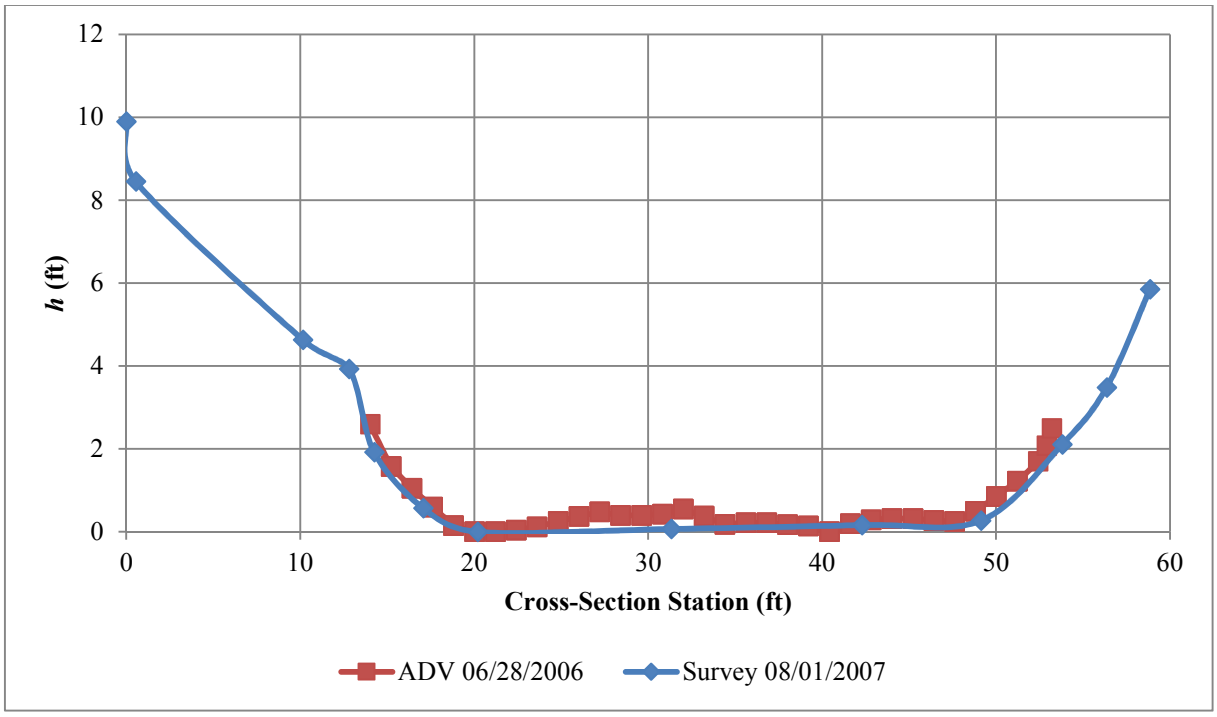

Figure 5-3 Comparison of cross-section geometry surveyed at RFH Canal Site 200 in June 2006 and in August 2007

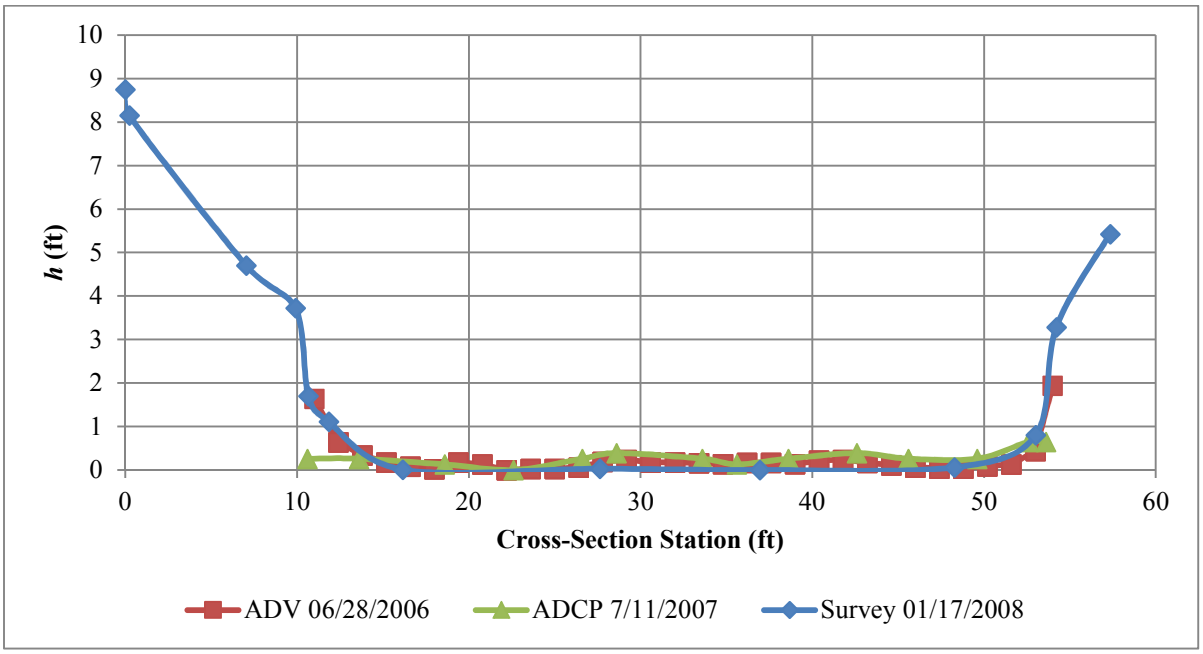

Figure 5-4 Comparison of cross-section geometry estimated with ADV measurement in June 2006, with ADCP measurement in July 2007, and with level survey in January 2008 at RFH Canal Site 201

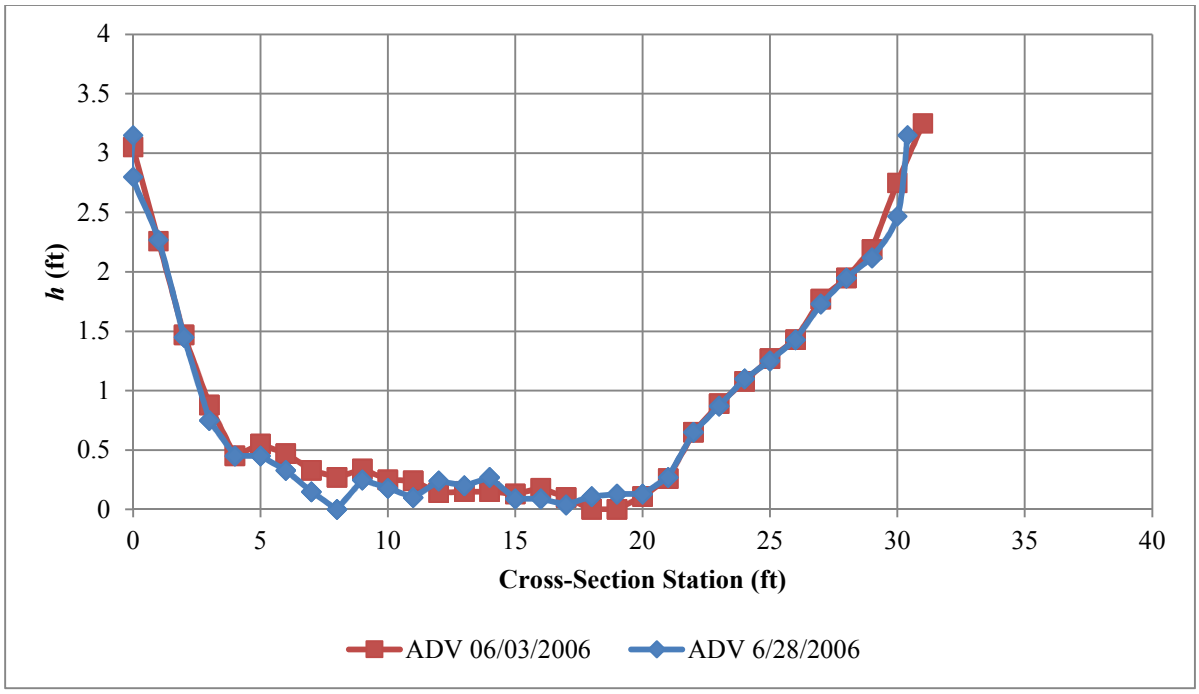

Figure 5-5 Comparison of cross-section geometry estimated with ADV measurement at the beginning and end of a 25-day interval in June 2006 at RFH Canal Site 202

5.1.2 Measurement Error in Characterizing Canal Hydraulic Geometry

Measurement error in hydraulic geometry is associated with the surveying process, during which error sources may include improper leveling of the total station or level, not holding the survey rod vertical, mis-reading of the Philly rod, a misaligned cross-section that is not perpendicular to the principal flow direction, sinking of the survey rod into the canal bed, or displacement of a survey pin.

Measurement errors likely occurred when conducting cross-section surveys along the RFH and Catlin canal study reaches. To account for measurement error, a PDF was developed for each cross section for describing the distribution of random errors defined as the difference between couplets of P or T_w values estimated from surveys of channel cross-section perimeter and corresponding h values and fitted regression relationships between P or T_w and h. The

random error associated with estimating P from h at a cross section is designated as ε_P and that associated with estimating T_w from h as ε_{Tw}, and the development their respective PDFs is discussed in this section.

The following steps were taken to develop the PDFs used to estimate and model values of ε_P and ε_T:

1. Fit regression relationships of P vs h and T_w vs h using surveyed cross-section data;
2. Calculate values of ε_P and ε_{Tw} from the measured data and fitted relationships; and
3. Assign a PDF to the values of ε_P and ε_{Tw}, unique to each surveyed cross-section.

Fitting Regression Relationships of P vs h and T_w vs h for each surveyed cross-section:

A function relating wetted perimeter, P, to thalweg flow depth, h, and a function relating water surface top width, T_w, to h were fit for each cross-section over the range of h values that were observed during field measurements. Multiple function types were considered including linear, logarithmic, power, polynomial, and exponential. In the end, it was discovered that a second order polynomial function was the most representative of both P vs. h and T_w vs. h. Buhman et al. (2002) found that for natural river channels a power function best fit the cross-sectional data. Although power functions fit the LARV canal data reasonably well for the majority of the cross-sections that were surveyed, they did not fit the surveyed cross-sections as well as second-order polynomial functions of the following form:

$$P = C_{P_1} h^2 + C_{P_2} h + C_{P_3} \tag{5.1}$$

$$T_w = C_{T_1} h^2 + C_{T_2} h + C_{T_3} \tag{5.2}$$

wherein C_{P_1} , C_{P_2}, C_{P_3}, C_{T_1}, C_{T_2}, and C_{T_3} are fitted least-squares regression coefficients.

Figure 5-6 and Figure 5-7 present example best-fit relationships of P and T_w to h using survey data for two cross-sections on the RFH Canal and Catlin Canal, respectively. Best-fit second-order polynomial coefficients and corresponding coefficients of determination, R^2, for the remainder of cross-sections on the Catlin Canal and RFH Canal are presented in Table 5-2 and Table 5-3, respectively.

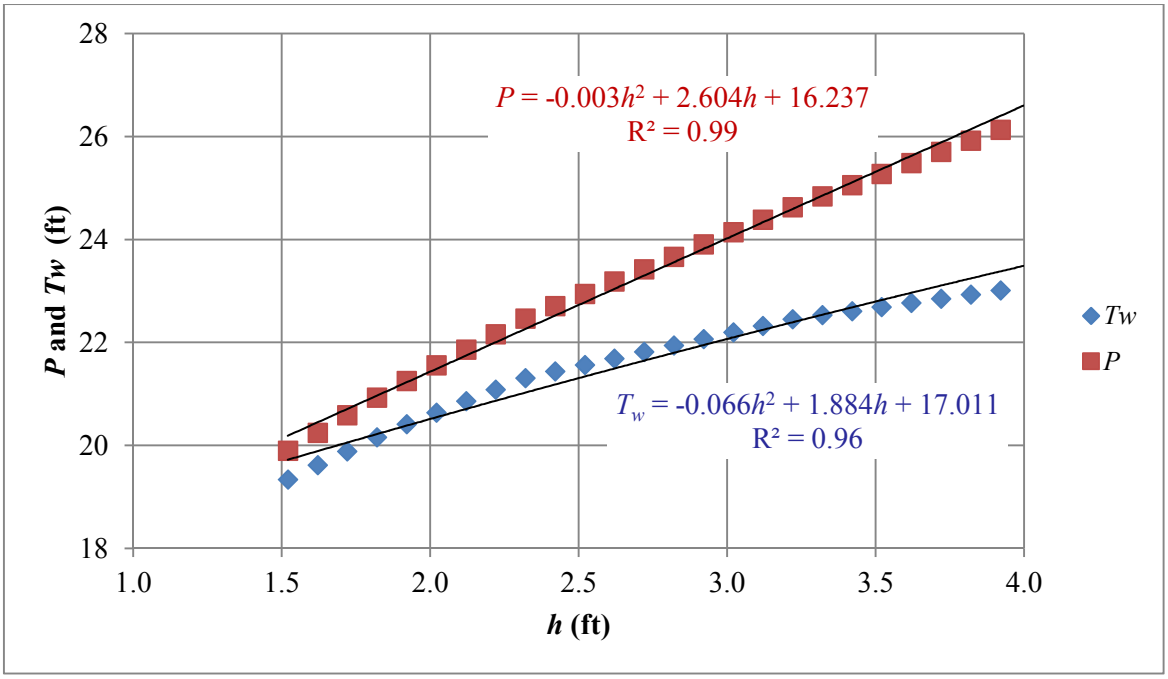

Figure 5-6 Best-fit P and T_w versus h relationships for cross-section at Sta. 1.93 on the Catlin Canal

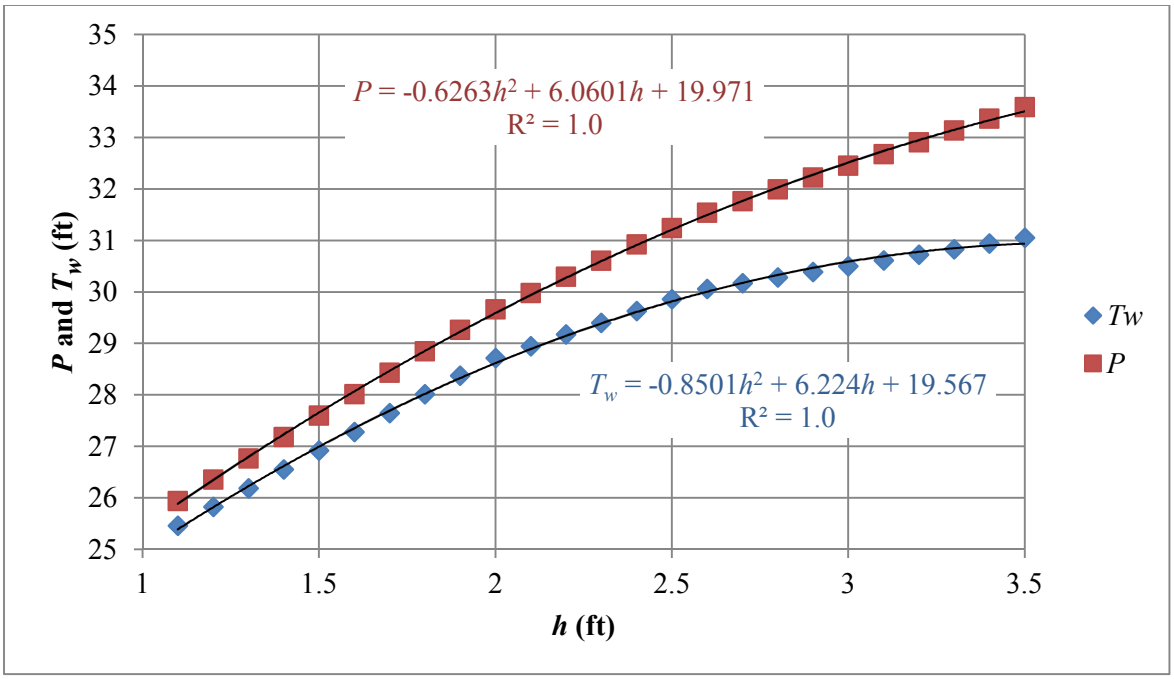

Figure 5-7 Best-fit P and T_w versus h relationships for cross-section at Sta. 1.76 on the RFH Canal

Table 5-2 Second-order polynomial coefficients and coefficients of determination for the Catlin Canal

Flow Measurement Site Number	Station (mi)	P				T_w			
		C_{P1}	C_{P2}	C_{P3}	R^2	C_{T1}	C_{T2}	C_{T3}	R^2
Site 202	0.00	0.32	0.60	17.17	1.00	0.46	-1.43	18.83	0.99
	0.16	1.05	-2.92	20.62	0.95	1.22	-5.45	22.56	0.79
	0.22	0.46	-0.05	19.81	0.99	0.56	-2.07	22.36	0.90
	0.39	0.02	2.21	13.77	1.00	-0.07	1.24	14.34	0.98
	0.44	1.07	-2.34	18.55	1.00	1.38	-5.49	20.94	0.99
	0.55	0.63	-0.97	21.73	0.99	0.73	-2.77	23.86	0.93
	0.79	1.18	-3.19	22.59	0.97	1.49	-6.07	24.93	0.92
	0.94	0.28	1.00	24.44	0.99	0.28	-0.69	26.02	0.72
	1.19	0.27	1.27	17.27	0.99	0.23	0.26	18.34	0.94
	1.33	0.25	1.18	22.99	1.00	0.49	-1.60	26.36	0.97
	1.57	0.31	1.23	18.43	1.00	0.49	-0.96	20.62	0.99
	1.74	-0.06	3.14	20.42	1.00	-0.10	2.40	21.24	0.99
	1.93	0.00	2.60	16.24	0.99	-0.07	1.88	17.01	0.96
	2.12	-0.15	3.65	14.87	1.00	-0.22	3.01	15.61	0.98
	2.26	-0.83	8.42	5.24	1.00	-1.02	8.66	4.91	1.00
Site 201	2.35	0.28	0.82	17.33	1.00	0.46	-1.60	20.21	0.96

Table 5-3 Second-order polynomial coefficients and coefficients of determination for the RFH Canal

Flow Measurement Site Number	Station (mi)	P				T_w			
		C_{P1}	C_{P2}	C_{P3}	R^2	C_{T1}	C_{T2}	C_{T3}	R^2
204	0.00	-0.19	3.19	28.39	1.00	-0.30	2.42	29.12	0.98
	0.18	-0.26	4.51	31.69	1.00	-0.35	4.16	31.80	1.00
	0.26	0.01	2.76	29.87	1.00	0.01	1.86	30.87	1.00
	0.38	-0.07	3.05	24.11	1.00	-0.07	1.95	25.12	1.00
	0.55	-0.63	6.34	22.27	1.00	-0.95	7.04	21.28	1.00
	0.80	-0.46	5.18	22.19	1.00	-0.73	5.44	21.98	0.99
	0.97	-0.35	5.25	22.45	1.00	-0.45	5.09	22.36	1.00
	1.17	-0.03	2.27	29.28	1.00	-0.05	0.94	30.67	0.99
	1.31	-0.14	3.77	27.20	1.00	-0.18	3.24	27.79	1.00
	1.55	-0.20	3.42	25.44	1.00	-0.25	2.52	26.49	0.99
	1.76	-0.63	6.06	19.97	1.00	-0.85	6.22	19.57	1.00
	1.97	-0.64	6.89	14.18	1.00	-0.75	6.76	14.25	1.00
	2.17	-0.52	5.19	21.91	0.99	-0.64	4.82	22.20	0.98
	2.37	-0.43	5.33	22.82	1.00	-0.49	4.92	23.10	1.00
	2.61	-0.41	5.53	15.77	1.00	-0.57	5.57	15.65	1.00
203	2.71	-0.47	5.97	11.82	1.00	-0.64	6.19	11.42	1.00
	3.01	0.01	2.45	21.07	1.00	0.00	1.44	22.05	0.99
	3.22	0.14	1.39	28.09	1.00	0.31	-1.06	30.50	1.00
	3.42	0.05	2.07	20.67	1.00	0.09	0.62	22.44	0.99
	3.61	-0.03	2.96	14.52	1.00	-0.02	1.82	15.43	1.00
	3.66	-0.08	3.02	16.18	1.00	-0.15	2.38	16.77	1.00
	3.76	0.01	2.53	20.16	1.00	-0.09	1.88	20.77	0.96
202	3.98	-0.08	2.61	23.69	1.00	-0.15	1.46	25.19	0.98
	4.13	-0.32	4.66	18.41	1.00	-0.56	5.14	17.70	1.00
	4.39	-0.18	3.98	18.58	1.00	-0.23	3.31	19.36	1.00
	4.59	-0.12	2.86	24.31	1.00	-0.23	2.00	25.54	0.99
	4.68	-0.33	5.64	12.01	1.00	-0.41	5.53	11.78	1.00
	4.79	-0.08	3.05	31.62	1.00	-0.08	1.99	32.90	0.99
	4.99	-0.11	3.08	29.47	1.00	-0.19	2.50	30.17	1.00
	5.08	0.10	4.60	17.65	1.00	0.18	3.46	17.84	0.99
	5.19	-0.32	4.72	20.41	1.00	-0.52	4.97	19.77	1.00
	5.27	-0.10	3.75	20.23	1.00	-0.15	3.30	20.33	1.00
	5.40	-0.42	5.50	24.69	0.99	-0.53	5.20	25.02	0.98
	5.59	0.10	2.19	27.69	1.00	0.15	0.96	28.76	1.00
	5.68	0.03	2.69	17.68	0.99	-0.05	2.06	18.76	0.97
	5.79	0.00	2.44	24.28	1.00	0.01	1.39	25.67	1.00
	5.86	-0.11	2.91	34.41	1.00	-0.16	2.00	35.54	1.00
	6.20	-0.09	3.52	33.06	1.00	-0.11	2.78	33.57	1.00
	6.41	-0.48	5.09	33.18	1.00	-0.72	5.11	33.20	1.00
201	6.44	-0.03	2.42	39.59	1.00	-0.04	1.18	40.81	0.99
	6.62	-0.48	5.85	23.93	1.00	-0.56	5.29	24.72	1.00
	6.80	-0.77	8.85	12.79	1.00	-0.87	8.86	12.76	1.00
	7.00	-0.94	9.13	9.25	0.99	-1.14	9.32	9.22	0.96
	7.20	-0.25	5.47	15.93	1.00	-0.28	5.10	16.26	1.00
	7.41	-0.26	4.32	27.77	1.00	-0.34	3.80	28.53	0.98
	7.60	-0.02	2.40	29.94	1.00	-0.02	1.27	30.97	1.00
	7.81	-0.05	2.93	20.93	1.00	-0.05	1.92	21.85	1.00
	8.00	-0.18	3.93	27.03	1.00	-0.28	3.66	27.26	1.00
	8.20	-0.04	2.47	40.36	1.00	-0.05	1.29	41.41	1.00
200	8.49	-0.44	5.85	30.00	1.00	-0.53	5.55	30.17	1.00

Calculation of residual values between the measured data and fitted curves

The residuals, ε_P and ε_T, between values of P and T_w estimated by direct geometric analysis of the surveyed cross section and the values predicted using Equations 5.1 and 5.2 were calculated for every 0.1 feet of h for each cross section, as illustrated for a few examples in Figure 5-8.

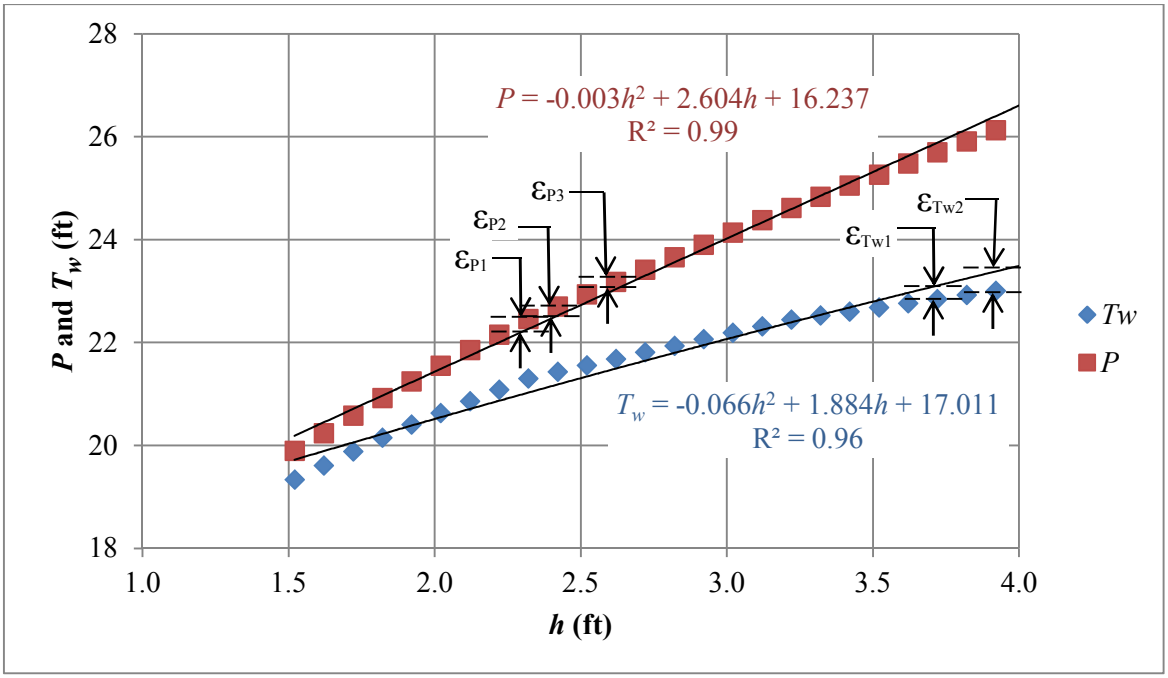

Figure 5-8 Examples of ε_P and ε_T values for P and T_w versus h relationships for cross-section at Sta. 1.93 on the Catlin Canal

Assigning a PDF to the residual values, unique to each surveyed cross-section:

Using @RISK software, a PDF was then fit to the ε_P and ε_{Tw} values computed for each surveyed cross section. It was determined that logistic PDF fit the datasets best based upon Chi-Squared, Anderson-Darling, and Kolmogorov-Smirnov goodness-of-fit measures in @RISK. These fitted PDFs were used to generate possible values of ε_P and ε_{Tw} with Monte Carlo simulation for assessing uncertainty in P and T_w estimates, as described in Section 5.1.3.1 below.

Examples of the 136 PDFs used to calculate ε_P and ε_{Tw} values for 68 surveyed cross-sections along the Catlin Canal are presented for the cross section at Station 0.0 in Figure 5-9 and Figure 5-10, respectively.

The presence of spatial trends in the values of the shape parameter, α, and scale parameter, β, of the fitted logistic PDFs of ε_P and ε_{Tw} along the canals was investigated. The α and β parameters for each surveyed cross-section were plotted versus canal station. Coefficients of determination, R^2, were generally less than 0.2, and statistically significant spatial trends could not be detected.

Cross-correlation between ε_P and ε_T values at individual cross sections was explored to account for the likelihood that if measurement error in a survey of cross-section geometry resulted in an overestimation of P, then it would also result in an overestimation of T_w, as they both increase in a similar fashion with increasing h. Pearson cross-correlation coefficients were calculated for ε_P and ε_{Tw} values (datasets from values computed at 0.1 increments of h) at each cross section and were found to be statistically significant at $\alpha = 0.05$. The correlation coefficients were used in the correlation matrix in @RISK for generating possible values of ε_P and ε_{Tw} in Monte Carlo simulation. A summary of the Pearson cross-correlation coefficients for ε_P and ε_{Tw} is presented in Table 5-4 and Table 5-5 for the Catlin and RFH canals, respectively.

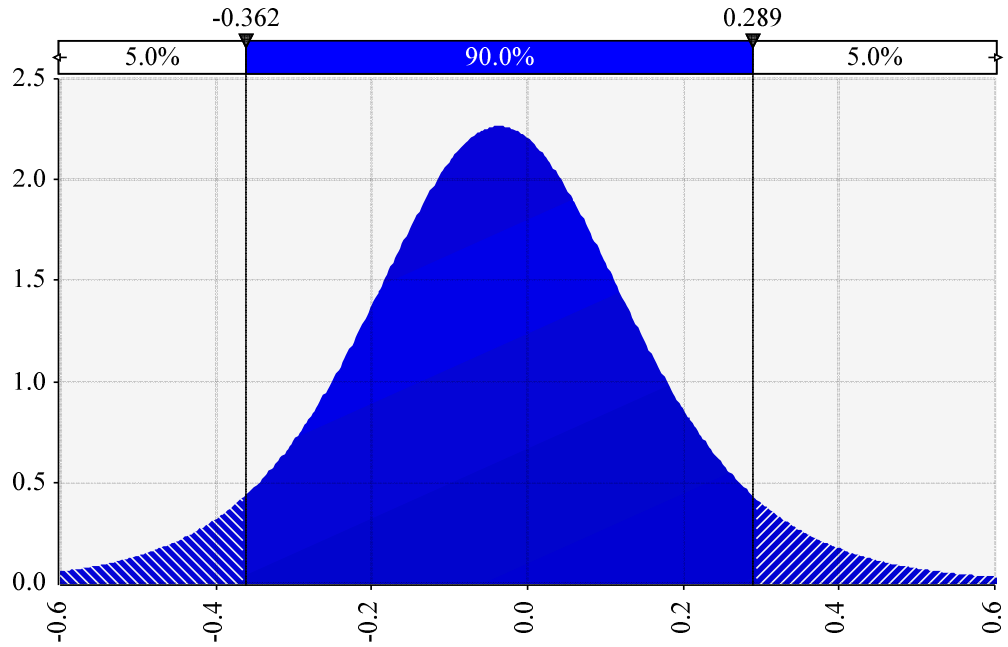

Figure 5-9 Fitted logistic PDF for ε_{Tw} for the cross-section at Sta 0.0 on the Catlin Canal (α = -0.036 and β = 0.111)

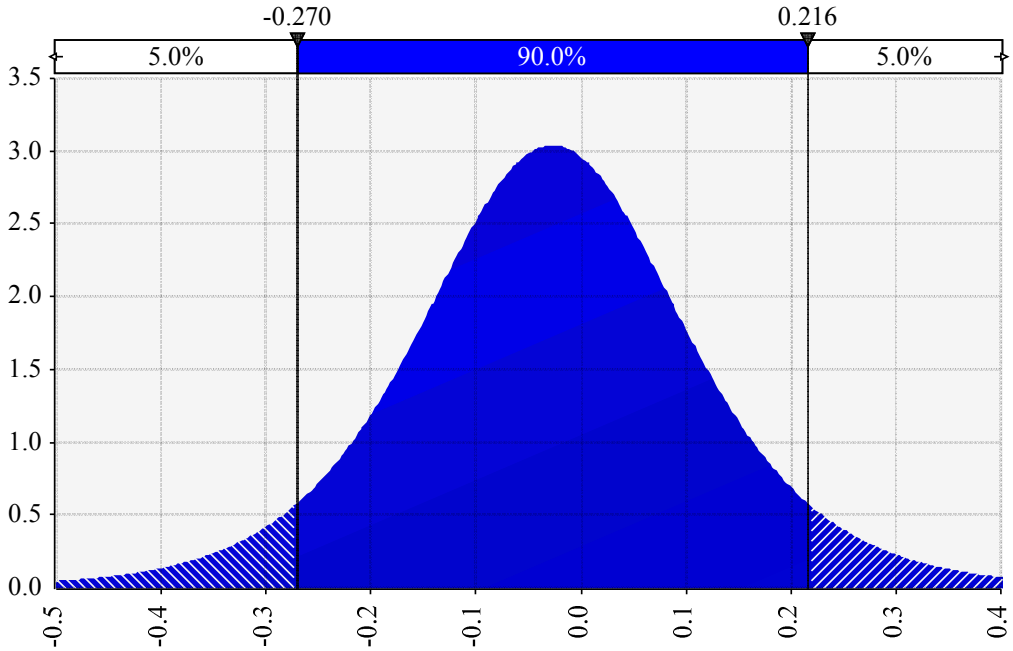

Figure 5-10 Fitted logistic PDF for ε_P for the cross-section at Sta 0.0 on the Catlin Canal (α = -0.027 and β = 0.082)

Table 5-4 Pearson Cross-Correlation Coefficients between ε_P and ε_{Tw} for the Catlin Canal

Flow Measurement Site Number	**Station (mi)**	**Pearson Cross-Correlation Coefficient**
Site 202	0.00	0.980
	0.16	1.000
	0.22	0.998
	0.39	0.913
	0.44	0.956
	0.55	0.974
	0.79	0.998
	0.94	0.994
	1.19	0.994
	1.33	0.999
	1.57	0.982
	1.74	0.998
	1.93	0.998
	2.12	0.985
	2.26	0.974
Site 201	2.35	0.996

Table 5-5 Pearson Cross-Correlation Coefficients between ε_p and ε_{Tw} for the RFH Canal

Flow Measurement Site Number	Station (mi)	Pearson Cross-Correlation Coefficient	Flow Measurement Site Number	Station (mi)	Pearson Cross-Correlation Coefficient
Site 204	0.00	0.962		4.59	0.947
	0.18	1.000		4.68	0.990
	0.26	0.998		4.79	0.997
	0.38	0.969		4.99	1.000
	0.55	0.978		5.08	1.000
	0.80	0.958		5.19	0.879
	0.97	0.995		5.27	0.997
	1.17	0.997		5.40	0.999
	1.31	0.995		5.59	1.000
	1.55	0.996		5.68	0.998
	1.76	1.000		5.79	0.999
	1.97	0.996		5.86	0.977
	2.17	0.998		6.20	1.000
	2.37	1.000		6.41	0.994
	2.61	0.978	Site 201	6.44	0.999
Site 203	2.71	0.991		6.62	0.988
	3.01	1.000		6.80	1.000
	3.22	0.955		7.00	0.999
	3.42	1.000		7.20	0.999
	3.61	0.653		7.41	0.995
	3.66	0.985		7.60	0.996
	3.76	0.975		7.81	1.000
Site 202	3.98	1.000		8.00	0.999
	4.13	0.995		8.20	1.000
	4.39	0.999	Site 200	8.49	0.999

5.1.3 Spatial Variability in Canal Hydraulic Geometry

Canal cross sections were surveyed at least every 0.2 miles and hydraulic geometry was found to vary substantially along the canal study reaches. Thus, there is uncertainty regarding the shape and size of the canal perimeter along segments of the tested canal reach between the locations of the surveyed cross sections. This spatial variability in hydraulic geometry

contributes to uncertainty in estimating canal storage change during the inflow-outflow tests for estimating canal seepage.

The data presented in Table 5-2 and Table 5-3 were used to create "along-the-canal" plots (Figure 5-11 through Figure 5-16) describing the spatial variation along the canal of the second-order polynomial coefficients used to predict P and Tw as functions of h at each surveyed cross –section. These plots display how each coefficient varies along the canal study reaches. They were created so that P and Tw versus h coefficients could be predicted based upon the distance along the canal reach and upon PDFs that describe the random variability of the coefficients about this trendline. That is, each second-order polynomial coefficient, Ci, was modeled as the sum of a deterministic component, $\hat{C}_i$, described by the trendline function of distance x along the canal and a random component, C_i' :

$$C_i = \hat{C}_i + C_i' \tag{5.3}$$

Along-the-canal trendline functions, for estimating the deterministic components of the coefficients in the *P* and T_w versus *h* relationships at each surveyed cross section, were estimated by least-squares regression, and are shown for the inflow-outflow test reach along the Catlin Canal in Figure 5-11, Figure 5-12, and Figure 5-13. The trendline functions for C_{P1} and C_{T1} are presented in Figure 5-11, for C_{P2} and C_{T2} in Figure 5-12, and for C_{P3} and C_{T3} in Figure 5-13. Similarly, the along-the-canal trendline functions for estimating the deterministic components of the coefficients in the *P* and T_w versus *h* relationships at each surveyed cross section for the RFH Canal are presented in Figure 5-14, Figure 5-15, and Figure 5-16. Values of R^2 and associated *p* values are shown for each fitted regression function. A summary of *p* values for the fitted trendline curves for each canal is provided in Table 5-6.

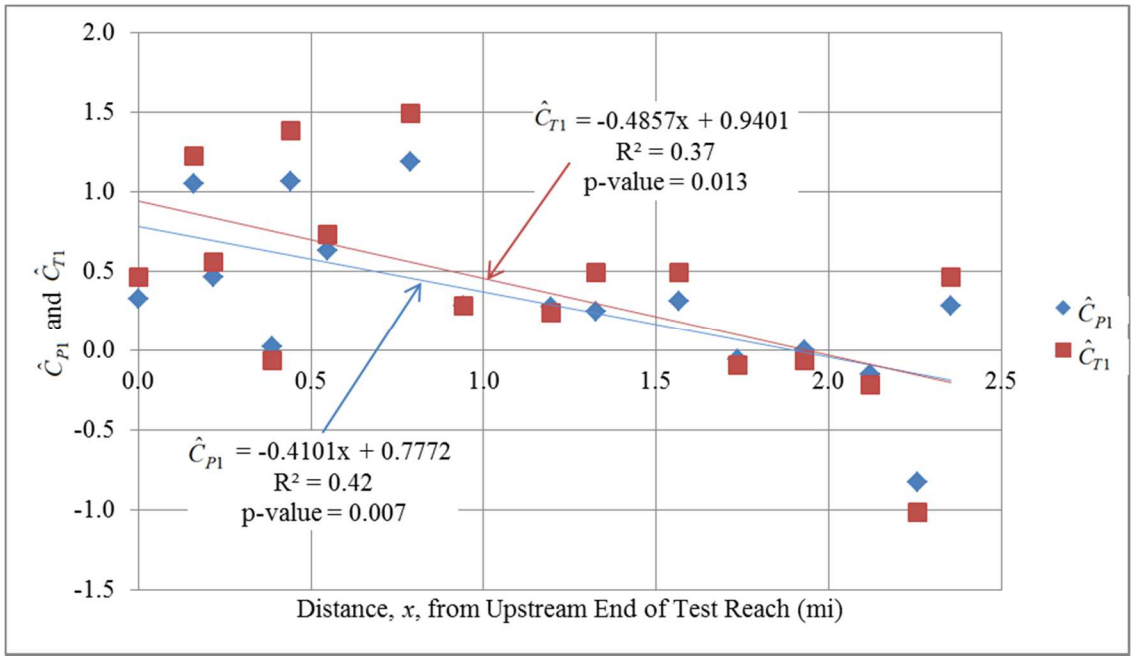

Figure 5-11 Best-fit functions for estimating the deterministic trend components of the coefficients $\hat{C}_{P1}$ and $\hat{C}_{T1}$ for the Catlin Canal

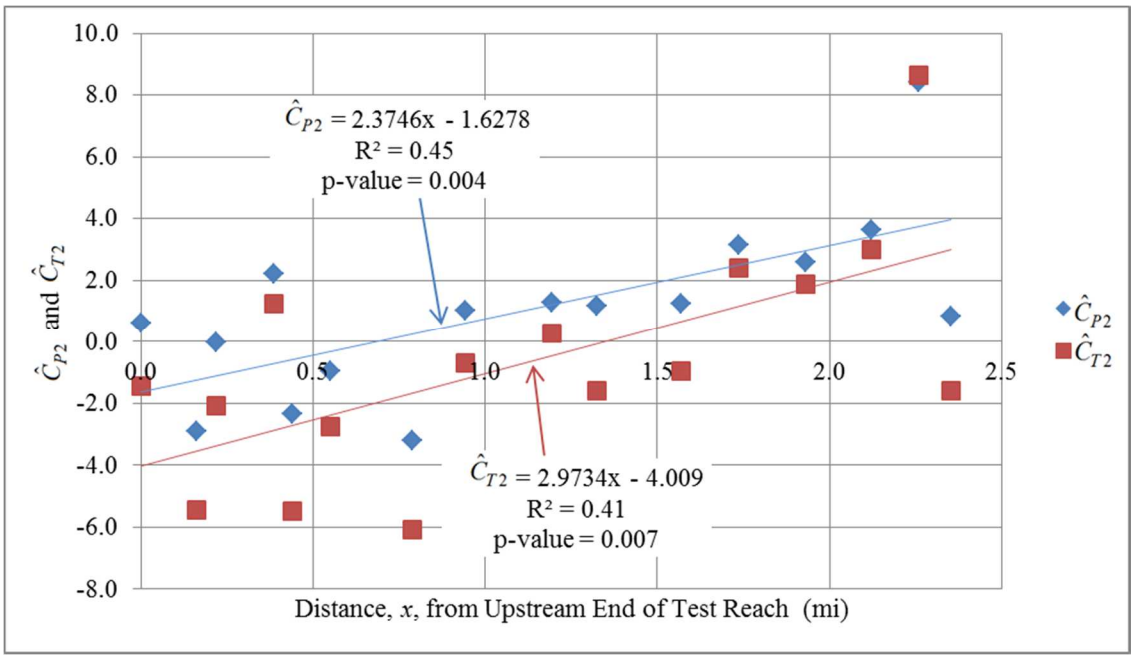

Figure 5-12 Best-fit functions for estimating the deterministic trend components of the coefficients $\hat{C}_{P2}$ and $\hat{C}_{T2}$ for the Catlin Canal

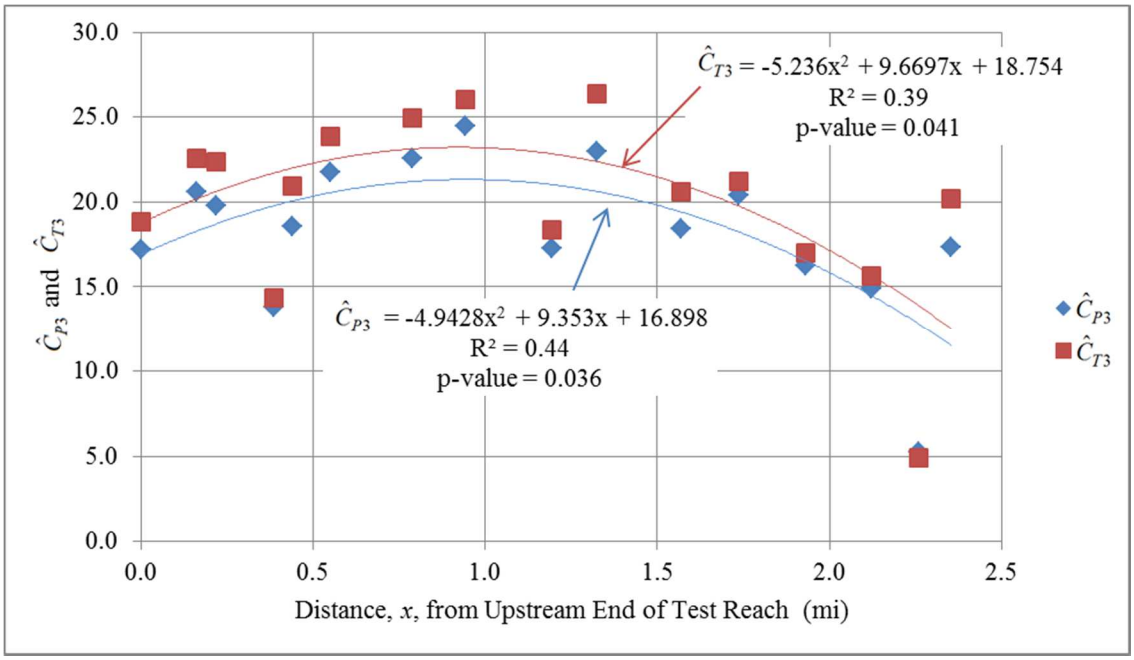

Figure 5-13 Best-fit functions for estimating the deterministic trend components of the coefficients $\hat{C}_{P3}$ and $\hat{C}_{T3}$ for the Catlin Canal

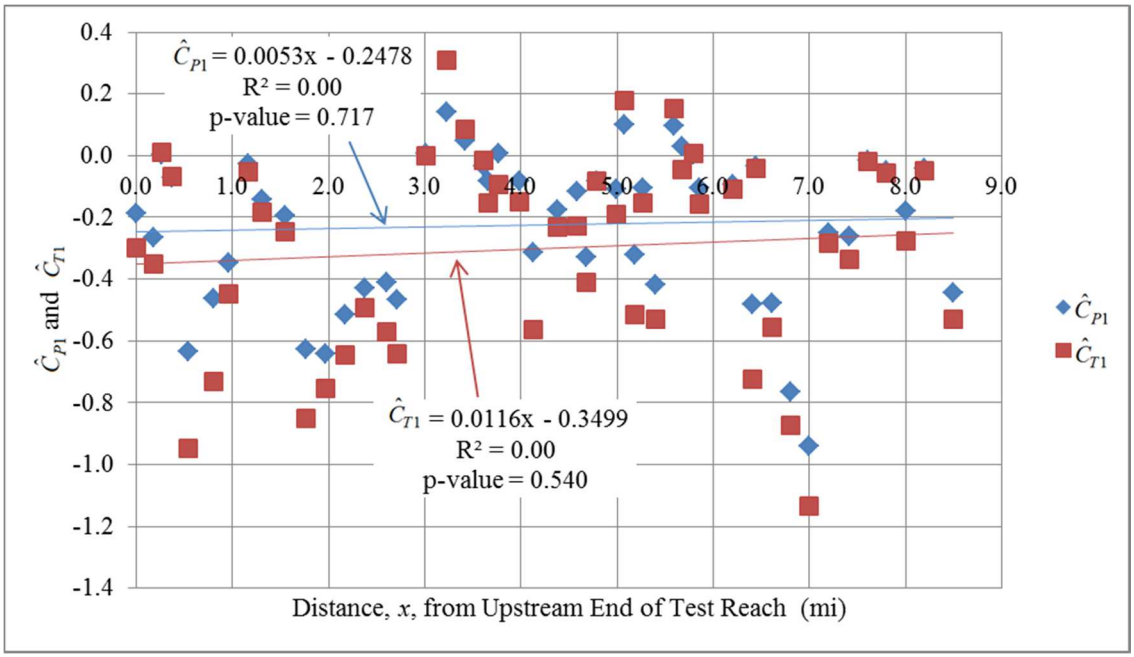

Figure 5-14 Best-fit functions for estimating the deterministic trend components of the coefficients $\hat{C}_{P1}$ and $\hat{C}_{T1}$ for the RFH Canal

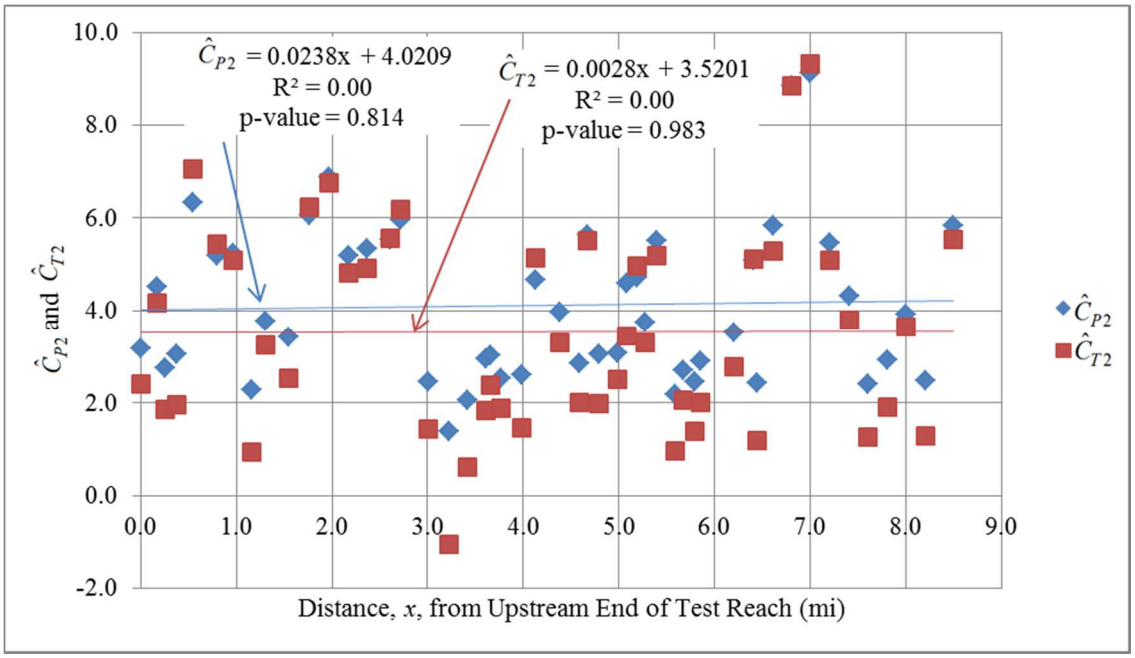

Figure 5-15 Best-fit functions for estimating the deterministic trend components of the coefficients $\hat{C}_{P2}$ and $\hat{C}_{T2}$ for the RFH Canal

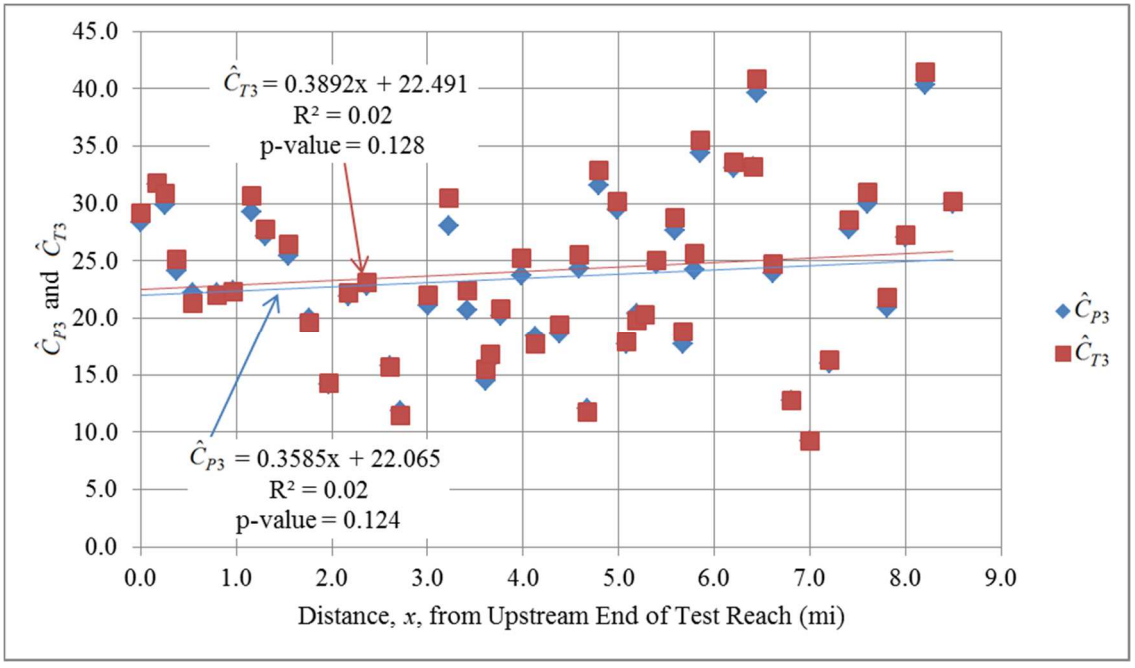

Figure 5-16 Best-fit functions for estimating the deterministic trend components of the coefficients $\hat{C}_{P3}$ and $\hat{C}_{T3}$ for the RFH Canal

Table 5-6 p values for fitted trendline functions for estimating the deterministic components of the coefficients in the P and T_w versus h relationships at cross sections along the Catlin and RFH canals

Deterministic Component of Cross Section Geometry Coefficient (with Fitted Trendline)	**Catlin Canal**	**RFH Canal**
$\hat{C}_{P1}$	0.01	0.72
$\hat{C}_{P2}$	0.00	0.81
$\hat{C}_{P3}$	0.04	0.12
$\hat{C}_{T1}$	0.01	0.54
$\hat{C}_{T2}$	0.01	0.98
$\hat{C}_{T3}$	0.04	0.13

Based upon the data summarized in Table 5-6, the following conclusions and decisions were made:

- For the Catlin canal,
    - p-values are less than 0.05 for all along-the-canal trendline coefficients, indicating that the curves are statistically significant.
    - Along-the-canal trendlines were used to estimate random values of P and T_w for the Catlin Canal in the @RISK model.
- For the RFH canal,
    - p-values are greater than 0.05 for all along-the-canal trendline coefficients, indicating the curves are *not* statistically significant.
    - Along-the-canal trendlines were not used to estimate random values of P and T_w for the RFH Canal in the @RISK model.

Spatial variability was modeled differently for the Catlin Canal than for the RFH Highline, as a result of the fitted trend equations for the P and T_w coefficients being statistically significant for the Catlin canal but not statistically significant for the RFH canal. The procedures used to model spatial variability in P and T_w for each canal are discussed in Sections 5.1.3.1 and 5.1.3.2, respectively.

5.1.3.1 Modeling Spatial Variability of Hydraulic Geometry in the Catlin Canal

The equations for describing deterministic trends in P and T_w coefficients (Figure 5-11, Figure 5-12, and Figure 5-13) cannot represent channel geometry with certainty. As such, probability distributions were used to model random residuals, C_{P1}', C_{P2}', C_{P3}', C_{T1}', C_{T2}', and C_{T3}', from the deterministic trend along the Catlin canal. PDFs were inferred from field data to describe the probability of occurrence of the random residual values. Thus, possible values of the random residuals from the trend at a given location along the canal were generated from the appropriate PDFs using the @RISK software. These random along-the-canal residual values were added to the estimated deterministic trend and adjusted by a random at-a-station residual value to calculate random values of P and T_w for a given flow depth h at the given location along the canal:

$$P = \left(\hat{C}_{P1} + C_{P1}'\right)h^2 + \left(\hat{C}_{P2} + C_{P2}'\right)h + \left(\hat{C}_{P3} + C_{P3}'\right) + \varepsilon_P \tag{5.4}$$

$$T_w = \left(\hat{C}_{T1} + C_{T1}'\right)h^2 + \left(\hat{C}_{T2} + C_{T2}'\right)h + \left(\hat{C}_{T3} + C_{T3}'\right) + \varepsilon_{Tw} \tag{5.5}$$

A summary of the deterministic trend component of the P and T_w coefficients (calculated from the curves in Figure 5-11, Figure 5-12, and Figure 5-13) appear in Table 5-7. The difference

between the deterministic trend and the actual value of coefficients calculated at each surveyed cross section are presented in Table 5-8.

Table 5-7 Deterministic trend component of the second order polynomial coefficients for P and T_w for the Catlin Canal

Station (mi)	$\hat{C}_{P1}$	$\hat{C}_{P2}$	$\hat{C}_{P3}$	$\hat{C}_{T1}$	$\hat{C}_{T2}$	$\hat{C}_{T3}$
0	0.78	-1.63	16.90	0.94	-4.01	18.75
0.16	0.71	-1.24	18.29	0.86	-3.53	20.19
0.22	0.69	-1.11	18.71	0.83	-3.36	20.62
0.39	0.62	-0.71	19.78	0.75	-2.86	21.71
0.44	0.60	-0.58	20.06	0.73	-2.70	22.00
0.55	0.55	-0.32	20.55	0.67	-2.37	22.49
0.79	0.45	0.25	21.20	0.56	-1.66	23.12
0.94	0.39	0.61	21.32	0.48	-1.21	23.22
1.19	0.29	1.21	21.02	0.36	-0.46	22.83
1.33	0.23	1.52	20.61	0.30	-0.07	22.37
1.57	0.13	2.09	19.41	0.18	0.65	21.05
1.74	0.06	2.50	18.23	0.10	1.15	19.76
1.93	-0.01	2.96	16.53	0.00	1.73	17.90
2.12	-0.09	3.41	14.50	-0.09	2.30	15.71
2.26	-0.15	3.73	12.82	-0.16	2.70	13.90
2.35	-0.19	3.96	11.52	-0.20	2.99	12.50

Table 5-8 Residuals of estimated second order polynomial coefficients for P and T_w from the deterministic trend component of the for the Catlin Canal

Station (mi)	$C_{P1} - \hat{C}_{P1}$	$C_{P2} - \hat{C}_{P2}$	$C_{P3} - \hat{C}_{P3}$	$C_{T1} - \hat{C}_{T1}$	$C_{T2} - \hat{C}_{T2}$	$C_{T3} - \hat{C}_{T3}$
0	-0.45	2.23	0.27	-0.48	2.58	0.07
0.16	0.34	-1.68	2.33	0.36	-1.92	2.37
0.22	-0.23	1.06	1.09	-0.28	1.29	1.74
0.39	-0.60	2.91	-6.00	-0.82	4.10	-7.37
0.44	0.47	-1.76	-1.51	0.66	-2.79	-1.06
0.55	0.08	-0.65	1.18	0.05	-0.39	1.37
0.79	0.73	-3.44	1.39	0.93	-4.41	1.80
0.94	-0.11	0.39	3.12	-0.20	0.51	2.80
1.19	-0.02	0.06	-3.75	-0.13	0.71	-4.49
1.33	0.01	-0.34	2.38	0.19	-1.54	3.99
1.57	0.17	-0.87	-0.99	0.31	-1.61	-0.43
1.74	-0.13	0.64	2.19	-0.19	1.24	1.48
1.93	0.01	-0.35	-0.29	-0.07	0.15	-0.89
2.12	-0.06	0.24	0.37	-0.13	0.71	-0.11
2.26	-0.68	4.69	-7.59	-0.86	5.96	-8.99
2.35	0.47	-3.14	5.81	0.67	-4.59	7.71

PDFs were fit to each column of Table 5-8 using @RISK to account for residual values from the along-the-canal trendline estimates of P and T_w. For example, a distribution was fit to all $C_{P1} - \hat{C}_{P1}$ values, a separate distribution was fit to all $C_{P2} - \hat{C}_{P2}$ values, and so on. Logistic PDFs appeared to fit the datasets best using Chi-Squared, Anderson-Darling, and Kolmogorov-Smirnov fit ranking methods and were adopted for all of the coefficients. Frequency histograms of the computed residual values along with the logistic PDFs used for randomly generating C_{P1}', C_{P2}', C_{P3}', C_{T1}', C_{T2}', and C_{T3}' for the Catlin Canal in the @RISK model are presented in Figure 5-17 through Figure 5-22, respectively.

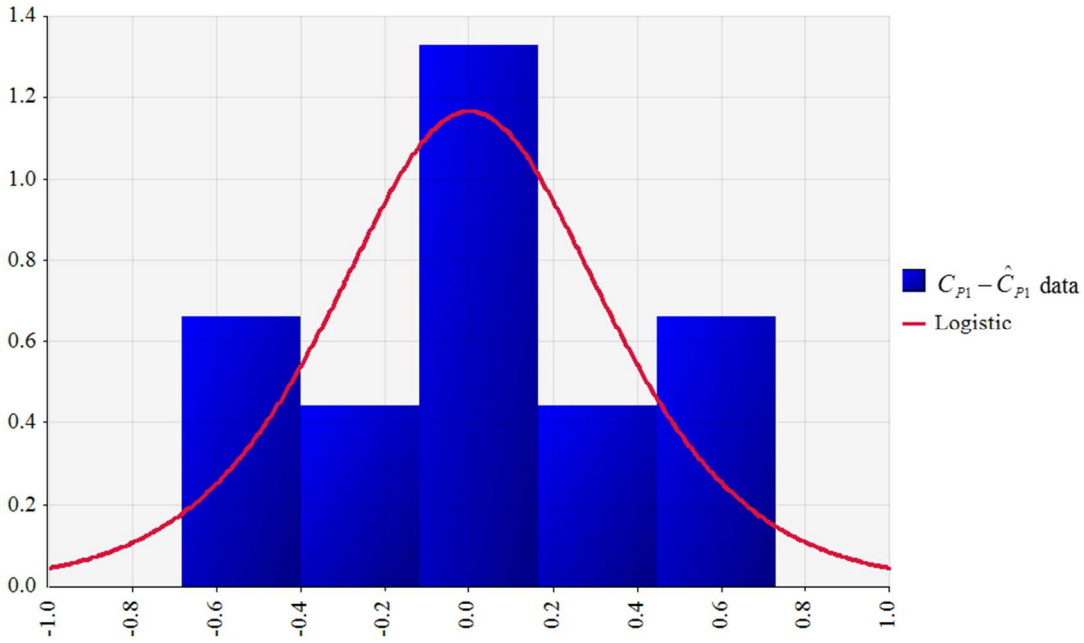

Figure 5-17 Frequency histogram of computed along-the-canal residual values and fitted Logistic PDF for C_{P1}' on the Catlin Canal (μ = 0.0005 and s = 0.214)

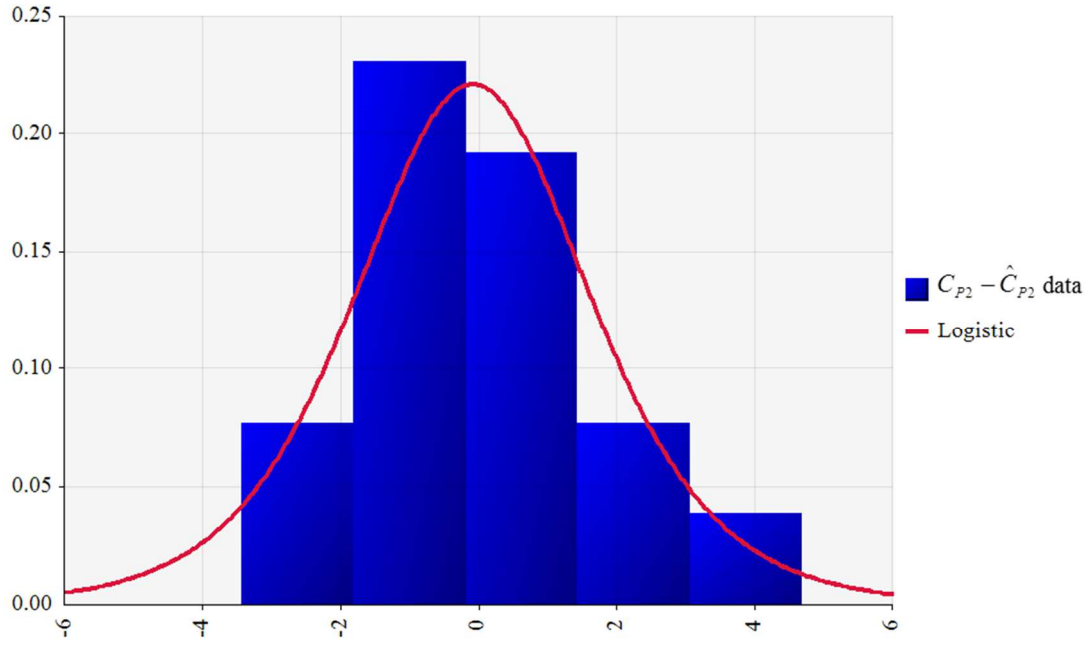

Figure 5-18 Frequency histogram of computed along-the-canal residual values and fitted Logistic PDF for C_{P2}' on the Catlin Canal (μ = -0.088 and s = 1.132)

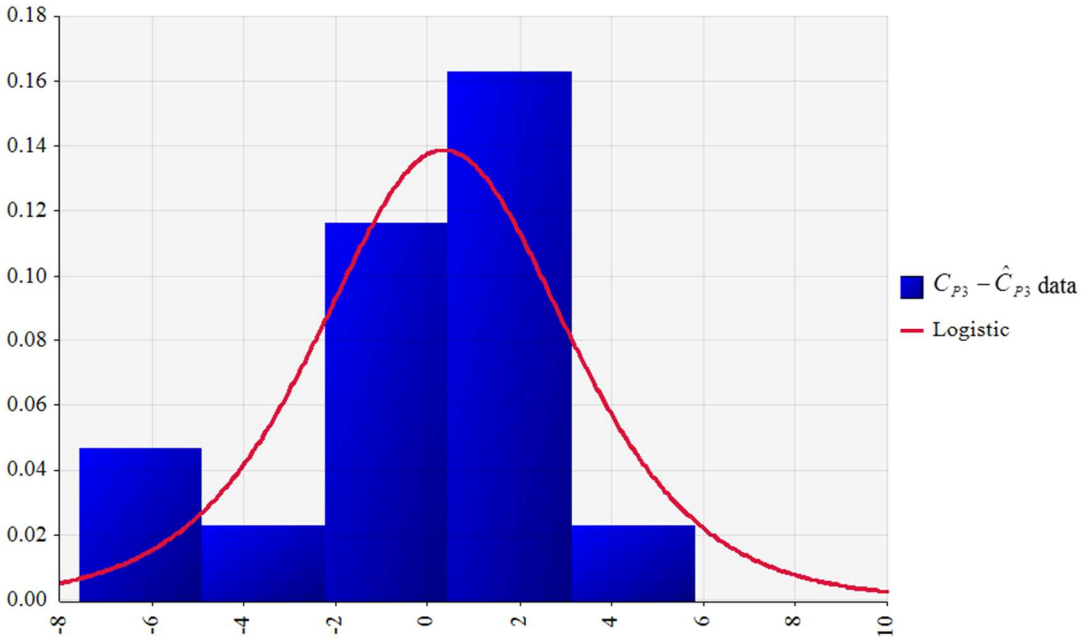

Figure 5-19 Frequency histogram of computed along-the-canal residual values and fitted Logistic PDF for C_{P3}' on the Catlin Canal (μ = 0.348 and s = 1.801)

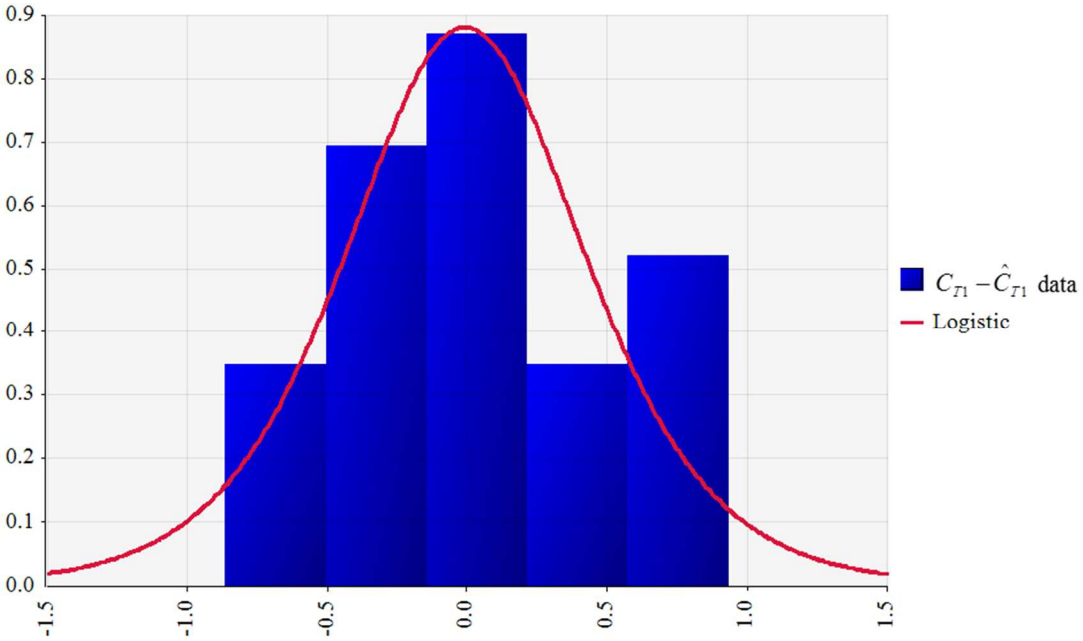

Figure 5-20 Frequency histogram of computed along-the-canal residual values and fitted Logistic PDF for C_{T1}' on the Catlin Canal (μ = -0.007 and s = 0.284)

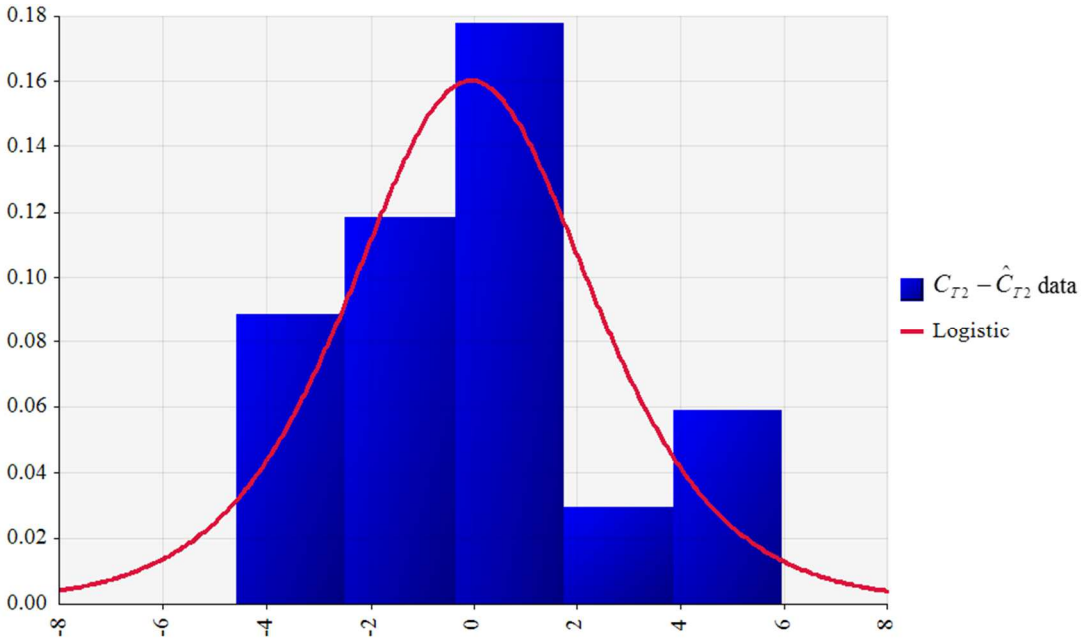

Figure 5-21 Frequency histogram of computed along-the-canal residual values and fitted Logistic PDF for C_{T2}' on the Catlin Canal (μ = -0.052 and s = 1.561)

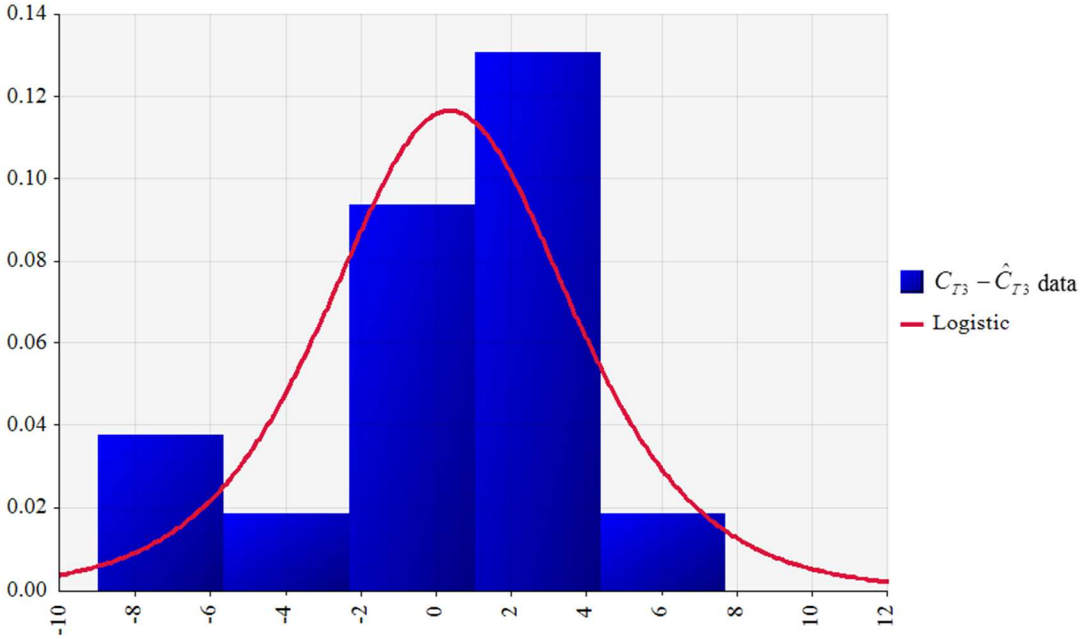

Figure 5-22 Frequency histogram of computed along-the-canal residual values and fitted Logistic PDF for C_{T3}' on the Catlin Canal (μ = 0.362 and s = 2.145)

The cross-correlation among the values of C_{P1}', C_{P2}', C_{P3}', C_{T1}', C_{T2}', and C_{T3}' was calculated using the correlation function in Excel and used in generating random values using @RISK. For example, the correlation factor was determined between the 16 values of $(C_{P1} - \hat{C}_{P1})$ and the 16 values of $(C_{P2} - \hat{C}_{P2})$ along the Catlin Canal to form the correlation between C_{P1}' and C_{P2}'. The associated correlation matrices for the along-the-canal residuals for the Catlin Canal are presented in Table 5-9.

Table 5-9 Correlation matrix for the along-the-canal residuals on the Catlin Canal

	C_{P1}'	C_{P2}'	C_{P3}'	C_{T1}'	C_{T2}'	C_{T3}'
C_{P1}'	1					
C_{P2}'	-0.980	1				
C_{P3}'	0.585	-0.685	1			
C_{T1}'	0.988	-0.967	0.603	1		
C_{T2}'	-0.969	0.985	-0.698	-0.981	1	
C_{T3}'	0.626	-0.721	0.988	0.660	-0.753	1

5.1.3.2 Modeling Spatial Variability in the RFH Canal

For the RFH Canal, along-the-canal trendlines were determined to be statistically insignificant for the coefficients used to calculate P and T_w. As such, a different approach was taken to account for spatial variability of hydraulic geometry along the RFH Canal.

The plots of C_{P1} and $C_{T1;}$ C_{P2} and $C_{T2;}$ and C_{P3} and C_{T3} for the RFH Canal (Figure 5-14, Figure 5-15, and Figure 5-16, respectively) display no clear underlying deterministic pattern or trend, as indicated by the p-values. However, these coefficients can vary greatly from one cross

section to the next. As such, PDFs were developed to randomly generate the second-order polynomial coefficients used to predict P and T_w. Values of C_{P1}, C_{P2}, C_{P3}, $C_{T1,}$ $C_{T2,}$ and C_{T3} derived from all 50 surveyed cross sections (presented in Table 5-3) were implemented in the development of the respective PDFs. Thus values at any given cross section were generated from these PDFs simply as random along-the-canal values (where the trend component is taken to be zero): C_{P1}', C_{P2}', C_{P3}', C_{T1}', C_{T2}', and C_{T3}'. For example, the 50 values of C_{P1} from Table 5-3 were used to fit the PDF for generating C_{P1}'.

The frequency histograms of the values of C_{P1}, C_{P2}, C_{P3}, $C_{T1,}$ $C_{T2,}$ and C_{T3} calculated from survey data along the RFH Canal along with fitted PDFs for use in generating the random values C_{P1}', C_{P2}', C_{P3}', C_{T1}', C_{T2}', and C_{T3}' are presented as Figure 5-23, Figure 5-24, Figure 5-25, Figure 5-26, Figure 5-27, and Figure 5-28, respectively. Normal PDFs fit the datasets best using Chi-Squared, Anderson-Darling, and Kolmogorov-Smirnov goodness-of-fit tests. The normal PDFs were truncated to prevent generation of physically-unrealistic values of P and T_w. The truncations were calibrated through a trial and error process such that the PDFs generated random variables that represented realistic values of P and T_w for the given range of observed flow depths. For the RFH Canal, P and T_w were calculated using Equations 5.3 and 5.4, respectively, with the deterministic trends set equal to zero.

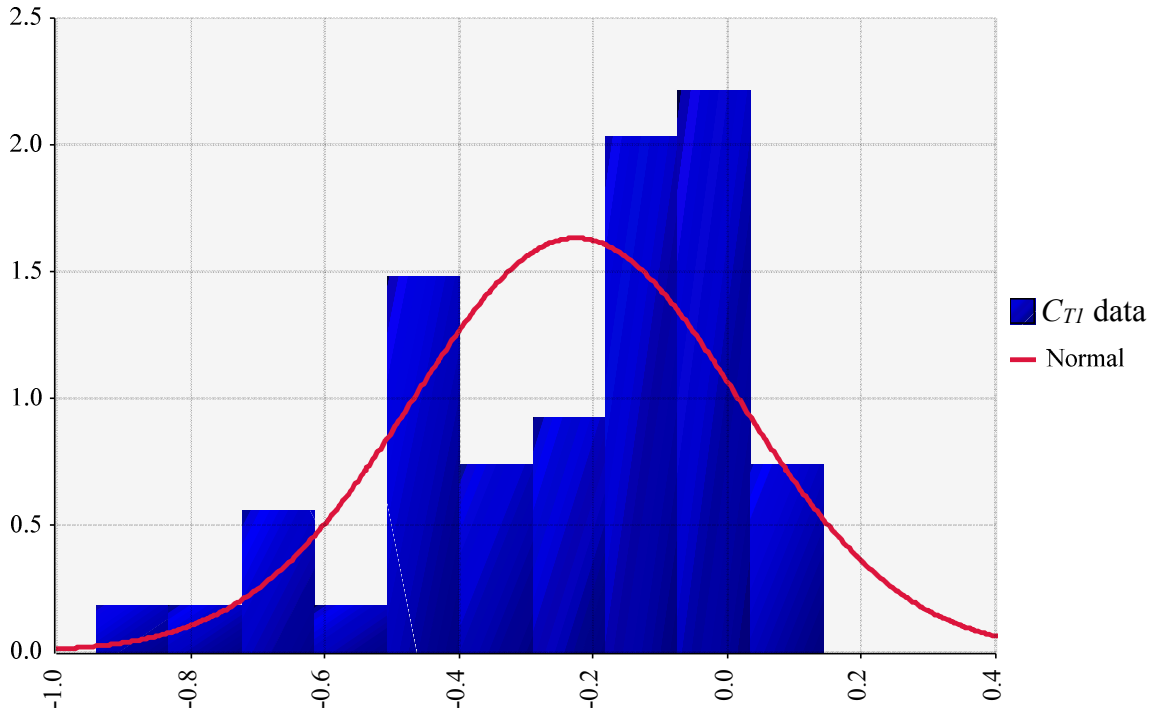

Figure 5-23 Frequency histogram of computed values and fitted normal PDF for $C_{T1} = C_{T1}$' on the RFH Canal (μ = -0.226 and σ = 0.245)

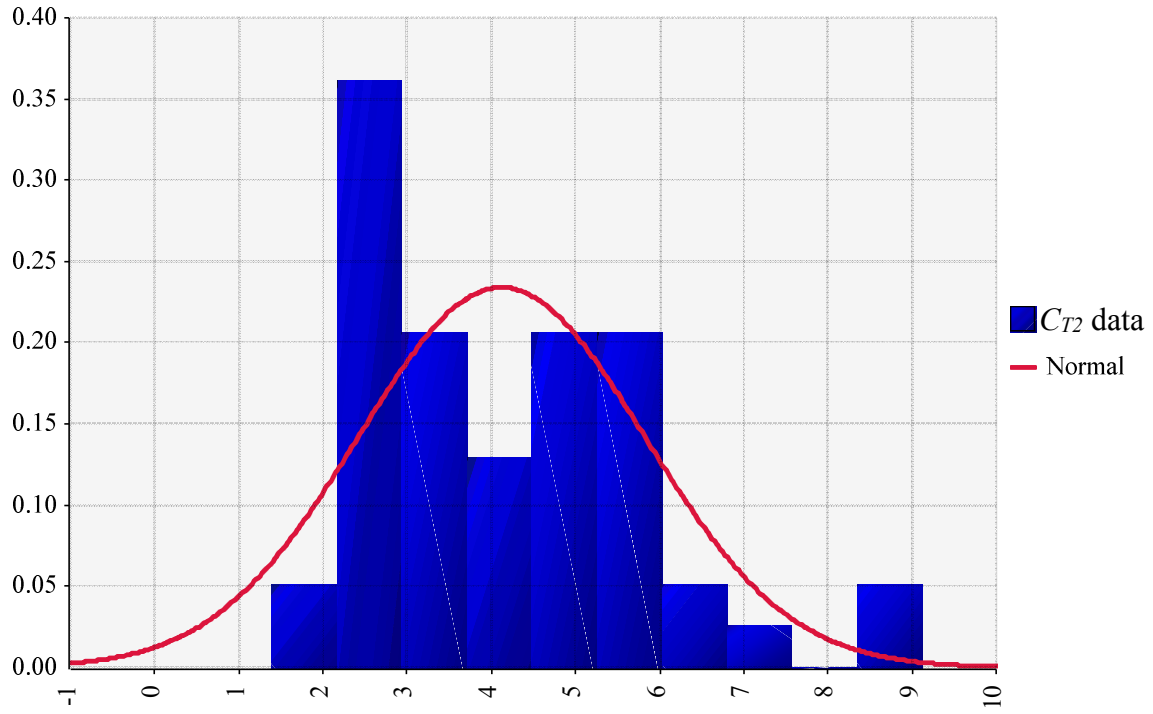

Figure 5-24 Frequency histogram of computed values and fitted normal PDF for $C_{T2} = C_{T2}$'on the RFH Canal (μ = 4.121 and σ = 1.705)

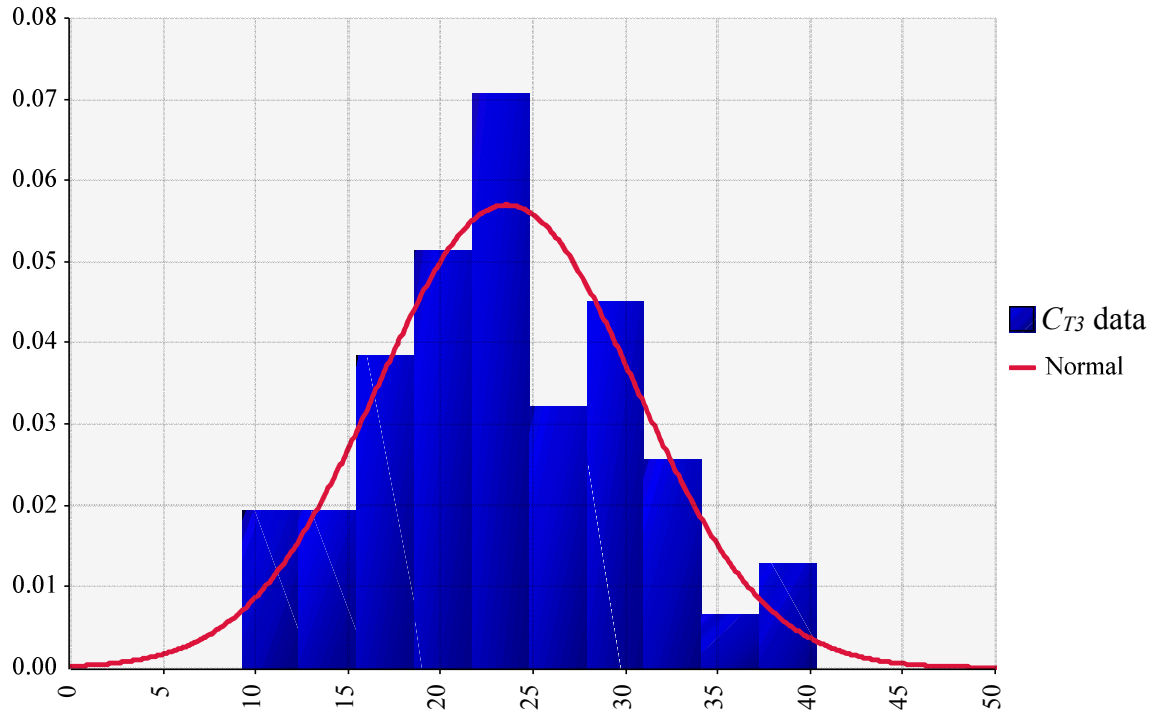

Figure 5-25 Frequency histogram of computed values and fitted normal PDF for $C_{T3} = C_{T3}$'on the RFH Canal ($\mu = 23.578$ and $\sigma = 7.000$)

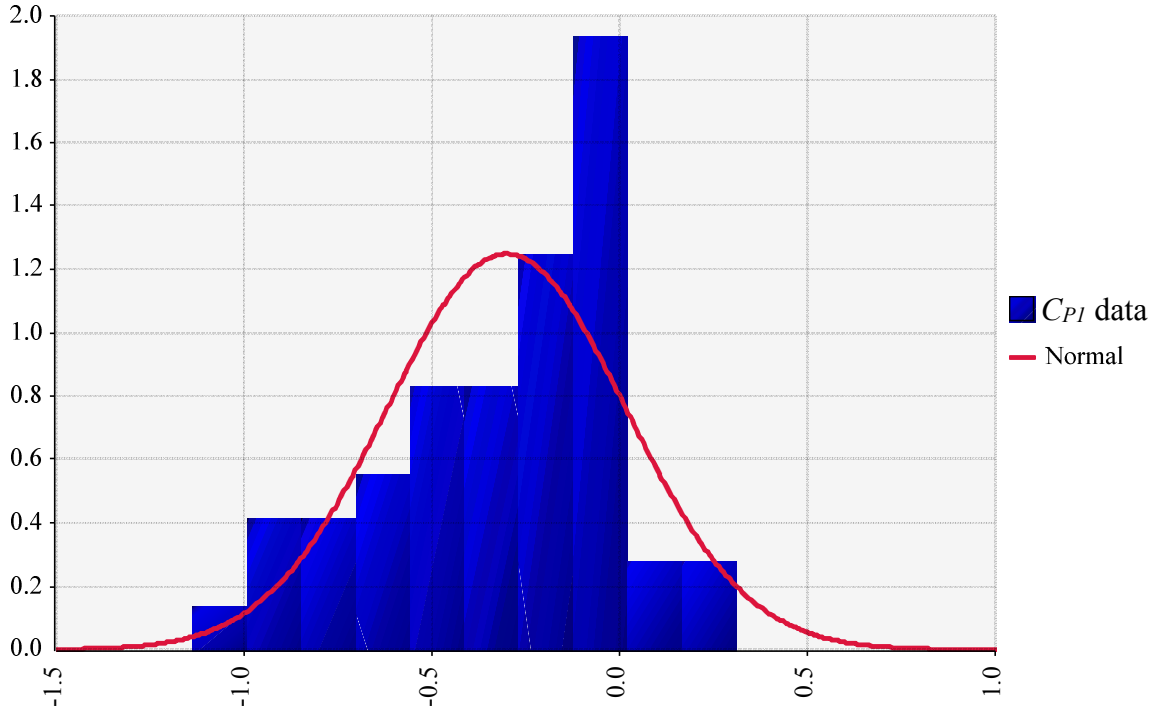

Figure 5-26 Frequency histogram of computed values and fitted normal PDF for $C_{P1} = C_{P1}$' on the RFH Canal ($\mu = -0.301$ and $\sigma = 0.320$)

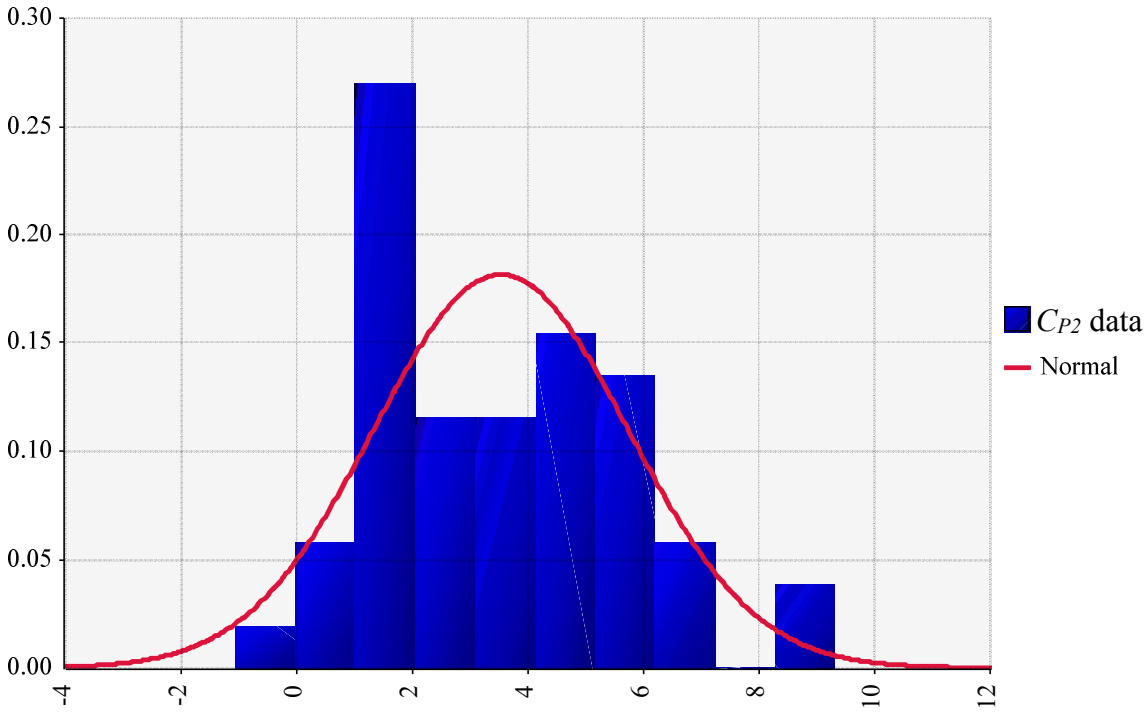

Figure 5-27 Frequency histogram of computed values and fitted normal PDF for $C_{P2} = C_{P2}$'on the RFH Canal ($\mu = 3.532$ and $\sigma = 2.198$)

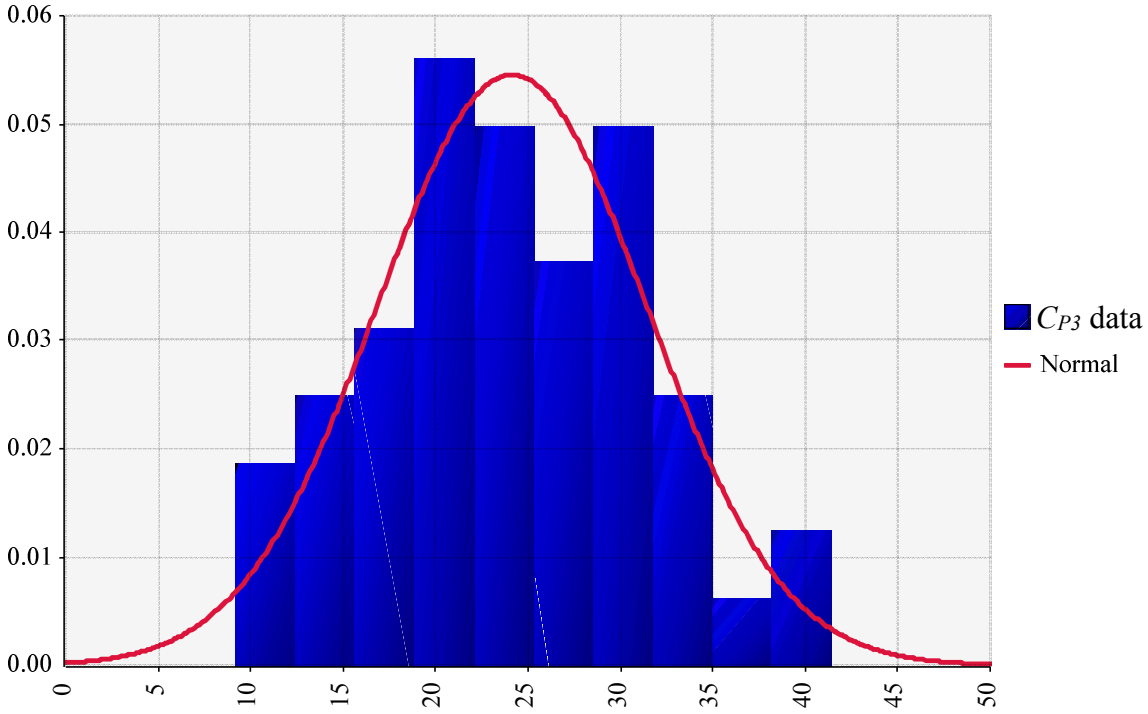

Figure 5-28 Frequency histogram of computed values and fitted normal PDF for $C_{P3} = C_{P3}$'on the RFH Canal ($\mu = 24.133$ and $\sigma = 7.316$)

5.1.4 Uncertainty in Water Surface Profiles

As described in Section 3.2.3, the water surface was interpolated along canal reaches at locations where staff gages and pressure transducers were not installed, so that the flow geometry of the entire canal study reach could be estimated. Measured water surface elevations were linearly interpolated along canal reaches between locations where the water surface elevation was measured with a staff gage or pressure transducer. These interpolated values define what will be referred to as the "predicted" water surface. In order to check the accuracy of the water surface interpolation calculations in the Catlin Canal, the flow depth (physically measured at surveyed cross sections with a wading rod on three different dates immediately after flow rate measurements) was used to define the "measured" water surface. The predicted and measured water surface profiles on those three days were compared to estimate errors in the water surface interpolation methodology.

Plots of predicted and measured water surface profiles along the Catlin Canal study reach for three separate dates are presented in Figure 5-29. The predicted and measured water surface elevations along the canal reach appear to match fairly closely at the cross-sections located in the vicinity of staff gages or pressure transducers. They do not compare as well towards the center of the study reaches, illustrating that, installation of stage measurement equipment over long intervals increases uncertainty in water surface elevation calculations, which also increases uncertainty in the calculation of hydraulic geometry parameters such as P and T_w.

(a)

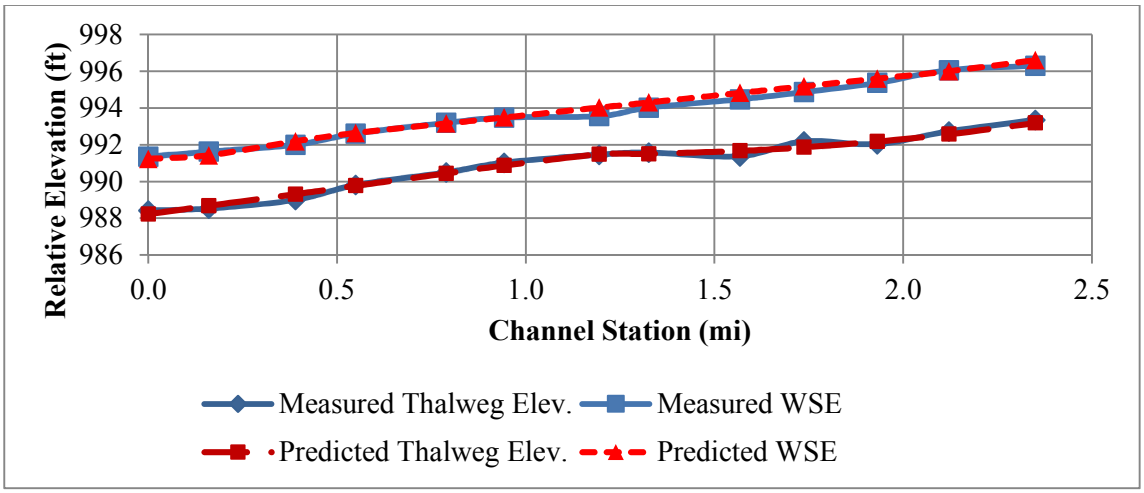

(b)

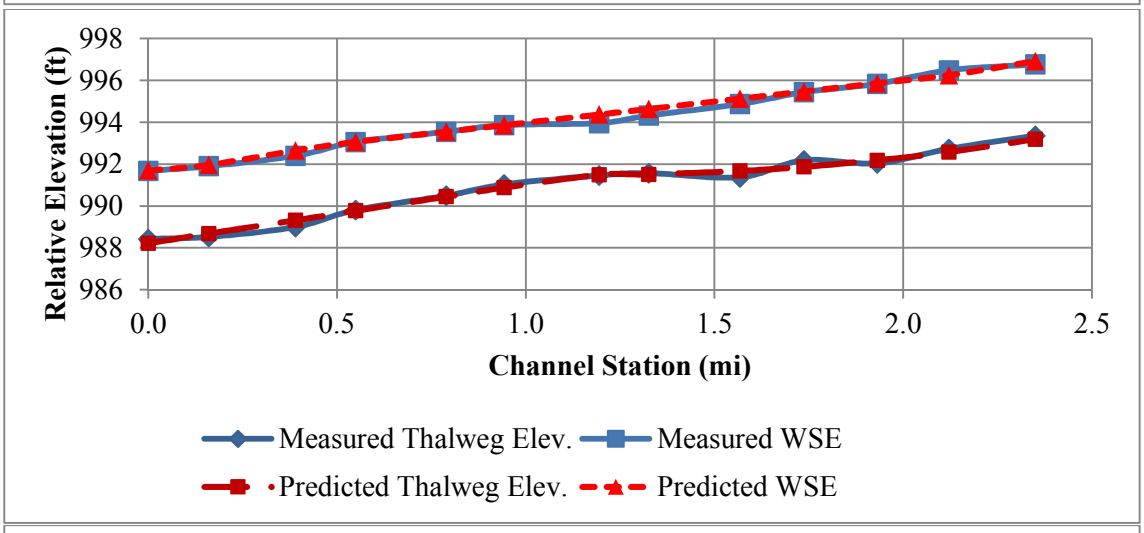

(c)

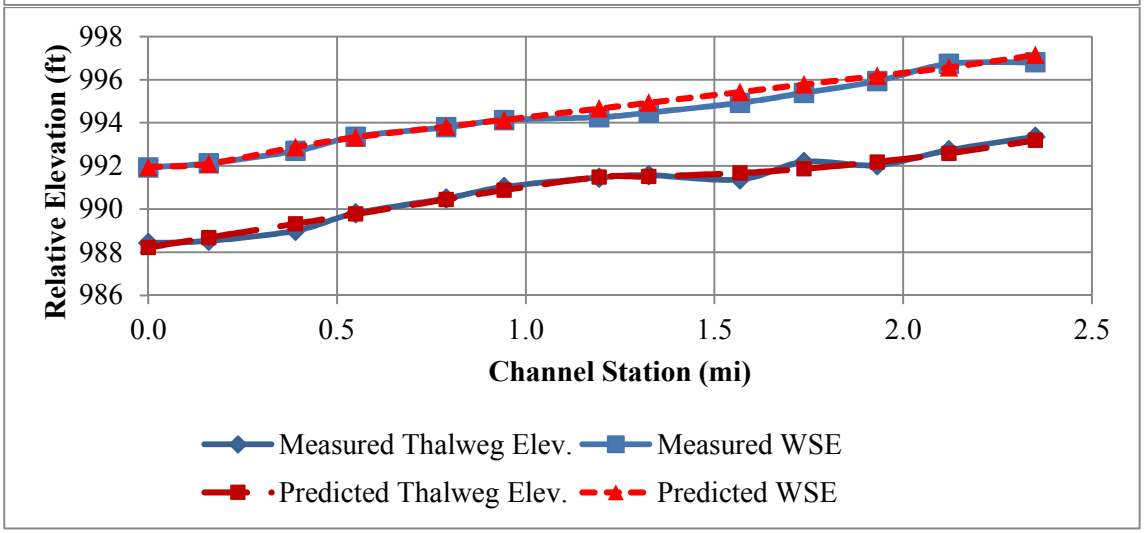

Figure 5-29 Measured water surface profiles versus predicted water surface profiles on the Catlin Canal for data on (a) 6/14/2007, (b) 6/20/2007, and (c) 7/23/2007

5.1.5 Uncertainty in Predicting Canal Thalweg Elevations

Thalweg flow depth, h, defined as the vertical difference between the water surface elevation, WSE, and the point of lowest elevation in the canal cross section (the thalweg elevation, TH_{el}), is used to calculate hydraulic geometry parameters T_w and P:

$$h = WSE - TH_{el} \tag{5.5}$$

Values of TH_{el} vary spatially along a canal and temporally due to sedimentation and erosion processes. To account for such variability, TH_{el} was modeled by (a) describing a deterministic trend component using channel bed survey data and (b) fitting and using a PDF to randomly generate a random error term (ε_{TH}). Trendline residuals (difference between measured and trendline predicted elevations) were used to develop the PDF. Chi-Squared, Anderson-Darling, and Kolmogorov-Smirnov ranking methods were implemented in @Risk, and a normal PDF was adopted for randomly generating ε_{TH} at a given cross-section that was surveyed. Example PDFs used to generate ε_{TH} values are presented as Figure 5-32 and Figure 5-33 for the RFH and Catlin canals, respectively.

Longitudinal profiles of surveyed thalweg elevations for the RFH and Catlin canals are presented as Figure 5-30 and Figure 5-31, respectively. The following equations used for estimating TH_{el} at a given location (station) along the canal reach, include a fitted regression function of the location, x, that represents the deterministic trend along the canal reach and a random error term:

RFH Canal – Sta. 0.0 to 3.6:

$$TH_{el} = -0.3979x^2 + 2.1161x + 976.6 + \varepsilon_{TH} \tag{5.6}$$

RFH Canal – Sta. 3.7 to 6.41:

$$TH_{el} = 2.3598x + 970.7 + \varepsilon_{TH} \tag{5.7}$$

RFH Canal – Sta. 6.44 to 8.5:

$$TH_{el} = 0.5015x^2 - 5.1235x + 997.8 + \varepsilon_{TH} \tag{5.8}$$

Catlin Canal – Sta. 0.0 to 1.0:

$$TH_{el} = -0.019x^2 + 2.8379x + 988.2 + \varepsilon_{TH} \tag{5.9}$$

Catlin Canal – Sta. 1.2 to 2.35:

$$TH_{el} = 1.2335x^2 - 2.9079x + 993.18 + \varepsilon_{TH} \tag{5.10}$$

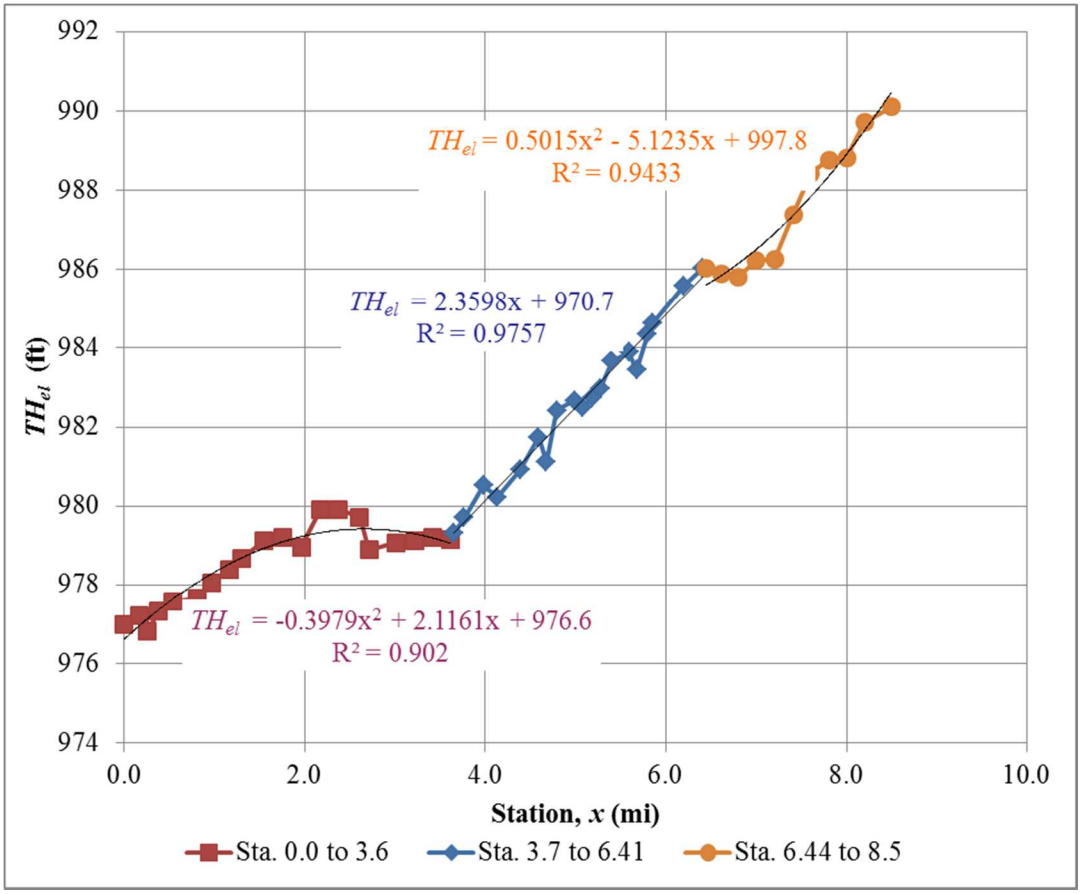

Figure 5-30 Thalweg elevations and trendline curves of best fit for the RFH Canal study reach

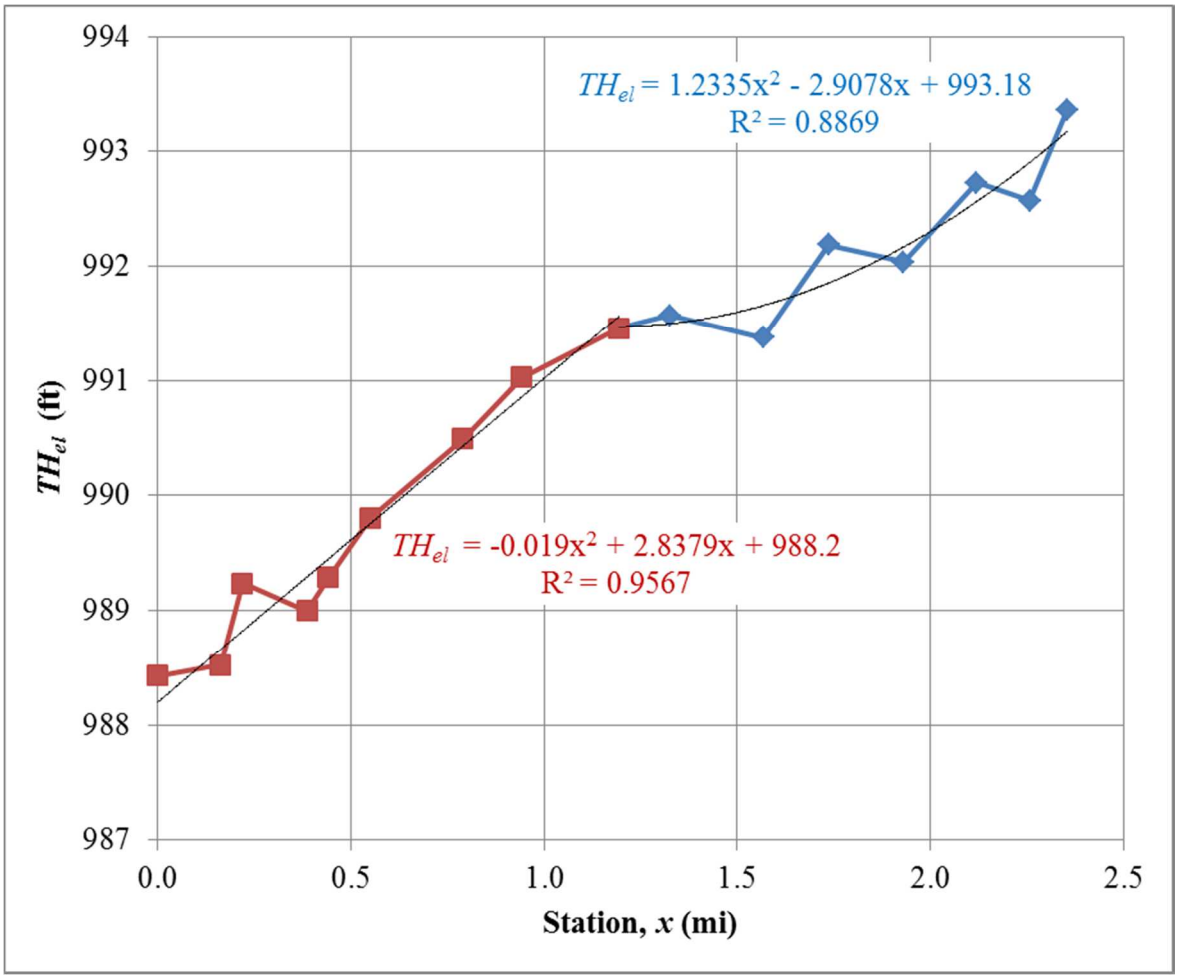

Figure 5-31 Thalweg elevations and trendline curves of best fit for the Catlin Canal study reach

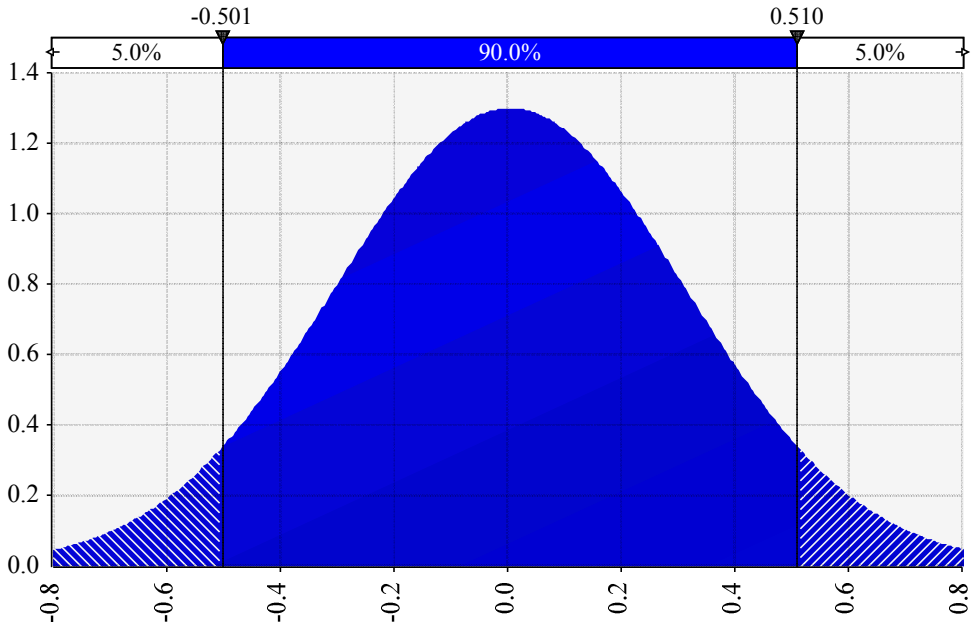

Figure 5-32 Fitted PDF for generating ε_{TH} on the RFH Canal between Stations 0.0 and 3.6 miles

($\mu = 0.004$ and $\sigma = 0.307$)

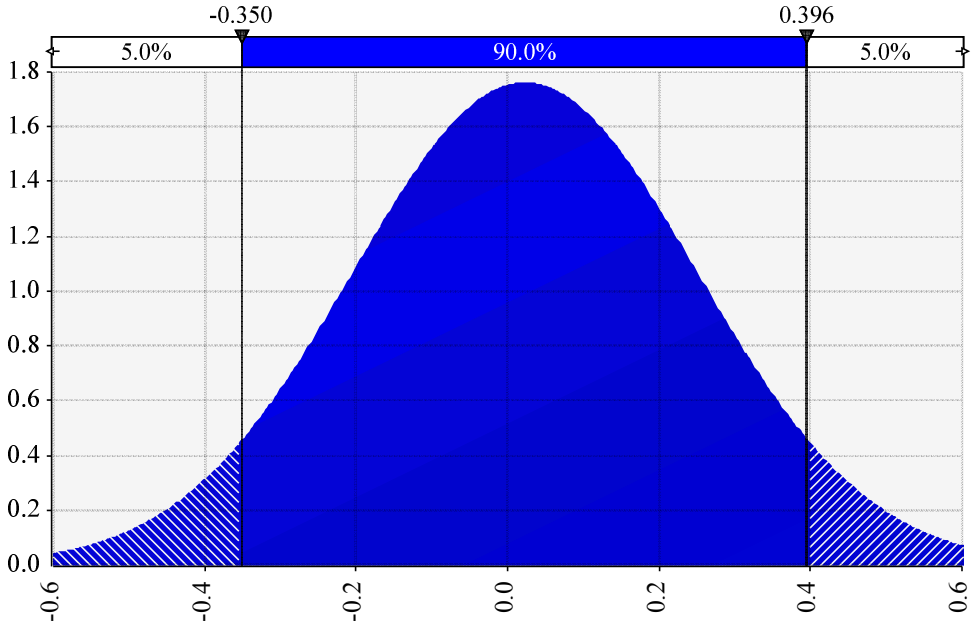

Figure 5-33 Fitted PDF for generating ε_{TH} on the Catlin Canal between Stations 0.0 and 1.0 miles

($\mu = 0.023$ and $\sigma = 0.227$)

5.2 FLOW RATE MEASUREMENT UNCERTAINTY ANALYSIS

This section pertains to the calculation of Q_{US}, Q_{DS}, Q_I, and Q_D of Equation 2.1 for estimating seepage rates via the inflow-outflow volumetric method. Based upon studies presented in Section 1 of this report, the accuracy of flow measurement was assumed to be +/- 5% at the 90% IR using ADV and ADCP technology. As such, the measured flow rate was multiplied by a randomly generated number from a normal PDF that ranged from 0.95 to 1.05 at the 5th and 95th percentiles, respectively, in @RISK. The PDF that was used in @RISK is presented as Figure 5-34. As an example, if the flow rate was measured to be 100 ft^3/s with an ADCP and the randomly generated value from the normal PDF was 0.98 for a given Monte Carlo realization, then the flowrate used for that realization would be 98 ft^3/s (100 ft^3/s times 0.98). This procedure implies that the measured flow rate by an ADV or ADCP is equivalent to the mean of the distribution. Although it is unlikely that the measured value is the true value due to measurement error, assigning a probable error range is expected to capture the full range of probable flow rates. It should be noted that sensitivity analysis was conducted for the probable error range of flow rate measurements, in which PERs of +/- 2%, +/- 5%, and +/- 8% at the 90% IR were considered. These results are presented in Section 6.4.

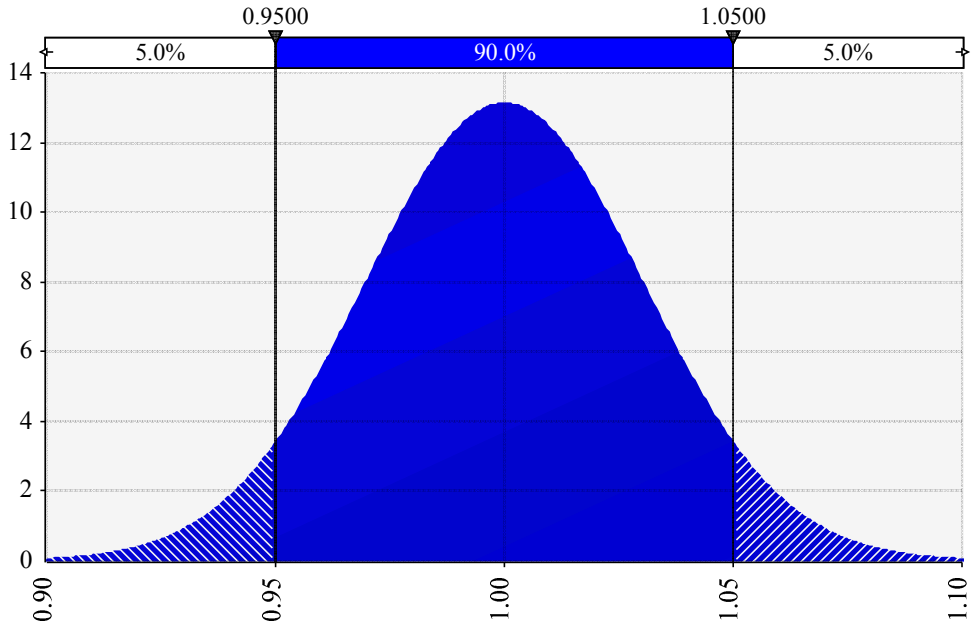

Figure 5-34 Normal PDF for the PERs of ADV and ADCP flow rate measurements ($\mu = 1.00$ and $\sigma = 0.0304$)

Correlation matrices were developed for discharge and average channel velocity on the RFH and Catlin canals, presented as Table 5-10 and Table 5-11, respectively. As discharge increases, the average channel velocity would expectedly increase also. The correlation values between discharge and average channel velocity at a given cross section were developed using measured values from the 2006 and 2007 flow rate measurements. The correlation between discharge measurement could vary depending on if the same equipment type was used to measure discharge, if the same measurement unit was used to measure discharge, and if the same personnel conducted discharge measurements at all locations within a study reach. As such, sensitivity analysis on the correlation factors between Q_{US} and Q_{DS} measurements was conducted, and is presented in Section 6.4.2.2.

Table 5-10 Correlation matrix for discharge and velocity on the RFH Canal used in @RISK

	Discharge at	Discharge at	Discharge at	Velocity at	Velocity at	Velocity at
Discharge at	1					
Discharge at	0	1				
Discharge at	0	0	1			
Velocity at Site 201	0.944	0	0	1		
Velocity at Site 203	0	0.203	0	0	1	
Velocity at Site 204	0	0	0.879	0	0	1

Table 5-11 Correlation matrix for discharge and velocity on the Catlin Canal used in @RISK

	Discharge at Site 201	Discharge at Site 202	Velocity at Site 201	Velocity at Site 202
Discharge at Site 201	1			
Discharge at Site 202	0	1		
Velocity at Site 201	0	0.90	1	
Velocity at Site 202	0.93	0	0	1

5.2.1 Predicting Q_{US} and Q_{DS} for Various Flow Measurement Conditions

Seepage measurements were conducted with either simultaneous flow rate measurements or with lagged flow rate measurements. The following definition will be used herein for simultaneous seepage measurements and lagged seepage measurements:

- *simultaneous seepage measurement* – measurement of Q_s where Q_{US} and Q_{DS} are measured over the same time period by multiple devices and sets of personnel.
- *lagged seepage measurement* – measurement of Q_s where Q_{US} was measured first, then Q_{DS} was measured in succession generally by the same device and personnel.

Refer to Figure 5-35 for an illustration of the difference between simultaneous and lagged seepage measurements. The time period over which Q_{US} is not being measured (during travel time, setup time, and the duration of Q_{DS} measurement) herein will be referred to as the "unmeasured" time period $\Delta t_A = t_4 - t_2$, and vice versa, time period $\Delta t_B = t_3 - t_1$ for Q_{DS} where t_1 is the time at the start of the upstream flow measurement, t_2 is the time at the end of the upstream flow measurement, t_3 is the time at the start of the downstream flow measurement, and t_4 represents the time at the end of the downstream flow measurement (Figure 5-35).

For steady flow conditions, the values of Q_{US} and Q_{DS} would be unchanging over $\Delta t = t_4 - t_1$ and the estimates derived from simultaneous and lagged measurements should be the same. However, for unsteady flow conditions, simultaneous and lagged measurement must be analyzed differently. For simultaneous measurements during unsteady flow, measured values of Q_{US} and Q_{DS} are interpreted as averages over Δt. For lagged measurements, Q_{US} and Q_{DS} are changing over the respective unmeasured time periods Δt_A and Δt_B and the measured values may not adequately represent the average values over the full duration of the seepage measurement Δt.

The procedures to evaluate uncertainty Q_{US} and Q_{DS} measurements during (a) steady conditions or unsteady conditions with simultaneous flow measurements or (b) unsteady lagged flow measurements are presented in the following sections.

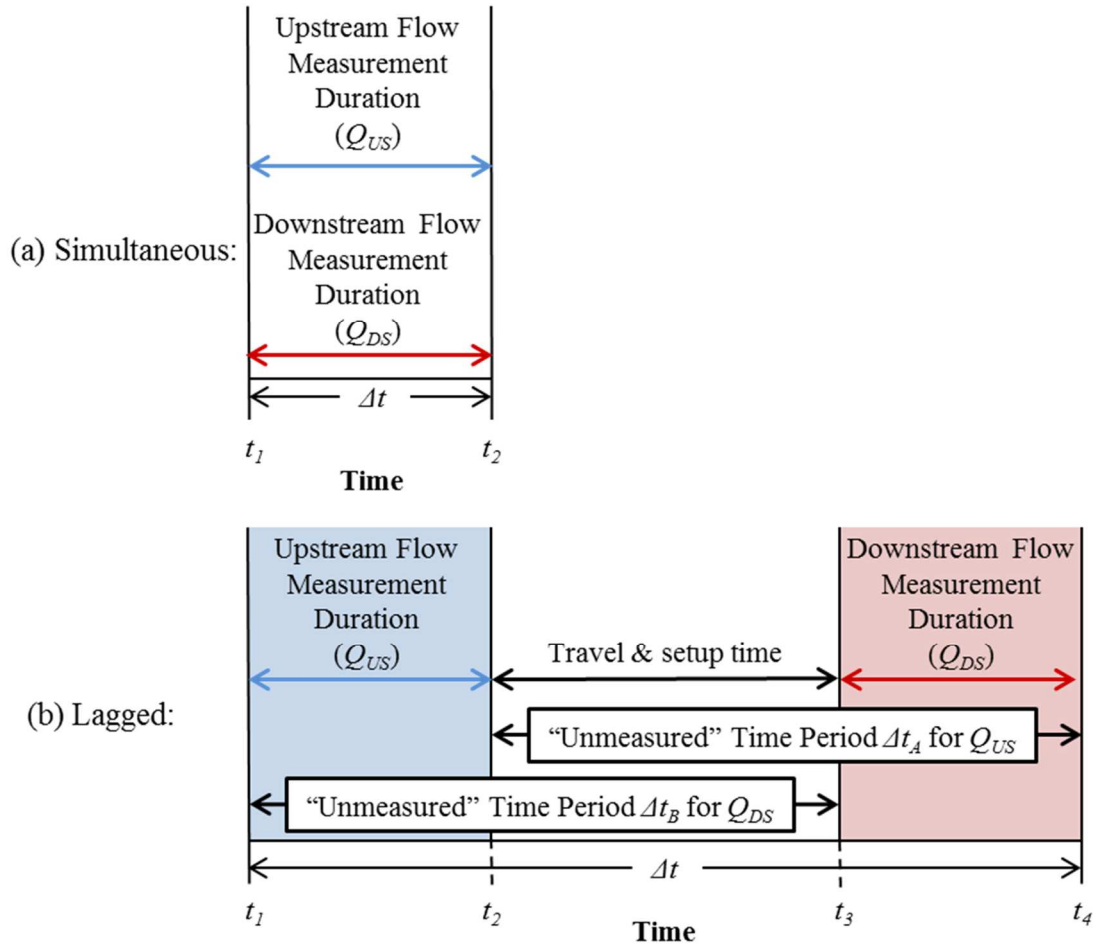

Figure 5-35 Depiction of (a) simultaneous seepage measurement versus (b) lagged seepage measurement

5.2.1.1 Simultaneous Seepage Measurements and Steady Lagged Seepage Measurements

For simultaneous seepage measurements and steady lagged seepage measurements, Q_{US} and Q_{DS} were calculated as described in the first paragraph of Section 5.2. This procedure generates a range of expected flow rates based upon the measured value and the assigned PER.

5.2.1.2 Unsteady Lagged Seepage Measurement

For unsteady flow conditions with lagged measurements, flow rates are changing over the inflow-outflow test duration Δt (Figure 5-36) and, as such, the Q_{US} value measured over Δt_A does not represent the average flow rate at the upstream boundary over Δt. During the processes of relocating the instrumentation and measuring Q_{DS} at the downstream boundary, Q_{US} likely has changed.

In other words, Q_{US} is measured, but while relocating and measuring Q_{DS}, Q_{US} has changed (unsteady flows) and is no longer equal to the measured value. Yet, $\frac{\Delta S}{\Delta t}$ is calculated over Δt using changes in H which correspond in part to Q_{US} values occurring during the unmeasured time period. The same would be true in relation to the measured value of Q_{DS}, but the unmeasured time period Δt_B occurs at the beginning of the test duration as opposed to the end. However, if the values of Q_{US} and Q_{DS} over the respective unmeasured time periods Δt_A and Δt_B can be estimated, then the average values of Q_{US} and Q_{DS} over Δt can be predicted as the weighted average of the measured flow rates and the flow rates estimated over the unmeasured time periods. This was accomplished by relating Q_{US} and Q_{DS} to the stage measured in the canal at the upstream boundary, H_{US}, and the stage measured at the downstream boundary, H_{DS}, respectively. Each flow rate estimated at a given time using H data also was adjusted by a random error. The PDF that was used to generate this random error was developed by fitting a normal distribution to residuals calculated as the difference between measured flow rate (Q_{US} or

Q_{DS}) and flow rate predicted from a trendline fit to the relationships of Q_{US} vs. H or Q_{DS} vs. H. This method was used to describe the error that occurs when predicting a flow rate using a stage-discharge relationship.

Referring to the illustration in Figure 5-37, the average value of Q_{US} and Q_{DS} over Δt was estimated using Equations 5.6 and 5.7, respectively.

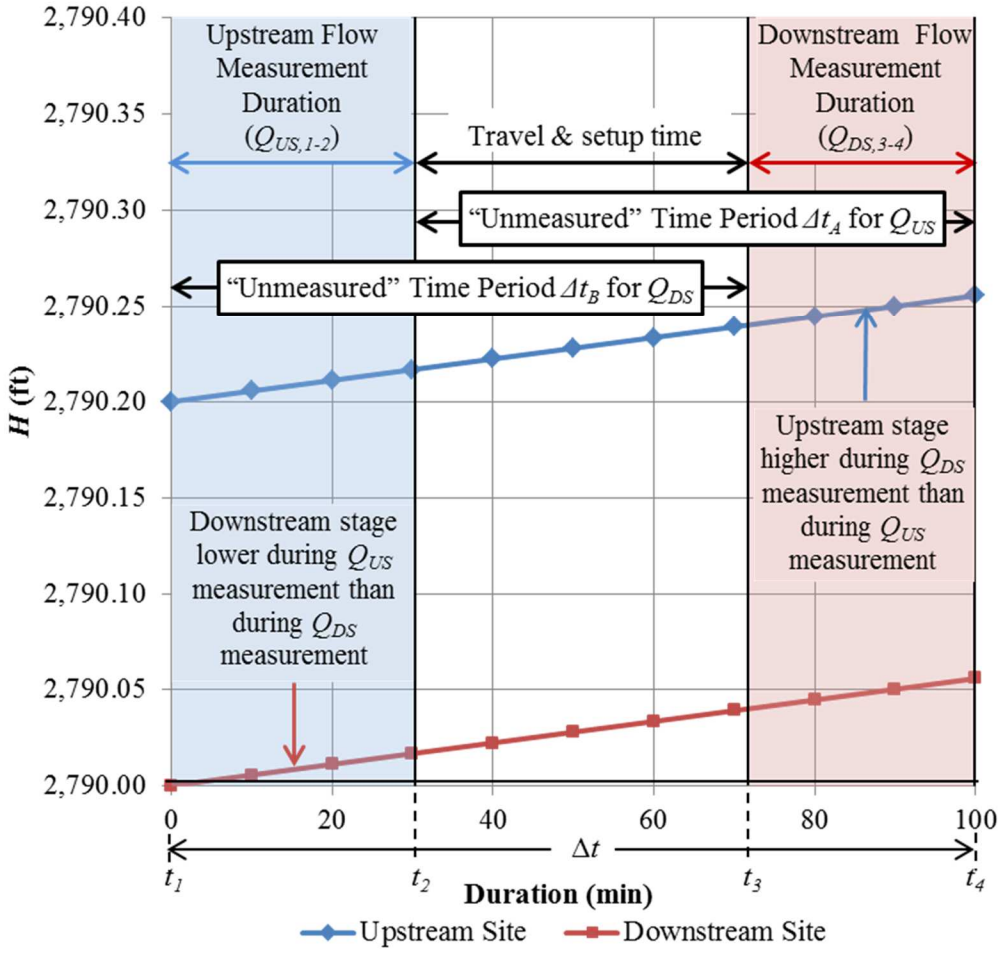

Figure 5-36 Illustration of lagged seepage measurement with unsteady flow conditions

$$Q_{US} = \frac{\left[(Q_{US,1-2} + \varepsilon_{Q_{US,1-2}})(t_2 - t_1)\right] + \left[\left(\frac{Q_{US,1-2} + Q'_{US,3}}{2}\right)(t_3 - t_2)\right] + \left[\left(\frac{Q'_{US,3} + Q'_{US,4}}{2}\right)(t_4 - t_3)\right]}{\Delta t} \quad (5.6)$$

wherein

$Q_{US,1-2}$ = measured flow rate at the upstream boundary of the test reach of the canal between t_1 and t_2 by the ADV or ADCP (ft^3/s),

$Q'_{US,3}$ = upstream flow rate at time t_3 estimated using Q vs. H relationship (ft^3/s) = $Q_{US,1-2} + \left(\frac{\Delta Q}{\Delta H}\right)_{US} \Delta H_{US,2-3} + \varepsilon_{Q_{US,3}}$,

$Q'_{US,4}$ = upstream flow rate at t_4 estimated using Q vs. H relationship (ft^3/s) = $Q_{US,1-2} + \left(\frac{\Delta Q}{\Delta H}\right)_{US} \Delta H_{US,2-4} + \varepsilon_{Q_{US,4}}$,

$\left(\frac{\Delta Q}{\Delta H}\right)_{US}$ = change in flow rate with flow stage at the upstream boundary, as developed using flow rate and pressure transducer data [$(ft^3/s)/ft$],

$\Delta H_{US,2-3}$ = measured stage change at the upstream boundary between t_2 and t_3 (ft),

$\Delta H_{US,2-4}$ = measured stage change at the upstream boundary between t_2 and t_4 (ft),

$\varepsilon_{Q_{US,1-2}}$ = randomly generated flow rate error for estimation of $Q_{US,1-2}$ (ft^3/s),

$\varepsilon_{Q_{US,3}}$ = randomly generated flow rate error for estimation of $Q'_{US,3}$ (ft^3/s),

$\varepsilon_{Q_{US,4}}$ = randomly generated flow rate error for estimation of $Q'_{US,4}$ (ft^3/s),

t_1 = time at the start of the upstream flow measurement,

t_2 = time at the end of the upstream flow measurement,

t_3 = time at the start of the downstream flow measurement, and

t_4 = time at the end of the downstream flow measurement.

$$Q'_{DS} = \frac{\left[\left(\frac{Q'_{DS,1}+Q'_{DS,2}}{2}\right)(t_2 - t_1)\right] + \left[\left(\frac{Q'_{DS,2}+Q_{DS,3-4}}{2}\right)(t_3 - t_2)\right] + \left[(Q_{DS,3-4} + \varepsilon_{QDS,3-4})(t_4 - t_3)\right]}{(t_4 - t_1)} \quad (5.7)$$

wherein

$Q_{DS,3-4}$ = measured flow rate at the downstream boundary of the test reach of the canal between t_3 and t_4 by the ADV or ADCP (ft^3/s),

$Q'_{DS,1}$ = downstream flow rate at time t_1 estimated using Q vs. H relationship (ft^3/s) = $Q_{DS,3-4} + \left(\frac{\Delta Q}{\Delta H}\right)_{DS} \Delta H_{DS,1-3} + \varepsilon_{Q_{DS,1}}$,

$Q'_{DS,2}$ = downstream flow rate at t_2 estimated using Q vs. H relationship (ft^3/s) = $Q_{DS,3-4} + \left(\frac{\Delta Q}{\Delta H}\right)_{DS} \Delta H_{DS,2-3} + \varepsilon_{Q_{DS,2}}$,

$\left(\frac{\Delta Q}{\Delta H}\right)_{DS}$ = change in flow rate with flow stage at the downstream boundary, as developed using flow rate and pressure transducer data [$(ft^3/s)/ft$],

$\Delta H_{DS,1-3}$ = measured stage change at the downstream boundary between t_1 and t_3 (ft),

$\Delta H_{DS,2-3}$ = measured stage change at the upstream boundary between t_2 and t_3 (ft),

$\varepsilon_{Q_{DS,3-4}}$ = randomly generated flow rate error for estimation of $Q_{DS,3-4}$ (ft^3/s),

$\varepsilon_{Q_{DS,1}}$ = randomly generated flow rate error for estimation of $Q'_{DS,1}$ (ft^3/s), and

$\varepsilon_{Q_{DS,2}}$ = randomly generated flow rate error for estimation of $Q'_{DS,2}$ (ft^3/s)

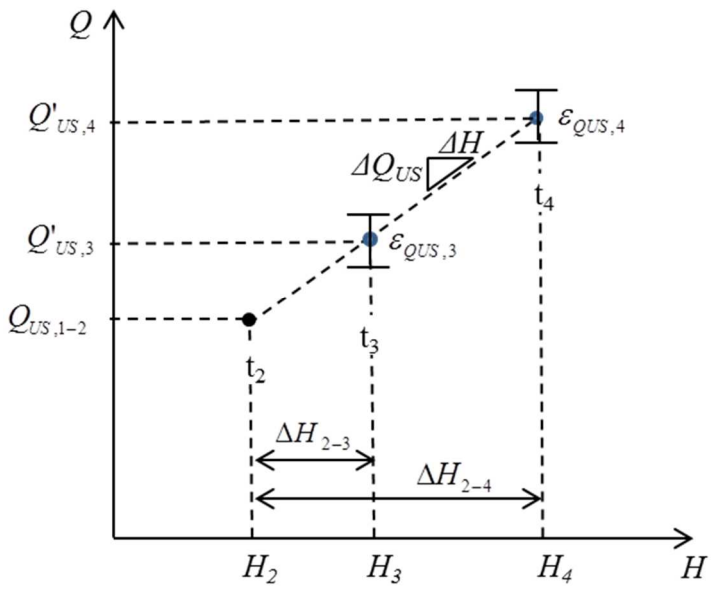

Figure 5-37 Depiction of stage increase at upstream cross-section during unsteady lagged seepage measurement

Each of the variables in the Equations 5.6 and 5.7 were measured in the field during a seepage test, with the exception of $Q'_{US,3}$, $Q'_{US,4}$, $Q'_{DS,1}$, $Q'_{DS,2}$. However, these unmeasured variables can be estimated using a relationship between flow rate and stage (Q vs. h) based upon pressure transducer data that recorded stage continuously during the full duration of seepage measurement. The values of $\left(\frac{\Delta Q}{\Delta H}\right)_{US}$ and $\left(\frac{\Delta Q}{\Delta H}\right)_{DS}$ were estimated from available pressure transducer and flow rate measurements at the upstream and downstream ends of the test reach and overall were relatively consistent for the available measured datasets. For the period of this study they were calculated by plotting measured values of Q_{US} vs. H_{US} and Q_{DS} vs. H_{DS} and fitting linear trendlines to each data set [statistically significant ($\alpha = 0.05$) R^2 of 0.92 and 0.94, respectively]. The observed range of H varied by less than 1.6 ft, and the relationship between Q

and H was linear in all cases over the measured data sets with $\left(\frac{\Delta Q}{\Delta H}\right)_{US}$ and $\left(\frac{\Delta Q}{\Delta H}\right)_{DS}$ calculated as the slope of the fitted trend lines. Note that pressure transducers were not installed in 2006, so this analysis could only be conducted for 2007 measurements.

The measured flow rate was plotted versus stage measurement by the pressure transducers and a trendline was fit to the data, as presented in Figure 5-38 for Site 201 and Site 202 on the Catlin Canal. Pressure transducer #1 (PT #1)were used for Site 201 (0.09 miles downstream), and data from pressure transducer #5 (PT #5) was used for Site 202 (0.22 miles upstream). These pressure transducers were located closest to their respective flow measurement sites, which is why they were selected. Based upon Figure 5-38, it is clear that measured flow rate and stage (as measured by the nearest pressure transducer) are correlated. With the relationship between flowrate and stage at the upstream and downstream cross-sections determined [$\left(\frac{\Delta Q}{\Delta h}\right)_{US}$ and $\left(\frac{\Delta Q}{\Delta h}\right)_{DS}$, respectively], the predicted change in flowrate (ΔQ) could be calculated for a given change in stage (Δh). It is acknowledged that the relationship between Q and h, as developed from pressure transducers, has an associated degree of error due to multiple potential factors including (a) temporal changes in vegetation within the canal, (b) operational of gates within the canal, (c) the pressure transducers are located outside of the flow measurement cross-section, etc. To account for this uncertainty, the randomly generated error terms $\varepsilon_{QDS,1}$, $\varepsilon_{QDS,2}$, $\varepsilon_{QUS,3}$, and $\varepsilon_{QUS,4}$ were added into the Equations 5.13 and 5.16. They are randomly generated value from a PDF developed by residuals of the $\frac{\Delta Q}{\Delta h}$ relationship.

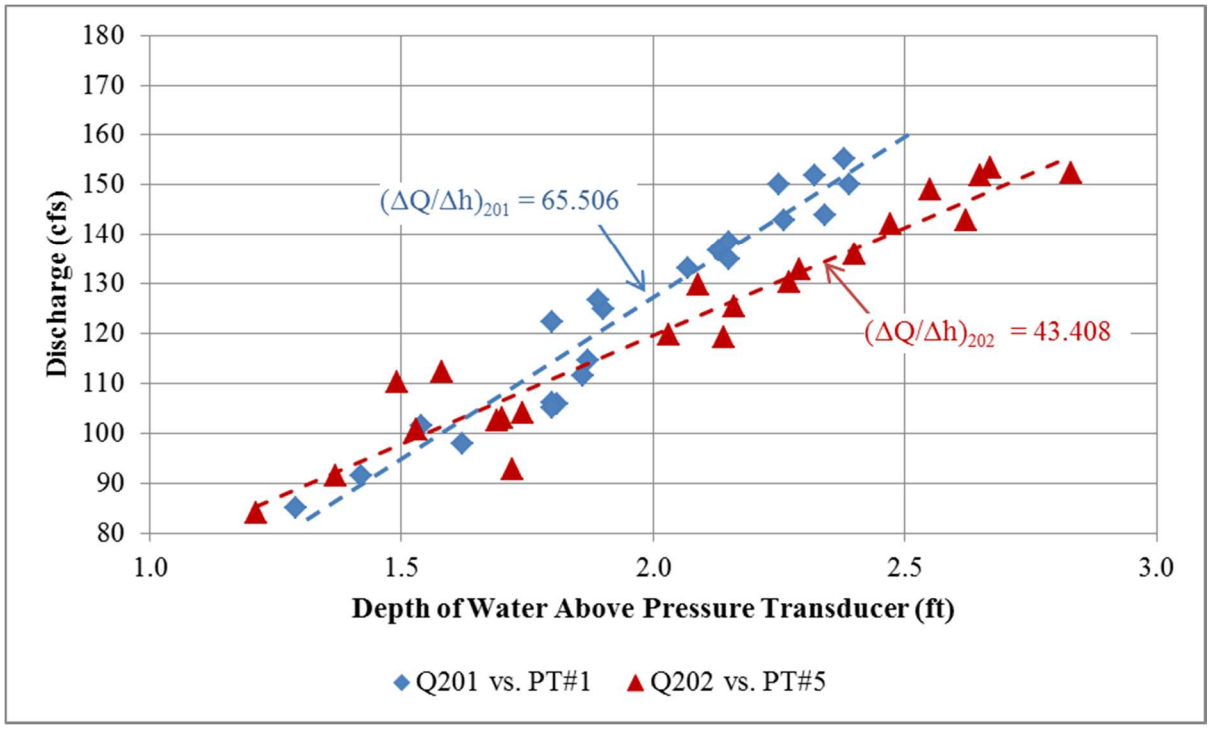

Figure 5-38 Relationship between flow rate and stage on the Catlin Canal in 2007

The PER for $\varepsilon_{QDS,1}$, $\varepsilon_{QDS,2}$, $\varepsilon_{QUS,3}$, and $\varepsilon_{QUS,4}$ were adjusted such that that unrealistic values of ΔQ could not be generated. For example, a stage increase of 0.01 feet would not realistically produce a flow rate increase of 10 ft^3/s for the Catlin canal where the top width is approximately 20 feet (incremental area would be 0.2 ft^2, which would mean that the average velocity over ΔH would be 10 ft^3/s /0.2 ft^2 = 50 ft/sec which is unrealistic). Based upon relationships of $\left(\frac{\Delta Q}{\Delta H}\right)$ at different times of the year, it was discovered that $\left(\frac{\Delta Q}{\Delta H}\right)$ is typically within 15% of the values presented in Figure 5-38. As such, the PER for $\varepsilon_{QDS,1}$, $\varepsilon_{QDS,2}$, $\varepsilon_{QUS,3}$, and $\varepsilon_{QUS,4}$ was set at +/-15% error. The error terms $\varepsilon_{QDS,1}$, $\varepsilon_{QDS,2}$, $\varepsilon_{QUS,3}$, and $\varepsilon_{QUS,4}$ were calculated by generating a random value using a normally distributed PDF with a mean of zero and the 5th and 95th percentiles at -0.15 and+0.15 (+/- 15% error), respectively. Four PDFs

were created; one for each of the four error terms. This procedure accounted for error in estimating ΔQ based upon ΔH, while limiting the generated error to realistic values.

For the Monte Carlo simulation in @RISK, the PDFs used to calculated $\varepsilon_{QDS,1}$ and $\varepsilon_{QDS,2}$ were correlated by a factor of 1.0 and the PDFs used to calculated $\varepsilon_{QUS,3}$ and $\varepsilon_{QUS,4}$ were correlated by a factor of 1.0, since the relationship between flow depth and flow rate would be the same at t_3 and t_4 for Site 201 and the same at t_1 and t_2 for Site 202 (i.e. the magnitude that a change in flow depth has on the flow rate would be the same despite the time of the measurement, because the short duration between measurements). This assumption could not be made for long durations, as the relationship between H and Q could vary more significantly.

Impact of storage changes on predicted flow rates:

An example of the impact that storage change can have on the average measured flow rate for lagged discharge measurements is presented in Figure 5-39. The distribution for Q_{US} and Q_{DS} are presented as Figure 5-39 (a) and (b), respectively. The calculated flowrate using the aforementioned methodology for estimating discharge over the unmeasured time period during a stage change, was illustrated in Figure 5-36. For this example, the seepage test was conducted on the Catlin Canal while stage was decreasing on June 14, 2007 (negative storage change in the control volume). It can be seen that the "predicted" Q_{US} is greater than "measured" Q_{US} in Figure 5-36. Since Q_{US} was measured at the beginning of the seepage measurement when stage was at its highest, "measured" Q_{US} is higher than "predicted" Q_{US} over the full seepage measurement duration. Similarly for the downstream flow measurement, "Q_{DS} calculated" is higher than " Q_{DS} measured" because the downstream flow rate was measured at the end of the seepage measurement period when stage was at its lowest point. For clarification, the

"calculated" flow rates were used to calculate final seepage results. Note that for each Monte Carlo simulation, Δh changes because a new measurement error term is randomly generated for every realization, which also impacts the estimated value of ΔQ.

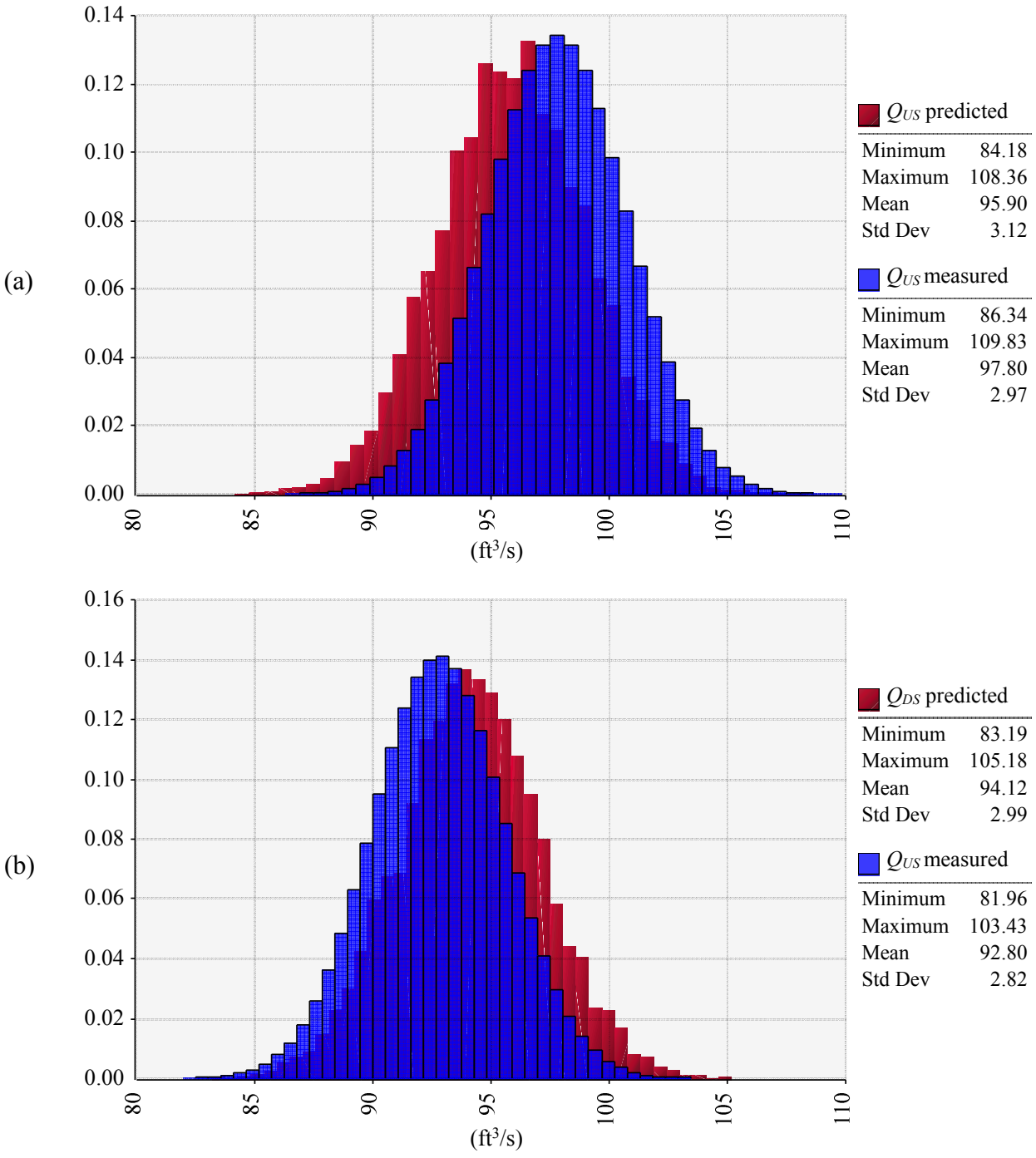

Figure 5-39 Comparison between generated distributions of measured and predicted values of (a) Q_{US} and (b) Q_{DS} for a lagged seepage test with unsteady flow on the Catlin Canal on 6/14/2007

5.3 EVAPORATION CALCULATION UNCERTAINTY ANALYSIS

A literature review of the error and uncertainty of free-water evaporation measurements is presented in Chapter 1. Few dependable studies were found, and most studies made comparisons among measurement techniques or compared results using different equations, as opposed to conducting controlled studies to estimate the accuracy of each method.

It is recognized that error in evaporation calculations stems from (1) the equation used to calculate evaporation and (2) measurement error of atmospheric data. As such, it was decided that modeling uncertainty by lumping these two sources together would be an acceptable approach since not enough information was found to be able to quantify the two sources of uncertainty individually. In addition, estimating the accuracy of weather station data is very difficult and exceeds the scope of this study.

The depth rate of free water evaporation from the canal water surface over the seepage study reach was estimated with the Penman combination hydrometeorological equation (Dingman, 2002) using data collected at the closest weather stations associated with Colorado State University's CoAgMet program (CoAgMet, 2006 and 2007). A CoAgMet weather station located about 1.0 km southeast of Avondale (ID: AVN01), and about 22 km from the midpoint of RFH Canal study reach, was used for the RFH Canal. For the Catlin C, data were taken from a weather station location near Rocky Ford (ID: RFD01), which is approximately 8.5 km from the Catlin Canal study reach midpoint.

Based upon studies reported by Ham (2002) it was assumed that free-water evaporation from a canal's water surface can be estimated as a random variable within +/-20% of the value predicted by the Penman combination equation over the 90th IR. In the @Risk model, the depth rate of free-water evaporation (calculated from the Penman Combination Equation) was multiplied by a randomly generated value from a normal PDF (presented as Figure 5-40), with a

mean of 1.0, a value of 0.80 is at the 5% interval, and a value of 1.20 is at the 95% interval. To obtain Q_E, the depth rate of evaporation was multiplied by A_{WS} along the control volume.

For example, if the evaporation rate was calculated to be 6.0 mm/day (0.02 ft/day) using the Penman Combination Equation and the randomly generated variable from the PDF was 1.1 for a given Monte-Carlo realization, then the evaporation rate used for that realization would be 6.6 mm/day (6.0 mm/day multiplied by 1.1) or 0.022 ft/day. For the next simulation realization, the randomly generated variable may be 0.95, in which case the evaporation rate for that realization would be 5.7 mm/day (6.0 mm/day multiplied by 0.95) or 0.019 ft/day. This approach was used to estimate a probable range of evaporation rates during a given seepage test.

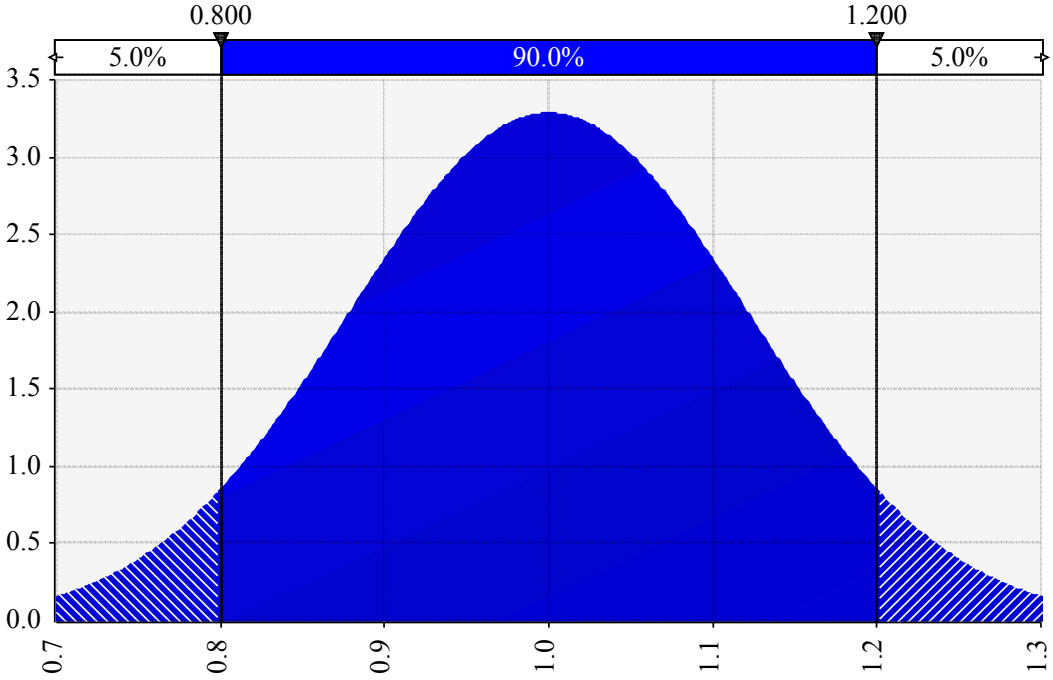

Figure 5-40 Normal probability distribution function used to generate uncertainty in free-water evaporation measurement ($\mu = 1.0$ and $\sigma = 0.1215$)

5.4 STAGE MEASUREMENT UNCERTAINTY ANALYSIS

Temporal variability in canal water levels are associated with changes in the volume of water stored within a canal control volume. Main sources of such variability include changing inflow rates at the canal system's source (river), changes in diversion rates from the canal, adjustments to the settings of regulating structures (i.e. sluice gates and overshot weirs), changes in channel hydraulic geometry and hydraulic resistance, and atmospheric variability.

For this study, stage measurements were conducted using staff gages, ONSET HOBO pressure transducers, and In-Situ pressure transducers.

Water level fluctuations were monitored at upstream and downstream cross-sections where Q_{US} and Q_{DS} were measured and, in some cases, at intermediate cross-sections over Δt. Staff gages were mounted at the upstream and downstream cross-sections so that readings of H could be collected during flow rate measurements. Pressure transducers with data loggers also were used to monitor water levels along the study reaches, although they were not installed at upstream and downstream flow measurement cross-sections and only were used in 2007. Manual readings of H using staff gages typically were recorded every 5 to 15 minutes during inflow-outflow tests, and readings with pressure transducers were recorded automatically every 15 minutes.

5.4.1 Pressure Transducer Stage Measurement Error

Pressure transducers installed at intermediate locations along the canal study reach were used to measure the absolute pressure, p_{abs}, due to the water column above the transducer. One pressure transducer also was employed near each canal study reach to measure barometric pressure p_{baro}, needed to convert p_{abs} into gage pressure, p_{gage}, from which the height of the water column above the pressure transducer was calculated using average water density, γ_w, for the

range of temperatures recorded. Therefore, each stage measurement is subject to error from two pressure transducers, and the total error associated with a stage measurement using pressure transducers was calculated as the sum of errors associated with P_{abs} (unique to each stage measurement location) and P_{baro} (uniform for all stage measurement locations on a canal).

From the pressure transducer's technical specifications, it was found that the ONSET HOBO pressure transducers are accurate within 0.03 feet and that the In-Situ pressure transducers are accurate within 0.035 feet (In-Situ 2009; ONSET 2008). For this study, measurement error for P_{abs} and P_{baro} were both assumed to be +/- 0.04 feet of water over the 90th IR of a normal PDF, using the manufacturer's specifications as a reference.

The normal PDF used to generate random errors related to pressure transducer measurements is presented as Figure 5-41. The error value generated from the PDF in Figure 5-41 was added to the stage measured by the pressure transducers. The randomly generated error terms for P_{abs} and P_{baro} were assigned variables ε_{abs} and ε_{baro}, respectively, and the height of the water column above a pressure transducer, h_{PT} was calculated as follows:

$$h_{PT} = \frac{P_{abs} - P_{baro}}{\gamma_w} + \varepsilon_{abs} + \varepsilon_{baro} = \frac{P_{gage}}{\gamma_w} + \varepsilon_{abs} + \varepsilon_{baro} \tag{5.8}$$

The water column above a pressure transducer (h_{PT}) was converted to H in the canal using longitudinal survey data. For each surveyed canal cross-section, a survey pin was installed on the channel bank and the longitudinal survey captured these survey pins. This allowed for relative elevations of all survey points, as well as the elevation of each installed pressure transducer, EL_{PT}, to be linked together and relative H values to be calculated as the elevation of the pressure transducer plus the error-adjusted water column height. Values of H at cross

sections not equipped with pressure transducers were estimated using linear interpolation between values at cross sections with pressure transducers.

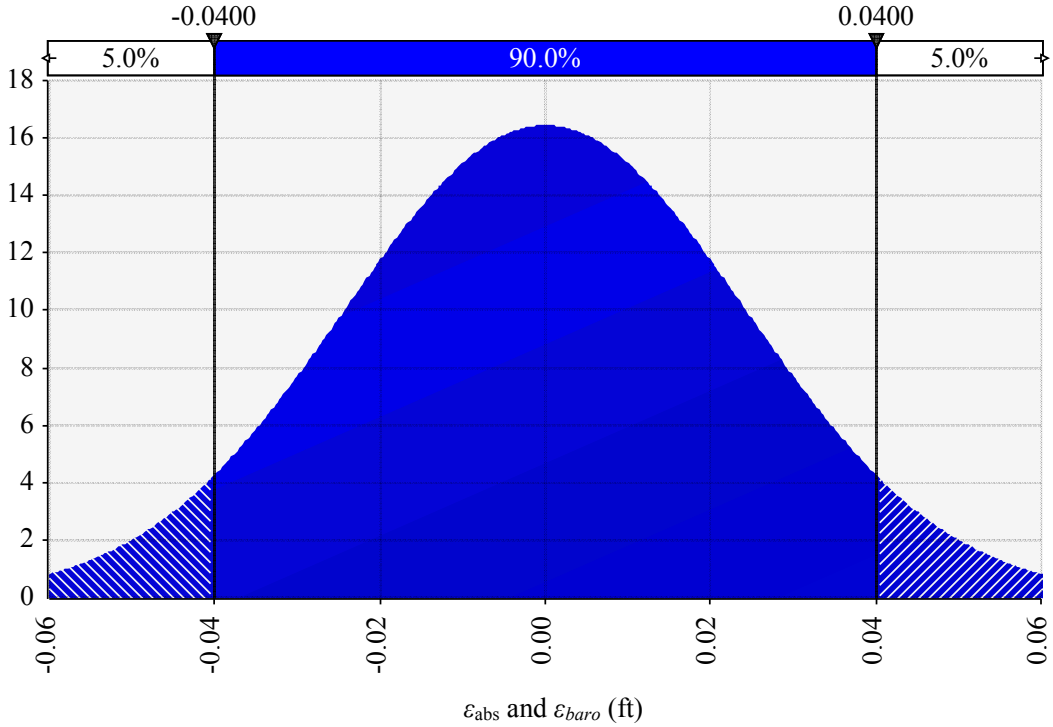

Figure 5-41 Normal probability distribution function used to generate ε_{abs} and ε_{baro} ($\mu = 0$ and $\sigma = 0.0243$)

5.4.2 Staff Gage Stage Measurement Uncertainty Analysis

When reading a staff gage, user error is involved due to wave action and the subjective nature of human interpretation. Staff gages were placed along canal banks where velocities were slower so wave action caused by the interference of flow from the staff gage/mounting post was minimal, but present, and interpretations of stage are subjective. Therefore, based upon personal field experience, it was assumed that measurement error was +/-0.04 feet (~0.5 inch) at the 90% IR. The normal PDF used to generate random errors related to staff gage measurements is presented as Figure 5-42. The error value generated from the PDF (ε_{sg}) in Figure 5-42 was added to the stage measured using a staff gage. For example, if the canal stage was measured to

be 1.50 feet and ε_{sg} was generated to be -0.02 feet for a given Monte-Carlo realization, then the stage from the staff gage measurement used for that realization was 1.48 feet (1.50 feet minus 0.02 feet).

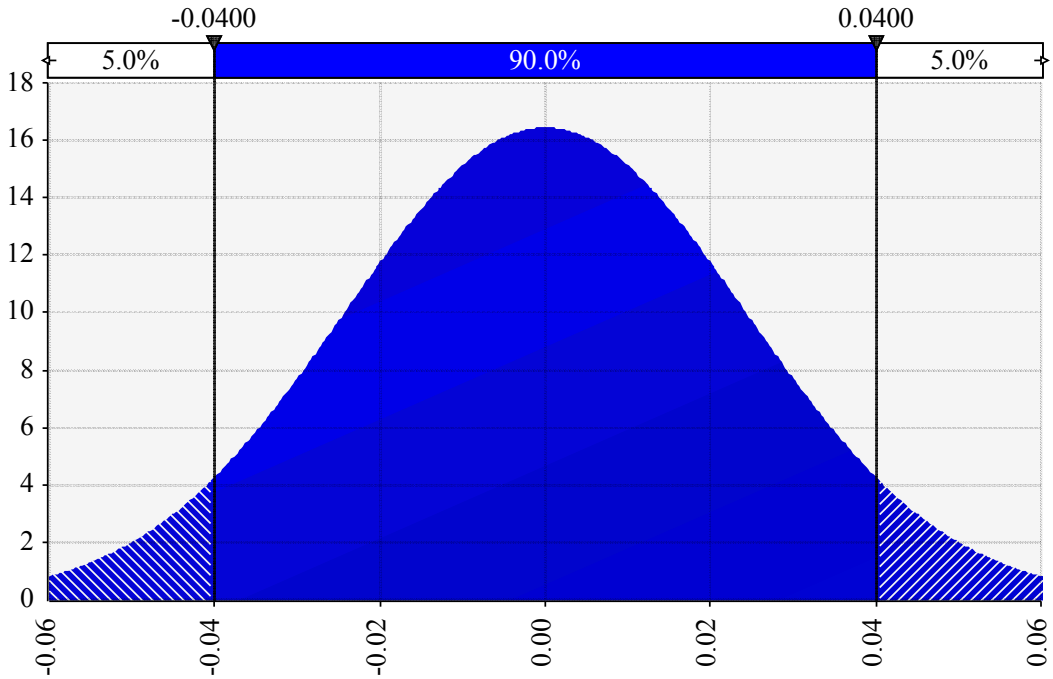

Figure 5-42 Normal probability distribution function used to generate ε_{sg} ($\mu = 0$ and $\sigma = 0.0243$)

5.4.3 Stage Estimates during Unsteady Flow Conditions

When unsteady flow occurred in the canal test reaches, the measured values of p_{abs} typically were found to oscillate due to short-term wave action about a linear trendline over Δt. To smooth out this behavior, a general linear trend over Δt was fit to the water column data derived from p_{gage} values calculated from measured p_{abs} and p_{baro} along the test reach and was used to compute total changes in H at locations with installed pressure transducers (example in Figure 5-43). Only manual staff gage readings were recorded at the upstream and downstream boundaries, where Q_{US} and Q_{DS} were measured, near the beginning and end of the relatively short measurement durations Δt_A and Δt_B which were typically on the order of 15 to 20 minutes.

As such, oscillations in H were not always apparent from manual staff gage readings; thus, the total changes in H over Δt_A and Δt_B at the upstream and downstream boundaries also were estimated by projecting the fitted linear trend in the water column estimated from the p_{gage} data along the test reach.

To account for uncertainty in estimating H by projecting a linear trend line ($H_{PTtrend}$), a random error, $\varepsilon_{PTtrend}$, was generated from a normal PDF, which was inferred from residuals computed as the difference between the oscillating H measurements and the corresponding value predicted from the linear trend line. Note that this measurement error is only associated with pressure measurements in the canal, so ε_{baro} was also added to the equation for estimating H.

As such, H was estimated during unsteady flow conditions as the following, where H_{t_i} is the predicted stage at a time t_i during the seepage test, and H_{t_1} is the measured stage at t_1:

$$H_{ti} = \left(H_{t_1} + \frac{\Delta H}{\Delta t}(t_i - t_1) \right) + \varepsilon_{PTtrend} + \varepsilon_{baro} = \left(H_{PTtrend} \right) + \varepsilon_{PTtrend} + \varepsilon_{baro} \tag{5.9}$$

$$\Delta H = H_{t4} - H_{t1} \tag{5.10}$$

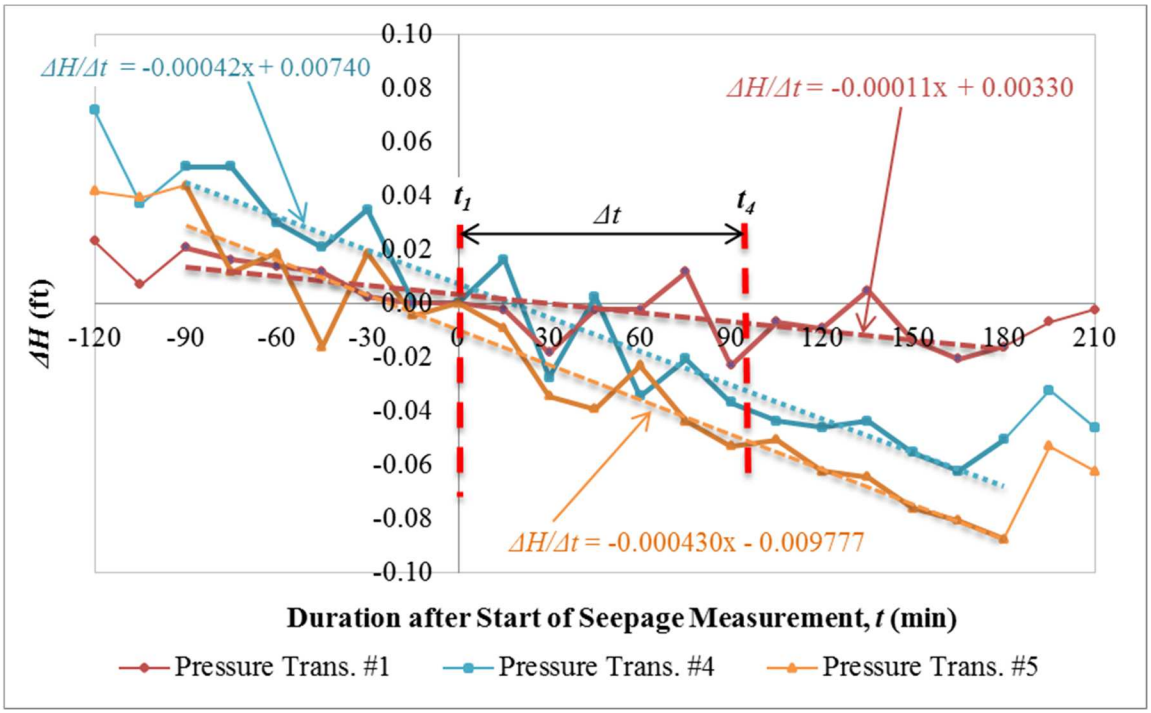

Figure 5-43 Example of trendlines fit to pressure transducer stage data (7/10/2007 on Catlin Canal) used to calculate $H_{PTtrend}$

5.5 STORAGE CHANGE ESTIMATION UNCERTAINTY ANALYSIS

In 2007 pressure transducers were installed into the canals which helped to track stage changes along the study reaches which could be used to estimate $\Delta S/\Delta t$. The pressure transducers made storage changes easier to identify and simplified calculations of ΔS. Manual staff gage readings could also be compared the pressure transducer stage data as a comparison and to assist in calculation of ΔS. In 2006, no pressure transducers were installed in the canals so the only source of stage data came from manual staff gage readings at flow measurement locations (Q_{US} and Q_{DS} boundaries). Since staff gages were only read over the duration of the flow measurements, tracking changes in the stored volume was much more difficult. The calculations of ΔS in the study reach were solely dependent upon these staff gage readings over a

relatively short period of time. Without having data at intermediate locations (locations between Q_{US} and Q_{DS} boundaries) the change in volume is more uncertain. Uncertainty associated with not having stage data at intermediate locations could not be quantified, but it is important to acknowledge its existence, and the importance of intermediate stage readings is noted.

The total volume of storage gained or lost in the canal reach control volume during a seepage test was calculated by analyzing H data along the study reaches. Rising or falling H was tracked over Δt and the total volume of water associated with the changes was calculated over the measurement duration. To obtain ΔS, the average change in H measured at the upstream and downstream end of each subreach j was estimated and multiplied by the average water surface area over that subreach, which is the product of channel length between two stage measurement stations, L_j, and average top width, $\overline{T}_{w_j}$. Summing all N subreach storage changes and dividing by Δt yielded the total rate of storage change over the entire canal study reach:

$$\frac{\Delta S}{\Delta t} = \frac{\sum_{j=1}^{N}\left[\frac{\left(\Delta H_{1\text{–}4}\right)_{US_j} + \left(\Delta H_{1\text{–}4}\right)_{DS_j}}{2}\left(L_j \overline{T}_{w_j}\right)\right]}{\Delta t} \tag{5.11}$$

Where:

$\left(\Delta H_{1\text{–}4}\right)_{US_j}$ = measured stage change over Δt at the stage measurement location on the upstream end of subreach j (ft) and

$\left(\Delta H_{1\text{–}4}\right)_{DS_j}$ = measured stage change over Δt at the stage measurement location on the downstream end of subreach j (ft).

Uncertainty in estimates of $\frac{\Delta S}{\Delta t}$ is captured in Equation 5.11 due to dependence on the random variables H and T_w as described above.

6 RESULTS AND DISCUSSION

This section presents results and discussions for the following:

- Canal seepage estimates from a deterministic approach using the inflow-outflow method.
- Canal seepage estimates from a stochastic approach using the inflow-outflow method.
- Relationships between canal seepage, cross-section averaged flow velocity, and turbidity.
- Analysis of sensitivity of estimated canal seepage to variables used in the inflow-outflow method.
- Effectiveness of PAM applications in reducing canal seepage using
    - deterministic estimates of seepage rates, and
    - stochastic estimates of seepage rates.

6.1 DETERMINISTIC SEEPAGE RESULTS

Analysis of inflow-outflow seepage measurements using a deterministic approach are presented in this section for the Catlin, RFH, Lamar, and Fort Lyon canals. The deterministic approach assumes that the field-measured values for the variables in the water balance Equation (3.1) are known with certainty. Effectiveness of PAM applications is discussed in Section 6.5.

Note that negative values of Q_s indicate that the canal control volume was gaining water, which is unlikely but possible.

Catlin Canal

Deterministic estimates of Q_s from Equation (3.1) for the inflow-outflow tests on the Catlin Canal in 2006 are presented in Table 6-1 and plotted in Figure 6-1. Deterministic Q_s and $\hat{Q}_S$ values for the Catlin Canal in 2007 are presented in Table 6-2 and plotted in Figure 6-2. In 2006,

the PAM application on the Catlin Canal was performed on June 3rd, which was the first day of seepage measurements. As such, pre-application seepage measurements were limited to one test using ADVs and one test using an ADCP to measure Q_{US} and Q_{DS}. Prior to the PAM applications, measured Q_s values were 1.38 $ft^3/s/acre$ and 0.64 $ft^3/s/acre$. The day after PAM application, measured Q_s values from three tests were 0.14 $ft^3/s/acre$, 0.23 $ft^3/s/acre$, and -0.72 $ft^3/s/acre$, all of which were less than the day before (when PAM had yet to be applied). Throughout the remainder of the irrigation season, an additional seven seepage tests were conducted, with estimates of Q_s ranging between -0.34 and 0.55 $ft^3/s/acre$. In summary, estimates of $\hat{Q}_s$ were lower for all 2006 post-PAM application measurements than for the two pre-PAM application measurements, indicating that seepage was reduced.

Table 6-1 Deterministic canal seepage estimates for the Catlin Canal in 2006

Date	Measurement Equipment and Method	Canal Storage Change?	A_P (acre)	Q_{US} (ft^3/s)	Q_{DS} (ft^3/s)	Q_D (ft^3/s)	Q_I (ft^3/s)	$\Delta S/\Delta t$ (ft^3/s)	Q_E (ft^3/s)	Q_s (ft^3/s)	$\hat{Q}_s$ [(ft^3/s)/acre]
6/3/06	ADCP, Lagged	No	7.1	112.0	102.0	0	0	0	0.2	9.8	1.38
6/3/06	ADV, Simultaneous	No	7.2	105.9	101.1	0	0	0	0.2	4.6	0.63
PAM APPLICATION – June 3, 2006											
6/4/06 A	ADV, Simultaneous	Yes	7.3	113.7	113.2	0	0	-0.8	0.3	1.0	0.14
6/4/06 B	ADCP, Lagged	No	7.3	131.0	129.0	0	0	0	0.3	1.7	0.23
6/4/06 C	ADCP, Lagged	No	7.3	128.0	133.0	0	0	0	0.3	-5.3	-0.72
6/22/06 A	ADV, Simultaneous	Yes	7.1	100.1	101.4	0	0	1.0	0.2	-2.4	-0.34
6/22/06 B	ADV, Simultaneous	Yes	7.1	100.4	101.4	0	0	-0.5	0.2	-0.8	-0.11
6/26/06	ADV, Lagged	No	7.1	103.0	99.4	0.7	0	0	0.2	2.7	0.38
7/20/06	ADCP, Lagged	No	7.1	103.0	103.5	0	0	0	0.2	-0.7	-0.10
8/10/06	ADCP, Lagged	No	7.1	107.0	103.0	0	0	0	0.1	3.9	0.55
9/28/06	ADCP, Lagged	No	6.6	71.2	70.6	0.5	0	0	0.1	0.0	0.00
11/2/06	ADCP, Lagged	No	6.6	64.5	63.5	0	0	0	0.1	0.9	0.14

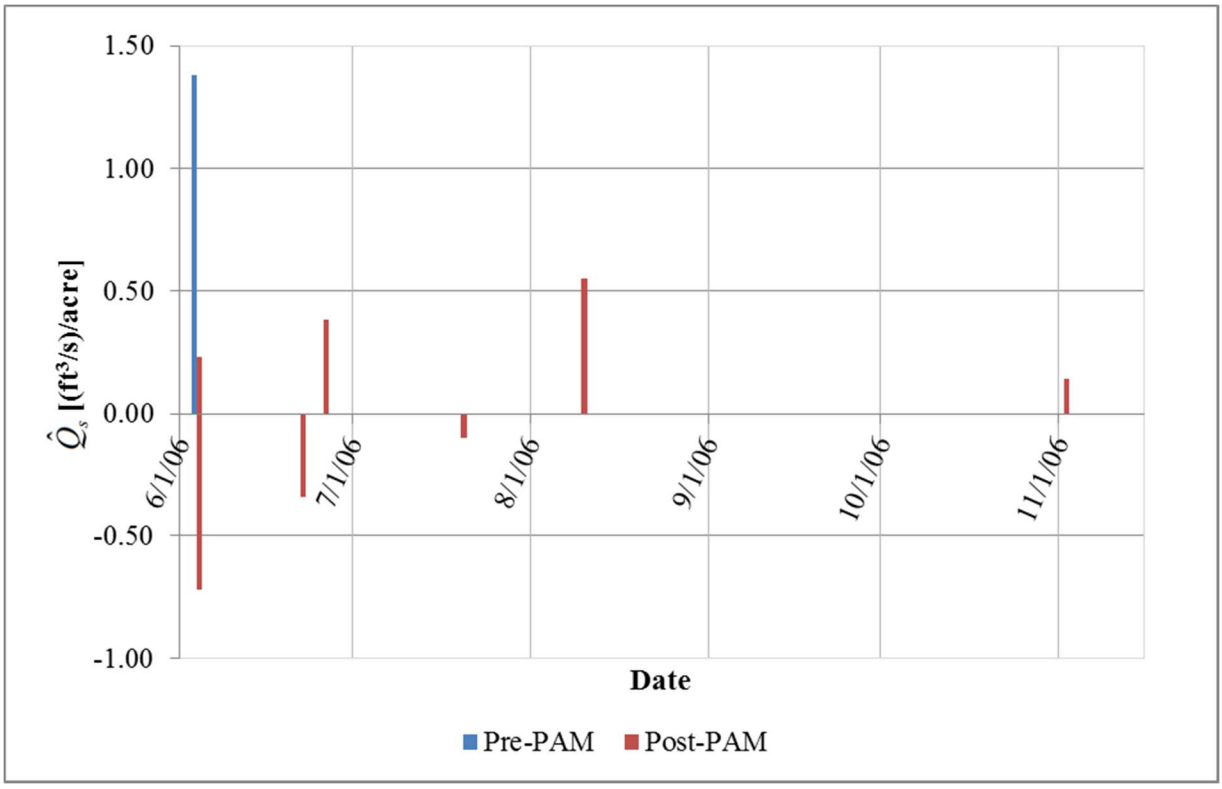

Figure 6-1 Pre- and post-PAM application deterministic $\hat{Q}_s$ estimated from inflow-outflow tests on the Catlin Canal in 2006

In 2007, PAM was applied to the Catlin Canal on August 7th, allowing for $\hat{Q}_s$ to be measured multiple times before and after the application. There were fourteen pre-application measurements and twelve post-application measurements of $\hat{Q}_s$. The same study reach on the Catlin Canal was used for the tests conducted in both 2006 and 2007, as described in Section 2.3.

Pre-application measurements of $\hat{Q}_s$ ranged from 0.02 to 1.53 $ft^3/s/acre$, and post-application measurements of $\hat{Q}_s$ ranged from -0.37 to 0.28 $ft^3/s/acre$ in 2007. Three seepage tests were conducted the week prior to PAM application, resulting in $\hat{Q}_s$ estimates of 0.85, 1.01, and 1.14 $ft^3/s/acre$. Five seepage tests were conducted the week after PAM application, resulting

in $\hat{Q}_s$ estimates of 0.11, -0.37, -0.38, 0.17, and -0.18 $ft^3/s/acre$, all of which were less than estimates of $\hat{Q}_s$ the week before PAM was applied, indicating a reduction in seepage loss.

Table 6-2 Deterministic canal seepage estimates for the Catlin Canal in 2007.

Date	Measurement Equipment and Method	Canal Storage Change?	A_P (acre)	Q_{US} (ft^3/s)	Q_{DS} (ft^3/s)	Q_D (ft^3/s)	Q_I (ft^3/s)	$\Delta S/\Delta t$ (ft^3/s)	Q_E (ft^3/s)	Q_s (ft^3/s)	$\hat{Q}_s$ [(ft^3/s)/acre]
4/25/2007	ADCP, Lagged	No	6.9	92.4	90.5	0	0	0	0	1.9	0.28
4/28/2007	ADCP, Lagged	No	6.9	87.0	84.8	0.3	0.0	0.0	0.1	1.8	0.26
5/23/2007	ADCP, Lagged	No	7.1	119.6	114.9	0.3	0.0	0.0	0.1	4.3	0.61
6/14/2007	ADCP, Lagged	Yes	7.1	95.9	94.1	0.3	0.0	-2.6	0.1	4.0	0.56
6/20/2007	ADCP, Lagged	No	7.4	124.8	119.3	0.3	0.0	0.0	0.2	5.0	0.68
7/10/2007	ADCP, Lagged	Yes	7.2	105.8	104.6	1.0	0.0	-1.3	0.0	1.4	0.20
7/11/2007 A	ADCP, Lagged	Yes	7.1	105.1	102.6	1.0	0.0	0.4	0.1	1.0	0.14
7/11/2007 B	ADCP, Lagged	Yes	7.2	106.2	103.0	1.0	0.0	-0.1	0.2	2.1	0.29
7/23/2007	ADCP, Lagged	Yes	7.6	142.5	130.6	1.0	0.0	-1.0	0.3	11.7	1.53
7/24/2007	ADCP, Lagged	No	7.3	114.6	112.4	1.0	0.0	0.0	0.2	1.0	0.14
7/25/2007	ADCP, Lagged	Yes	7.1	111.5	110.4	1.0	0.0	-0.3	0.3	0.2	0.02
8/2/2007	ADCP, Lagged	Yes	7.5	136.7	129.9	1.5	0.0	-1.1	0.0	6.4	0.84
8/6/2007	ADCP, Lagged	No	7.9	150.0	142.0	0.0	0.0	0.0	0.1	7.9	1.01
8/7/07 A	ADCP, Lagged	No	7.9	152.0	143.0	0.0	0.0	0.0	0.1	8.9	1.13
PAM APPLICATION – August 7, 2007											
8/7/07 B	ADCP, Lagged	No	7.9	153.0	152.0	0.0	0.0	0.0	0.2	0.8	0.11
8/7/07 C	ADCP, Lagged	Yes	7.9	149.8	153.1	0.0	0.0	-0.5	0.0	-2.9	-0.37
8/8/2007	ADCP, Lagged	Yes	7.9	144.0	143.8	0.0	0.0	2.9	0.3	-3.0	-0.38
8/9/2007 A	ADCP, Lagged	No	7.6	134.8	133.3	0.0	0.0	0.0	0.2	1.3	0.17
8/9/2007 B	ADCP, Simult.	No	7.7	134.8	136.0	0.0	0.0	0.0	0.2	-1.4	-0.18
8/15/2007	ADCP, Lagged	No	7.5	133.2	132.9	0.0	0.0	0.0	0.2	0.1	0.01
8/17/2007	ADCP, Lagged	No	7.9	155.3	152.4	1.5	0.0	0.0	0.3	1.1	0.14
8/23/2007	ADCP, Lagged	Yes	7.4	122.4	119.9	1.0	0.0	-0.6	0.0	2.0	0.28
9/16/2007	ADCP, Lagged	Yes	7.4	126.6	126.2	1.0	0.0	-1.9	0.2	1.1	0.14
10/6/2007	ADCP, Lagged	No	6.9	91.5	91.6	1.0	0.0	0.0	0.1	-1.2	-0.18
10/25/2007	ADCP, Lagged	No	7.0	101.6	100.7	1.0	0.0	0.0	0.1	-0.2	-0.03
11/8/2007	ADCP, Lagged	No	6.8	85.1	83.9	1.0	0	0	0	0.2	0.03

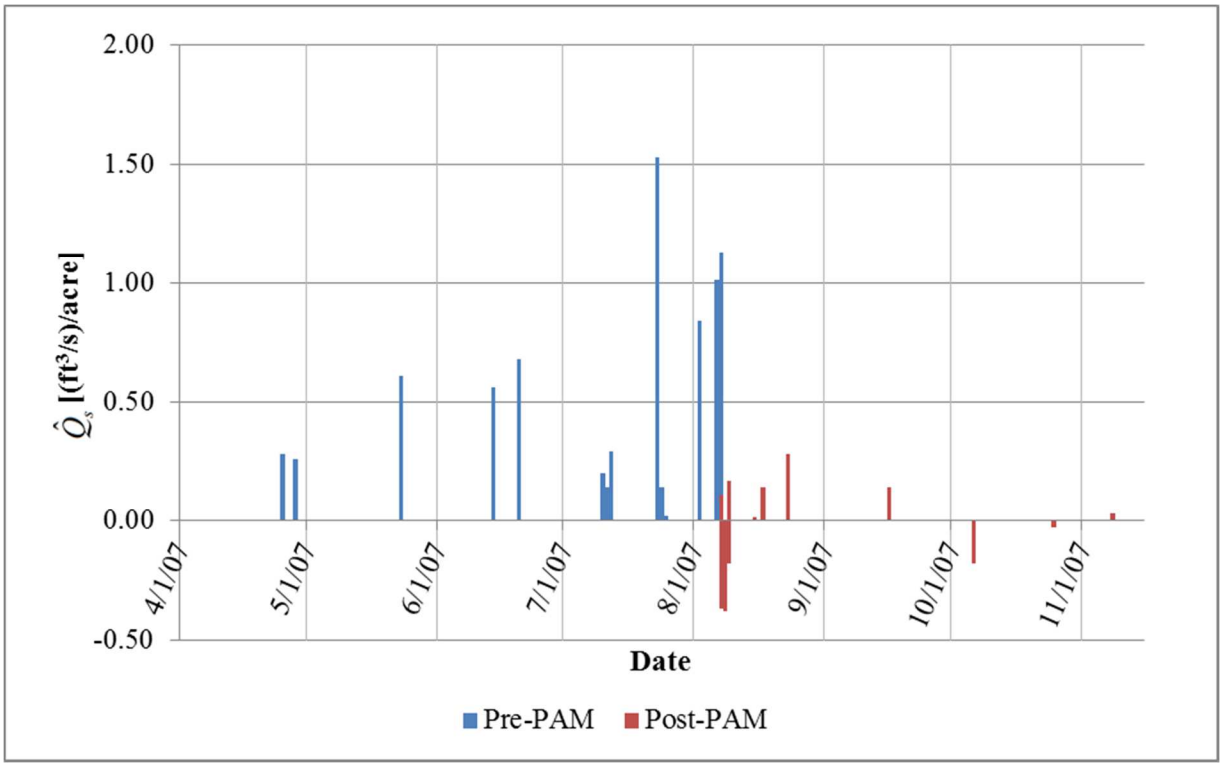

Figure 6-2 Pre- and post-PAM application deterministic $\hat{Q}_s$ estimated from inflow-outflow tests on the Catlin Canal in 2007

RFH Canal

Inflow-outflow tests were conducted on the RFH Canal in 2006 and 2007. The deterministic results are summarized in Table 6-3 and plotted in Figure 6-3 for each of the measurements taken in 2006. Results are presented in Table 6-4 and plotted in Figure 6-4 for measurements taken in 2007.

Two PAM applications were performed on the RFH Canal in 2006. The first application spanned from June 29, 2006 to June 30, 2006 over a 19.9 mile study reach, but did not appear to have significant impact on seepage reduction. The second application was conducted on July 20, 2006 on a shorter 2.5-mile study reach from Site 201 to Site 202. Estimates of $\hat{Q}_s$ ranged

between 0.39 and 1.09 $ft^3/s/acre$ over six seepage tests prior to the second application. After the second application, $\hat{Q}_s$ estimates ranged between 0.25 and 0.56 $ft^3/s/acre$ over six seepage tests. Five out of six post-application estimates were lower than all pre-application measurements of $\hat{Q}_s$, indicating that seepage was reduced between sites 201 and 202 as a result of the second PAM application on the RFH Canal.

PAM was not applied to the RFH Canal in 2007, but $\hat{Q}_s$ was measured several times over (a) a 3.7-mile reach between Site 201 and Site 203 or (b) a 6.4-mile reach between Site 201 and Site 204, depending on the irrigation schedule, as described in Section 0. In summary, estimates of $\hat{Q}_s$ ranged between -0.09 and 0.81 $ft^3/s/acre$, with an average $\hat{Q}_s$ of 0.30 $ft^3/s/acre$.

Table 6-3 Deterministic seepage estimates for the RFH Canal in 2006

Date	Measurement Equipment and Method	Study Reach	A_P (acre)	Q_{US} (ft^3/s)	Q_{DS} (ft^3/s)	Q_D (ft^3/s)	Q_I (ft^3/s)	$\Delta S/\Delta t$ (ft^3/s)	Q_E (ft^3/s)	Q_s (ft^3/s)	$\hat{Q}_s$ [(ft^3/s)/acre]
6/2/2006	ADCP, Lagged	201-202	10.5	132.6	123.7	0	0	0	0.4	8.5	0.81
6/28/2006 A	ADCP, Lagged	201-202	10.5	138	130	0	0	0	0.4	7.6	0.73
6/28/2006 B	ADV, Lagged	201-202	10.6	142.5	134.7	0	0	0	0.3	7.5	0.71
7/1/2006 A	ADCP, Lagged	201-202	10.6	144	135	0	0	0	0.5	8.5	0.81
7/1/2006 B	ADV, Lagged	201-202	10.6	142	137.5	0	0	0	0.4	4.1	0.38
7/19/2006	ADCP. Lagged	201-202	10.6	145	133	0	0	0	0.4	11.6	1.09
PAM APPLICATION – July 20, 2006											
7/21/2006	ADCP. Lagged	201-202	10.4	118	115	0	0	0	0.1	2.9	0.28
7/26/2006 A	ADCP. Lagged	201-202	10.3	118	114.2	0	0	0	0.4	3.4	0.33
7/26/2006 B	ADCP. Lagged	201-202	10.3	117.2	114.4	0	0	0	0.3	2.5	0.25
8/4/2006	ADCP. Lagged	201-202	10.3	115	109	0	0	0	0.2	5.8	0.57
8/10/2006	ADCP. Lagged	201-202	10.7	145	141	0	0	0	0.4	3.6	0.34
11/2/2006	ADCP. Lagged	201-202	10.4	96.1	93.5	0	0	0	0.0	2.6	0.25

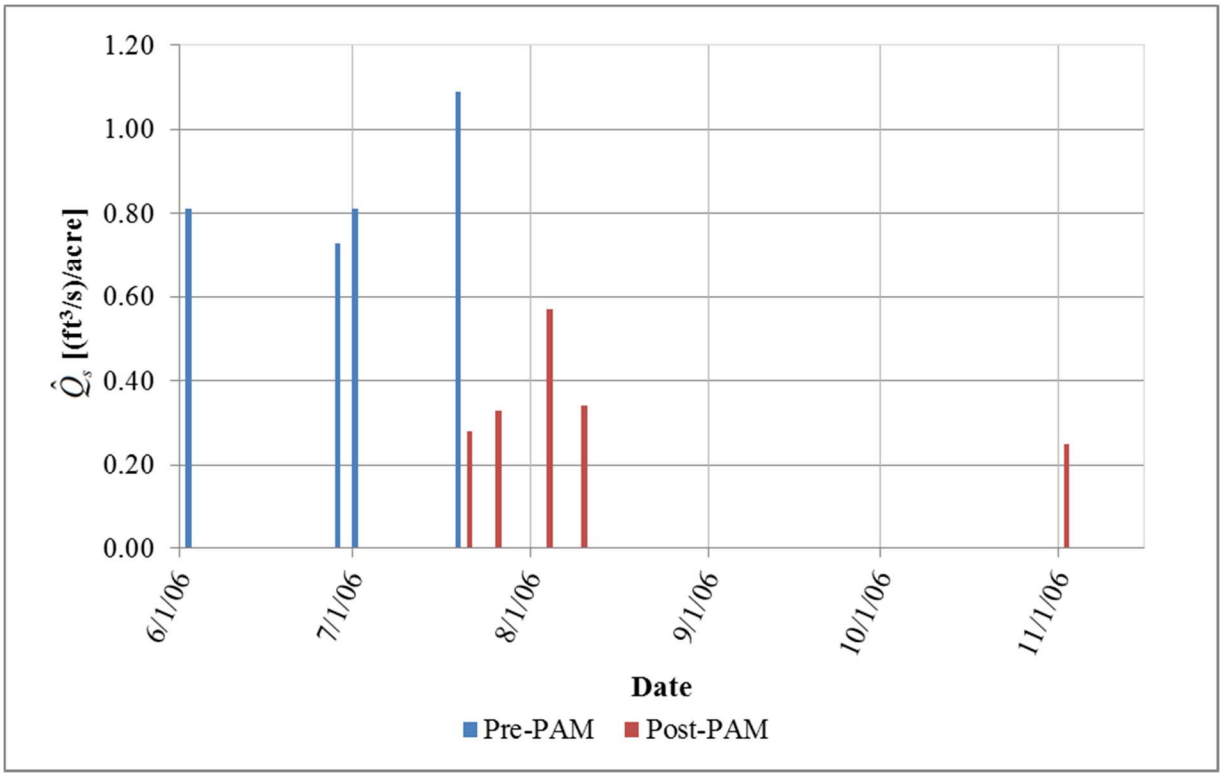

Figure 6-3 Pre- and post-PAM application deterministic $\hat{Q}_s$ estimated from inflow-outflow tests on the RFH Canal in 2006 – second PAM application

Table 6-4 Deterministic seepage estimates for the RFH Canal in 2007

Date	Measurement Equipment and Method	Study Reach	A_P (acre)	Q_{US} (ft^3/s)	Q_{DS} (ft^3/s)	Q_D (ft^3/s)	Q_I (ft^3/s)	$\Delta S/\Delta t$ (ft^3/s)	Q_E (ft^3/s)	Q_s (ft^3/s)	$\hat{Q}_s$ [(ft^3/s)/acre]
6/28/2007	ADCP, Lagged	201-204	25.3	127.1	115.2	0	0	0	0.8	11.1	0.44
7/11/2007	ADCP, Lagged	201-203	16.1	199.7	192.6	0	0	0	0.3	6.8	0.42
7/22/2007	ADCP, Lagged	201-203	15.9	196.6	182.9	0.6	0	0	0.3	12.8	0.81
7/25/2007	ADCP, Lagged	201-203	15.9	191.6	181.8	0	0	0	0.5	9.3	0.58
8/6/2007	ADCP, Lagged	201-204	28.4	184.6	182.0	0	0	0	1.1	1.5	0.05
8/15/2007	ADCP, Lagged	201-204	28.2	181.1	182.7	0	0	0	0.9	-2.5	-0.09
8/23/2007	ADCP, Lagged	201-203	15.9	184.7	183.3	0	0	0	0.2	1.2	0.08
9/1/2007	ADCP, Lagged	201-204	27.7	169.0	163.0	0	0	0	0.9	5.1	0.18
9/13/2007	ADCP, Lagged	201-203	14.8	126.9	120.6	0	0	0	0.5	5.8	0.39
10/6/2007	ADCP, Lagged	201-204	26.4	122.5	116.4	0	0	0	1.1	5	0.19
10/25/2007	ADCP, Lagged	201-203	14.8	125	120.6	0	0	0	0.0	4.4	0.30
11/8/2007	ADCP, Lagged	201-203	14.2	94.4	90.5	0	0	0	0.1	3.8	0.27

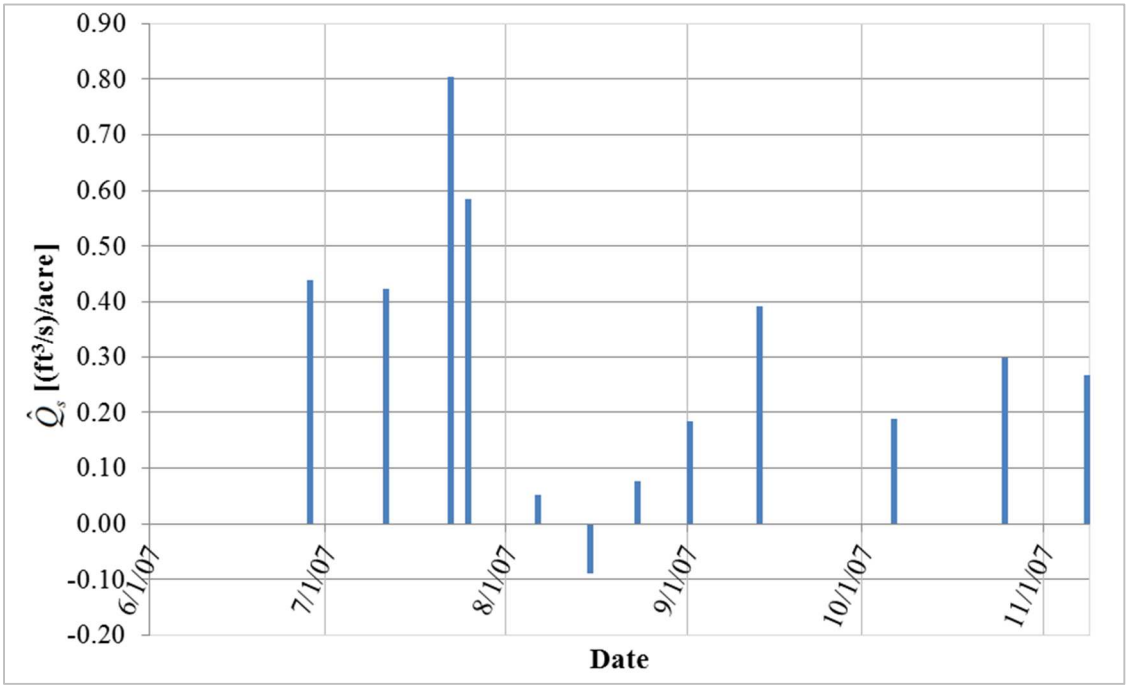

Figure 6-4 Pre-PAM application deterministic $\hat{Q}_s$ estimated from inflow-outflow tests on the RFH Canal in 2007

Lamar Canal

Inflow-outflow measurements were conducted on the Lamar Canal in 2006. PAM was applied to the Lamar Canal on June 7, 2006. Deterministic estimates of Q_s and $\hat{Q}_s$ are presented in Table 6-5 and plotted in Figure 6-5. The Lamar Canal study reach spanned either (a) 5.8 miles from Site 401 to Site 405 or (b) 7.4 miles from Site 400 to Site 405, as indicated in the table. Water level changes along the reach were not measured, although undetected canal storage changes were suspected due to variable results.

In summary, pre-application estimates of $\hat{Q}_s$ ranged between 0.57 and 1.06 $ft^3/s/acre$, with an average of 0.84 $ft^3/s/acre$, and post-application estimates of $\hat{Q}_s$ ranged between 0.41 and 0.60 $ft^3/s/acre$, with an average of 0.54 $ft^3/s/acre$. Effectiveness of the PAM application is discussed in Section 6.5.1.

Table 6-5 Deterministic seepage estimates for the Lamar Canal in 2006

Date	Measurement Equipment and Method	Study Reach Sites	A_P (acre)	Q_{US} (ft^3/s)	Q_{DS} (ft^3/s)	Q_D (ft^3/s)	Q_I (ft^3/s)	$\Delta S/\Delta t$ (ft^3/s)	Q_E (ft^3/s)	Q_s (ft^3/s)	$\hat{Q}_s$ [(ft^3/s)/acre]
6/1/2006 A	ADCP, Lagged	401-405	13.5	56.5	35.8	6.0	0	0	0.4	14.3	1.06
6/1/2006 B	ADV, Lagged	400-405	18.1	55.3	35.6	9.0	0	0	0.4	10.3	0.57
6/6/2006 A	ADCP, Lagged	401-405	13.9	51.7	34.0	3.6	0	0	0.5	13.6	0.98
6/6/2006 B	ADV, Lagged	401-405	13.9	50.0	35.8	3.6	0	0	0.5	10.1	0.73
PAM APPLICATION – June 7, 2006											
6/8/2006 A	ADCP, Lagged	400-405	18.3	59.7	47.5	4.0	0	0	0.7	7.5	0.41
6/8/2006 B	ADV, Lagged	401-405	14.3	59.9	46.7	4.0	0	0	0.6	8.6	0.60
6/14/2006	ADCP, Lagged	400-405	13.3	38.4	30.0	0	0	0	0.7	7.7	0.58
7/21/2006	ADCP, Lagged	400-405	13.5	45.2	28.2	9.0	0	0	0.2	7.8	0.57
9/8/2006	ADCP, Lagged	400-405	13.5	45.7	25.8	12.0	0	0	0.4	7.5	0.56

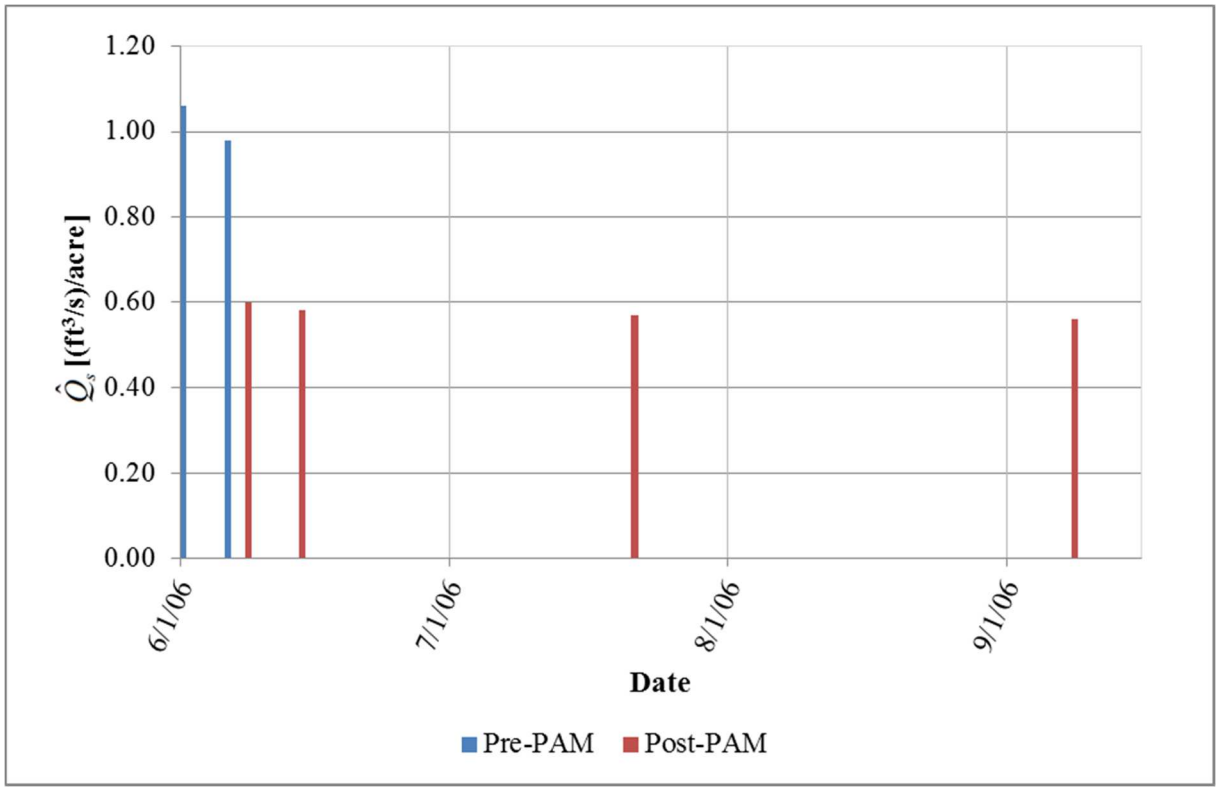

Figure 6-5 Pre- and post-PAM application deterministic $\hat{Q}_s$ estimated from inflow-outflow tests on the Lamar Canal in 2006

Fort Lyon Canal

Seepage tests were conducted on the Fort Lyon Canal in 2007, but a PAM application was not conducted. Deterministic seepage results are presented in Table 6-6. Seepage was measured over a 25-mile stretch of the Las Animas Division and over a 17.1-mile stretch of the Limestone Division, as described in Section 2.4. Pressure transducers were not always installed or working properly in the study reaches during inflow-outflow tests; however, canal managers indicated that flow conditions were relatively steady during the tests and stage was visually observed not to vary during flow rate measurement. Hence, it was assumed that canal storage changes were negligible.

Table 6-6 Deterministic seepage estimates for the Fort Lyon Canal in 2007

Division	Date	Measurement Equipment and Method	A_{wp} (acre)	Q_{US} (ft^3/s)	Q_{DS} (ft^3/s)	Q_D (ft^3/s)	Q_I (ft^3/s)	$\Delta S/\Delta t$ (ft^3/s)	Q_E (ft^3/s)	Q_s (ft^3/s)	$\hat{Q}_s$ [(ft^3/s)/acre]
Las Animas	9/14/2007	ADCP, Lagged	155.3	267.3	233.2	0	0	0	3.8	30.4	0.20
	11/9/2007	ADCP, Lagged	158.5	300.0	279.0	0	0	0	3.0	18.0	0.11
Limestone	7/13/2007	ADCP, Lagged	118.3	374.2	329.9	0	0	0	4.1	40.2	0.34
	8/1/2007	ADCP, Lagged	108.3	285.4	240.1	0	0	0	3.3	41.9	0.39
	10/4/2007	ADCP, Lagged	109.3	293.0	253.0	0	0	0	3.2	36.8	0.34
	11/9/2007	ADCP, Lagged	109.3	279.0	259.0	0	0	0	1.9	18.1	0.17

6.2 STOCHASTIC CANAL SEEPAGE RESULTS USING MONTE CARLO SIMULATION

In contrast to deterministic analysis, stochastic analysis implements probability distributions to account for uncertainty due to measurement error and spatiotemporal variability in the variables within the water balance Equation (3.1). The probability distributions that were presented in Chapter 5 were used within the @RISK model to develop a distribution of possible Q_s values by Monte Carlo solutions of Equation (3.1). Stochastic results obtained from Monte Carlo simulations in @RISK are presented in Table 6-7, Table 6-8, and Table 6-9 for the RFH Canal 2006, RFH Canal 2007, and Catlin Canal 2006 inflow-outflow measurements, respectively. Results for the RFH Canal include tests conducted between sites 201 and 203 only (excluding site 204 which was not included in all tests) for comparison purposes. Stochastic analysis was not conducted for the Lamar and Fort Lyon canals because hydraulic geometry was not surveyed due to time constraints. The stochastic results for the Catlin Canal in 2007 had to be divided into two tables because of the large data set. As such, seepage results from tests conducted between 4/28/2007 and 8/6/2007 are presented in Table 6-10, and seepage results for tests between

8/7/2007 and 10/25/2007 are presented in Table 6-11. For each inflow-outflow test, some basic statistics of the distributions of values generated for each variable of the water balance equation are presented, including the generated mean, 5th and 95th percentile values, standard deviation (Stdev), and coefficient of variation (CV = |Stdev / mean|).

The CV values presented in the results should be interpreted with caution, especially for mean seepage estimates that are near zero or negative. As mean seepage rates approach zero, the CV value will approach infinity. Seepage rates that are negative indicate that the canal control volume was gaining water, which is unlikely but possible.

The standard deviations for Q_{US}, Q_{DS}, Q_D, and Q_E values were specified to equal a constant fraction of the measured value, so CV remains constant for these parameters for every test. The only exception to this rule, is for conditions of unsteady flow with lagged discharge measurement where Q_{US} and Q_{DS} were also a function of the change in stage during the "unmeasured" time period. These conditions only occurred during the 2007 tests on the Catlin Canal, because unsteady flow was not observed on the RFH Canal and pressure transducers were not installed in the Catlin Canal in 2006. However, note that the CV values of Q_{US} and Q_{DS} for unsteady flow with lagged measurements are no different than for steady or simultaneous measurements. This indicates that the uncertainty in estimating Q_{US} and Q_{DS} was not greatly impacted by the stage change. This likely is because stage changes were typically on the order of a couple hundredths of a foot, which results in relatively small changes in Q_{US} and Q_{DS} when compared to the direct measurement error of Q_{US} and Q_{DS} at +/- 5%.

On the Catlin Canal, the CVs of A_P and A_{WS} were generally about 0.08 and 0.10, respectively. These values were about 0.03 and 0.05 on the RFH Canal, respectively. For the Catlin Canal, the 5th and 95th percentiles of the generated distributions for A_P generally were

different from the mean by about 1.0 acre, which is generally about 14% of the mean, in both 2006 and 2007. This indicates that the uncertainty in estimating A_P on the Catlin Canal was typically +/- 14% for the 90th IR. Similarly, the uncertainty of estimating A_P on the RFH Canal was typically +/- 10% for the 90th IR in 2006 and +/- 5% for the 90th IR in 2007. Canal stage was significantly higher in 2007 than in 2006 on the RFH Canal, which can explain the reduction in relative uncertainty - as measurement error from pressure transducers became a smaller percentage of the total stage height, so the uncertainty in predictions of P became a smaller percentage of total P values.

The results indicate that uncertainty due to spatial variability and at-a-station measurement error can have a significant impact on estimating the hydraulic geometry of a canal study reach. The degree of uncertainty clearly is dependent upon the size and uniformity of the reach.

Estimated mean values of $\hat{Q}_S$ varied across the 60 tests on the two canals from as low as -0.73 (ft^3/s)/acre (gain) to as high as 1.53 (ft^3/s)/acre, averaging 0.32 (ft^3/s)/acre with a standard deviation of 0.43 (ft^3/s)/acre and CV of 0.19 (ft^3/s)/acre. For RFH Canal reaches untreated with LA-PAM sealant, mean values of Q_s and $\hat{Q}_S$ ranged from -4.2 to 12.8 ft^3/s and -0.26 to 1.09 (ft^3/s)/acre, respectively, with averages of 5.5 ft^3/s and 0.44 (ft^3/s)/acre. For reaches on the Catlin Canal untreated with LA-PAM, mean values of Q_s and $\hat{Q}_S$ ranged from 0.2 to 11.7 ft^3/s and 0.02 to 1.53 (ft^3/s)/acre, respectively, with averages of 4.7 ft^3/s and 0.63 (ft^3/s)/acre. For reaches on the RFH Canal and Catlin Canal treated with LA-PAM, mean $\hat{Q}_S$ values ranged from 0.25 to 0.57 (ft^3/s)/acre, averaging 0.33 (ft^3/s)/acre, and from -0.73 to 0.55 (ft^3/s)/acre, averaging -0.01 (ft^3/s)/acre, respectively.

Table 6-7 Stochastic seepage results for the RFH Canal in 2006

		Date of Seepage Measurement											
		6/2	6/28	6/28	7/1	7/1	7/19	7/21	7/26	7/26	8/4	8/10	11/2
Lagged (L) or Simultaneous (S)		L	L	L	L	L	L	L	L	L	L	L	L
Q Equipment		ADCP	ADCP	ADV	ADCP	ADV	ADCP	ADCP	ADCP	ADCP	ADCP	ADCP	ADCP
Q_S (ft^3/s)	5%	-0.5	-2.0	-2.3	-1.4	-5.8	1.7	-5.4	-4.7	-5.7	-2.1	-6.6	-4.2
	mean	8.5	7.6	7.5	8.5	4.1	11.6	2.9	3.4	2.5	5.8	3.6	2.6
	95%	17.5	17.1	17.1	18.2	14.0	21.4	11.0	11.5	10.8	13.8	13.7	9.2
	stdev	5.5	5.8	5.9	6.0	6.0	6.0	5.0	5.0	5.0	4.8	6.2	4.1
	CV	0.65	0.76	0.79	0.70	1.48	0.52	1.75	1.47	1.99	0.83	1.71	1.58
$\hat{Q}_s$ ($ft^3/s/acre$)	5%	-0.05	-0.19	-0.22	-0.13	-0.55	0.16	-0.52	-0.46	-0.55	-0.21	-0.63	-0.41
	mean	0.81	0.73	0.71	0.81	0.38	1.09	0.28	0.33	0.25	0.57	0.34	0.25
	95%	1.69	1.63	1.64	1.73	1.33	2.05	1.07	1.13	1.05	1.34	1.29	0.89
	stdev	0.53	0.55	0.57	0.57	0.57	0.57	0.49	0.48	0.49	0.47	0.58	0.40
	CV	0.65	0.76	0.80	0.70	1.48	0.52	1.75	1.47	1.99	0.83	1.72	1.59
Q_{US} (ft^3/s)	5%	126.0	131.1	135.4	136.8	134.9	137.7	112.1	112.1	111.3	109.2	137.7	91.3
	mean	132.6	138.0	142.5	144.0	142.0	145.0	118.0	118.0	117.2	115.0	145.0	96.1
	95%	139.2	144.9	149.6	151.2	149.1	152.2	123.9	123.9	123.1	120.7	152.2	100.9
	stdev	4.0	4.2	4.3	4.4	4.3	4.4	3.6	3.6	3.6	3.5	4.4	2.9
	CV	0.03	0.03	0.03	0.03	0.03	0.03	0.03	0.03	0.03	0.03	0.03	0.03
Q_{DS} (ft^3/s)	5%	117.5	123.5	128.0	128.2	130.6	126.3	109.2	108.5	108.7	103.5	133.9	88.8
	mean	123.7	130.0	134.7	135.0	137.5	133.0	115.0	114.2	114.4	109.0	141.0	93.5
	95%	129.9	136.5	141.4	141.7	144.4	139.6	120.7	119.9	120.1	114.4	148.0	98.2
	stdev	3.8	4.0	4.1	4.1	4.2	4.0	3.5	3.5	3.5	3.3	4.3	2.8
	CV	0.03	0.03	0.03	0.03	0.03	0.03	0.03	0.03	0.03	0.03	0.03	0.03
Q_D (ft^3/s)	5%	0	0	0	0	0	0	0	0	0	0	0	0
	mean	0	0	0	0	0	0	0	0	0	0	0	0
	95%	0	0	0	0	0	0	0	0	0	0	0	0
	stdev	0	0	0	0	0	0	0	0	0	0	0	0
	CV	0	0	0	0	0	0	0	0	0	0	0	0
Q_E (ft^3/s)	5%	0.3	0.3	0.2	0.4	0.4	0.3	0.1	0.3	0.2	0.1	0.3	0.0
	mean	0.4	0.4	0.3	0.5	0.4	0.4	0.1	0.4	0.3	0.2	0.4	0.0
	95%	0.5	0.5	0.4	0.6	0.5	0.5	0.2	0.5	0.3	0.2	0.5	0.0
	stdev	0.1	0.1	0.0	0.1	0.1	0.1	0.0	0.1	0.0	0.0	0.1	0.0
	CV	0.14	0.14	0.14	0.14	0.14	0.14	0.14	0.14	0.14	0.13	0.14	0.14
$\Delta S/\Delta t$ (ft^3/s)	5%	0	0	0	0	0	0	0	0	0	0	0	0
	mean	0	0	0	0	0	0	0	0	0	0	0	0
	95%	0	0	0	0	0	0	0	0	0	0	0	0
	stdev	0	0	0	0	0	0	0	0	0	0	0	0
	CV	0	0	0	0	0	0	0	0	0	0	0	0
A_P (acre)	5%	9.6	9.6	9.7	9.7	9.7	9.7	9.5	9.4	9.4	9.4	9.8	9.5
	mean	10.5	10.5	10.6	10.6	10.6	10.6	10.4	10.3	10.3	10.3	10.7	10.4
	95%	11.4	11.4	11.5	11.5	11.5	11.5	11.2	11.2	11.2	11.2	11.6	11.3
	stdev	0.5	0.5	0.5	0.5	0.5	0.6	0.5	0.5	0.5	0.5	0.6	0.5
	CV	0.05	0.05	0.05	0.05	0.05	0.05	0.05	0.05	0.05	0.05	0.05	0.05
A_{WS} (acre)	5%	8.9	8.9	8.9	8.9	8.9	9.0	8.8	8.8	8.8	8.8	9.0	8.9
	mean	9.9	9.9	9.9	9.9	9.9	10.0	9.8	9.8	9.8	9.8	10.0	9.8
	95%	10.9	10.9	10.9	10.9	10.9	11.0	10.8	10.8	10.7	10.7	11.0	10.8
	stdev	0.6	0.6	0.6	0.6	0.6	0.6	0.6	0.6	0.6	0.6	0.6	0.6
	CV	0.06	0.06	0.06	0.06	0.06	0.06	0.06	0.06	0.06	0.06	0.06	0.06

Table 6-8 Stochastic seepage results for the RFH Canal in 2007

		Date of Seepage Measurement											
		6/28	7/11	7/22	7/25	8/6	8/15	8/23	9/1	9/13	10/6	10/25	11/8
Lagged (L) or Simultaneous (S)		L	L	L	L	L	L	L	L	L	L	L	L
Q Equipment		ADCP	ADCP	ADCP	ADCP	ADCP	ADCP	ADCP	ADCP	ADCP	ADCP	ADCP	ADCP
Q_S (ft^3/s)	5%	-0.1	-7.1	-0.7	-3.9	-15.1	-17.0	-11.9	-10.2	-3.0	-5.8	-4.3	-2.8
	mean	8.6	6.8	12.8	9.3	-1.9	-4.2	1.2	1.8	5.8	2.8	4.4	3.8
	95%	17.4	20.9	26.4	22.5	11.1	8.7	14.3	13.8	14.6	11.3	13.1	10.3
	stdev	5.3	8.5	8.2	8.0	8.0	7.8	7.9	7.2	5.4	5.2	5.3	4.0
	CV	0.62	1.25	0.64	0.86	-4.24	-1.86	6.84	4.10	0.92	1.85	1.21	1.04
$\hat{Q}_s$ ($ft^3/s/acre$)	5%	0.00	-0.44	-0.05	-0.24	-0.95	-1.08	-0.75	-0.66	-0.20	-0.39	-0.29	-0.19
	mean	0.59	0.42	0.80	0.58	-0.12	-0.26	0.07	0.11	0.40	0.19	0.30	0.27
	95%	1.18	1.30	1.66	1.41	0.70	0.55	0.90	0.89	0.99	0.77	0.90	0.73
	stdev	0.36	0.53	0.52	0.50	0.50	0.49	0.50	0.47	0.37	0.36	0.36	0.28
	CV	0.62	1.25	0.65	0.86	-4.25	-1.87	6.85	4.11	0.92	1.85	1.21	1.04
Q_{US} (ft^3/s)	5%	120.7	189.7	186.8	182.0	175.4	172.0	175.5	160.5	120.6	116.4	118.7	89.7
	mean	127.1	199.7	196.6	191.6	184.6	181.1	184.7	169.0	126.9	122.5	125.0	94.4
	95%	133.5	209.7	206.4	201.2	193.8	190.2	193.9	177.4	133.2	128.6	131.3	99.1
	stdev	3.9	6.1	6.0	5.8	5.6	5.5	5.6	5.1	3.9	3.7	3.8	2.9
	CV	0.03	0.03	0.03	0.03	0.03	0.03	0.03	0.03	0.03	0.03	0.03	0.03
Q_{DS} (ft^3/s)	5%	112.1	183.0	173.8	172.7	176.6	175.6	174.1	158.4	114.6	113.0	114.6	86.0
	mean	118.0	192.6	182.9	181.8	185.9	184.8	183.3	166.7	120.6	119.0	120.6	90.5
	95%	123.9	202.2	192.0	190.9	195.2	194.0	192.5	175.0	126.6	124.9	126.6	95.0
	stdev	3.6	5.9	5.6	5.5	5.7	5.6	5.6	5.1	3.7	3.6	3.7	2.8
	CV	0.03	0.03	0.03	0.03	0.03	0.03	0.03	0.03	0.03	0.03	0.03	0.03
Q_D (ft^3/s)	5%	0	0	0.57	0	0	0	0	0	0	0	0	0
	mean	0	0	0.60	0	0	0	0	0	0	0	0	0
	95%	0	0	0.63	0	0	0	0	0	0	0	0	0
	stdev	0	0	0.02	0	0	0	0	0	0	0	0	0
	CV	0	0	0.00	0	0	0	0	0	0	0	0	0
Q_E (ft^3/s)	5%	0.4	0.3	0.3	0.4	0.5	0.4	0.2	0.4	0.4	0.5	0.0	0.0
	mean	0.5	0.3	0.3	0.5	0.6	0.5	0.2	0.5	0.5	0.7	0.0	0.1
	95%	0.6	0.4	0.4	0.6	0.7	0.6	0.3	0.7	0.6	0.8	0.0	0.1
	stdev	0.1	0.0	0.0	0.1	0.1	0.1	0.0	0.1	0.1	0.1	0.0	0.0
	CV	0.13	0.13	0.13	0.13	0.13	0.13	0.13	0.13	0.13	0.13	0.13	0.13
$\Delta S/\Delta t$ (ft^3/s)	5%	0	0	0	0	0	0	0	0	0	0	0	0
	mean	0	0	0	0	0	0	0	0	0	0	0	0
	95%	0	0	0	0	0	0	0	0	0	0	0	0
	stdev	0	0	0	0	0	0	0	0	0	0	0	0
	CV	0	0	0	0	0	0	0	0	0	0	0	0
A_P (acre)	5%	13.8	15.2	15.1	15.1	15.0	15.0	15.0	14.7	13.9	13.9	13.9	13.3
	mean	14.7	16.1	15.9	15.9	15.9	15.8	15.9	15.5	14.8	14.7	14.8	14.2
	95%	15.5	16.9	16.8	16.8	16.8	16.7	16.7	16.4	15.7	15.6	15.6	15.1
	stdev	0.5	0.5	0.5	0.5	0.5	0.5	0.5	0.5	0.5	0.5	0.5	0.5
	CV	0.04	0.03	0.03	0.03	0.03	0.03	0.03	0.03	0.04	0.04	0.04	0.04
A_{WS} (acre)	5%	13.2	14.0	13.9	13.9	13.9	13.9	13.9	13.7	13.2	13.2	13.2	12.8
	mean	14.0	14.8	14.8	14.8	14.8	14.7	14.7	14.6	14.1	14.1	14.1	13.7
	95%	14.9	15.7	15.6	15.6	15.6	15.6	15.6	15.4	15.0	14.9	14.9	14.6
	stdev	0.5	0.5	0.5	0.5	0.5	0.5	0.5	0.5	0.5	0.5	0.5	0.5
	CV	0.04	0.03	0.03	0.03	0.03	0.03	0.03	0.04	0.04	0.04	0.04	0.04

Table 6-9 Stochastic seepage results for the Catlin Canal in 2006

		Date of Seepage Measurement											
		6/3	6/3	6/4 A	6/4 B	6/4 C	6/22 A	6/22 B	6/26	7/20	8/10	9/28	11/2
Lagged (L) or Simultaneous (S)		L	S	S	L	L	S	S	L	L	L	L	L
Q Equipment		ADCP	ADV	ADV	ADCP	ADCP	ADV	ADV	ADV	ADCP	ADCP	ADCP	ADCP
Q_S (ft^3/s)	5%	2.4	-2.7	-7.0	-7.3	-14.5	-9.5	-7.8	-4.4	-8.0	-3.6	-5.0	-3.6
	mean	9.8	4.6	1.0	1.7	-5.3	-2.4	-0.8	2.7	-0.7	3.9	0.0	0.9
	95%	17.5	11.9	9.2	10.8	4.0	4.8	6.2	9.7	6.7	11.3	5.0	5.4
	stdev	4.6	4.4	4.9	5.6	5.6	4.3	4.3	4.3	4.4	4.5	3.0	2.8
	CV	0.47	0.97	4.79	3.29	1.06	1.78	5.57	1.61	6.60	1.17	375.8	3.06
$\hat{Q}_s$ ($ft^3/s/acre$)	5%	0.33	-0.37	-0.97	-1.00	-2.00	-1.34	-1.11	-0.61	-1.13	-0.52	-0.77	-0.56
	mean	1.39	0.64	0.14	0.23	-0.73	-0.34	-0.11	0.38	-0.10	0.55	0.00	0.14
	95%	2.51	1.66	1.25	1.50	0.54	0.67	0.89	1.38	0.97	1.63	0.77	0.83
	stdev	0.67	0.62	0.67	0.77	0.78	0.62	0.61	0.62	0.64	0.65	0.47	0.43
	CV	0.48	0.98	4.78	3.29	-1.07	-1.80	-5.57	1.62	-6.64	1.18	264.70	3.08
Q_{US} (ft^3/s)	5%	106.4	100.6	108.0	124.4	121.6	95.1	95.4	97.8	97.8	101.6	67.6	61.3
	mean	112.0	105.9	113.7	131.0	128.0	100.1	100.4	103.0	103.0	107.0	71.2	64.5
	95%	117.6	111.2	119.4	137.5	134.4	105.1	105.4	108.1	108.2	112.3	74.8	67.7
	stdev	3.4	3.2	3.5	4.0	3.9	3.0	3.1	3.1	3.1	3.3	2.2	2.0
	CV	0.03	0.03	0.03	0.03	0.03	0.03	0.03	0.03	0.03	0.03	0.03	0.03
Q_{DS} (ft^3/s)	5%	96.9	96.0	107.5	122.5	126.3	96.3	96.3	94.4	98.3	97.8	67.1	60.3
	mean	102.0	101.1	113.2	129.0	133.0	101.4	101.4	99.4	103.5	103.0	70.6	63.5
	95%	107.1	106.2	118.9	135.4	139.6	106.5	106.5	104.4	108.7	108.1	74.1	66.7
	stdev	3.1	3.1	3.4	3.9	4.0	3.1	3.1	3.0	3.1	3.1	2.1	1.9
	CV	0.03	0.03	0.03	0.03	0.03	0.03	0.03	0.03	0.03	0.03	0.03	0.03
Q_D (ft^3/s)	5%	0	0	0	0	0	0	0	0.7	0	0	0.5	0
	mean	0	0	0	0	0	0	0	0.7	0	0	0.5	0
	95%	0	0	0	0	0	0	0	0.7	0	0	0.5	0
	stdev	0	0	0	0	0	0	0	0.0	0	0	0.0	0
	CV	0	0	0	0	0	0	0	0.0	0	0	0.0	0
Q_E (ft^3/s)	5%	0.1	0.2	0.2	0.2	0.2	0.1	0.2	0.2	0.1	0.1	0.1	0.1
	mean	0.2	0.2	0.3	0.3	0.3	0.2	0.2	0.2	0.2	0.1	0.1	0.1
	95%	0.2	0.3	0.4	0.4	0.4	0.2	0.3	0.3	0.2	0.2	0.1	0.1
	stdev	0.0	0.0	0.0	0.0	0.0	0.0	0.0	0.0	0.0	0.0	0.0	0.0
	CV	0.16	0.16	0.16	0.16	0.16	0.16	0.16	0.16	0.16	0.16	0.17	0.17
$\Delta S/\Delta t$ (ft^3/s)	5%	0	0	-1.0	0	0	0.8	-0.5	0	0	0	0	0
	mean	0	0	-0.8	0	0	1.0	-0.5	0	0	0	0	0
	95%	0	0	-0.7	0	0	1.1	-0.4	0	0	0	0	0
	stdev	0	0	0.1	0	0	0.1	0.0	0	0	0	0	0
	CV	0	0	-0.10	0	0	0.10	-0.11	0	0	0	0	0
A_P (acre)	5%	6.1	6.2	6.4	6.4	6.4	6.1	6.1	6.2	6.1	6.1	5.5	5.6
	mean	7.1	7.2	7.3	7.3	7.3	7.1	7.1	7.1	7.1	7.1	6.6	6.6
	95%	8.1	8.2	8.3	8.3	8.3	8.1	8.1	8.1	8.1	8.1	7.6	7.6
	stdev	0.6	0.6	0.6	0.6	0.6	0.6	0.6	0.6	0.6	0.6	0.6	0.6
	CV	0.09	0.08	0.08	0.08	0.08	0.08	0.09	0.08	0.09	0.09	0.10	0.10
A_{WS} (acre)	5%	5.3	5.4	5.4	5.4	5.5	5.3	5.3	5.3	5.3	5.3	5.0	5.0
	mean	6.4	6.4	6.5	6.5	6.5	6.4	6.4	6.4	6.4	6.4	6.2	6.1
	95%	7.5	7.5	7.6	7.6	7.6	7.5	7.5	7.5	7.5	7.5	7.2	7.3
	stdev	0.7	0.7	0.7	0.6	0.6	0.7	0.7	0.7	0.7	0.7	0.7	0.7
	CV	0.11	0.10	0.10	0.10	0.10	0.10	0.11	0.10	0.11	0.11	0.11	0.11

Table 6-10 Stochastic seepage results for measurements between (4/28/2007 through 8/6/2007) on the Catlin Canal in 2007

		Date of Seepage Measurement											
		4/28	5/23	6/14	6/20	7/10	7/11A	7/11B	7/23	7/24	7/25	8/2	8/6
Lagged (L) or Simultaneous (S)		L	L	L	L	L	L	L	L	L	L	L	L
Q Equipment		ADCP	ADCP	ADCP	ADCP	ADCP	ADCP	ADCP	ADCP	ADCP	ADCP	ADCP	ADCP
Q_S (ft^3/s)	5%	-4.3	-3.9	-3.4	-3.7	-6.4	-6.9	-5.7	1.6	-6.9	-8.3	-4.1	-2.3
	mean	1.8	4.3	4.0	5.0	1.4	1.0	2.2	11.7	1.0	0.2	6.4	7.9
	95%	7.8	12.7	11.3	13.7	9.4	8.9	10.1	21.7	8.9	8.6	16.7	18.3
	stdev	3.7	5.0	4.5	5.3	4.8	4.8	4.7	6.2	4.9	5.2	6.3	6.2
	CV	2.08	1.16	1.13	1.05	3.41	4.80	2.14	0.53	4.72	32.91	0.99	0.79
$\hat{Q}_s$ ($ft^3/s/acre$)	5%	-0.63	-0.55	-0.49	-0.49	-0.90	-0.97	-0.80	0.21	-0.96	-1.19	-0.55	-0.29
	mean	0.26	0.61	0.56	0.68	0.20	0.15	0.30	1.53	0.14	0.02	0.85	1.01
	95%	1.14	1.81	1.61	1.87	1.33	1.26	1.42	2.89	1.24	1.23	2.22	2.36
	stdev	0.54	0.72	0.64	0.72	0.68	0.68	0.67	0.82	0.68	0.74	0.84	0.81
	CV	2.09	1.17	1.14	1.06	3.41	4.53	2.23	0.53	4.73	33.44	0.99	0.80
Q_{US} (ft^3/s)	5%	82.6	113.6	90.7	118.6	100.3	99.9	100.9	135.2	108.9	105.7	129.7	142.5
	mean	87.0	119.6	95.9	124.8	105.8	105.1	106.2	142.5	114.6	111.5	136.7	150.0
	95%	91.3	125.6	101.1	131.0	111.3	110.4	111.5	149.8	120.3	117.2	143.7	157.5
	stdev	2.6	3.6	3.1	3.8	3.4	3.2	3.2	4.4	3.5	3.5	4.2	4.6
	CV	0.03	0.03	0.03	0.03	0.03	0.03	0.03	0.03	0.03	0.03	0.03	0.03
Q_{DS} (ft^3/s)	5%	80.6	109.2	89.2	113.3	99.3	97.1	97.4	123.9	106.8	104.6	123.3	134.9
	mean	84.8	114.9	94.1	119.3	104.6	102.6	103.0	130.6	112.4	110.4	129.9	142.0
	95%	89.0	120.6	99.1	125.3	109.9	108.0	108.6	137.3	118.0	116.1	136.5	149.1
	stdev	2.6	3.5	3.0	3.6	3.2	3.3	3.4	4.1	3.4	3.5	4.0	4.3
	CV	0.03	0.03	0.03	0.03	0.03	0.03	0.03	0.03	0.03	0.03	0.03	0.03
Q_D (ft^3/s)	5%	0.3	0.3	0.3	0.3	0.9	1.0	1.0	0.9	0.9	0.9	1.4	0.0
	mean	0.3	0.3	0.3	0.3	1.0	1.0	1.0	1.0	1.0	1.0	1.5	0.0
	95%	0.3	0.3	0.3	0.3	1.0	1.1	1.1	1.0	1.0	1.0	1.6	0.0
	stdev	0.0	0.0	0.0	0.0	0.0	0.0	0.0	0.0	0.0	0.0	0.0	0.0
	CV	0.0	0.0	0.0	0.0	0.0	0.0	0.0	0.0	0.0	0.0	0.0	0.0
Q_E (ft^3/s)	5%	0.1	0.1	0.1	0.1	0.0	0.1	0.1	0.2	0.1	0.2	0.0	0.1
	mean	0.1	0.1	0.1	0.2	0.0	0.1	0.2	0.3	0.2	0.3	0.0	0.1
	95%	0.1	0.1	0.1	0.2	0.0	0.2	0.2	0.3	0.2	0.3	0.0	0.1
	stdev	0.0	0.0	0.0	0.0	0.0	0.0	0.0	0.0	0.0	0.0	0.0	0.0
	CV	0.2	0.2	0.2	0.2	0.2	0.2	0.2	0.2	0.2	0.2	0.2	0.2
$\Delta S/\Delta t$ (ft^3/s)	5%	0	0	-4.4	0	-3.4	-2.0	-2.0	-3.2	0	-3.2	-5.1	0
	mean	0	0	-2.6	0	-1.3	0.4	-0.1	-1.0	0	-0.3	-1.1	0
	95%	0	0	-0.9	0	0.8	2.9	1.6	1.1	0	2.5	2.8	0
	stdev	0	0	1.1	0	1.3	1.5	1.1	1.3	0	1.7	2.4	0
	CV	0	0	-0.42	0	-1.00	3.70	-11.00	-1.23	0.00	-5.61	-2.10	0
A_P (acre)	5%	5.9	6.1	6.1	6.4	6.2	6.1	6.2	6.7	6.3	6.1	6.6	6.9
	mean	6.9	7.1	7.1	7.4	7.2	7.1	7.2	7.6	7.3	7.1	7.5	7.9
	95%	7.9	8.1	8.1	8.4	8.1	8.1	8.1	8.6	8.2	8.1	8.5	8.8
	stdev	0.6	0.6	0.6	0.6	0.6	0.6	0.6	0.6	0.6	0.6	0.6	0.6
	CV	0.09	0.08	0.09	0.08	0.08	0.08	0.08	0.08	0.08	0.09	0.08	0.07
A_{WS} (acre)	5%	5.2	5.3	5.3	5.5	5.3	5.3	5.3	5.7	5.4	5.2	5.6	5.9
	mean	6.3	6.4	6.4	6.5	6.4	6.4	6.4	6.7	6.5	6.4	6.6	6.8
	95%	7.4	7.5	7.5	7.6	7.5	7.5	7.5	7.7	7.5	7.5	7.6	7.8
	stdev	0.7	0.7	0.7	0.7	0.7	0.7	0.7	0.6	0.7	0.7	0.6	0.6
	CV	0.11	0.10	0.11	0.10	0.10	0.11	0.10	0.09	0.10	0.11	0.09	0.09

Table 6-11 Stochastic seepage results for measurements between (8/7/2007 through 10/25/2007) on the Catlin Canal in 2007

		Date of Seepage Measurement											
		8/7 A	8/7 B	8/7 C	8/8	8/9 A	8/9 B	8/15	8/17	8/23	9/16	10/6/07	10/25/07
Lagged (L) or Simultaneous (S)		L	L	L	L	L	S	L	L	L	L	L	L
Q Equipment		ADCP	ADCP	ADCP	ADCP	ADCP	ADCP	ADCP	ADCP	ADCP	ADCP	ADCP	ADCP
Q_S (ft^3/s)	5%	-1.4	-9.8	-14.2	-18.7	-8.1	-11.0	-9.2	-9.8	-8.9	-8.4	-7.6	-7.3
	mean	8.9	0.8	-2.9	-3.0	1.3	-1.4	0.1	1.1	2.0	1.1	-1.2	-0.2
	95%	19.4	11.6	8.4	13.3	10.6	8.2	9.5	12.0	13.0	10.6	5.2	6.9
	stdev	6.3	6.5	6.9	9.8	5.7	5.8	5.7	6.6	6.7	5.7	3.9	4.3
	CV	0.71	7.75	2.37	3.28	4.37	4.24	81.33	5.86	3.29	5.47	3.25	20.54
$\hat{Q}_S$ ($ft^3/s/acre$)	5%	-0.18	-1.26	-1.80	-2.38	-1.07	-1.45	-1.24	-1.23	-1.21	-1.14	-1.13	-1.05
	mean	1.14	0.11	-0.37	-0.38	0.17	-0.18	0.01	0.14	0.28	0.14	-0.18	-0.03
	95%	2.51	1.47	1.06	1.71	1.40	1.08	1.26	1.53	1.77	1.44	0.76	1.01
	stdev	0.82	0.83	0.88	1.25	0.75	0.77	0.76	0.84	0.91	0.78	0.58	0.62
	CV	0.72	7.78	-2.38	-3.30	4.35	-4.28	78.14	5.84	3.29	5.57	-3.28	-21.12
Q_{US} (ft^3/s)	5%	144.4	145.3	142.1	136.8	128.1	128.1	126.5	147.5	115.7	120.0	86.9	96.5
	mean	152.0	153.0	149.8	144.0	134.8	134.8	133.2	155.3	122.4	126.6	91.5	101.6
	95%	159.6	160.7	157.5	151.2	141.5	141.5	139.9	163.1	129.0	133.2	96.1	106.7
	stdev	4.6	4.7	4.7	4.4	4.1	4.1	4.0	4.7	4.0	4.0	2.8	3.1
	CV	0.03	0.03	0.03	0.03	0.03	0.03	0.03	0.03	0.03	0.03	0.03	0.03
Q_{DS} (ft^3/s)	5%	135.8	144.4	145.3	130.4	126.6	129.2	126.3	144.8	113.8	119.9	87.0	95.7
	mean	143.0	152.0	153.1	143.8	133.3	136.0	132.9	152.4	119.9	126.2	91.6	100.7
	95%	150.1	159.6	161.0	157.2	140.0	142.8	139.5	160.0	126.1	132.5	96.2	105.7
	stdev	4.3	4.6	4.8	8.3	4.1	4.1	4.0	4.6	3.8	3.9	2.8	3.1
	CV	0.03	0.03	0.03	0.06	0.03	0.03	0.03	0.03	0.03	0.03	0.03	0.03
Q_D (ft^3/s)	5%	0	0	0	0	0	0	0	1.4	0.9	0.9	0.9	0.9
	mean	0	0	0	0	0	0	0	1.5	1.0	1.0	1.0	1.0
	95%	0	0	0	0	0	0	0	1.6	1.0	1.0	1.0	1.0
	stdev	0	0	0	0	0	0	0	0.0	0.0	0.0	0.0	0.0
	CV	0	0	0	0	0	0	0	0.0	0.0	0.0	0.0	0.0
Q_E (ft^3/s)	5%	0.1	0.1	0.0	0.2	0.1	0.1	0.2	0.2	0.0	0.2	0.1	0.1
	mean	0.1	0.2	0.0	0.3	0.2	0.2	0.2	0.3	0.0	0.2	0.1	0.1
	95%	0.1	0.2	0.1	0.3	0.2	0.2	0.3	0.3	0.0	0.3	0.1	0.1
	stdev	0.0	0.0	0.0	0.0	0.0	0.0	0.0	0.0	0.0	0.0	0.0	0.0
	CV	0.1	0.1	0.1	0.2	0.2	0.2	0.2	0.1	0.2	0.2	0.2	0.2
$\Delta S/\Delta t$ (ft^3/s)	5%	0	0	-3.8	-2.3	0	0	0	0	-7.0	-4.4	0	0
	mean	0	0	-0.5	2.9	0	0	0	0	-0.6	-1.9	0	0
	95%	0	0	2.9	8.4	0	0	0	0	6.0	0.5	0	0
	stdev	0	0	2.0	3.3	0	0	0	0	3.9	1.5	0	0
	CV	0	0	-4.08	1.13	0	0	0	0	-7.09	-0.78	0	0
A_P (acre)	5%	7.0	7.0	7.0	6.9	6.7	6.7	6.6	7.0	6.4	6.5	5.9	6.0
	mean	7.9	7.9	7.9	7.9	7.6	7.7	7.5	7.9	7.4	7.4	6.9	7.0
	95%	8.8	8.8	8.9	8.8	8.6	8.6	8.5	8.9	8.3	8.4	7.9	8.0
	stdev	0.6	0.6	0.6	0.6	0.6	0.6	0.6	0.6	0.6	0.6	0.6	0.6
	CV	0.07	0.07	0.07	0.07	0.08	0.07	0.08	0.07	0.08	0.08	0.09	0.09
A_{WS} (acre)	5%	5.9	5.9	5.9	5.8	5.7	5.7	5.6	5.9	5.5	5.5	5.1	5.2
	mean	6.8	6.8	6.9	6.8	6.7	6.7	6.6	6.9	6.5	6.6	6.3	6.3
	95%	7.8	7.8	7.8	7.8	7.7	7.7	7.6	7.8	7.6	7.6	7.4	7.4
	stdev	0.6	0.6	0.6	0.6	0.6	0.6	0.6	0.6	0.6	0.6	0.7	0.7
	CV	0.09	0.09	0.09	0.09	0.09	0.09	0.09	0.09	0.10	0.10	0.11	0.11

6.3 RELATIONSHIP BETWEEN SEEPAGE, VELOCITY, AND TURBIDITY

Time series plots of measured Q_s, average cross-sectional flow velocity, and turbidity were prepared to consider the impacts that velocity and turbidity may have on seepage. Turbidity, a measure of suspended sediment, could be related to measured Q_s due to its relation to sediment deposition along the canal perimeter. Moreover, canal velocity affects channel hydraulics, including sediment transport and suspension and perimeter shear stress, thereby potentially impacting Q_s. Time series plots of the three variables are presented as Figure 6-6 and Figure 6-7 for the Catlin Canal and RFH Canal, respectively, for the 2007 irrigation season.

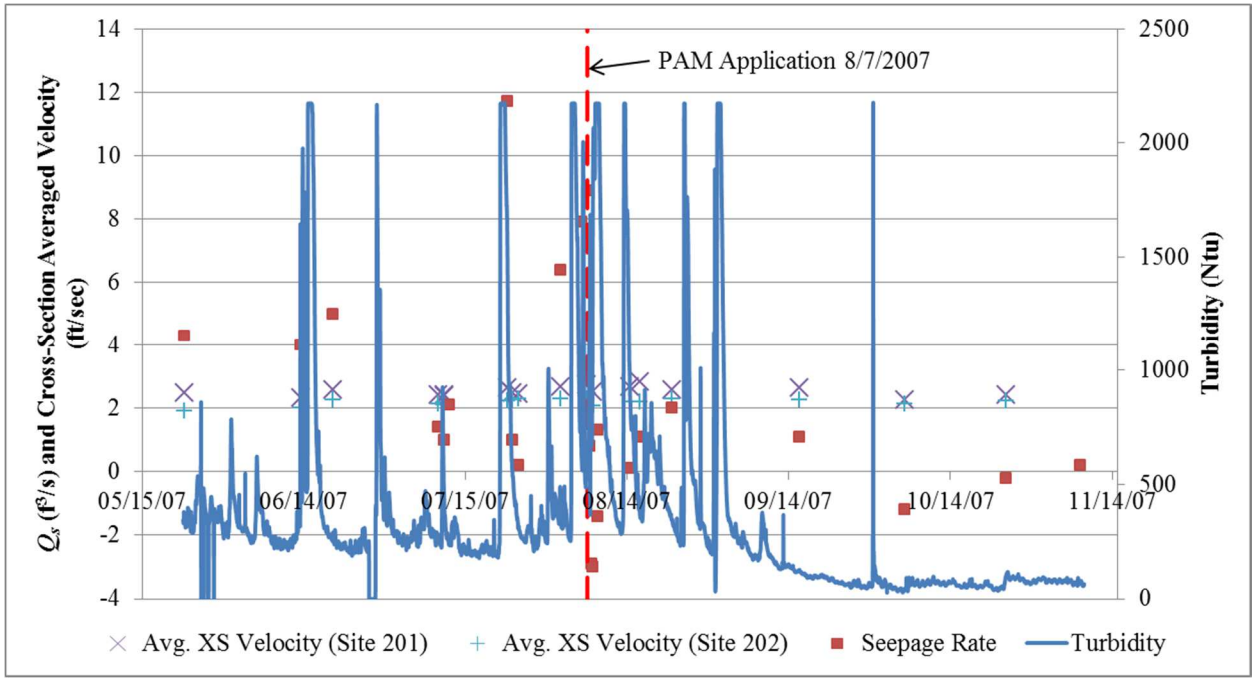

Figure 6-6 Time-series plot of measured Q_s, cross-section average flow velocity and turbidity for the Catlin Canal in 2007

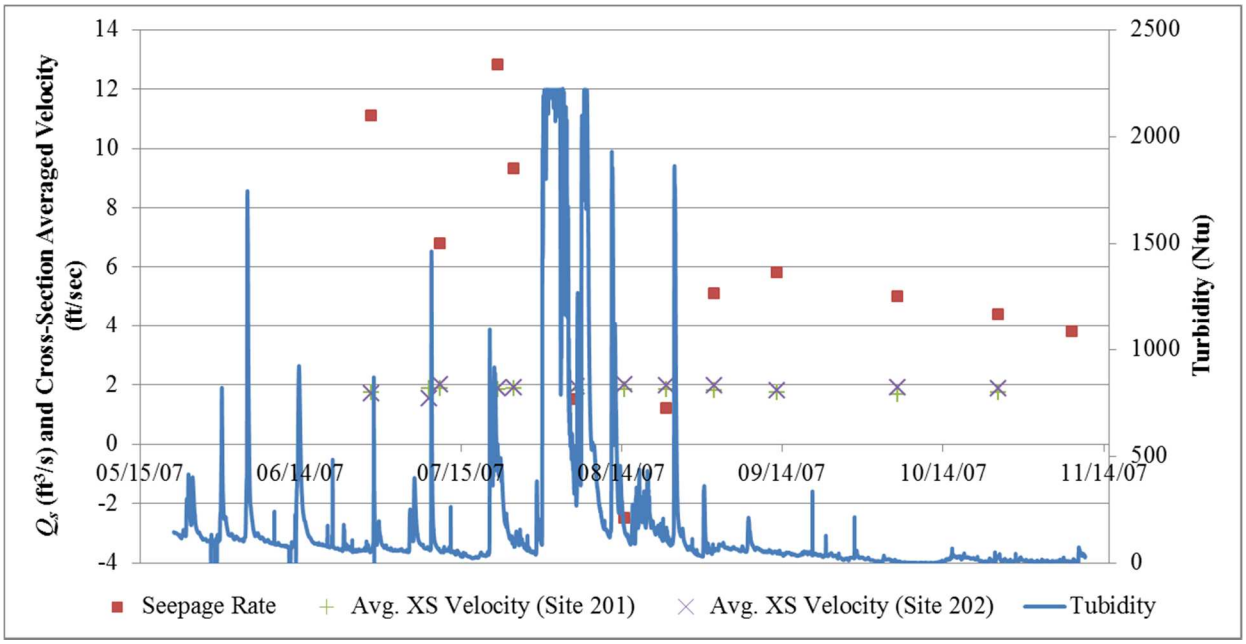

Figure 6-7 Time-series plot of measured Q_s, cross-section averaged velocity, and turbidity for the RFH Canal in 2007

Cross-section averaged velocity remained relatively consistent throughout irrigation seasons, and Q_s fluctuated without a correlated change in velocity for the range of values considered. Turbidity appeared to have affected Q_s in some instances but not in others, depending upon the duration over which turbidity levels were elevated. For example, the storm event that occurred around July 24, 2007 increased turbidity in the Catlin Canal to greater than 2,000 Ntu corresponding to a Q_s decrease from 11.9 ft^3/s on July 23rd to 1.0 ft^3/s on July 24th and to 0.2 ft^3/s on July 25th. However, Q_s estimates rose again prior to applying PAM on August 7th. The second example of apparent turbidity impact on seepage occurred on the RFH Canal between late July and mid-August of 2007 as a series of storm events contributed to sustained high tubidity levels in the canal water. Corresponding measured Q_s decreased from 9 to 12 ft^3/s in late-July to less than 2.0 ft^3/s through mid-August. However, the plots also indicate that

spikes in turbidity rates did not always result in natural sealing of the channel perimeter and reductions in measured seepage rates. Multiple spikes in turbidity on both the Catlin and RFH canals in 2007 had no observable impact on Q_s. The impact potentially is related to the duration over which turbidity is elevated and the opportunity time for sediment to be deposited along the canal perimeter. However, this topic exceeds the scope of this thesis and was not studied further.

Pearson correlation coefficients are presented in Table 6-12, and plots of turbidity and cross-section averaged velocity versus $\hat{Q}_s$ for the Catlin 2007 and RFH 2007 data sets are presented as Figure 6-8 and Figure 6-9, respectively. Turbidity values were measured at the time of the inflow-outflow test. The correlation coefficient values were calculated for the pre- and post-PAM application period for the Catlin Canal 2007 dataset, as well as for the full data set (pre- and post-PAM application data combined). For the RFH Canal 2007 dataset, the correlation coefficients for the full dataset and for the dataset between June and September were calculated. June through September was considered because turbidity levels declined significantly in October and November.

The results indicate that there was no statistically significant correlation (i.e. no p-values less than 0.05), as reported in Table 6-12, between Q_s and turbidity nor between Q_s and cross-section averaged velocity when comparing the full datasets for each canal. However, this does not take into account that turbidity levels may have been elevated and sediment deposition may have occurred in the days prior to the inflow-outflow test. Hence, the correlation values are apparently contradictory to some of the findings from qualitative examination of the time-series plots in Figure 6-6 and Figure 6-7.

Table 6-12 Correlation coefficient values for measured Q_s to turbidity and to cross-section averaged velocity

Canal	Period	Pearson Correlation Coefficient	
		Turbidity	Velocity
Catlin 2007	Pre-PAM	0.61	0.58
	Post-PAM	-0.41	0.23
	All	-0.05	0.04
RFH 2007	June - Sept	0.16	-0.05
	All	0.20	0.07

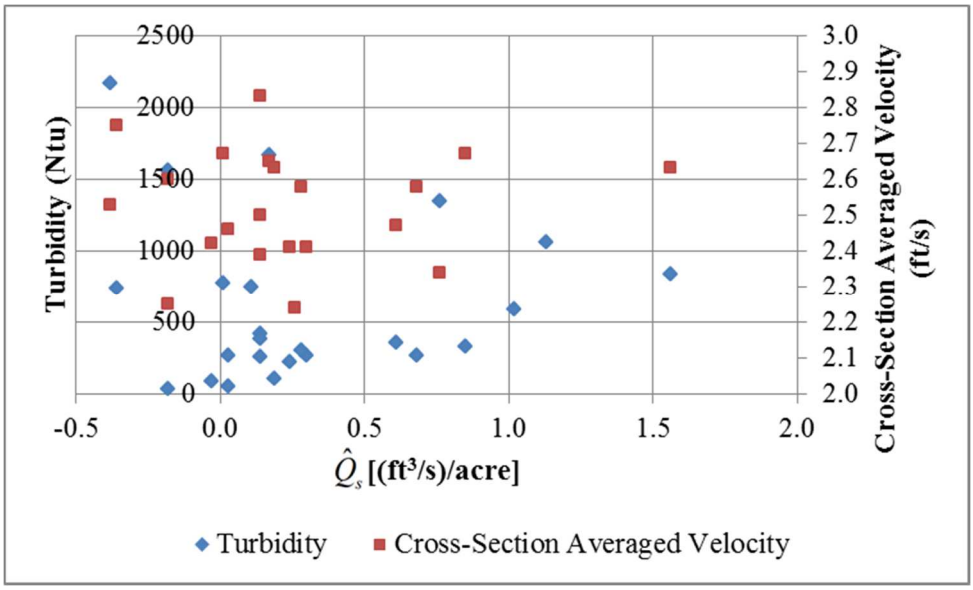

Figure 6-8 Measured $\hat{Q}_s$, average channel flow velocity and turbidity for the Catlin Canal in 2007

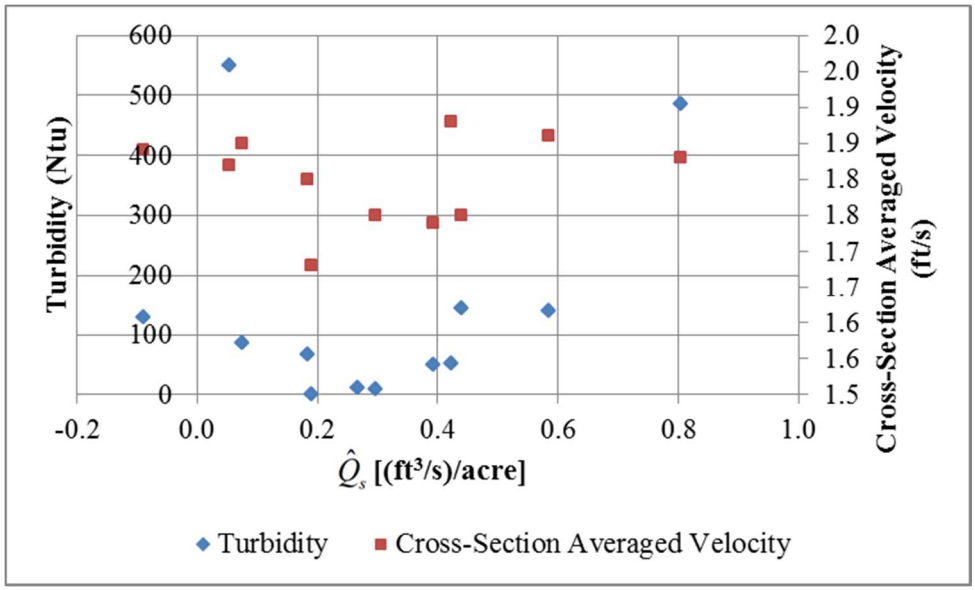

Figure 6-9 Measured $\hat{Q}_s$, cross-section averaged velocity and turbidity for the RFH Canal in 2007

6.4 SENSITIVITY ANALYSIS

6.4.1 Seepage Rate Sensitivity

Tornado plots were generated in @RISK to determine which variables and parameters most greatly impact the uncertainty in estimating canal seepage when using the inflow-outflow method. A tornado plot is a graphical method of displaying a ranking of random input variables in relation to their impact on a random output variable. The tornado plots present Spearman's rank correlation coefficients, which indicate the statistical dependence between two variables. A perfect Spearman correlation results in coefficients of -1.0 (inverse) or +1.0 (direct). Larger bars on the tornado plot indicate larger correlation coefficients between the assumed input probability distributions and the output probability distribution ($\hat{Q}_s$). Example tornado plots are presented only for results from a few representative inflow-outflow tests. To illustrate the full range of measurement conditions for inflow-outflow measurements, tornado plots for steady-

simultaneous, steady-lagged, unsteady- simultaneous, and unsteady-lagged tests are provided as Figure 6-10, Figure 6-11, Figure 6-12, and Figure 6-13, respectively. These plots are considered representative of all similar measurements conducted. There are only sixteen variables or parameters depicted in the tornado plots, which was maximum number allowed by @RISK. However, @RISK plots the sixteen variables or parameters with the largest correlation coefficients, so all other variables or parameters (that were not plotted) had correlation coefficients less than the minimum value on each tornado plot.

For inflow-outflow tests conducted under steady hydraulic conditions, uncertainty in Q_{US} and Q_{DS} accounted for the large majority of uncertainty in estimated seepage rates. This is true for both simultaneous and lagged inflow-outflow measurements, as indicated by the tornado plots of Figure 6-10 and Figure 6-11. The uncertainty of Q_{US} and Q_{DS} can vary based upon measurement error, measurement conditions, operator experience, and operation technique, and accuracy in estimating Q_{US} and Q_{DS} will have a far greater impact on estimating canal seepage than all other variables.

The second largest source of uncertainty stems from estimates in parameters associated with storage changes occurring within the canal study reach. Ideally, seepage tests would not be conducted when the canal flow is unsteady due to the added challenge of accurately estimating a storage change and discharge as the stage is changing.

Results indicate that evaporation rate uncertainty does not significantly impact uncertainty in $\hat{Q}_s$, especially in comparison to the impact of canal flow rate estimates. Evaporation rates may account for a respectable fraction of the total seepage rate, particularly for large study reaches with a large water surface area, but the impact on seepage uncertainty remains relatively small because the Q_E estimates are quite small compared to Q_{US} and Q_{DS}.

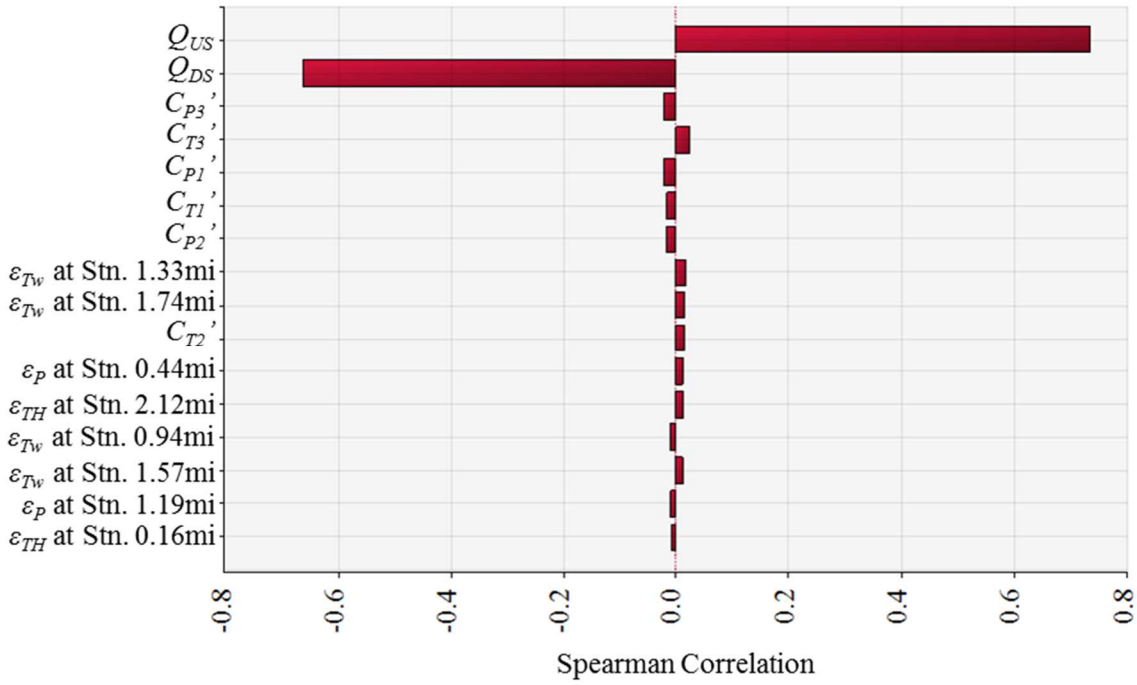

Figure 6-10 Tornado plots of Spearman rank correlation coefficients of steady-simultaneous $\hat{Q}_s$ with other variables estimated from the inflow-outflow tests on the Catlin Canal on 6/3/2006

(a)

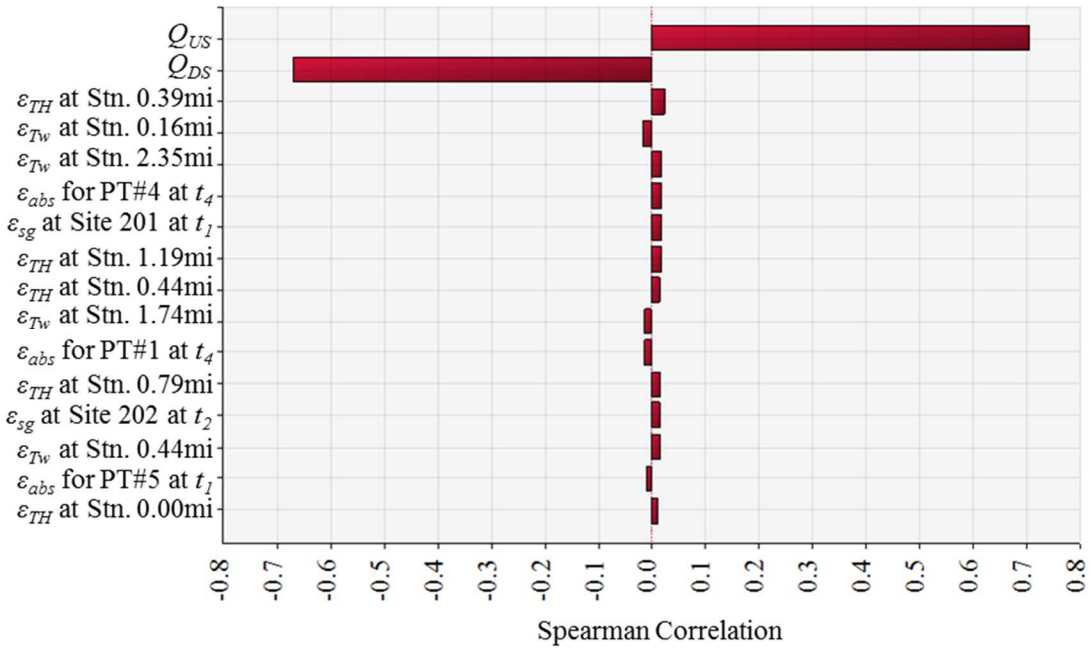

(b)

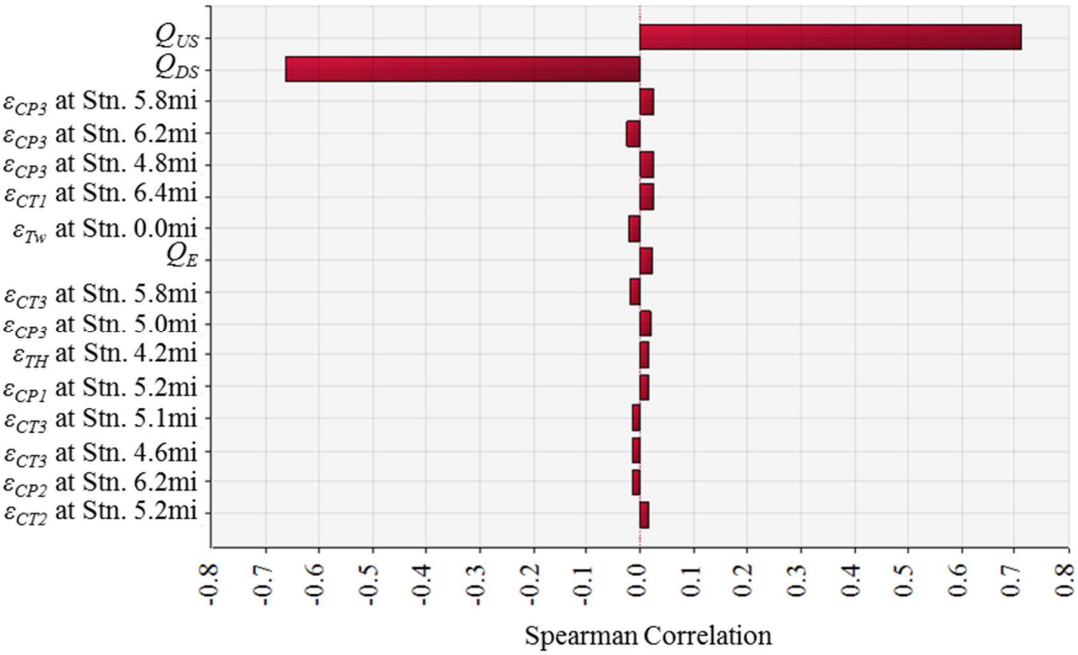

Figure 6-11 Tornado plots of Spearman rank correlation coefficients of steady-lagged $\hat{Q}_s$ with other variables estimated from the inflow-outflow tests on the (a) Catlin Canal on 8/6/2007 and (b) RFH Canal on 6/28/2006

(a)

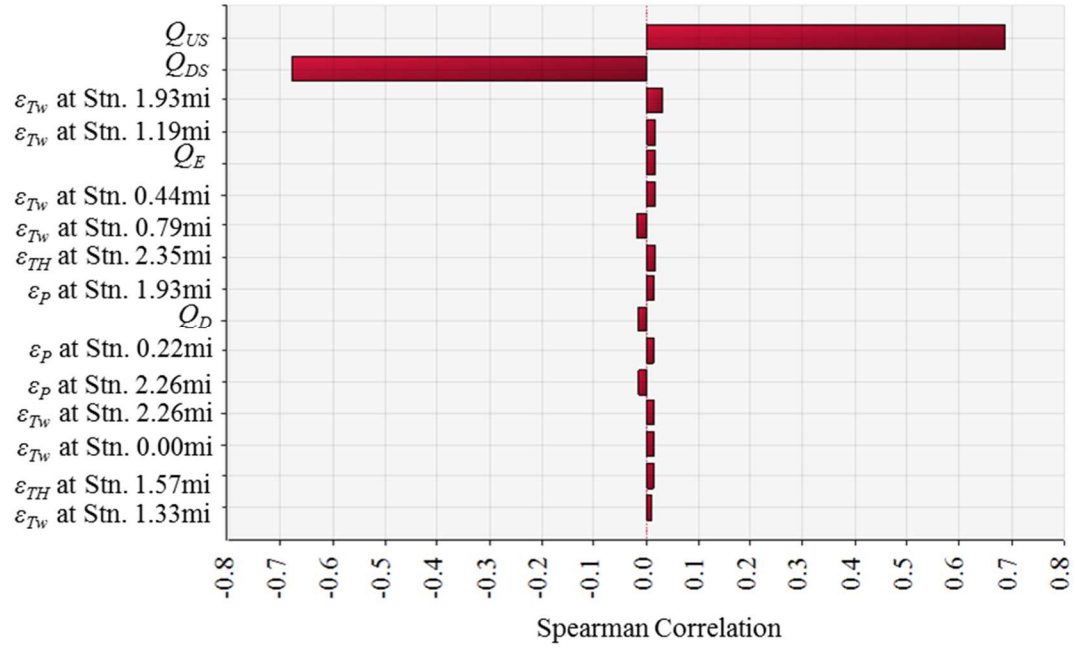

(b)

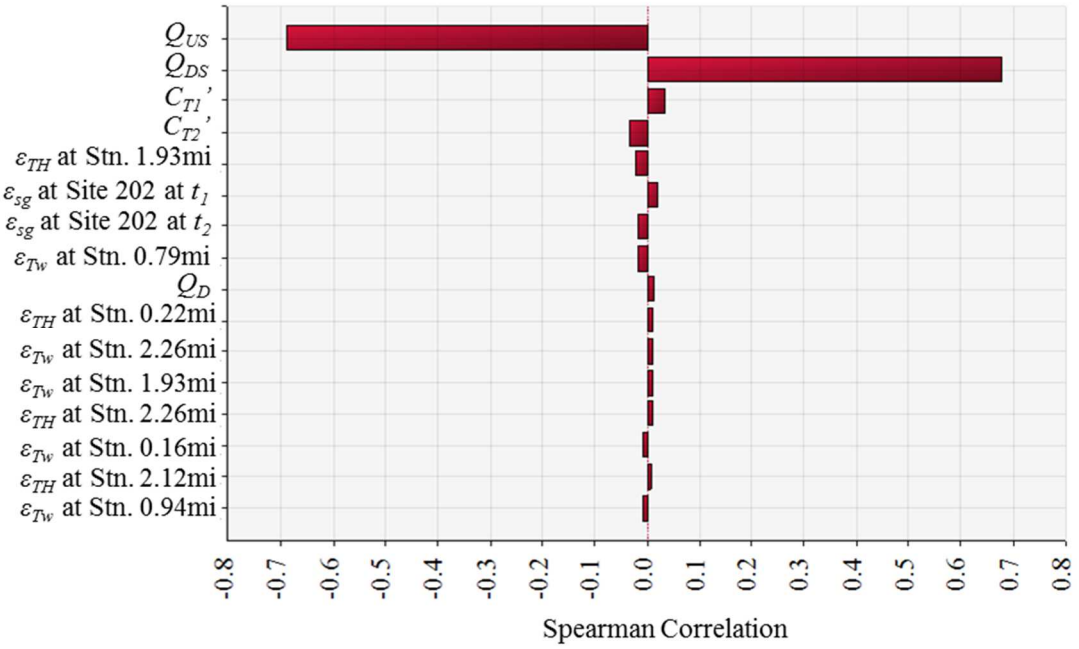

Figure 6-12 Tornado plots of Spearman rank correlation coefficients of unsteady-simultaneous $\hat{Q}_s$ with other variables estimated from the inflow-outflow tests on the (a) 6/4/2006 and (b) 6/22/2006 on the Catlin Canal

(a)

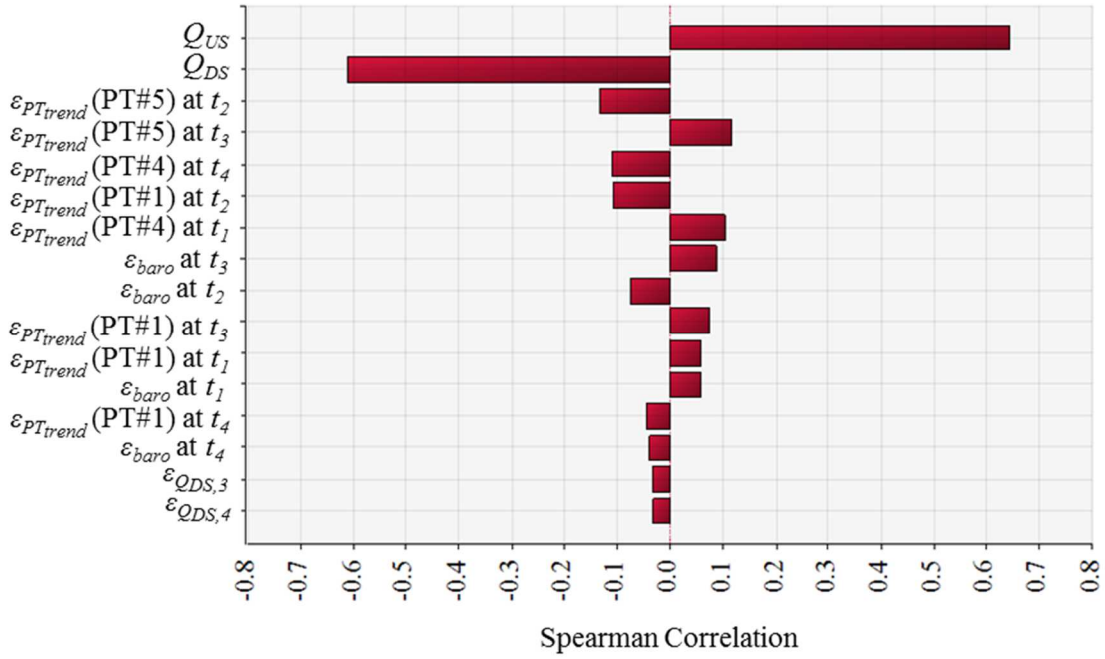

(b)

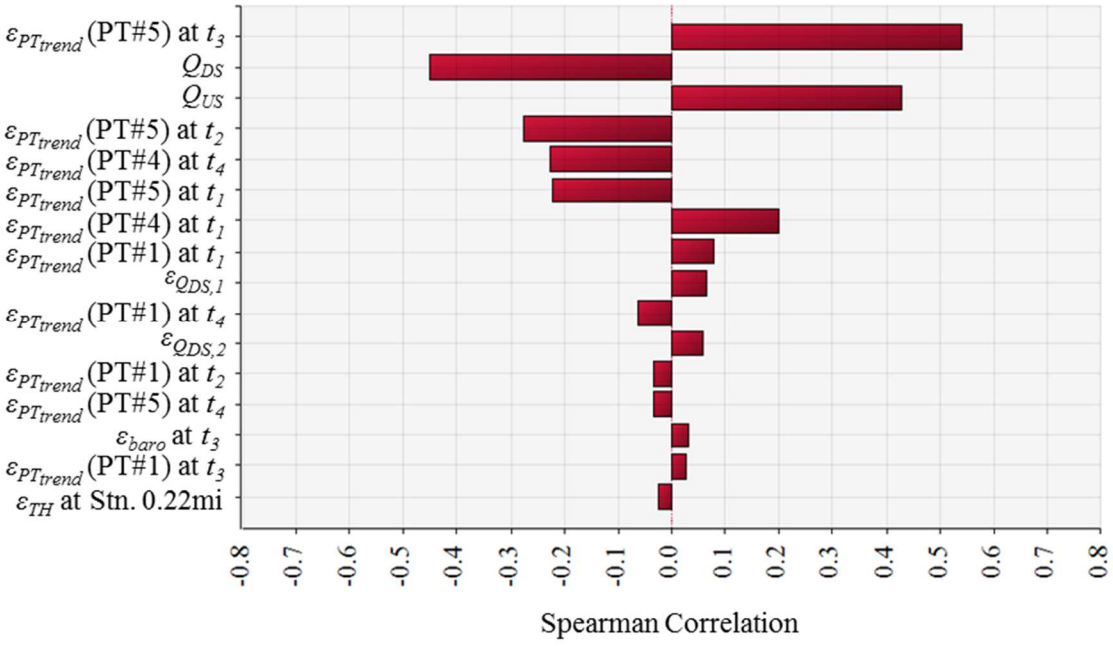

Figure 6-13 Tornado plots of Spearman rank correlation coefficients of unsteady-lagged $\hat{Q}_s$ with other variables estimated from the inflow-outflow tests on the (a) 6/14/2007 and (b) 8/8/2007 on the Catlin Canal

For tests with simultaneous canal flow rate measurements conducted when flow conditions were unsteady, uncertainty in Q_{US} and Q_{DS} also accounted for the large majority of uncertainty in estimated seepage, as presented in Figure 6-12. Uncertainty in stage measurement had little impact. This was likely due to the fact that canal flow rates were measured over the full duration of the seepage measurement (t_1 to t_4), so that Q_{US} and Q_{DS} did not have to be estimated during the "unmeasured" time period, as discussed is Section 5.2.1.2. For conditions of unsteady flow with lagged Q_{US} and Q_{DS} measurements, pressure transducer data had to be used to estimate Q_{US} and Q_{DS} when acoustic Doppler devices were not in use at the upstream and downstream cross-section, respectively (during travel time and during the flow measurement duration at the cross-section at the opposite end of the study reach). As such, it would be expected that the uncertainty related to stage measurements from pressure transducers would have a greater impact on the overall uncertainty related to seepage estimation in such cases. This is supported by the tornado plots in Figure 6-13, where the uncertainty of parameters associated with pressure transducer measurements of stage has a significant impact on uncertainty in seepage estimates for unsteady-lagged measurements. For both plots in Figure 6-13, the trendline residual for estimating stage from pressure transducer data significantly affected seepage uncertainty. The impacts were greater for the 8/8/2007 inflow-outflow tests than for the 6/14/2007 test, because a lower seepage value was calculated for 8/8/2007 (post-PAM application) and the estimated canal storage change was a much larger fraction of the calculated seepage. Figure 6-13 illustrates that canal storage changes can have a very significant impact on the uncertainty of estimated seepage, particularly for unsteady-lagged inflow-outflow measurements where the seepage value is relatively small.

Hence, from the tornado plots, the following conclusions can be drawn:

1. Q_{US} and Q_{DS} generally contribute the largest degree of uncertainty in estimating $\hat{Q}_s$.
2. For unsteady-lagged measurements, correlation coefficients for parameters related to stage measurement errors (i.e. ε_{baro}), stage measurement uncertainty (i.e. $\varepsilon_{PTtrend}$) spatial variability in hydraulic geometry (i.e. ε_{TH}), and uncertainty is estimating Q_{US} and Q_{DS} (i.e. $\varepsilon_{QUS,3}$ and $\varepsilon_{QUS,4}$) were higher than they were for steady-simultaneous, steady-lagged, and unsteady-simultaneous measurements.

6.4.2 Sensitivity Analysis for Flow Measurements Accuracy

6.4.2.1 Sensitivity to Q_{US} and Q_{DS} Measurement Error Range

The estimated measurement error for Q_{US} and Q_{DS} for this analysis was assumed to equal +/- 5% at the 90th IR based upon literature reviews of the accuracy of ADV and ADCP technologies. However, it is recognized that flow measurement error varies based upon hydraulic conditions, measurement location, turbulence, operator experience, equipment calibration, and other factors previously discussed. As such, sensitivity analysis was performed in this section to consider the impacts that a varying magnitude in the estimated flow measurement error has on canal seepage estimates. To make the comparison, five inflow-outflow test data sets from each of the Catlin 2006, Catlin 2007, RFH 2006, and RFH 2007 were considered. Data sets were selected so that the full range of canal flow rates and seepage rates encountered in this study could be represented in the analysis. Dates surrounding PAM applications (if applicable) also were considered in selecting the considered data sets. Measurement error ranges of +/- 2%, +/- 5%, and +/- 8% at the 90th IR were considered for Q_{US} and Q_{DS} for each seepage measurement. The +/- 8% error range was chosen based upon a study by Rehmel (2007), which indicated flow measurements using ADVs varied from flow rate measurements taken with other flow rate measurements technologies by as much as +/- 8% at the

90%IR. The +/- 2% error range was chosen for comparison purposes, assuming that measurement error associated with Q_{US} and Q_{DS} can be reduced by +/- 3 percentage points.

Table 6-13 presents the results. Examples of how the estimated seepage probability distributions are impacted by the considered alternative distribution in measured flow rate are presented in Figure 6-14. It is clear from these results that limiting flow measurement error can greatly reduce uncertainty in estimating seepage. As shown in Figure 6-14, the 90th IR for estimated seepage is substantially impacted by the degree of flow rate measurement error. The probability distribution of estimated seepage is greatly narrowed and the standard deviation is roughly proportional to one size of the 90th IR, being about one-fourth as large for a +/- 2% error range for Q_{US} and Q_{DS} as opposed to a +/- 8% error range. These observations are well known by the engineering community, as discussed in the literature review, but the results presented in Table 6-13 and Figure 6-14 provide a quantitative description of the importance of limiting flow measurement error in increasing the confidence in seepage rate estimated from inflow-outflow tests.

Table 6-13 Sensitivity analysis of uncertainty in estimated Q_S to measurement error range of Q_{US} and Q_{DS} at the 90th IR.

Canal and Year	Date	Measured Discharge (ft^3/s)		Q_S (ft^3/s)													
				+/- 2% at 90% IR					+/- 5% at 90% IR					+/- 8% at 90% IR			
		Q_{US}	Q_{DS}	5%	Mean	95%	CV	Stdev	5%	Mean	95%	CV	Stdev	5%	Mean	95%	CV	Stdev
Catlin 2006	6/3 A	112.0	102.0	6.8	9.8	12.8	0.18	1.8	2.4	9.8	17.5	0.47	4.6	-2.3	9.8	22.0	0.76	7.4
	6/3 B	105.9	101.1	1.6	4.6	7.5	0.39	1.8	-2.7	4.6	11.9	0.96	4.4	-6.8	4.6	16.2	1.54	7.1
	6/4 ADV	113.7	113.2	-2.1	1.0	4.2	1.90	1.9	-7.0	1.0	9.2	4.79	4.9	-11.6	1.0	13.9	7.80	7.8
	6/22 B	100.4	101.4	-3.6	-0.8	2.1	-2.13	1.7	-7.8	-0.8	6.2	-5.57	4.3	-12.3	-0.8	10.5	-8.63	6.9
	28/09/2006	71.2	70.6	-2.0	0.0	2.0	0.00	1.2	-5.0	0.0	5.0	0.00	3.0	-8.1	0.0	8.2	0.00	4.9
Catlin 2007	4/28	87.0	84.8	-0.7	1.8	4.2	0.83	1.5	-4.3	1.8	7.8	2.08	3.7	-7.9	1.8	11.4	3.28	5.9
	6/20	124.8	119.3	1.5	5.0	8.4	0.42	2.1	-3.7	5.0	13.7	1.05	5.3	-8.8	5.0	19.1	1.68	8.4
	8/7 A	152.0	143.0	4.7	8.9	13.1	0.28	2.5	-1.4	8.9	19.4	0.71	6.3	-8.0	8.9	25.7	1.15	10.2
	8/7 B	153.0	152.0	-3.5	0.8	5.2	3.25	2.6	-9.8	0.8	11.6	7.75	6.5	-16.3	0.8	18.2	13.13	10.5
	8/9 A	134.8	133.3	-2.5	1.3	5.0	1.77	2.3	-8.1	1.3	10.6	4.37	5.7	-13.8	1.3	16.4	7.08	9.2
RFH 2006	6/2	132.6	123.7	4.9	8.5	12.1	0.26	2.2	-0.5	8.5	17.5	0.65	5.5	-5.9	8.5	22.9	1.04	8.8
	7/1 A	144.0	135.0	4.5	8.5	12.5	0.28	2.4	-1.4	8.5	18.2	0.70	6.0	-7.1	8.5	24.3	1.11	9.4
	7/19	145.0	133.0	7.6	11.6	15.6	0.21	2.4	1.7	11.6	21.4	0.52	6.0	-4.4	11.6	27.1	0.83	9.6
	7/21	118.0	115.0	-0.4	2.9	6.2	0.70	2.0	-5.4	2.9	11.0	1.75	5.0	-10.3	2.9	16.0	2.82	8.1
	11/2	96.1	93.5	-0.1	2.6	5.2	0.63	1.6	-4.2	2.6	9.2	1.58	4.1	-8.2	2.6	13.3	2.53	6.5
RFH 2007	6/28	127.1	118.0	5.1	8.6	12.0	0.25	2.1	-0.1	8.6	17.4	0.62	5.3	-5.4	8.6	22.4	0.99	8.5
	7/22	196.6	182.9	7.4	12.8	18.1	0.25	3.2	-0.7	12.8	26.4	0.64	8.2	-8.4	12.8	34.3	1.02	13.1
	8/23	184.7	183.3	-4.1	1.2	6.4	2.67	3.2	-11.9	1.2	14.3	6.58	7.9	-19.8	1.2	21.8	10.50	12.6
	9/13	126.9	120.6	2.4	5.8	9.4	0.36	2.1	-3.0	5.8	14.6	0.93	5.4	-8.2	5.8	20.0	1.48	8.6
	11/8	94.4	90.5	1.3	3.8	6.5	0.42	1.6	-2.8	3.8	10.3	1.05	4.0	-6.6	3.8	14.2	1.66	6.3

(a)

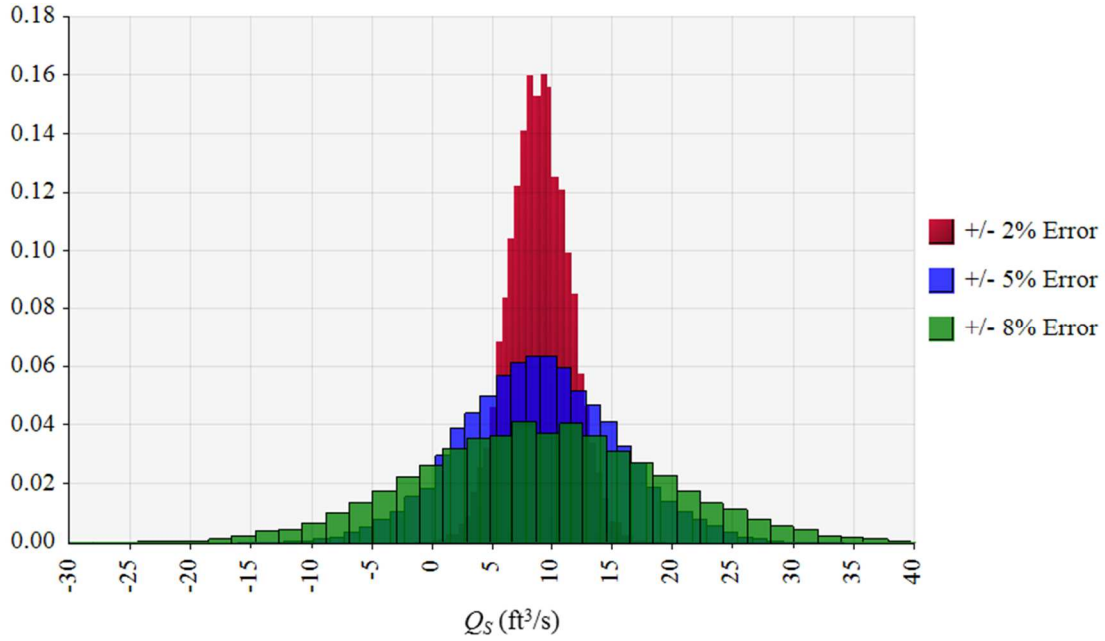

(b)

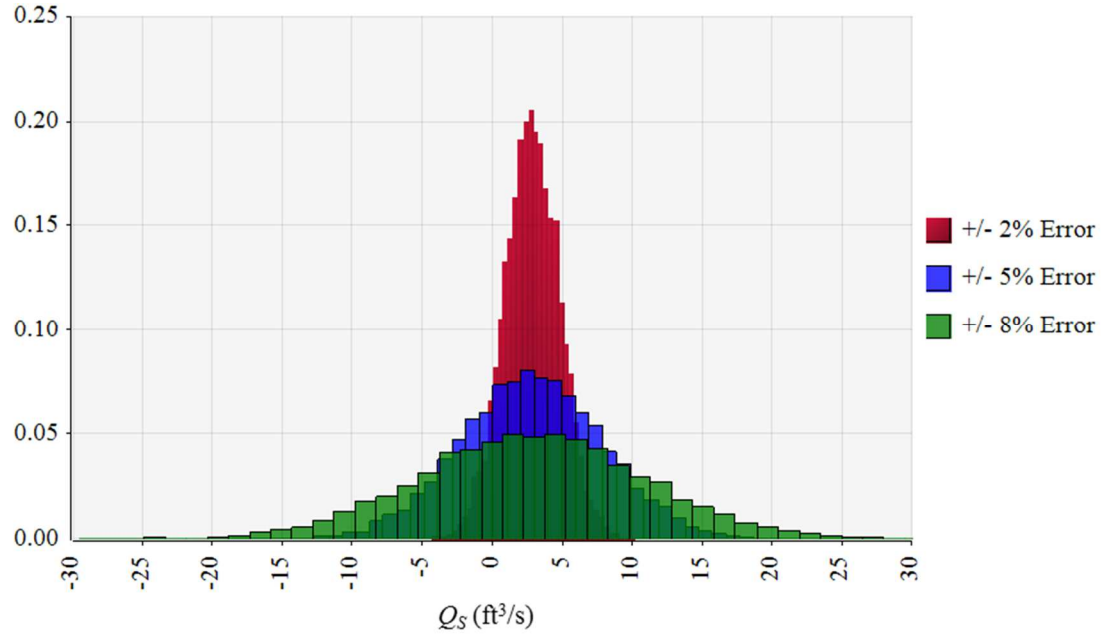

Figure 6-14 Probability distributions (frequency histograms) of estimated canal Q_S for different measurement error ranges (90th IR) for Q_{US} and Q_{DS} on (a) Catlin Canal 8/7/2007 and (b) RFH Canal on 7/21/2006

6.4.2.2 Sensitivity to Q_{US} and Q_{DS} Correlation

The Pearson correlation coefficient, r, between measurement of Q_{US} and Q_{DS} can vary based upon equipment technology, calibration of equipment, and operator experience and consistency. If flow measurements contain systematic errors and the same equipment is used to measure both Q_{US} and Q_{DS}, then r would be expected to be higher than if two different pieces of equipment were used to measure Q_{US} and Q_{DS}. Similarly, r would be impacted by equipment operators. If the same equipment operators measured both Q_{US} and Q_{DS}, then r would be expected higher than if different operators took the measurements due to differing levels of training, habits, and subjective interpretations. Such correlation between measurements is very difficult, if not impossible, to quantify due to the subjective nature of human interpretation and because equipment calibration and bias varies among each measurement and typically is unknown in the absence of detailed and controlled studies. As such, sensitivity analysis was performed to consider a range of plausible values for r and to evaluate the impact on uncertainty in estimation of Q_S.

Similar to the previous section, data sets from five representative inflow-outflow tests for each of the Catlin 2006, Catlin 2007, RFH 2006, and RFH 2007 were considered in examining the impact of r. The same five tests were used in this portion of the analysis, so that results could be compared to those for the examination of the assumed measurement error range for Q_{US} and Q_{DS} (presented in Section 6.4.2.1). Results are presented in Table 6-14. To illustrate the impact that r has on uncertainty in estimated seepage rates, relative frequency histograms and box plots generated from Monte Carlo simulations in @RISK are provided from the analysis of two seepage tests in Figure 6-15 and Figure 6-16. From the table and figures, it is evident that uncertainty in seepage estimation increases as the correlation between Q_{US} and Q_{DS} decreases. For example, typical CV values for estimated seepage increase by around 50% to 70% as r

decreases from 0.8 to 0.0. This reinforces the presumption that using the same flow measurement equipment and the same personnel, or least equally-trained personnel, can substantially reduce the uncertainty of canal seepage estimates when using the inflow-outflow method.

In comparison to the sensitivity analysis of assumed measurement error range for Q_{US} and Q_{DS}, r has less impact on uncertainty. For example, increasing r from 0 to 0.5 and from 0 to 0.8 reduces CV by about 30% and 50%, respectively, but reducing the measurement error range from +/- 5% to +/- 2% at the 90% IR reduces CV by about 60%. This indicates that generally it is more important to use more accurate and better-calibrated measurement equipment and methods than take measures to reduce r (i.e. having the same person(s) conduct Q_{US} and Q_{DS} measurements using the same piece of equipment).

Table 6-14 Sensitivity analysis of correlation factors for Q_{US} and Q_{DS}

Canal and Year	Date	Measured Discharge (ft^3/s)		Q_S (ft^3/s)													
				$r = 0$ (no correlation)					$r = 0.5$					$r = 0.8$			
		Q_{US}	Q_{DS}	5%	Mean	95%	CV	Stdev	5%	Mean	95%	CV	Stdev	5%	Mean	95%	CV	Stdev
Catlin 2006	6/3 A	112.0	102.0	2.4	9.8	17.5	0.47	4.6	4.0	9.8	15.5	0.36	3.5	4.9	9.8	14.8	0.31	3.0
	6/3 B	105.9	103.3	-2.7	4.6	11.9	0.96	4.4	-1.1	4.6	10.2	0.74	3.4	-0.2	4.6	9.3	0.63	2.9
	6/4 ADV	113.7	113.2	-7.0	1.0	9.2	4.79	4.9	-5.1	1.0	7.3	3.70	3.7	-4.3	1.0	6.2	3.20	3.2
	6/22 B	100.4	101.4	-7.8	-0.8	6.2	5.57	4.3	-6.2	-0.8	4.7	4.13	3.3	-5.5	-0.8	3.9	3.63	2.9
	9/28	71.2	70.6	-5.0	0.0	5.0	0.00	3.0	-3.8	0.0	3.8	0.00	2.3	-3.3	0.0	3.2	0.00	2.0
Catlin 2007	4/28	87.0	84.8	-4.3	1.8	7.8	2.08	3.7	-2.8	1.8	6.4	1.56	2.8	-2.2	1.8	5.8	1.33	2.4
	6/20	124.8	119.3	-3.7	5.0	13.7	1.05	5.3	-1.5	5.0	11.7	0.80	4.0	-0.5	5.0	10.7	0.68	3.4
	8/7 A	152.0	143.0	-1.4	8.9	19.4	0.71	6.3	0.8	8.9	16.7	0.54	4.8	2.2	8.9	15.6	0.46	4.1
	8/7 B	153.0	152.0	-9.8	0.8	11.6	7.75	6.5	-7.3	0.8	9.1	6.25	5.0	-6.2	0.8	7.9	5.38	4.3
	8/9 A	134.8	133.3	-8.1	1.3	10.6	4.37	5.7	-6.0	1.3	8.6	3.38	4.4	-4.9	1.3	7.4	2.92	3.8
RFH 2006	6/2	132.6	123.7	-0.5	8.5	17.5	0.65	5.5	1.4	8.5	15.4	0.50	4.2	2.5	8.5	14.4	0.43	3.6
	7/1 A	144.0	135.0	-1.4	8.5	18.2	0.70	6.0	1.0	8.5	16.1	0.54	4.6	2.0	8.5	15.0	0.46	3.9
	7/19	145.0	133.0	1.7	11.6	21.4	0.52	6.0	3.9	11.6	19.0	0.39	4.6	5.2	11.6	18.0	0.34	3.9
	7/21	118.0	115.0	-5.4	2.9	11.0	1.75	5.0	-3.4	2.9	9.2	1.31	3.8	-2.6	2.9	8.3	1.14	3.3
	11/2	96.1	93.5	-4.2	2.6	9.2	1.58	4.1	-2.5	2.6	7.7	1.19	3.1	-1.7	2.6	7.0	1.04	2.7
RFH 2007	6/28	127.1	118.0	-0.1	8.6	17.4	0.62	5.3	1.9	8.6	15.1	0.47	4.0	2.8	8.6	14.3	0.40	3.5
	7/22	196.6	182.9	-0.7	12.8	26.4	0.64	8.2	3.0	12.8	22.6	0.46	5.9	4.8	12.8	20.8	0.38	4.9
	8/23	184.7	183.3	-11.9	1.2	14.3	6.58	7.9	-8.4	1.2	10.7	4.98	5.8	-6.6	1.2	9.0	4.05	4.7
	9/13	126.9	120.6	-3.0	5.8	14.6	0.93	5.4	-0.5	5.8	12.3	0.67	3.9	0.6	5.8	11.2	0.55	3.2
	11/8	94.4	90.5	-2.8	3.8	10.3	1.05	4.0	-0.9	3.8	8.7	0.76	2.9	-0.1	3.8	7.8	0.63	2.4

(a)

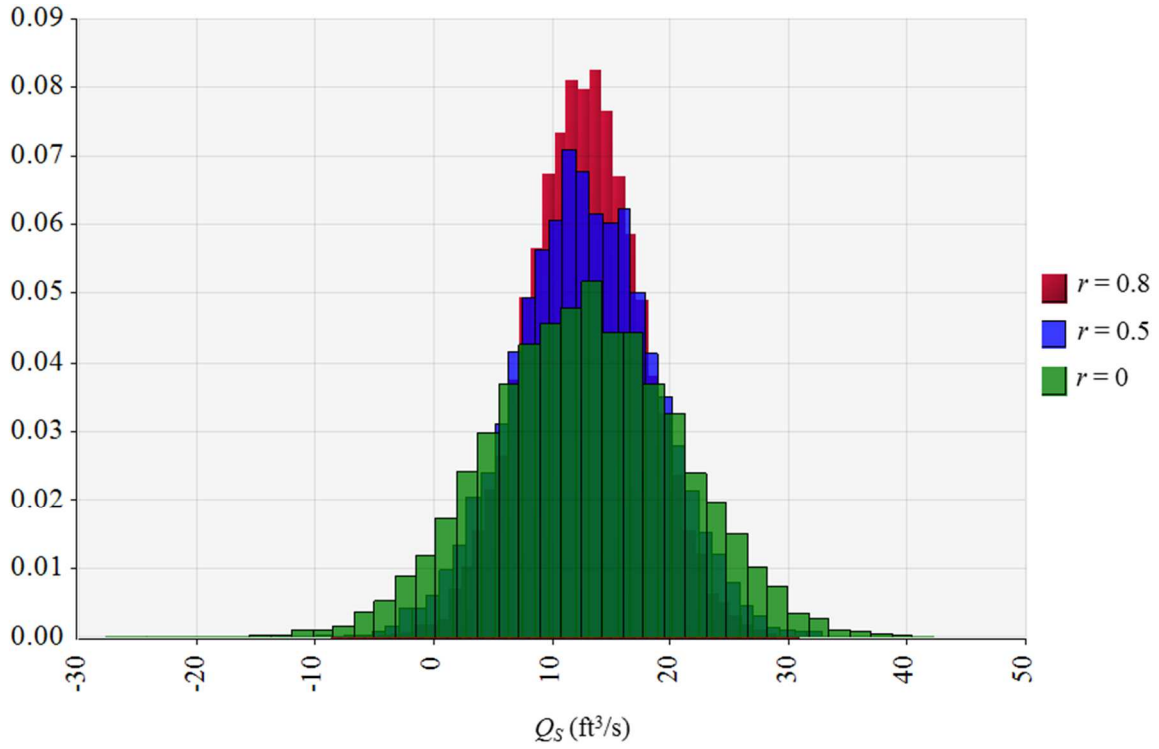

(b)

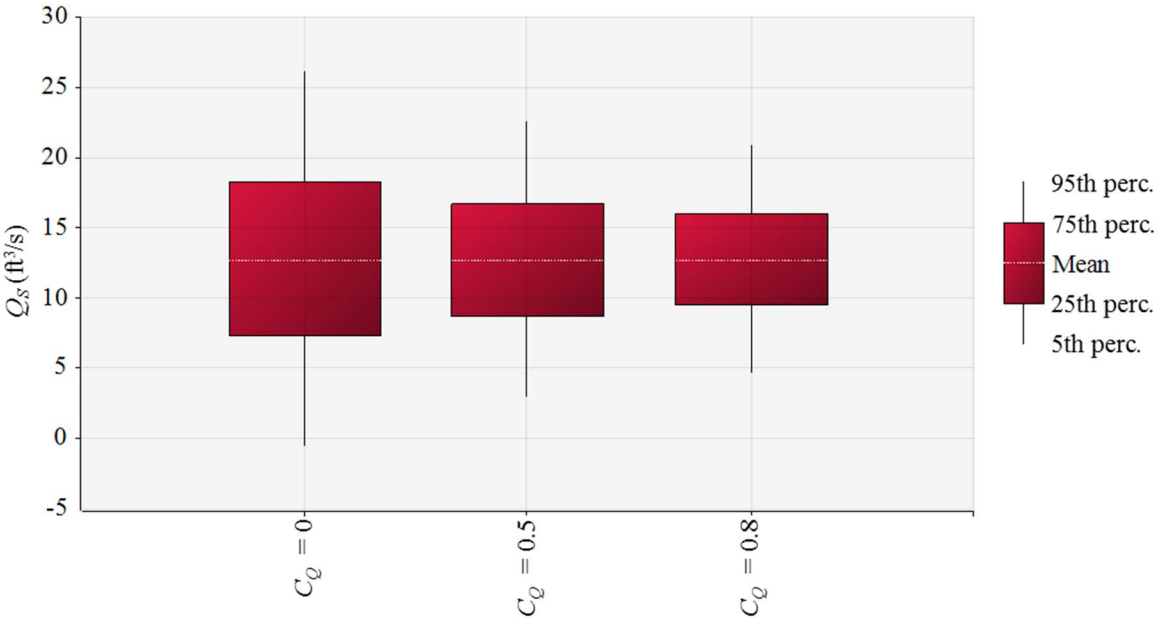

Figure 6-15 Generated estimates of canal Q_S as (a) relative frequency histograms and (b) box plots for r values of 0.0, 0.5, and 0.8 (RFH Canal on 7/22/2007)

(a)

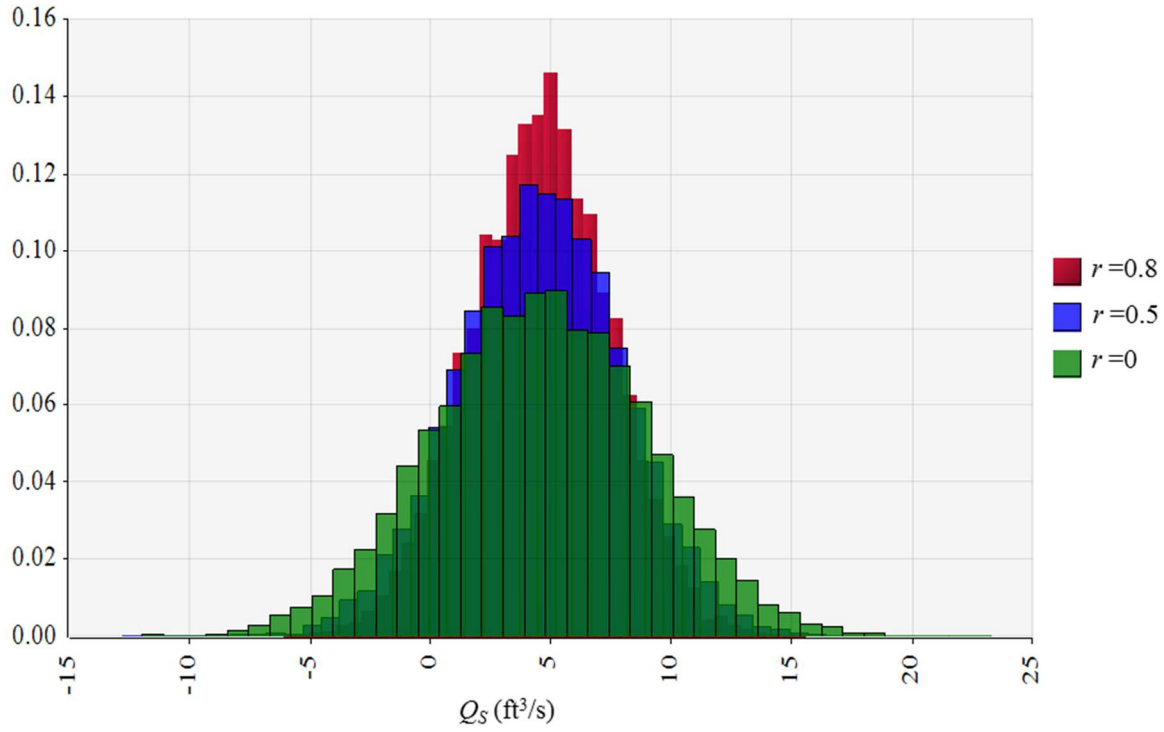

(b)

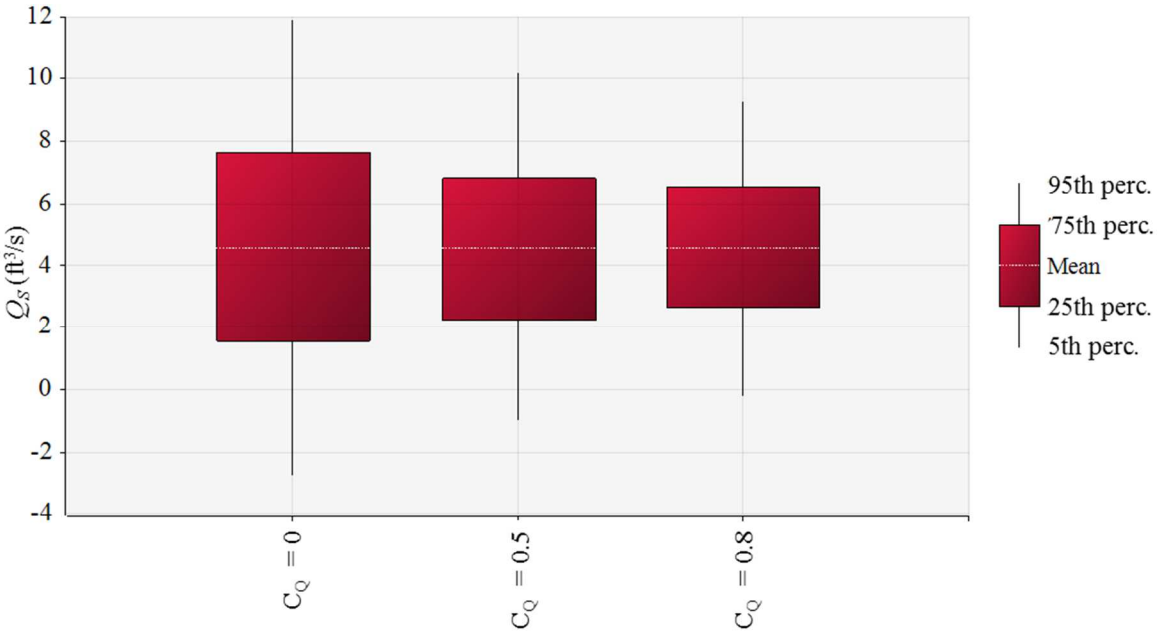

Figure 6-16 Generated estimates of canal Q_S as (a) relative frequency histograms and (b) box plots for r values of 0.0, 0.5, and 0.8 (Catlin Canal on 6/3/2006 B)

6.4.3 Sensitivity Analysis for Errors in Stage Measurement

Sensitivity analysis was performed for stage measurement error. The aforementioned expected error ranges for staff gages and pressure transducers were doubled for this sensitivity analysis and the resulting estimates of Q_S were compared to the original estimates. The adopted errors of +/- 0.04 feet for staff gages and +/- 0.04 feet for pressure transducers (absolute and barometric pressure measurements) at the 90th IR are labeled as Error Level A in Table 6-15. Error Level A results from Monte Carlo simulation of Q_S are compared against Error Level B results, which include stage measurement errors of +/- 0.08 feet for staff gages and +/-0.12 feet for pressure transducers at the 90^{th} IR. Four sets of inflow-outflow test data were compared to illustrate the sensitivity of uncertainty in estimated Q_S tests to uncertainty in stage measurements. Two tests where storage changes occurred were included in the analysis. These examples are considered to provide adequate representation of all other data sets.

Table 6-15 Sensitivity analysis results for uncertainty in estimated Q_S and other water balance components to assumed uncertainty in stage measurements

		Catlin 6/3/2006 A		Catlin 6/14/2007		Catlin 7/11/2007 B		RFH 9/13/2007	
Canal Storage Change?		No	No	Yes	Yes	Yes	Yes	No	No
Error Level		A*	B**	A*	B**	A*	B**	A*	B**
A_P (acre)	5%	6.1	6.1	6.1	6.1	6.2	6.2	13.9	13.9
	Mean	7.1	7.1	7.1	7.1	7.2	7.2	14.8	14.8
	95%	8.1	8.1	8.1	8.1	8.1	8.2	15.7	15.7
	Stdev	0.6	0.6	0.6	0.6	0.6	0.6	0.5	0.5
	CV	0.09	0.09	0.09	0.09	0.08	0.08	0.04	0.04
A_{WS} (acre)	5%	5.3	5.3	5.3	5.3	5.3	5.3	13.2	13.2
	Mean	6.4	6.4	6.4	6.4	6.4	6.4	14.1	14.1
	95%	7.5	7.5	7.5	7.5	7.5	7.5	15.0	14.9
	Stdev	0.7	0.7	0.7	0.7	0.7	0.7	0.5	0.5
	CV	0.11	0.11	0.11	0.11	0.10	0.10	0.04	0.04
Q_E (ft^3/s)	5%	0.12	0.12	0.05	0.05	0.14	0.14	0.37	0.37
	Mean	0.17	0.17	0.07	0.07	0.19	0.19	0.46	0.46
	95%	0.21	0.21	0.09	0.09	0.24	0.24	0.56	0.56
	Stdev	0.03	0.03	0.01	0.01	0.03	0.03	0.06	0.06
	CV	0.16	0.16	0.16	0.16	0.16	0.16	0.13	0.13
$\Delta S/\Delta t$ (ft^3/s)	5%	n/a	n/a	-4.4	-5.5	-2.0	-3.4	n/a	n/a
	Mean	n/a	n/a	-2.6	-2.6	-0.1	-0.1	n/a	n/a
	95%	n/a	n/a	-0.9	0.2	1.6	3.1	n/a	n/a
	Stdev	n/a	n/a	1.1	1.7	1.1	2.0	n/a	n/a
	CV	n/a	n/a	-0.42	-0.67	-11.00	-13.23	n/a	n/a
Q_S (ft^3/s)	5%	2.4	2.4	-3.4	-4.5	-5.7	-6.2	-3.0	-3.0
	Mean	9.8	9.8	4.0	4.0	2.2	2.2	5.8	5.8
	95%	17.5	17.3	11.3	12.4	10.1	10.5	14.6	14.6
	Stdev	4.6	4.6	4.5	5.1	4.7	5.1	5.4	5.4
	CV	0.47	0.47	1.13	1.29	2.14	2.35	0.92	0.92
$\hat{Q}_s$ [(ft^3/s)/acre]	5%	0.33	0.34	-0.49	-0.63	-0.80	-0.88	-0.20	-0.19
	Mean	1.39	1.39	0.56	0.56	0.30	0.30	0.40	0.40
	95%	2.51	2.49	1.61	1.76	1.42	1.48	0.99	0.98
	Stdev	0.67	0.66	0.64	0.73	0.67	0.72	0.37	0.36
	CV	0.48	0.47	1.14	1.29	2.23	2.37	0.92	0.91

* Error Level A: +/- 0.04 ft error for staff gages and +/- 0.04 ft for pressure transducers

** Error Level B: +/- 0.08 ft error for staff gages and +/- 0.12 ft for pressure transducers

As shown in Table 6-15, increased error in stage measurements has very little impact on uncertainty in A_P and A_{WS}. This is because the error in stage results in changes in T_w and P that are a very small percentage of the measured values. For example, if T_w and P were measured to

be 20 and 22 feet, respectively, and stage error were to increase by an additional 0.05 feet, then T_w across the channel would change to a maximum value of 20.1 feet and P would increase to around 22.1 (assuming vertical side slopes). In both cases, these increases are around 0.25% of the measured values, which is very minimal. As a result, evaporation rates also are minimally impacted since they are directly dependent upon A_{WS} (a function of T_w).

However, canal storage change estimates are impacted by the level of error in stage measurements, as seen in Table 6-15 for the 6/14/2007 and 7/11/2007 B seepage measurements on the Catlin Canal. The mean values of storage change were not impacted, because the error range was assumed centered around the measured value to estimate the true value, but the 5th and 95th percentile values were impacted as the degree of uncertainty increased. The increase in stage measurement error added an additional 2.2 ft^3/s and 2.9 ft^3/s to the 90th interpercentile intervals for storage changes for the 6/14/2007 and 7/11/2007 B seepage measurements, respectively, which amount to 55% and 73% of the respective mean values. Upon viewing the tornado plots in @RISK, uncertainty related to measuring Q_{US} and Q_{DS} has a significantly greater impact on the uncertainty in estimating Q_S than does uncertainty in stage measurement. Nevertheless, stage measurement error still has a measurable impact on Q_S uncertainty under unsteady flow conditions.

6.4.4 Sensitivity Analysis of Uncertainty in Evaporation Estimates

Based upon tornado plots for inflow-outflow test results, similar to those presented in Section 6.4.1, it is clear that uncertainty in Q_E had minimal impact on uncertainty in Q_S estimates. Values of Q_E can be significant on large canal reaches with a large water surface area, but the impact of uncertainty in flow rate measurements and calculation of storage changes substantially outweighs that of uncertainty in estimation of evaporation rates. For wider canals and hotter

weather conditions, evaporation may play a larger role in uncertainty estimation, but this was not the case for these studies. As such, a more detailed sensitivity study was not performed.

6.5 EFFECTIVENESS OF PAM APPLICATIONS

6.5.1 Deterministic Approach for Evaluating Effectiveness of PAM Applications

Canal seepage rates, calculated from the mass balance equation using a deterministic approach, are presented in Section 3.1 for each canal that was studied in 2006 and 2007. Plots of Q_S versus time also are presented, helping illustrate changes in estimated Q_S before and after PAM applications. From Figure 6-1 through Figure 6-5, it appears that overall the PAM applications had an impact on reducing canal seepage, although the degree of the impact is unclear. Average seepage reduction percentages are presented in Table 6-16. The results for the first RFH and first Lamar canal PAM applications are not presented in the table since estimates of Q_S were not presented in Section 6.2 and because it is acknowledged that the applications had no appreciable impact on Q_S reduction or that the studies were too flawed by error. If Q_S was estimated to be less than zero (presumably due to measurement error), that estimate was assigned a value of zero when calculating the reduction averages in Table 6-16, since there was no evidence that canals were gaining water from adjacent groundwater (based upon readings from groundwater monitoring wells immediately adjacent to the canal banks). The pre-PAM application Q_S values that were used to calculate the seepage reduction percentages were taken as the average of all values estimated from inflow-outflow tests conducted over the week prior to the application.

The second Lamar 2006 PAM application showed the lowest reduction in Q_S at around 34%, which may be attributed to lower suspended sediment concentrations due in part to the Lamar Canal being located on the Arkansas River at only about 22 miles downstream of a large

reservoir (John Martin Reservoir). The two applications on the Catlin Canal showed the largest reduction in deterministic estimates of Q_S - anywhere from near 100% to 84% at one week to three months after the application. The second application on the RFH Canal in 2006 showed a reduction in Q_S of 74% over the first week. For a couple of months after the PAM application, reduction in Q_S was estimated to be approximately 67%. PAM appeared to have maintained a relatively stable impact on reduction in Q_S for the 3 month period after PAM application for all cases presented in Table 6-16.

Table 6-16 Average estimated reduction in Q_S for PAM applications

Canal with Application	**Time after PAM Application**			
	~1 week	**~1 month**	**~2 months**	**~3 months**
Catlin 2006	91%	94%	89%	84%
Catlin 2007	100%	93%	92%	93%
Lamar 2006 – 2nd app.	35%	35%	34%	34%
RFH 2006 – 2nd app.	74%	67%	67%	69%

Note: Pre-PAM application Q_S values were taken as average of the values estimated from inflow-outflow tests over the week prior to application.

Seepage reduction likely can be attributed both to PAM applications and to natural occurences, such as storm events, that bring high concentrations of suspended sediment into the canal with resulting natural sealing of the channel perimeter upon settling. Two examples of storm events likely causing significant reductions in Q_S in the canal study reaches were discussed in Section 6.3. A plan to apply PAM to the RFH Canal in late July 2007 was abandoned as a result of the natural channel sealing that occurred due to these storm events. The second PAM application to the RFH Canal in 2006 was conducted on July 20th because a storm event had just increased suspended sediment concentrations in the canal water (turbidity levels exceeded 270 Ntu), thereby creating what was thought to be a good condition to enhance PAM effectiveness.

Results indicate that Q_S decreased after the PAM application. However, based upon the aforementioned knowledge that seepage rates can decrease due to natural channel sealing from storm events, it is unclear how extensive a role that PAM played in Q_S in this case since an adequate control reach in the canal was not developed. If an adequate control reach had been established, then an estimate of the degree of natural channel sealing could have been differentiated from the sealing brought about by the PAM application. Nevertheless, the combination of the PAM application in the presence of higher suspended sediment concentrations may explain why the second application in 2006 resulted in an estimated reduction in Q_S whereas the first application in 2006 was unsuccessful. The impact of the July 24, 2007 storm (without a PAM application) on the Catlin Canal lasted only a couple of weeks; whereas, on the RFH Canal, the impact of the storm coupled with a PAM application on July 20, 2006 lasted about three months. Additional explanation and description of factors that affect the success of PAM applications are presented in Susfalk et al. (2008).

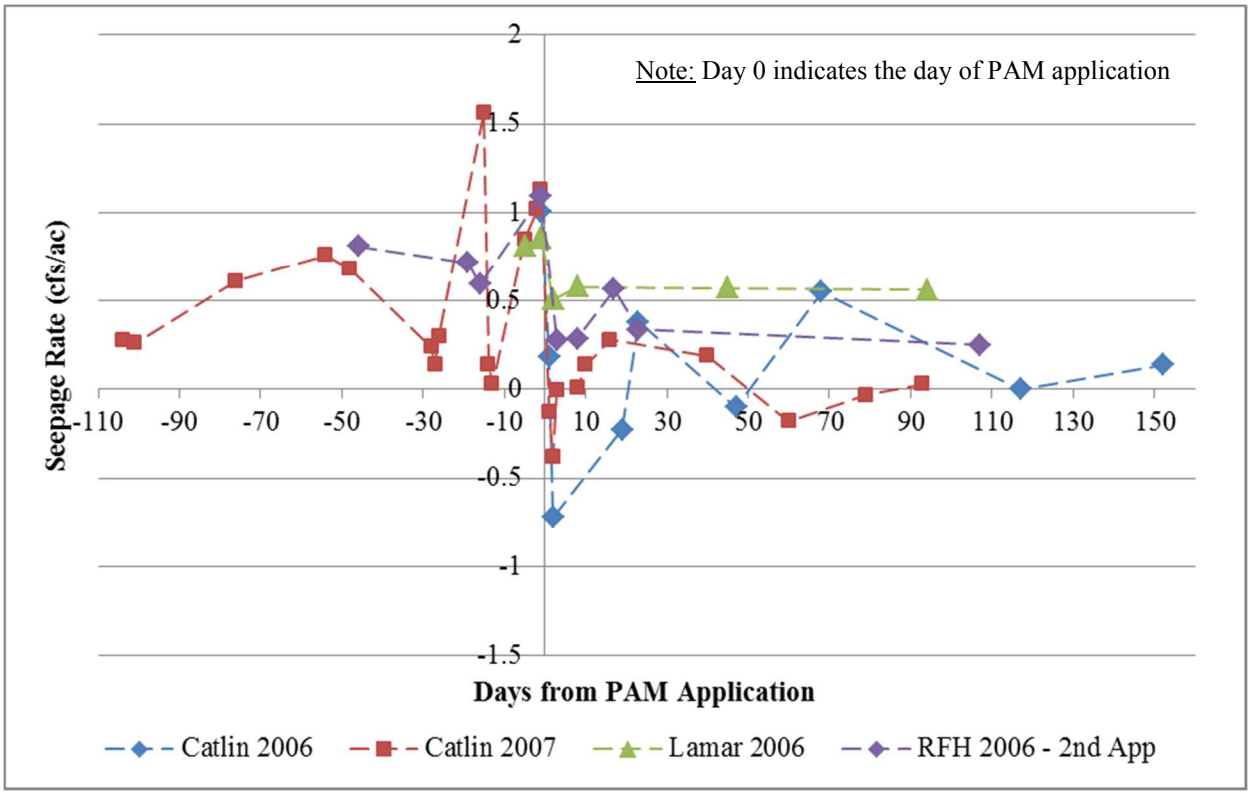

Figure 6-17 Time series plots of deterministic estimates of Q_S

6.5.2 Stochastic Approach for Evaluating Effectiveness of PAM Applications

Probability distributions of Q_S estimates for pre- and post-PAM application tests were generated by solving the inflow-outflow volume balance with Monte Carlo simulation and were compared to estimate potential changes in Q_S due to PAM application. Distributions of percent differences in were calculated for 5000 realizations of estimated pre- and post-PAM application Q_S values. In other words, the percent difference was calculated using the first generated realization of post-PAM seepage rate and the first generated pre-PAM seepage rate, then the same for the remaining 4999 generated pairs of realizations. The resulting cumulative frequency plots are presented in Figure 6-18, Figure 6-19, Figure 6-20, and Figure 6-21 for the RFH 2006B, Catlin 2006 (with ADVs), Catlin 2006 (with ADCPs), and Catlin 2007 seepage reduction studies,

respectively. The percent differences were cutoff at +/- 400% for plotting purposes and for clarity on the graphs.

Percent differences greater than zero indicate a reduction in seepage from pre- to post-PAM seepage measurement as a result of the PAM application. The plots indicate that 87.7%, 80.3%, 89.0%, and 86.0% of plotted realizations had a percent difference greater than zero for the RFH Canal 2006B, Catlin 2006 (with ADVs), Catlin 2006 (with ADCPs), and Catlin 2007 studies, respectively. As such, at least 80% of all realizations indicated that PAM reduced seepage to some degree. The mean percent differences for the four data sets were 67.1%, 74.3%, 78.8%, and 86.0%, respectively. Percent differences greater than 100% indicate the post-PAM Q_S estimate was negative for a given realization.

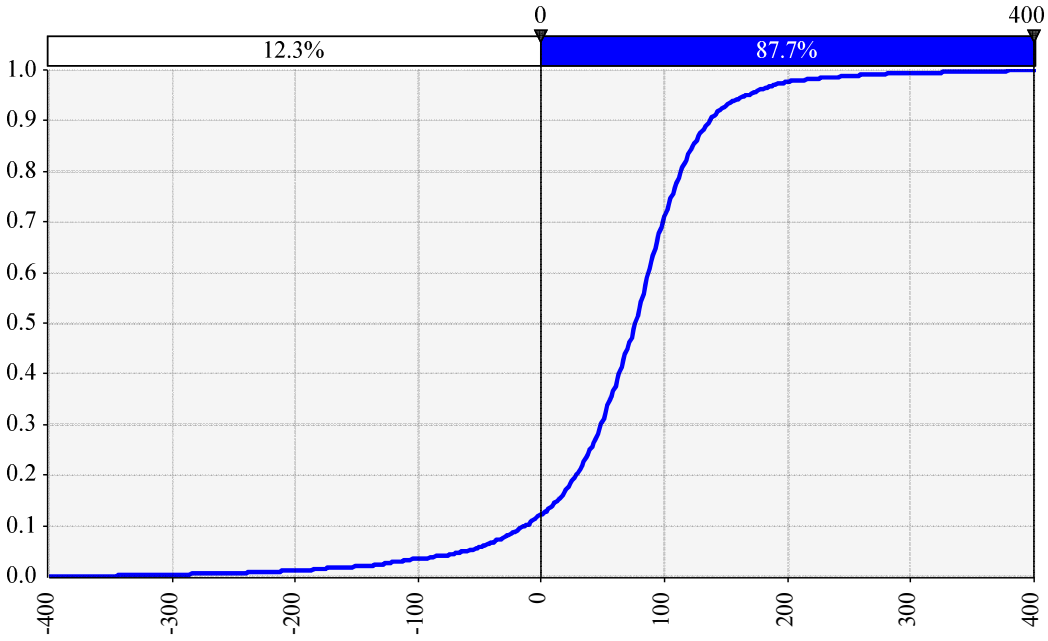

Figure 6-18 Cumulative frequencies of percent difference in estimated Q_S for pre- and post-PAM measurements on the RFH Canal in 2006

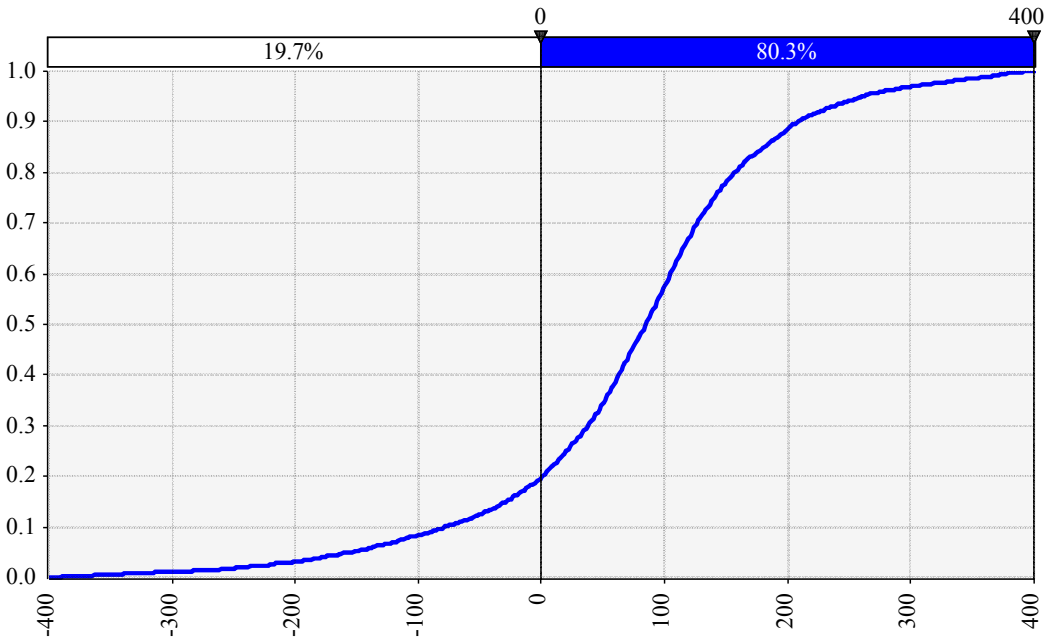

Figure 6-19 Cumulative frequencies of percent difference in estimated Q_S for pre- and post-PAM measurements on the Catlin Canal in 2006 using ADVs

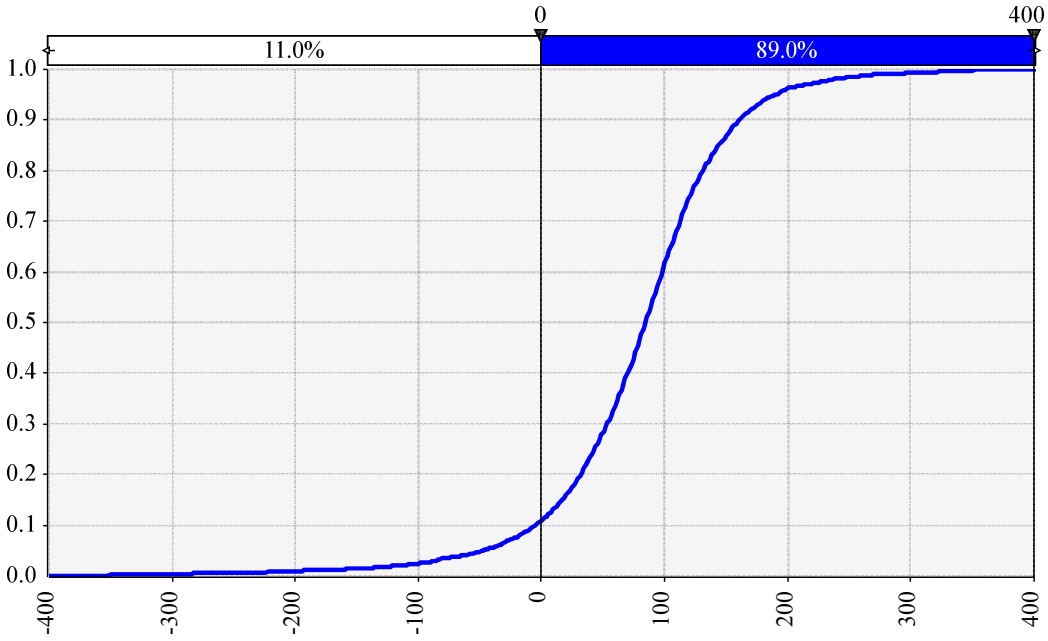

Figure 6-20 Cumulative frequencies of percent difference in estimated Q_S for pre- and post-PAM measurements on the Catlin Canal in 2006 using ADCPs

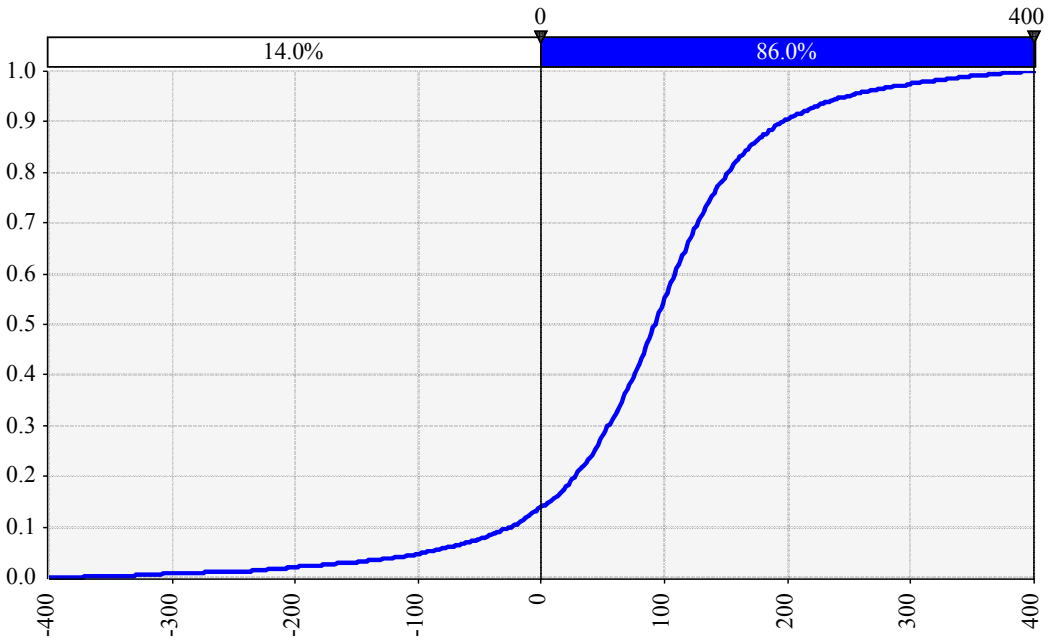

Figure 6-21 Cumulative frequencies of percent difference in estimated Q_S for pre- and post-PAM measurements on the Catlin Canal in 2007

For the Catlin 2006 PAM application, the distributions of estimated $\hat{Q}_s$ that were generated via Monte Carlo simulation with @RISK are presented in the relative frequency histograms and box-and-whisker plots of Figure 6-22. The solid-bars represent relative frequency of pre-application $\hat{Q}_s$ estimates and the "stair-step" lines represent relative frequency of post-application $\hat{Q}_s$ estimates. The two pre-application measurements were conducted on June 3, 2006 which was the morning prior to applying PAM. These were the only two seepage tests conducted for this study. The three post-application tests that are presented in Figure 6-22 were all taken the day after the application. From plots in Figure 6-22, it is clear that the generated possible $\hat{Q}_s$ values overlap, with the mean values of the post-application distribution less than those of the post-application distributions. The pre-application $\hat{Q}_s$ was estimated once

from a test where canal flow was measured with an ADV and once where canal flow was measured using an ADCP, each giving different results. The application of PAM appears to have been more effective when considering the pre-application seepage test using the ADCP (colored solid blue in Figure 6-22) than when considering the ADV results (colored solid red in Figure 6-22).

For the PAM application on Catlin Canal study reach in 2007, the relative frequency histogram and box plots for $\hat{Q}_s$ values estimated from pre- and post-application measurements are more disparate (as shown in Figure 6-23) than for the 2006 study. The estimates of $\hat{Q}_s$ for three nearest pre-application and three post-application tests, all of which were conducted within a week of the application, are provided in Figure 6-23. Again, the relative frequency histograms of the $\hat{Q}_s$ estimate for the pre-PAM tests are presented with solid-bars in Figure 6-23, and histograms for post-PAM tests are represented with "stair-step" lines. The distributions of $\hat{Q}_s$ for pre- and post-application tests overlap, indicating that PAM could have been less effective at reducing canal seepage than indicated by deterministic analysis. However, the fact that the means of all post-application estimates of $\hat{Q}_s$ are less than the means of all pre-application estimates provides support to the conclusion that PAM likely was effective in reducing seepage. The box plot in Figure 6-23 shows a clear shift in the distribution of post-application estimates; however, using this approach hypothesis testing cannot be conducted to evaluate the statistical significance of the difference. As a side note, the distribution on 8/8/07 is wider than the other distributions depicted in Figure 6-23 because a canal storage change occurred during the 8/8/07 test which induced more uncertainty in the $\hat{Q}_s$ values estimated from the test data. This

illustrates the need to conduct inflow-outflow tests when canal flow conditions are relatively steady.

Plots of frequency histograms of generated estimates of $\hat{Q}_s$ estimated for the PAM application study on the RFH Canal in 2006 (second application) are presented in Figure 6-24. The three nearest pre-application and three post-application estimated values of $\hat{Q}_s$ are provided in Figure 6-24. The plots indicate no substantial difference between the generated pre-application and post-application estimates. However, two of the pre-application tests were conducted on July 1, 2006 which was 19 days prior to the PAM application. When considering just the pre-application measurement on July 19th (the day before the PAM application), the difference between pre-application and post-application estimates of $\hat{Q}_s$ is much greater, suggesting that PAM was effective in reducing $\hat{Q}_s$.

(a)

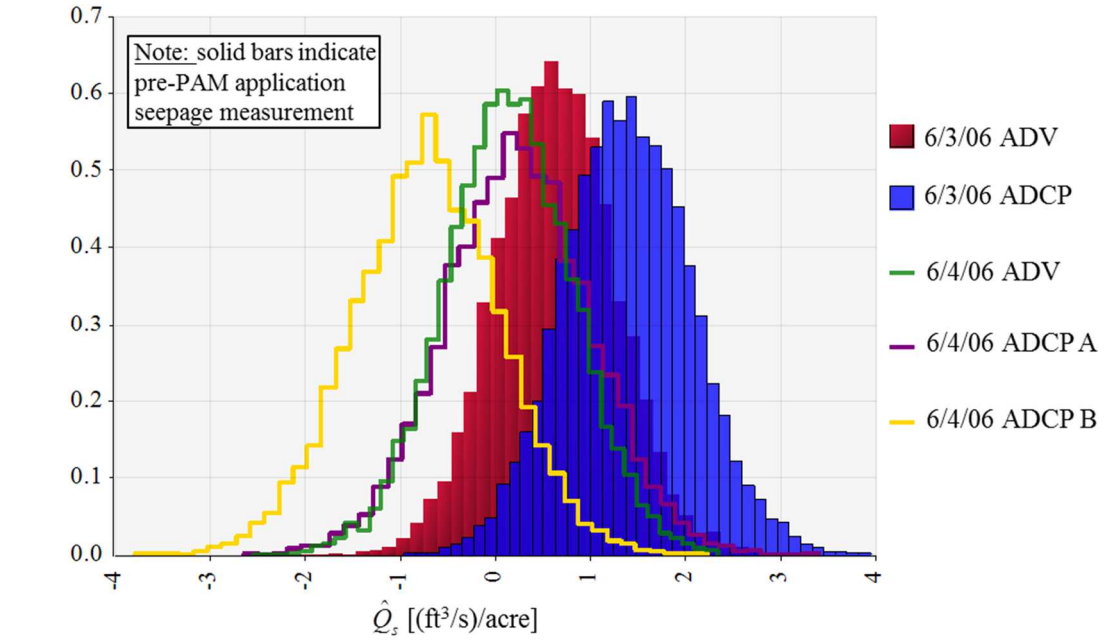

(b)

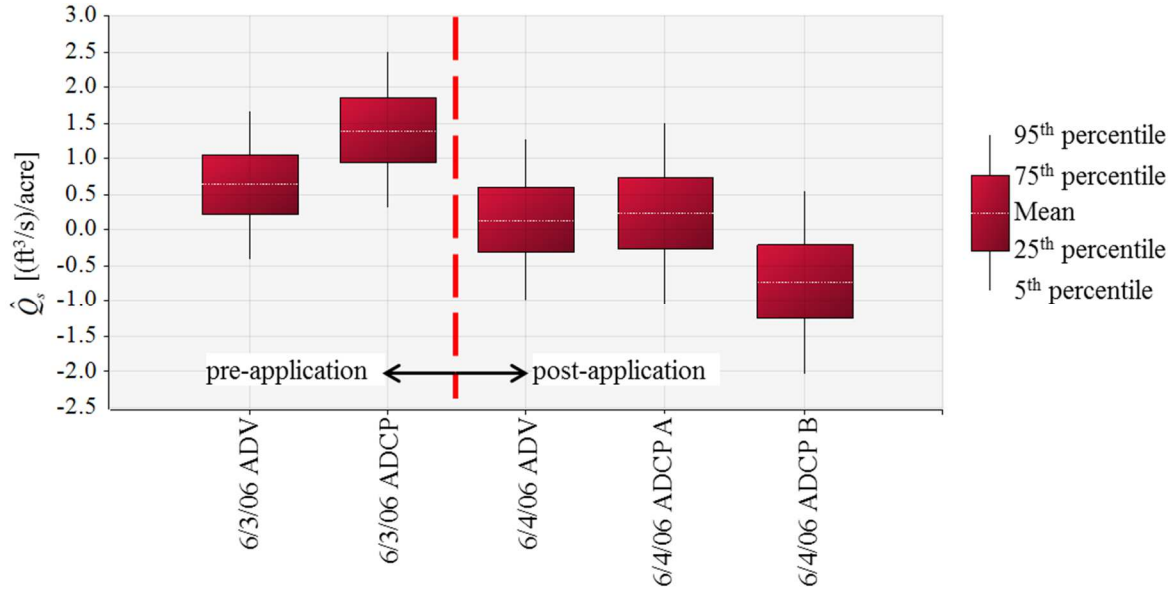

Figure 6-22 Generated pre- and post-PAM application estimates of $\hat{Q}_s$ for the Catlin Canal in 2006 as (a) relative frequency histograms and (b) box plots

(a)

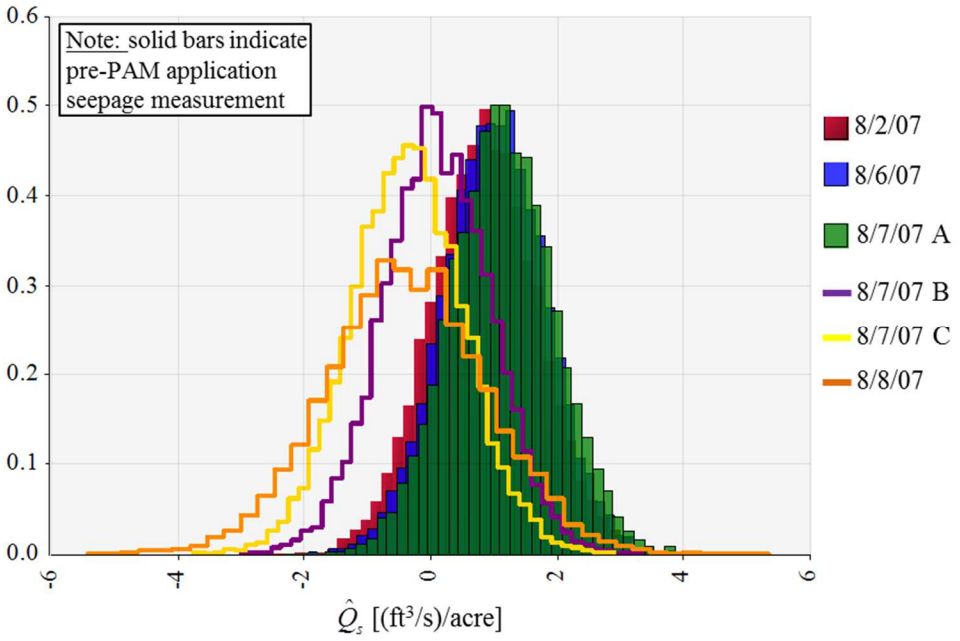

(b)

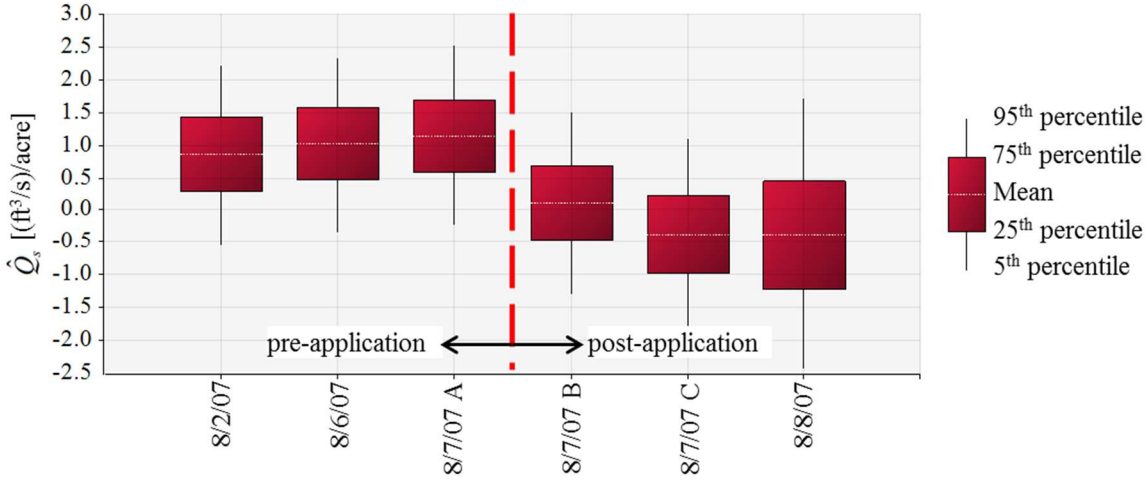

Figure 6-23 Generated pre- and post-PAM application estimates of $\hat{Q}_s$ for the Catlin Canal in 2007 as (a) relative frequency histograms and (b) box plots

(a)

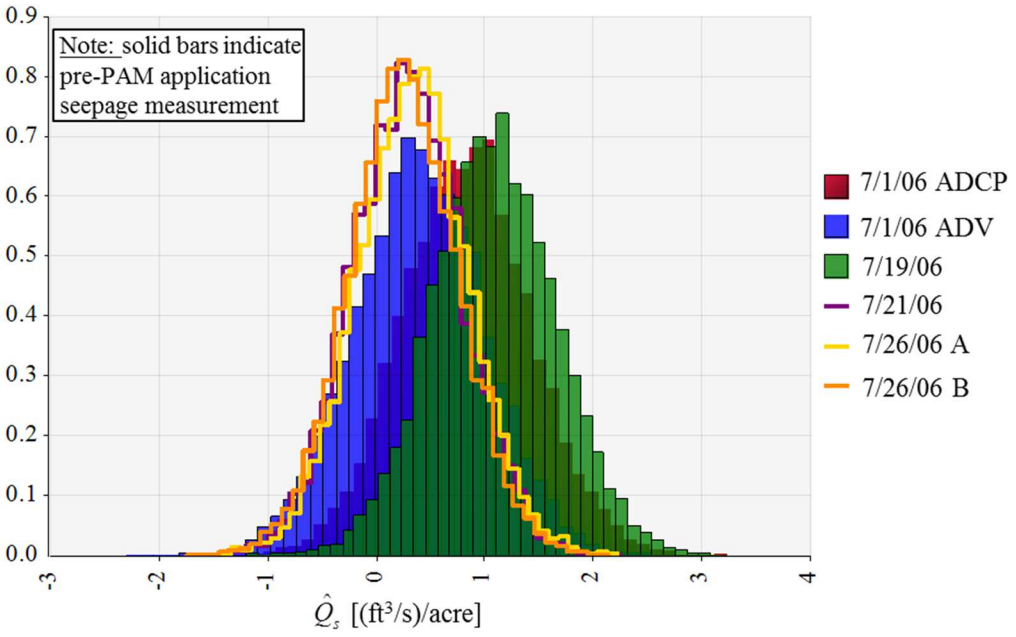

(b)

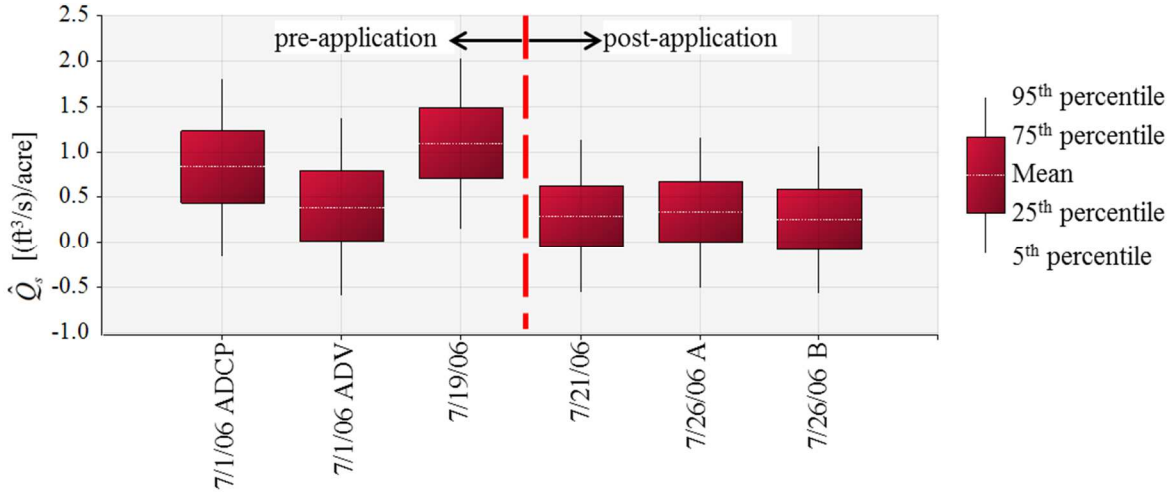

Figure 6-24 Generated pre- and post-PAM application estimates of canal $\hat{Q}_s$ for the RFH Canal in 2006 (2nd application) as (a) relative frequency histograms and (b) box plots

7 SUGGESTIONS FOR CONDUCTING CANAL SEEPAGE MEASUREMENTS

This chapter presents suggestions for conducting canal seepage measurement based upon lessons learned from this study. Suggestions are for pre-test preparations, data collection before and during seepage tests, assessments of seepage reduction technologies (specifically PAM), and measurement methods of variables within the inflow-outflow equation:

7.1 SUGGESTIONS FOR CONDUCTING STUDIES ON THE EFFECTIVENESS OF SEALANT APPLICATIONS

Establishing a Control Reach

If performing a study on the effectiveness of sealant (i.e. PAM) applications, it is very important to establish an adequate control reach on the canal. A "control reach" is a section of canal where sealant is not applied but Q_S is measured at the same frequency as the "application reach" (the reach where the sealant is applied). Ideally, the control reach and the application reach would have similar $\hat{Q}_s$ values and seepage patterns. Establishing a control reach is important so any potential seepage reductions can be distinguished from the sealant application or natural occurrences.

Tests should be conducted in the control reach just as frequently as on the application reach. Comparing the control reach and application reach allows for temporal changes in $\hat{Q}_s$ due to other factors to be identified and differentiated from changes due to the sealant's impact. This is particularly important if storm events bring sediment into a canal, which can reduce $\hat{Q}_s$ due to

natural sediment deposition and sealing of the channel perimeter, so that the magnitude and longevity of $\hat{Q}_s$ reduction is not entirely attributed to the polymer application. The control reach does not necessarily have to be directly adjacent to the application reach, but the closer the better because impacts of sediment deposition due to a storm event will vary spatially along the canal.

Timing of the PAM Application and Seepage Tests

To consider the effectiveness of a PAM application, coordinate the PAM application with conditions the canal flow rates and conditions can be steady for a few days. Ideally, conduct several pre-application tests and several post-application tests such that a distribution for each can be developed then evaluated for significant difference using statistical hypothesis testing. The number of tests required, however, would likely prove very costly and difficult to complete.

7.2 SUGGESTIONS FOR COLLECTION OF STAGE DATA

Pressure transducers should be installed near the upstream boundary, downstream boundary, and at intermediate locations of a seepage study reach of canal. This data is useful for tracking and estimating storage changes. If pressure transducers are not available then staff gages can be installed and read manually, although this generally will require additional personnel stationed along the canal.

Before and after conducting a seepage test, collect/download canal stage data along the canal. By assessing the canal stage data prior to a seepage test, it can be determined if flow conditions are steady or unsteady. This will assist in deciding whether conditions are steady enough to provide trustworthy results. By assessing canal stage data after a seepage test, it can be determined if a storage change was occurring within the study reach during the seepage test. The data can also be used to estimate $\Delta S/\Delta t$ in the inflow-outflow equation.

Using Pressure Transducers

Prior to launching pressure transducers, check the calibration. This easily can be done by launching every pressure transducer and submerging them in bucket of water (trash cans work best). Measure the depth of water in the bucket and check this depth against the depth that each pressure transducer is recording. Do this for at least 3 different depths of water. This process works best by starting with the shallowest depth, then adding water for the 2nd and 3rd water levels. Remember to subtract atmospheric pressure from the measured absolute pressure prior to calculating water depth. This requires launching an atmospheric pressure transducer while the calibration process is taking place. Launching the pressure transducers to record at short time intervals will make this process go faster.

Install a permanent pressure transducer at upstream and downstream flow measurement locations. This allows for stage to be continuously measured throughout a seepage test. This is particularly important for lagged flow measurements, when manual staff gages at the opposite measurement location cannot be measured because they are unattended.

If possible, install two barometric pressure transducers along the canal study reach. P_{baro} is required to convert P_{abs} (recorded by each pressure transducer that is submerged in the canal) to P_{gage}, which is used to calculate water depth above the pressure transducers. As such, P_{baro} is very important; so, installing a second barometric pressure transducer will provide backup in case the other malfunctions. P_{baro} should not change significantly along a canal reach, unless is it several miles long ($\geq$10 miles) or a storm system passes near the reach.

Record the actual time that each pressure transducer is downloaded, and record the time that the pressure transducer records when downloaded (the pressure transducer should log the download time). This will ensure that the pressure transducer has the correct timestamp. It is

very important to use P_{baro} and P_{abs} that were measured at the same time, so P_{gage} can accurately be estimated and for synchronizing storage changes with flow rate. If the pressure transducer's timestamp is incorrect, then make sure it is corrected.

Record when daylight savings time occurs. Some pressure transducers do not recognize daylight savings time changes, so the timestamps need to be adjusted manually. Also, some pressure transducers adjust the timestamp in recognition of daylight savings time (DST) change, but the date at which the adjustment is made may be incorrect. For example, the atmospheric pressure transducers on the Catlin and RFH canal test reaches recognized DST on 10/28, but it should have been on 11/4 (other countries recognized it on 10/28 in 2007, but not the USA). DST changes typically occur in mid-March and late October/early November.

Periodically check that the mount for the pressure transducers has not moved over time due to settling, hydrodynamic forces, debris buildup, or impact from debris or animals (i.e. cows). Remove accumulated debris as necessary to reduce drag forces on the mounts.

7.3 CHECKING FOR DIVERSIONS

Prior to, during, and after a seepage test, drive along the canal reach and check to ensure that flow offtakes are closed or open as expected. If an offtake gate is open, then this flow rate must be taken into account in the seepage estimate. Flow rates typically can be estimated fairly accurately by canal operators, so always ask the canal operator how much water is being diverted by each offtake. Also conduct a separate measurement of the offtake rate. This can be done by using an ADV, checking a flume that may be installed in the offtake channel, implementing a pump stage-discharge curve, or even measuring the time required to fill a bucket of known volume (smaller offtake rates). The sum of all offtake rates is used as Q_D in the inflow-outflow equation.

7.4 WEATHER CONDITIONS DURING SEEPAGE TESTS

Be aware of the effects of weather conditions during flow rate measurements with an ADCP. Windy conditions may cause an ADCP to travel across the canal cross section with additional movement and can create waves on the water surface that push the ADCP around. Wind can create inverted velocity profiles that results in additional error for the depth-velocity curves that are extrapolated to the canal surface during data processing used in estimating the unmeasured flow rate near the water surface. This can lead to flow measurement errors; thus, avoid conducting ADCP measurements in windy conditions.

Rain storms can introduce a Q_I and Q_P that are difficult to measurement with accuracy. Rain intensity may vary along the test reach, and permanent rain gages likely are not installed near the reach. This is more important for longer canal study reaches (large volume of water entering the control volume) and more important for lagged flow measurements than for simultaneous flow measurement.

Storm events also will cause atmospheric pressure to vary temporally and spatially. Such variations will impact processing of P_{baro} *and* P_{abs} measurements, which are used to estimate P_{gage} and canal stage.

7.5 SUGGESTIONS FOR CONDUCTING LAGGED OR SIMULTANEOUS FLOW MEASUREMENTS

Simultaneous measurements of Q_{US} and Q_{DS} are likely to result in the most accurate estimates of Q_S if there is the possibility of unsteady flow conditions because they limit the error caused by storage changes in the canal control volume. If it is expected that the canal flow will be steady, then lagged measurements may provide better accuracy than simultaneous measurements, because the same equipment can be used by the same operators, thereby limiting

measurement errors. Lagged measurements will result in higher correlation between measured values of Q_{US} and Q_{DS}.

Simultaneous Flow Measurements

For simultaneous flow measurements, Q_{US} and Q_{DS} are measured at the same time. The advantages of this type of measurement are limiting the degree of storage changes during unsteady flow (due to shorter measurement duration). The disadvantages include using different equipment to measure Q_{US} and Q_{DS} (adds systematic error) and different operators which introduces uncertainty associated with differing skill and subjective interpretations. Systematic equipment errors can be assessed by using multiple pieces of equipment to measure discharge at the same cross-section at the same time to check how the measurements compare. Operator errors can be limited by ensuring that the operators are properly trained and that common techniques are being implemented.

Lagged Flow Measurements

For lagged flow measurements, the Q_{US} is measured then the Q_{DS} is measured in sequence. The advantages of this type of measurement are that the same equipment and operators can be used for Q_{US} and Q_{DS} measurements and it requires fewer operators and equipment than simultaneous measurements. The disadvantages include longer measurement durations which increase the likelihood of canal storage changes occurring. It is very important to check pressure transducers to ensure that the canal stage is stable prior to and while conducting a seepage measurement, otherwise storage changes due to unsteady flow can greatly increase the uncertainty in estimating Q_S. Stage data should be downloaded at the end of a seepage

measurement, then the storage change should be calculated if applicable. When considering stage changes, the general trend of stage change should be considered when estimating channel flow depth because stage can fluctuate up and down due to surface waves, measurement error, etc.

7.6 SUGGESTIONS FOR COLLECTING AND PROCESSING SURVEY DATA

When surveying the canal to describe hydraulic geometry, keep the following items in mind:

- Survey the full length of the canal study reach where seepage is being measured.
- Survey a cross section along the canal at every location where geometry appears to change significantly (i.e. gets wider or changes shape).
- Surveying is most easily performed when the canal is dry (i.e. during winter or early spring). Flowing water in the canal can limit access or be unsafe for access. Flowing water can make it difficult to hold a surveying rod steady and vertically. Moving channel bed material can make the location of the canal bed subjective. If the canal is surveyed when the canal contains water, it cannot easily be determined if the canal bed is changing shape underneath the water surface; it can only be determined that the canal's top width is changing. Not being able to see variations in channel geometry causes difficulties in deciding on spacing between surveyed cross-sections.
- Use a surveying rod with a flat bottom. Do not use a rod with a pointed bottom because it will sink into a soft canal bed.
- When fitting regression functions for flow area, wetted perimeter, and top width versus flow depth for each cross section, use the same type of function for every cross section (e.g. use second order polynomial or power equation for all cross sections). Only fit the functions for the range of flow depths that were observed during the inflow-outflow tests.

Fitting the function to a range of flow depths that exceeds the range that was observed during the seepage tests may result in a function less representative.

- Install a bright-colored flag in the ground were each canal cross section was surveyed and take GPS coordinates. Label the stationing of the cross section on the flag, or install a more permanent identifier (i.e. wooden stake) with stationing indicated. This is important for checking the water surface interpolation, as discussed below.
- When surveying a canal cross section, install a temporary benchmark (i.e. wooden stake pounded into the ground) on the canal bank. Survey across the cross section using this benchmark. Use the surveyed elevation of each benchmark to determine the relative elevations of each surveyed when performing a longitudinal survey along the canal.
- Water surface elevations will have to be interpolated from one pressure transducer or staff gage location to another along the canal test reach to estimate water surface elevations for surveyed cross sections that do not contain pressure transducers or staff gages. If possible, the use of more pressure transducers should result in less error in interpolated elevations. To check the interpolated elevations, manually measure the canal thalweg depth at each surveyed cross section during a seepage test. This requires the ability to wade into the canal.

7.7 SUGGESTIONS FOR CROSS-SECTION LOCATIONS FOR FLOW MEASUREMENTS

For flow measurements, choose adequate cross-section locations with the following characteristics:

- Low turbulence,
- Minimal eddies,

- Flow parallel with banks,
- No obstructions,
- Minimal moving bed,
- No ineffective flow areas,
- Relatively regular geometry (no debris or riprap on the channel bed), and
- Easy access on both sides of the channel. Bridges may be required to reach the opposite bank if the channel is too deep to wade across.

7.8 SUGGESTIONS FOR ADCP FLOW MEASUREMENTS

This section provides suggestions for conducting flow measurements with an ADCP based upon experience from this study. It is also suggested that ADCP operators read Mueller et al. (2008), which provides a more robust set of practices for conducing flow measurements with ADCPs.

Channel Maintenance

For flow measurement, prepare the cross-section prior to starting. Remove thick vegetation on banks that will interfere with the travel of the ADCP, that limit how close the ADCP can get to the bank, or that create eddies. Position pins/pulleys in the left and right bank such that the cross-section is approximately perpendicular to the principal direction of flow.

Number of Transects

For flow measurement with an ADCP, the number of transect measurements should be dependent upon the conditions. USGS (2002) says to conduct four transect measurements, then if any one of those four measurements is more than +/-5% from the mean of the four transects,

then four additional transects measurement should be completed for a total of eight transects. Oberg and Mueller (2007) suggest conducting at least 12 minutes of measurement (i.e. four transects at 3-minute passes, or 12 transects at 1-minute passes).

From the experience gained in these studies, the number of transects and the measurement duration of each transect should be dependent upon the size and hydraulic conditions of each measurement cross section. The most important factor in establishing precision of measured flow rate among the transects is preventing "fishtailing" of the ADCP. Fishtailing causes the ADCP's transducer to rotate back and forth on the surface and therefore to measure both positive and negative travel distance as it pass from one side of the canal to the other, which is an unnecessary form of error. Thus, it is better to conduct shorter duration (faster) transects to prevent fishtailing. As a rule, maximize the duration of each transect without introducing fishtailing (but it is not advised to conduct transects less than 1-minute). If all of the first four transects measure flow rate that is within 5% of the collective mean, then a case could be made for ending the measurement, but it is advised to perform at least eight transects. The ADCP operator can keep track of how the mean flow rate changes with the addition of each transect. If the mean is not changing significantly as more transects are being collected, then there is no reason to collect additional transects. Taking additional transects will only increase the chance of collecting an outlier measurement that affects the mean.

Traversing the ADCP across the Canal Cross Section

Prior to conducting the first transect, traverse the ADCP across the canal to decide the targeted duration of each transect using the suggestions above. Place pulleys on the left and right bank so the cross-section is approximately perpendicular to the principal direction of flow. The

pulleys must be placed in stable soil, so the cables (rope) can be tightened adequately. String rope through the pulley system and tighten the rope so there is little sag. Sag will cause a bow-shaped travel path from the left pulley pin to the right pulley pin. The path of travel should be as linear as possible. The rope must be high enough off the water surface that the ADCP can attach and travel smoothly across the water without submergence.

Processing ADCP Data

Upon processing the ADCP measurement, disregard transect flow rates that are obvious outliers when calculating the mean if necessary. Check the various water surface velocity extrapolation methods in the data processing software and select the most appropriate method for each measurement. This can be done through sensitivity analysis, comparing each extrapolation method.

8 CONCLUSIONS

The inflow-outflow method can be a useful tool for estimating seepage loss rates in canals under normal operating conditions. Using the inflow-outflow method and field measurements directly in estimating seepage-related variables, deterministic seepage rates were estimated for 77 seepage tests on four canals in the LARV. Canal flow rates varied between 25.8 and 374.2 ft^3/s and averaged 127.9 ft^3/s, while deterministic estimates of seepage varied between -0.72 and 1.53 (ft^3/s)/acre with an average of 0.36 (ft^3/s) per acre of wetted perimeter of canal for all 77 tests. However, the parameters used to estimate seepage rates using this volume-balance procedure are subject to considerable uncertainty that affects confidence in the results. This uncertainty is derived both from measurement error and from spatiotemporal variability and it extends to the interpretation of comparative seepage tests for evaluating the effectiveness of technologies used for reducing canal seepage. To account for this uncertainty, variables of the inflow-outflow method were treated as random with associated PDFs for 60 tests conducted on the Catlin and RFH Canals. Using Monte-Carlo simulation with @Risk software, pseudorandom numbers were used to generate multiple successive realizations for each of the random variables in the inflow-outflow equation and their associated parameters. Over the 90^{th} IR, the error in flow measurement using ADV and ADCP technology was assumed to be +/- 5%, the error in evaporation estimates was assumed to be +/-20%, and stage measurement error was assumed to be +/-0.04 feet. To describe hydraulic geometry within the seepage test reaches of the Catlin and RFH canals, canal cross-sections were surveyed at 25 and 16 locations, respectively. PDFs were assigned to parameters used to estimate wetted perimeter and top width for each cross-section to account for measurement error and spatial uncertainty in hydraulic geometry. From stochastic

analysis of these 60 seepage tests, mean values of estimated seepage were between -0.73 (ft^3/s)/acre (gain) and 1.53 (ft^3/s)/acre, averaging 0.32 (ft^3/s)/acre with an average of the CV computed over all of the tests being 240% and the average of the 90th IR being 2.04 (ft^3/s)/acre. For the RFH Canal reaches untreated with LA-PAM sealant, mean values of $\hat{Q}_S$ ranged from -0.26 to 1.09 (ft^3/s)/acre, respectively, and averaged 0.44 (ft^3/s)/acre over all inflow-outflow tests. For reaches on the Catlin Canal untreated with LA-PAM, mean values of seepage ranged from 0.02 to 1.53 (ft^3/s)/acre, respectively, and averaged 0.63 (ft^3/s)/acre. For reaches on the RFH Canal and Catlin Canal treated with LA-PAM, mean $\hat{Q}_S$ values ranged from 0.25 to 0.57 (ft^3/s)/acre, averaging 0.33 (ft^3/s)/acre, and from -0.73 to 0.55 (ft^3/s)/acre, averaging -0.01 (ft^3/s)/acre, respectively. The likelihood that marked seepage reduction can be achieved with LA-PAM was demonstrated by comparisons of the probability distributions of seepage rates estimated for canal reaches pre- and post-treatment.

The degree of uncertainty in estimating seepage rates from inflow-outflow tests was found to be largely dependent upon flow rate measurement errors at the upstream and downstream boundaries of a test reach in both steady and unsteady flow conditions. If the error associated with measurement of upstream and downstream flow rates can be limited, then the uncertainty in canal seepage estimation decreases dramatically. For unsteady flow conditions, the uncertainty related to calculation of canal storage change also was found to have a sizeable impact on the magnitude and uncertainty of seepage estimates, particularly for lagged flow measurements at the upstream and downstream ends of the test reach.

When using inflow-outflow tests to analyze the effectiveness of a seepage reduction technology, ambiguity in seepage estimation becomes especially challenging. Seepage losses must be assessed for tests conducted both before and after the canal is treated. Since the seepage

rate will approach zero if a technology is effective, the expected value of the estimated seepage rate for the post-treatment test will become a smaller fraction of the relative variance in the estimate. This variance is predominantly affected by errors in upstream and downstream flow rates and, for unsteady flow, by uncertainty in canal storage change estimates which can be larger than the seepage rate being estimated from the water-balance equation. Unless the expected value of the pre-treatment seepage is markedly larger, the calculated difference between pre- and post-treatment values becomes overwhelmed by the relative variances. As discussed in this thesis, a key to combating this dilemma is to conduct repeated seepage tests both before and after the seepage reduction technology is applied so that consistency can be examined. Due to the potentially large degree of uncertainty associated with the inflow-outflow method, computed differences between some individual pairs of pre- and post-application tests may be difficult to interpret. However, if comparisons of multiple test pairs predominately indicate that seepage rates are less after the technology was applied than before, then a conclusion can be drawn more confidently about that technology's effectiveness.

Another issue that arises when testing a seepage reduction technology using the inflow-outflow method is that seepage rates change temporally in canals due to a variety of factors; thus, an apparent change in a seepage rate may not be solely attributable to the technology. A reduction in seepage could be in part due to natural occurrences (e.g. sediment deposition from a recent storm event, an increase in the adjacent groundwater table that reduces the groundwater gradient from the canal interface, etc.). As such, it was concluded from the studies in the LARV that establishing a control reach along the canal is important when assessing the effectiveness and longevity of a seepage reduction technology. If the longevity of a technology is not a question to be answered, then several seepage tests should be conducted both immediately prior

to and immediately after the seepage reduction technology is applied so that they can be compared under nearly constant hydraulic and sediment conditions in the canal.

Seepage studies conducted on the Lamar, Catlin, RFH canals in southeastern Colorado indicated that linear anionic PAM can reduce seepage rates from earthen irrigation canals. Results of deterministic analysis of pre- and post-PAM application tests on these canals indicated that seepage could be reduced by 34-35%, 84-100%, and 66-74% for each canal, respectively. Monte Carlo simulation was conducted to estimate the uncertainty associated with differences in seepage estimates from pre- and post-application seepage tests on the Catlin Canal in 2006 and 2007 and on the RFH canal in 2006. Statistical analysis indicated that 80.3%, 89.0%, 86.0%, and 87.7% of the realizations of computed differences between pre- and post-PAM seepage rates were positive for the Catlin 2006 (with ADVs), Catlin 2006 (with ADCPs), Catlin 2007, and RFH Canal 2006B studies, respectively. Due to the relatively time-consuming nature of inflow-outflow tests and because of the potential for canal conditions to become unsteady, pre- and post-PAM application seepage tests were conducted within a few days to a few weeks before or after PAM application, as opposed to repeatedly over a brief period (within no more than two days) just before and after application. The lack of a control reach during the seepage tests also challenged the interpretation of the difference between pre- and post-PAM results because seepage reduction rates due to PAM could not be distinguished from seepage reduction rates due to natural occurrences, such as sediment deposition from an intervening storm event. However, comparison of pre- and post-application tests consistently indicated a reduction in seepage rates.

The best ways to limit seepage estimation uncertainty when using the inflow-outflow method are to limit flow measurement error by properly calibrating flow measurement equipment, operating the equipment correctly and consistently, and performing the

measurements under steady flow conditions; and to account for canal flow unsteadiness by installing multiple stage measurement devices within a canal reach to quantify water surface elevation changes and by describing canal hydraulic geometry using surveys of multiple cross sections along the test reach. Results show that increased correlation of flow measurements at the upstream and downstream end of the study reach can lower the uncertainty of seepage estimation. Such increased correlation presumably could be achieved by using the same flow measurement devices (reduces systematic error bias) and the same personnel (reduces subjective interpretation bias) to conduct both measurements, which implies implementing the lagged flow measurement method. Lagged measurements, however, require longer measurement durations than simultaneous measurements, rendering the results more susceptible to impacts from unsteady flow conditions and canal storage changes. As such, simultaneous flow measurement should be implemented if it is likely that flow conditions will be unsteady.

9 REFERENCES

Abt, Steven R., et al. (1995), 'Settlement and Submergence Adjustments for Parshall Flume', Journal of Irrigation and Drainage Engineering, 121 (5), 317-21.

Ajwa, Husein A. and Trout, Thomas J. (2006), 'Polyacrylamide and Water Quality Effects on Infiltration in Sandy Loam Soils', Soil Sci Soc Am J, 70 (2), 643-50.

Akram, M, Kemper, W. D., and Sabey, J.D. (1981), 'Water Levels and Losses and Cleaning in Watercourses', American Society of Agricultural and Biological Engineers, 24 (3), 0643-50.

Alam, M. M. and Bhutta, M. N. (2004), 'Comparative evaluation of canal seepage investigation techniques', Agricultural Water Management, 66 (1), 65-76.

ANCID (2003), 'Open Channel Seepage and Control Vol 1.4 - Best Practice Guidelines for Channel Seepage Identification and Measurement', (Tatura, Victoria, Australia: Australian National Committee on Irrigation and Drainage).

ANCID (2004), 'Open Channel Seepage and Control - Guidelines for Channel Seepage Remediation', (Tatura, Victoria, Australia: Australian National Committee on Irrigation and Drainage).

Bakry, Mohamed Fawzy and Awad, Ahmed Abd El-Megeed (1997), 'Practical Estimation of Seepage Losses Along Earthen Canals in Egypt', Water Resources Management, 11 (3), 197-206.

Barvenik, F. W. (1994), 'Polyacrylamide characteristics related to soil applications', Soil science, 158 (4), 235-43.

Beim, A. A. and Beim, A. M. (1994), 'Comparative ecological – toxicological data on determination of maximum permissible concentrations (MPC) for several flocculants', Environmental Technology, 15 (2), 195-98.

Bell, Stephanie (1999), Measurement Good Practice Guide No. 11 (Issue 2) - A Beginner's Guide to Uncertainty of Measurement (Crown. Centre for Basic, Thermal and Length Metrology - National Physical Laboratory).

Bjorneberg, D.L., Aase, J.K., and Sojka, R. E. (2000), 'Sprinkler Runoff and Erosion Control with Polyacrylamide', National Irrigation Symposium (Phoenix, Arizona).

Bouwer, Herman, Ludke, Jamie, and Rice, Robert C. (2001), 'Sealing pond bottoms with muddy water', Ecological Engineering, 18 (2), 233-38.

Budd, P. M. (1996), 'Polymer and Water: An Overview', in C. A. Finch (ed.), Industrial Water Soluble Polymers (Aylesbury, UK: Pentafin Associates), 1-9.

Buhman, Daniel L., Gates, Timothy K., and Watson, Chester C. (2002), 'Stochastic Variability of Fluvial Hydraulic Geometry: Mississippi and Red Rivers', Journal of Hydraulic Engineering, 128 (4), 426-37.

Burkhalter, J. Philip and Gates, Timothy K. (2005), 'Agroecological Impacts from Salinization and Waterlogging in an Irrigated River Valley', Journal of Irrigation and Drainage Engineering, 131 (2), 197-209.

Burt, Charles M., Orvis, Sierra, and Alexander, Nadya (2010), 'Canal Seepage Reduction by Soil Compaction', Journal of Irrigation & Drainage Engineering, 136 (7), 479-85.

CDWR (2006 and 2007), Colorado Division of Water Resources < http://www.dwr.state.co.us>, accessed 2006 and 2007.

Chow, Ven T. (1959), Open-Channel Hydraulics (New York: McGraw-Hill).

CoAgMet 'Atmospheric Data', <http://coagmet.com/>, accessed 2006 and 2007.

Cox, M., Harris, P., and Siebert, B. R. L. (2003), 'Evaluation of Measurement Uncertainty Based on the Propagation of Distributions Using Monte Carlo Simulation', Measurement Techniques, 46 (9), 824-33.

Darcy, H. (1856), Les Fontaines Publiques de la Ville de Dijon (Dalmont, Paris).

De Boodt, M. (1975), 'Use of soil conditioners around the world', Soil Conditioners, Soil Sci. Soc. Am. Special Publication, 1–12.

Engelbert, P. J., Hotchkiss, R. H., and Kelly, W. E. (1997), 'Integrated remote sensing and geophysical techniques for locating canal seepage in Nebraska', Journal of Applied Geophysics, 38 (2), 143-54.

Fipps, Guy (2005), 'Potential Water Savings in Irrigated Agriculture for the Rio Grande Planning Region (Region M), 2005 Update'.

Gates, T., et al. (1992), 'Optimal Irrigation Delivery System Design under Uncertaint', Journal of Irrigation and Drainage Engineering, 118 (3), 433-49.

Gates, T.K. and Al-Zahrani, M.A. (1996b), 'Spatiotemporal Stochastic Open-Channel Flow. I: Model and Its Parameter Data', Journal of Hydraulic Engineering, 122 (11), 641-51.

Gates, T.K. and Al-Zahrani, M.A. (1996a), 'Spatiotemporal Stochastic Open-Channel Flow. II: Simulation Experiments', Journal of Hydraulic Engineering, 122 (11), 652-61.

Gates, T.K., Garcia, L.A., and Labadie, J.W. (2006), 'Toward Optimal Water Management in Colorado’s Lower Arkansas River Valley: Monitoring and Modeling to Enhance Agriculture and Environment', (Department of Civil and Environmental Engineering, Colorado State University).

Gates, T.K., et al. (2012), 'Irrigation Practices, Water Consumption, & Return Flows in Colorado's Lower Arkansas River Valley - Field and Model Investigations', (CWI Completion Report No. 221 CAES Report No. TR12-10; Colorado State University).

Green, V. S. and Stott, D. E. (eds.) (2001), Polyacrylamide: A Review of the Use, Effectiveness, and Cost of a Soil Erosion Control Amendment, eds. DE Scott, RH Mohtar, and GC Steinhardt (Sustaining the Global Farm) 384-89.

Gregory, J. (1996), 'Polymer adsorption and flocculation', in C. A. Finch (ed.), Industrial Water Soluble Polymers (Aylesbury, UK: Pentafin Associates), 62–75.

Haan, C.T. (1977), Statistical Methods in Hydrology (Ames Iowa: The Iowa State University Press).

Haan, C.T. (1989), 'Parametric Uncertainty in Hydrologic Modeling', American Society of Agricultural Engineers, 32 (1), 137-46.

Ham, J. M. (2002), 'Uncertainty Analysis of the Water Balance Technique for Measuring Seepage from Animal Waste Lagoons', J. Environ. Qual., 31 (4), 1370-79.

Harmel, R.D. and Smith, Patricia K. (2007), 'Consideration of measurement uncertainty in the evaluation of goodness-of-fit in hydrologic and water quality modeling', Journal of Hydrology, 337 (3–4), 326-36.

Herschy, R. W. (2004), 'Estimation of Uncertainties in Hydrometric Measurements', in Sehlke Gerald, F. Hayes Donald, and K. Stevens David (eds.), (138: ASCE), 206.

Herschy, R.W. (2002), 'The uncertainty in a current meter measurement', Flow Measurement and Instrumentation, 13 (5–6), 281-84.

Herschy, Reg (1993), 'The velocity-area method', Flow Measurement and Instrumentation, 4 (1), 7-10.

Herschy, Reginald W. (2009), Streamflow measurement (London ;: Routledge).

Hunkeler, D. and Hamielec, A. E. (1991), 'Mechanism and Kinetics of the Persulfate-Initiated Polymerization of Acrylamide', in S. W. Shalaby, C. L. McCormick, and G. B. Butler (eds.), Water-soluble polymers: synthesis, solution properties and applications (American Chemical Society).

Hunkeler, D. and Hernandez-Barajas, J. (1996), 'A concise review of the influence of synthesis and technological factors on the structure and properties of polyacrylamides', in C. A. Finch (ed.), Industrial Water Soluble Polymers (Aylesbury, UK: Pentafin Associates), 10–27.

In-Situ (2009), 'Technical Specifications for Level Troll 100, 200, 300, 500, and 700', (In-Situ Inc.).

Islam, Md. Zahurul (1999), 'Variation of Seepage Loss over Time in the Lined and Unlined Canals of the Teesta Barrage Project ', Rural and Environmental Engineering 36 (2), 20-34.

ISO (1973), 'Measurement of Liquid Flow in Open Channels', Dilution Methods for Measurement of Steady Flow - Constant-Rate Injection Method (Geneva, Switzerland: International Organization for Standardization).

ISO (1979), 'Liquid Flow Measurement in Open Channels', Velocity-Area Methods (Geneva, Switzerland: International Organization for Standardization).

ISO (1995), 'Guide to Expression of Uncertainty in Measurement', (Geneva, Switzerland: International Organization for Standardization).

Johnson, Peggy A. and Heil, Thomas M. (1996), 'Uncertainty in Estimating Bankfull Conditions', Journal of the American Water Resources Association, 32 (6), 1283-91.

Kahlown, M. A. and Kemper, W. D. (2004), 'Seepage losses as affected by condition and composition of channel banks', Agricultural Water Management, 65 (2), 145-53.

Keery, John, et al. (2007), 'Temporal and spatial variability of groundwater–surface water fluxes: Development and application of an analytical method using temperature time series', Journal of Hydrology, 336 (1–2), 1-16.

Kinzli, Kristoph-Dietrich, et al. (2010), 'Using an ADCP to determine canal seepage loss in an irrigation district', Agricultural Water Management, 97 (6), 801-10.

Lentz, R D, Sojka, R E, and Robbins, C W (1998), 'Reducing Phosphorus Losses from Surface-Irrigated Fields: Emerging Polyacrylamide Technology', Journal of Environmental Quality, 27 (2), 305-12.

Lentz, R. D., et al. (1992), 'Preventing Irrigation Furrow Erosion with Small Applications of Polymers', Soil Sci. Soc. Am. J., 56 (6), 1926-32.

Lentz, R. D. and Sojka, R. E. (2000), 'Applying polymers to irrigation water: Evaluating strategies for furrow erosion control', Transactions of the ASAE, 43 (6), 1561-68.

Lentz, R. D. (2003), 'Inhibiting water infiltration with polyacrylamide and surfactants: Applications for irrigated agriculture', Journal of Soil and Water Conservation, 58 (5), 290-300.

Lentz, Rodrick D. (2007), 'Inhibiting Water Infiltration into Soils with Cross-linked Polyacrylamide: Seepage Reduction for Irrigated Agriculture', Soil Sci Soc Am J, 71 (4), 1352-62.

Lentz, Rodrick D. and Freeborn, Larry L. (2007), 'Sediment and Polyacrylamide Effects on Seepage From Channeled Flows', Soil science, 172 (10), 770-89 10.1097/ss.0b013e3180de4a33.

Lentz, R. D. and Kincaid, D.C. (2008), 'Polyacrylamide Treatments for Reducing Seepage in Soil-Lined Reservoirs: A Field Evaluation', American Society of Agricultural and Biological Engineers, 51 (2), 535-44.

Lu, J. H., Wu, L., and Letey, J. (2002), 'Effects of soil and water properties on anionic polyacrylamide sorption', Soil Science Society of America Journal, 66 (2), 578-84.

Mason, L. B., et al. (2005), 'Reducing Sediment and Phosphorus in Tributary Waters with Alum and Polyacrylamide', Journal of Environmental Quality, 34 (6), 1998.

McLaughlin, Richard A. and Bartholomew, Nathanael (2007), 'Soil Factors Influencing Suspended Sediment Flocculation by Polyacrylamide', Soil Sci Soc Am J, 71 (2), 537-44.

Milligan, V. (1976), 'Field Measurement of Permeability in Soil and Rock', In Situ Measurement of Soil Properties (2; New York: American Society of Civil Engineers), 3-36.

Minsk, L.M., Kenyon, W.O., and Van Campen, J.H. (1949), 'Process for Polymerizing Acrylamide', in United States Patent Office (ed.), (No. 2,486,191; USA).

Mitchell, A. R. (1986), 'Polyacrylamide Application in Irrigation Water Ot Increase Infiltration', Soil science, 141 (5), 353-58.

Moran, E.A. (2007), 'Laboratory studies to examine the impacts of polyacrylamide (PAM) on soil hydraulic conductivity', (University of Nevada Las Vegas).

Mueller, D.S., Wagner, C.R., and Winkler, M.F. (2008). 'Best Practices for Measuring Discharge with Acoustic Doppler Current Profilers', United States Geological Survey and United States Army Corps of Engineers.

Muir, M. M., Kosteretz, K. G., and Lech, J. J. (1997), 'Localization, depuration, bioaccumulation and impairment of ion regulation associated with cationic polymer exposure in rainbow trout (Oncorhynchus mykiss)', Xenobiotica, 27 (10), 1005-14.

NOAA (2006), National Climatic Data Center <http://www.ncdc.noaa.gov/oa/ncdc.html>, assessed 2006.

NRCS (2005), 'Irrigation Water Conveyance Anionic Polyacrylamide Ditch and Canal Treatment', Code 754 (Natural Resources Conservation Service, Interim Conservation Practice Standard).

Oberg, Kevin and Mueller, David S. (2007), 'Validation of Streamflow Measurements Made with Acoustic Doppler Current Profilers', Journal of Hydraulic Engineering, 133 (12), 1421-32.

Oblinger, Jennifer A., et al. (2010), 'A pragmatic method for estimating seepage losses for small reservoirs with application in rural India', Journal of Hydrology, 385 (1–4), 230-37.

ONSET (2008), 'Technical Specifications for HOBO U20 Water Lever Logger', (ONSET Computer Corporation).

Ray, D. T. and Hogg, R. (1987), 'Agglomerate Breakage in Polymer-Flocculated Suspensions', J. Colloid Interface Sci. 116, 256, 1987.

Rehmel, Michael (2007), 'Application of Acoustic Doppler Velocimeters for Streamflow Measurements', Journal of Hydraulic Engineering, 133 (12), 1433-38.

Rosenberry, Donald O., et al. (2007), 'Comparison of 15 evaporation methods applied to a small mountain lake in the northeastern USA', Journal of Hydrology, 340 (3–4), 149-66.

Sauer, Vernon B., Meyer, R. W., and Geological, Survey (1992), Determination of error in individual discharge measurements (Norcross, Ga.; Denver, CO: U.S. Dept. of the Interior, U.S. Geological Survey ; Books and Open-File Reports Section [distributor]).

Seybold, C. A. (1994), 'Polyacrylamide review: soil conditioning and environmental fate', Communications in soil science and plant analysis, 25 (11-12), 2171-85.

Sharma, H.D. (1975), 'Manual of Canal Lining, Technical Report No. 14', (New Dehli: Central Board of Irriation and Power).

Shaw, R. D. and Prepas, E. E. (1990), 'Groundwater-lake interactions: I. Accuracy of seepage meter estimates of lake seepage', Journal of Hydrology, 119 (1–4), 105-20.

Sheng, Z., et al. (2003), 'Seepage Losses for the Rio Grande Project (Franklin Canal Case Study)', (TAMU, Agricultural Research and Extension Center, El Paso Texas Agricultural Experiment Station).

Shepard, J. S., Wallender, W. W., and Hopmans, J. W. (1993), 'One-Point Method for Estimating Furrow Infiltration', American Society of Agricultural Engineers, 36 (2), 395-404.

Simpson, M. R. (2002), Discharge Measurements Using a Broad-band Acoustic Doppler Current Profiler (US Dept. of the Interior, US Geological Survey; Information Services distributor).

Sirjacobs, D., et al. (2000), 'Polyacrylamide, Sediments, and Interrupted Flow Effects on Rill Erosion and Intake Rate', Soil Sci. Soc. Am. J., 64 (4), 1487-95.

Skogerboe, G. V., et al. (1999), 'Inflow-outflow channel losses and canal lining cost-effectiveness in the Fordwah Eastern Sadiqia (South) Irrigation and Drainage Project. IWMI Research Reports, Report No. R-85'.

Sojka, R. E., et al. (2007), 'Polyacrylamide in agriculture and environmental land management', Adv. Agron, 92, 75-162.

Stone, Mark C., et al. (2008), 'Impacts of Shear Stress on Saturated Hydraulic Conductivity of a Polyacrylamide Treated Soil', in W. Babcock Roger, Jr, and Walton Raymond (eds.), (316: ASCE), 102.

Susfalk, R.B., Young, M.H., and Smith, D.M. (2007), 'Application Guidelines: Use of Granular, Linear Anionic Polyacrylamide (LA-PAM) in Water Delivery Canals for Seepage Control', (DHS Publication No. 41239).

Susfalk, R., et al. (2008), 'Evaluation of Linear Anionic Polyacrylamide (LA-PAM) Application to Water Delivery Canals for Seepage Reduction', (Desert Research Institute, Reno and Las Vegas, NV and Colorado State University, Fort Collins, CO).

Swamee, Prabhata K. (1995), 'Optimal Irrigation Canal Sections', Journal of Irrigation and Drainage Engineering, 121 (6), 467-69.

Swamee, Prabhata K., Mishra, Govinda C., and Chahar, Bhagu R. (2000), 'Design of Minimum Seepage Loss Canal Sections', Journal of Irrigation and Drainage Engineering, 126 (1), 28-32.

Swihart, Jay (2007), 'U.S. Bureau of Reclamation, personal communication regarding cost of granular polyacrylamide.'.

Swihart, J. and Haynes, J. (2002), 'Canal-Lining Demonstration Project Year 10 Final Report', (R-02-03: United States Department of the Interior Bureau of Reclamation).

Tanji, K.K. and Kielen, N.C (2002), 'Agricultural drainage water management in arid and semi-arid areas', FAO irrigation and drainage paper 61, Rome: 135-60.

Tanny, J., et al. (2008), 'Evaporation from a small water reservoir: Direct measurements and estimates', Journal of Hydrology, 351 (1–2), 218-29.

Theng, B. K. G. (1982), 'Clay-polymer interactions; summary and perspectives', Clays and Clay Minerals, 30 (1), 1-10.

Trout, T. J. and Mackey, B. E. (1988), 'Inflow-Outflow Infiltration Measurement Accuracy', Journal of Irrigation and Drainage Engineering, 114 (2), 256-65.

Upadhyaya, A. and Chauhan, H. S. (2001), 'Water table fluctuations due to canal seepage and time varying recharge', Journal of Hydrology, 244 (1-2), 1-8.

USDL (2014), 'CPI Inflation Calculator', <http://www.bls.gov/data/inflation_calculator.htm>, accessed 1 June 2014.

USGS (1990), 'National Water Supply Summary, 1987: Hydrologic Events and Water Supply and Use', (Paper 2350; Denver, CO: United States Geological Survey).

USGS (2002), 'Policy and Technical Guidance on Discharge Measurements using Acoustic Doppler Current Profilers', (Office of Surface Water Technical Memorandum No. 2002.02).

Valiantzas, J. D. (2006), 'Simplified versions for the Penman evaporation equation using routine weather data', Journal of Hydrology, 331 (3–4), 690-702.

Valliant, J. (2000), 'Canal seepage reduction demonstration using polyacrylamides in the ditch and water: Arkansas River Valley of Colorado. Phases I, II, and III.'.

Vicens, Guillermo J., Rodriguez-Iturbe, Ignacio, and Schaake, John C., Jr. (1975), 'A Bayesian framework for the use of regional information in hydrology', Water Resources. Res., 11 (3), 405-14.

Wallace, A. and Wallace, G.A. (1990), 'Soil and crop improvement with water-soluble polymers', Soil Techn., 3:1-8.

WHO (1985), 'Acrylamide', (Geneva, Switzerland: World Health Organization, Environmental Health Criteria, No. 49).

Young, M., et al. (2007a), 'Risk Characterization: Using Linear Anionic Polyacrylamide (LA-PAM) to Reduce Water Seepage from Unlined Water Delivery Canal Systems', DHS Publication No. 41226 (University of Nevada Reno and Desert Research Institute).

Young, M.H., et al. (2009), 'Reducing Saturated Hydraulic Conductivity of Sandy Soils with Polyacrylamide', Soil Science Society of America Journal, 73, 13-20.

Young, M.H., et al. (2007b), 'Technical Report: Results of Laboratory Experiments in Support of PAM-Related Research', (Desert Research Institute, Division of Hydrologic Sciences Publication No. 41237).

Yu, Jian, et al. (2003), 'Infiltration and Erosion in Soils Treated with Dry PAM and Gypsum', Soil Sci Soc Am J, 67 (2), 630-36.

Yussuff, Sheik M. H., et al. (1994), 'Transient Canal Seepage to Sloping Aquifer', Journal of Irrigation and Drainage Engineering, 120 (1), 97-109.

Zhu, J. and Young, M.H. (2009), 'Sensitivity of Unlined Canal Seepage to Hydraulic Properties of Polyacrylamide-Treated Soil', Soil Science Society of America Journal, 73 (3), 695-703.